Durham University

Durham E-Theses

Atmospheric pressure metal-organic vapour phase epitaxy of InP, (GaIn)as, and (GaIn)(AsP) alloys

Butler, Barry R.

How to cite:

Butler, Barry R. (1989) *Atmospheric pressure metal-organic vapour phase epitaxy of InP, (GaIn)as, and (GaIn)(AsP) alloys*, Durham theses, Durham University. Available at Durham E-Theses Online: http://etheses.dur.ac.uk/6545/

Use policy

The full-text may be used and/or reproduced, and given to third parties in any format or medium, without prior permission or charge, for personal research or study, educational, or not-for-profit purposes provided that:

- a full bibliographic reference is made to the original source
- a link is made to the metadata record in Durham E-Theses
- the full-text is not changed in any way

The full-text must not be sold in any format or medium without the formal permission of the copyright holders.

Please consult the full Durham E-Theses policy for further details.

Academic Support Office, The Palatine Centre, Durham University, Stockton Road, Durham, DH1 3LE
e-mail: e-theses.admin@durham.ac.uk Tel: +44 0191 334 6107
http://etheses.dur.ac.uk

Abstract

Atmospheric Pressure Metal-Organic Vapour Phase Epitaxy
of InP, (GaIn)As, and (GaIn)(AsP) Alloys.

Barry R. Butler

An introduction to optical communications and opto-electronic devices is given, which demonstrates the motivation for research into III/V devices, and materials. Different epitaxial growth techniques are compared, an introduction to Metal-Organic Vapour Phase Epitaxy (MOVPE) is given, and the author's reactor is described.

The reaction chemistry of MOVPE is discussed and results from studies of the passivation of p-type InP are used to confirm the surface nature of reactions.

Results upon the background doping of MOVPE grown InP and the effect of growth conditions are discussed. High electron mobility results from InP layers are presented. The growth of epitaxial alloy layers of (GaIn)As and (GaIn)(AsP) is described with particular reference to crystallinity, lattice matching and composition control. A novel method of monitoring the dynamic vapour pressure of metal alkyls is described, and theoretical and practical results upon the factors affecting gas mixing and alloy uniformity are presented.

Results on the intentional doping of epitaxial layers with dimethylzinc, hydrogen selenide, and silane and the effect of varying the growth conditions are presented; and the use of other dopants is reviewed. The passivation of zinc acceptors by hydrogen in p-type InP is reported and discussed in detail. Results upon the use of ferrocene as a semi-insulating dopant are presented and the literature is reviewed.

Photoluminescence and transmission electron microscopy results are presented upon the growth of low dimensional structures, containing layers of less than 100Å thickness. Systematic studies of growth conditions are reported which have led to an understanding of the factors affecting hetero-interface abruptness.

Experimental results are reported upon distributed feedback lasers and all MOVPE double heterostructure and ridge waveguide lasers.

A discussion on safety aspects of MOVPE is included, with particular reference to the toxicity of arsine and phosphine, and the prevention of environmental pollution.

Atmospheric Pressure Metal-Organic Vapour Phase Epitaxy of InP, (GaIn)As and (GaIn)(AsP) Alloys.

Barry R. Butler

This thesis was submitted to the Faculty of Science of the University of Durham, for the degree of Master of Science.

1989

The copyright of this thesis rests with the author. No quotation from it should be published without his prior written consent and information derived from it should be acknowledged.

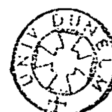

26 JAN 1990

The copyright of this thesis rests with the author. No quotation from it should be published without his prior written consent and information derived from it should be acknowledged.

Contents

	Page
Abstract	
Preface	
Chapter 1: Introduction	
Optical Fibre Communications	1
Optical Fibres	2
Cost Advantages of Optical Fibres	3
Optical Fibre Communication Systems	4
Opto-Electronic Devices	8
III/V Semiconductors	10
Device Fabrication	11
Epitaxial Layer Growth	12
Liquid Phase Epitaxy	13
Vapour Phase Epitaxy	14
Metal Organic Vapour Phase Epitaxy	15
Molecular Beam Epitaxy	16
Metal Organic Molecular Beam Epitaxy	17
Summary	17
Chapter 2: MOVPE Chemistry	
Reaction Mechanism for MOVPE	18
Metal Organic Compounds	21
Group V Precursors	23
Preparation of Metal Organic Compounds	25

Chapter 3: InP Epitaxy

Crystal Structure of InP	28
Epitaxial Crystal Growth	28
Substrates	30
Substrate Preparation	30
InP Growth Conditions	31
Background Doping of InP	32
Variation of InP Background Doping Level with Growth Conditions	33
Interface Carrier Concentration Spikes	34
Source of Background Doping	35
Single Epilayer Mobilities	37

Chapter 4: (GaIn)(AsP) Alloy Epitaxy

III/V Alloy Systems	40
Lattice Matching of Alloys	41
(GaIn)As	42
(GaIn)(AsP)	45
Alloy Uniformity	47
Non-Uniformity Due to Slow Arrival of Reactants	47
Ultrasonic Binary Gas Composition Monitoring	48
Trimethylindium Vapour Pressure Rise Time Measurements	51
Run to Run Vapour Pressure Stability	52
Trimethylindium Source Exhaustion Characteristics	53
Gas Mixing	54
Turbulent Mixing	56
Diffusion Mixing of Gases	58
Interface Abruptness: The Effect of Gas Diffusion	59
Interface Abruptness: Effect of Parabolic Velocity Profile	60
Entrance Effects	61
Longitudinal Compositional Uniformity	62
Thickness Uniformity	63

Chapter 5: Impurity Doping of InP and (GaIn)As

n-type Dopants	64
Silane	65
Disilane	67
Hydrogen selenide	67
Hydrogen sulphide	68
Diethyltelluride	68
Tetraethyllead	68
p-type Dopants	69
Dimethylzinc and Diethylzinc	69
Dimethylcadmium	71
Magnesium Doping	72
Manganese Doping	72
Hydrogen Passivation of Acceptors in p-type InP	73
Hydrogen Incorporation in p-InP/p+(GaIn)As Structures	73
Hydrogen Incorporation into p-InP Layers	77
Relevance of Hydrogen Incorporation to Reaction Mechanism	78
Bonding Mechanism for Hydrogen in p-InP	79
Rare Earth Element Doping	80
Iron Doping of InP	80
Cobalt Doping	83

Chapter 6: Low Dimensional Structures

Background	84
Device Applications	86
Growth on Mismatched Substrates	87
Growth of Low Dimensional Structures	88
Photoluminescence Studies of (GaIn)As/InP Quantum Wells	90
TEM Studies of (GaIn)As/InP Quantum Wells	92
Double Crystal X-ray Analysis of (GaIn)As/InP Quantum Wells	95
(GaIn)(AsP) Quantum Well Structures	95

Chapter 7: Semiconductor Lasers Grown by MOVPE

History 97
Theory of Operation 98
Heterostructures 101
Double Heterostructure Lasers 102
Ideal Device Performance 104
Ridge-Waveguide Lasers 105
Distributed Feedback Lasers 106
Contact Layers 108
p and n-Type Doping of InP Confining Layers 108
Reliability of Lasers 109
Buried Heterostructure Lasers 110
The Use of Semi-Insulating Materials in Buried Heterostructure Lasers 112
Quantum Well InP Based Lasers 113

Chapter 8: MOVPE Safety

Metal-Organic Chemicals 115
Phosphorus 116
Hydrogen 116
The Toxicity of Arsine and Phosphine 117
Safe Reactor Design and Operation 117
Gas Containment upon Equipment Failure 118
Cylinder Changing, Handling and Storage 119
Medical Aspects of Exposure to Arsine and Phosphine 120
Arsine and Phosphine Monitoring 120
Alternative Group V Sources 121
Environmental Protection 122
Charcoal Adsorption 122
Wet Scrubbers 123

Future Developments 124

Appendix 1: Atmospheric Pressure MOVPE Reactor B at STL

Vent-Run Design 125
Pressure and Flow Balancing 125
Mass Flow Controllers and Reactant Lines 126
Metal-Organic Sources 126
Gaseous Sources 127
Reaction Chamber 127
Exhaust and Toxic Gas Monitoring 127
Computer Control and In-situ Monitoring 128
Leak Testing and Vacuum System 128

Acknowledgements 129

References

Tables are incorporated within the text.

References are denoted using square brackets: [n].

Figures

Figures are included at the end of each chapter.

1.1 Summary of telecommunication systems and opto-electronic components.

1.2 Attenuation in silica optical fibres.

1.3 Semiconductor laser fabrication steps.

3.1 Growth of InP upon a non-planar surface.

3.2 InP background doping level as a function of growth temperature.

3.3 SIMS profile through InP grown at different temperatures.

3.4 InP background doping level as a function of growth rate.

3.5 SIMS profile through InP grown at different rates.

3.6 InP background doping level as a function of V/III ratio.

3.7 SIMS profile through InP grown under different V/III ratios.

3.8 Electrochemical profile through high mobility InP.

3.9 Low temperature photoluminescence spectrum for high purity InP.

4.1 Lattice matching and band-gap contours for compositions of ternary and quaternary alloys.

4.2 Morphology of good and poor quality (GaIn)As.

4.3 Morphology of (GaIn)As grown using different arsine over-pressures.

4.4 77K photoluminescence from a 1.3μm quaternary layer.

4.5 X-ray rocking curve for 1.18μm quaternary material.

4.6 X-ray rocking curve for 1.3μm quaternary material.

4.7 Diagram of reactor trimethylindium line and ultrasonic reagent monitor.

4.8 Time response of trimethylindium vapour pressure at 50°C.

4.9 Time response of the ultrasonic reagent monitor.

4.10 Time response of trimethylindium vapour pressure at 40°C.

4.11 Run to run repeatability of trimethylindium vapour pressure.

4.12 Trimethylindium vapour pressure source exhaustion characteristics.

4.13 Lateral composition of epitaxial (GaIn)As.

4.14 Lateral composition of epitaxial (GaIn)As after reversal of the gas manifold inlet configuration.
4.15 Lateral composition of epitaxial (GaIn)As grown with an increased trimethylgallium injection velocity.
4.16 Lateral composition of epitaxial (GaIn)As grown using a protruding inlet gas switching manifold.
4.17 Lateral composition of epitaxial (GaIn)As grown using a high impedance gas mixing nozzle.
4.18 Calculation for diffusion of trimethylgallium in hydrogen.
4.19 Photoluminescence map of (GaIn)As grown using a dual line reactor.
4.20 Photoluminescence map of 1.55μm quaternary material.
4.21 Variation of gallium content as a function of growth tube temperature.
4.22 Variation of arsenic content as a function of growth tube temperature.

5.1 Doping of InP and (GaIn)As using silane.
5.2 Dependence of InP electron concentration upon silane flow-rate.
5.3 Dependence of silane doped InP electron concentration upon growth temperature.
5.4 Dependence of silane doped InP electron concentration upon growth rate.
5.5 Dependence of InP electron concentration upon hydrogen selenide flow-rate.
5.6 Dependence of InP hole concentration upon dimethylzinc flow-rate.
5.7 Hole mobility in zinc doped InP.
5.8 Dependence of dimethylzinc doped InP hole concentration upon growth rate.
5.9 Dependence of growth rate of zinc doped InP upon doping level.
5.10 Dependence of dimethylzinc doped InP hole concentration upon growth temperature.
5.11 Structure used to study hydrogen passivation of p-InP.
5.12 Electrochemical profile through a passivated p^+(GaIn)As/p-InP heterostructure.

5.13 Electrochemical profile through a p^+(GaIn)As/p-InP heterostructure following thermal pulse annealing.
5.14 Electrochemical profile through a p^+(GaIn)As/p-InP /n-InP/p-InP heterostructure.
5.15 SIMS profile through a p^+(GaIn)As/p-InP/n-InP/p-InP heterostructure.
5.16 Electrochemical profiles through structures demonstrating the hydrogen blocking effect of n-type (GaIn)As.
5.17 Variation of hydrogen passivation with annealing conditions.
5.18 Doping levels for p-InP cooled under different conditions.
5.19 SIMS profiles through p-InP layers cooled under different conditions.
5.20 Electrochemical profile through p-n-p InP.
5.21 SIMS profile through p-n-p InP.
5.22 Electrochemical profile through iron and silicon doped InP.

6.1 (GaIn)As/InP quantum well structure.
6.2 4.5K photoluminescence from a (GaIn)As/InP quantum well structure.
6.3 (GaIn)As/InP structure containing thin quantum wells.
6.4 5K photoluminescence from a (GaIn)As/InP structure containing thin quantum wells.
6.5 Photoluminescence fwhm as a function of quantum well width.
6.6 TEM image from a (GaIn)As/InP structure containing thin quantum wells.
6.7 Repeated (GaIn)As/InP quantum well structure.
6.8 (GaIn)As/InP quantum well structure grown to investigate the effect of growth temperature upon interface quality.
6.9 (GaIn)As/InP quantum well structure grown to investigate the effect of V/III ratio upon interface quality.
6.10 (GaIn)As/InP quantum well structure grown to investigate the effect of growth rate upon interface quality.
6.11 Marked (GaIn)As/InP quantum well structure grown to investigate the onset of interface non-planarity.
6.12 TEM image of a (GaIn)As/InP quantum well structure containing InAs marker layers.

6.13 TEM image of a (GaIn)As/InP quantum well structure containing (GaIn)(AsP) marker layers.

6.14 (GaIn)As/InP quantum well structure grown to investigate the effect of growth pauses upon interface quality.

6.15 TEM image of a (GaIn)As/InP quantum well structure grown with (GaIn)As surfaces paused under arsine.

6.16 TEM image of a (GaIn)As/InP quantum well structure grown with (GaIn)As surfaces paused under hydrogen.

6.17 X-ray rocking curve for a repeated (GaIn)As/InP quantum well structure.

6.18 Repeated (GaIn)(AsP)/InP quantum well structure.

6.19 TEM image of a repeated (GaIn)(AsP)/InP quantum well structure.

6.20 X-ray rocking curve of a repeated (GaIn)(AsP)/InP quantum well structure.

6.21 (GaIn)(AsP)/InP quantum well structure containing wells of different thickness.

6.22 4.2K photoluminescence from a (GaIn)(AsP)/InP quantum well structure.

7.1 Inverted rib waveguide laser structure.

7.2 Ridge waveguide laser structure.

7.3 Sequence of epitaxial layers grown for a double heterostructure laser.

7.4 Light-current characteristic for an MOVPE double heterostructure laser.

7.5 Sequence of epitaxial layers grown for a ridge waveguide laser.

7.6 Light-current characteristic for an MOVPE ridge waveguide laser.

7.7 Distributed feedback laser fabrication steps.

7.8 Light-current characteristic for a distributed feedback laser.

7.9 Eye diagram for a distributed feedback laser.

7.10 Structure of a buried heterostructure laser.

A.1 Schematic diagram of MOVPE reactor B at STL.

Preface

This thesis was written during 1988 and 1989, for submission to the University of Durham for the degree of Master of Science, under regulation 2a of the University calendar. The subject of the thesis is the Metal Organic Vapour Phase Epitaxy (MOVPE) of indium phosphide (InP), and gallium indium arsenide phosphide (GaIn)(AsP) layers, which are subsequently used in the fabrication of opto-electronic components. The experimental work reported is that of the author, unless otherwise stated, albeit with considerable contributions from colleagues, due to the team nature of research and development work in this field. References are made to information gained through valuable discussions with other workers.

The author was employed in opto-electronic research and development, in the advanced sources group of STC Technology Ltd., (S.T.L.), in Harlow, Essex, U.K., until November 1988. The majority of the experimental work presented, was undertaken at S.T.L., using an atmospheric pressure MOVPE reactor which is detailed in appendix 1. During November 1988, the author transferred to the Optical Devices Division of STC Defence Systems Ltd., where the development work from S.T.L. was transferred to production. Some information is presented upon this latter work, although it was undertaken upon a low pressure MOVPE reactor.

During the 12 months taken to write the thesis, the early chapters have required continual revision in the light of new results. It is hoped that much of what is presented stands the test of time, however the thesis should be read in the context of the state of the art of the technology in 1988/89.

The opinions and conclusions expressed in this thesis are those of the author, and do not necessarily reflect the opinions of STC plc or the author's colleagues.

No information contained in this thesis has previously been submitted by the author for a degree at any university.

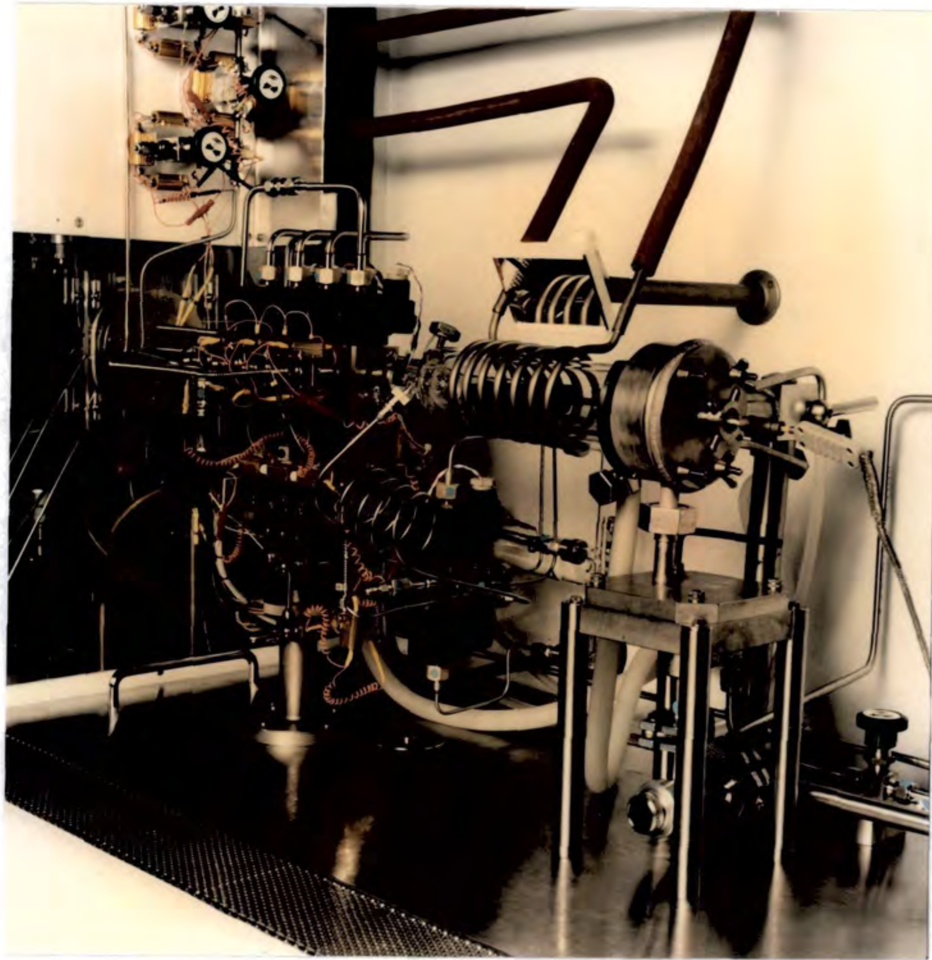

MOCVD Reactor "B" at STL.

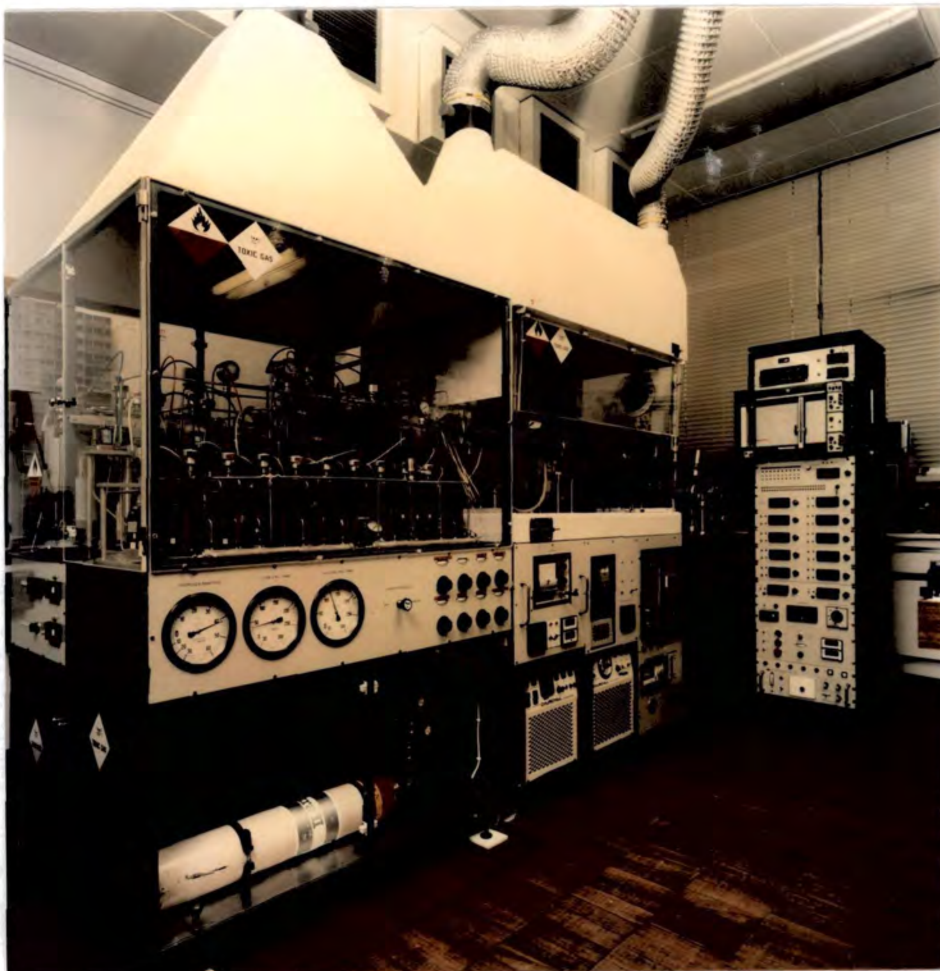

Chapter 1

Introduction

Metal Organic Vapour Phase Epitaxy (MOVPE), is an epitaxial growth technique used to manufacture many electronic devices. The particular materials discussed in this thesis are used in the fabrication of opto-electronic devices which are subsequently incorporated into optical communication systems. In order to understand the motivation driving the research and development of opto-electronics and MOVPE, an introduction to optical-fibre communications, system costs, and epitaxial crystal growth techniques is given.

Optical Fibre Communications

It was recognised during the 1960s, that the information capacity of trunk telecommunication systems required expansion. Fixed microwave metal waveguide links were being developed which would greatly expand the telephone system capacity through enlarged band-width. In retrospect the high material and engineering costs of this approach are daunting when compared with electrical systems using twisted pair or coaxial cables.

The guiding of light in a jet of water was demonstrated by Tyndall in 1870. The lateral step of using guided electromagnetic waves of a higher frequency than microwaves, namely light, to carry information was shown to be theoretically possible by Kao and Hockman in their paper on fibre-optic communication of 1966 [1]. In order for the predictions of Kao and Hockman to be realised, many years of development of fibre-optic components have been necessary. These components may be separated into the light guide or optical fibre, the opto-electronic transducers such as modulators, light emitters and detectors, and associated high speed electronic circuits to interface between the optical system and the normal electronic levels of information technology. The latter, usually silicon integrated circuits operating to several GHz are in themselves advanced components, and are the result of parallel developments in other

electronic fields, so are not expanded upon here. An overview of how the components are combined with each other to give an optical communication system is illustrated in figure (1.1).

Optical Fibres

The principal of the guiding of light in optical fibres is explained in many texts [2]. Two approaches are normally taken; for large diameter core fibres the ray model is used, whereby rays of light are repeatedly totally internally reflected within the fibre due to a decrease in refractive index towards the exterior of the fibre. The other model, applied especially to light propagation in fibres of less than 10μm diameter, involves solutions of Maxwell's equations with application of suitable boundary conditions in a similar manner to the guiding of microwaves by waveguides. Most modern telecommunication applications use optical fibres where an inner 5-10μm core of silica glass is surrounded with a lower refractive index cladding glass to increase the strength of the cable. Such fibres are termed single mode fibres since only a single fundamental mode of electromagnetic radiation is able to propagate along the fibre.

The optical fibres available at the time of the Kao and Hockman paper, had an attenuation of 1000dB/km. The techniques of fabrication of optical fibres have greatly improved, spurred on by the demands and rewards of the communications revolution. Attenuation levels as low as 0.2dB/km have now been achieved. The level of attenuation within a silica optical fibre is a function of the optical wavelength of the light being transmitted (figure 1.2). The attenuation is due to absorption of light due to the infra-red and ultra-violet band edges of the silica, Rayleigh scattering, and impurity absorption. The first two factors are fundamental to the silica itself, and the Rayleigh scattering is due to the glassy disordered state of the material. Impurities such as transition metals have to be kept at levels of less than a few parts per billion. The increase in attenuation at 1.4μm wavelength is due to OH^- resonance resulting from water being present during manufacture. It can be seen from figure (1.2) that whilst the more easily fabricated 0.85μm wavelength GaAs light emitters can be used for short distance communication links, for longer distance

applications it is better to use wavelengths such as 1.3μm and 1.55μm.

Another important property of optical fibres is material dispersion, that is the variation of the refractive index of silica with wavelength. The effect of material dispersion is that different wavelengths of light travel at different speeds within the fibre, and for a semiconductor laser with typically a 3nm band-width, light pulses become spread out along the fibre with increasing propagation distance. The maximum distance-bitrate product of the system is therefore limited by material dispersion as well as by fibre attenuation. However zero dispersion is encountered at a wavelength of 1.3μm. For this reason, whilst the attenuation minimum of standard optical fibres is at 1.55μm, most present optical communication systems operate at the slightly attenuated wavelength of 1.3μm. More recently, narrower band-width sources such as the distributed feedback laser have become more common, and new system implementations are tending to operate at 1.55μm.

A common optical fibre production method is to fabricate glass preforms which are rods of highly pure silica, intentionally doped with the impurities required in the core and cladding layers of the final fibre. The preforms are subsequently heated and pulled through a small die to form continuous lengths of fibre which are then coated for protection, and are strong enough to be used in conventional fabrication procedures.

Cost Advantages of Optical Fibres

Driving this technology forward are the advantages of optical fibre communication systems over conventional copper systems and satellite communication systems. The advantages may be briefly summarised as increased repeater spacings for long haul routes, small physical size, weight and flexibility, low material costs, and immunity from electromagnetic interference. Systems can be easily upgraded since fibres can be left in the ground whilst transmitters and receivers are replaced by more advanced products. An early disadvantage of optical fibres was the difficulty of splicing cables together. This has largely been overcome by the use of fusion splicers. The original difficulty encountered in tapping fibres has also been overcome, making them less secure than they used to be.

All of the above advantages result in an overall lower cost for an optical communications system of modest data rate, compared with either copper cables or satellite systems of similar capacity, without beginning to exploit the increased band-width of the systems. As a result, the major telephone operators have ceased to deploy copper trunk systems since the mid 1980's, and are now deploying optical systems. The laying of TAT-8, the undersea optical cable between Europe and America in 1988, heralded a change from copper to optical systems here too. TAT-8 has a similar information carrying capacity to the total capacity of all the previous copper cables.

Optical Fibre Communication Systems

The driving force for much of the development of optical fibres and optical emitters and receivers, derives from communication systems, and the desire to transmit large amounts of information at high data rates, selectively from one user to another. The applications extend from long distance telecommunication systems through to local area networks, and even to optical links within computers. For information to be transmitted through a medium, a carrier, in this case light, requires modulating. In the simplest form of optical communications technology, and the one commonly implemented to date, the light source is turned on and off to give digital pulse code modulation, without the use of an additional modulator on the output light beam from the source. The data rates achieved are then limited by the modulation and demodulation capabilities of the transmitting and receiving components, and the material dispersion of the fibre.

The initial application of optical systems was to the trunk telecommunication networks operated by the major telephone companies. The use of high cost components was justified by the greatly increased capacity of the long distance routes between major switching centres or exchanges. Companies such as British Telecom in the U.K. have adopted a policy of deploying optical cables in trunk networks instead of copper cables. The earliest demonstration of these systems was in 1977, and consisted of an optical fibre link between Hitchin and Stevenage in the U.K., which operated at a wavelength of 0.85μm. Much of the capital cost of long distance communication systems lies in the

cost of repeaters. Twisted wire pair 8Mb/s links require repeaters every 1-3km, and coaxial links require repeaters every 1-2km. By comparison, optical links can operate at speeds of up to 2.4Gb/s and repeater spacings of many tens of kilometres have been achieved. The cost of an opto-electronic repeater is higher than a purely electronic repeater, however the cost per bit of information is lower, making implementation of optical systems favourable.

Inter-continental communications traffic, formerly achieved by satellite and submarine coaxial cables, was also at the centre of the development of fibre-optic communications. For a considerable time, optical systems were not deployed beneath the oceans, whilst component reliability was assessed. Once determined as reliable, optical communications cables have completely superseded coaxial links in new systems. The first example of a commercial undersea optical cable was TAT-8, opened for traffic in 1988 between Europe and America, and operating at a wavelength of 1.3μm. Much cable capacity is presently leased to investors before cables are laid. The optical systems are cost competitive compared with satellites, it is said that they are a factor of three cheaper.

The next generation of optical fibre submarine systems such as TAT-9, will operate at 1.55μm wavelength where the attenuation of the fibre is at a minimum, and repeater spacings significantly greater. The problem of fibre dispersion is overcome by the use of narrower spectral line-width distributed feedback laser sources.

The penetration of optical technology into the trunk and international telecommunications arena is nearly total. The exception is perhaps third world applications where users are fewer and more dispersed, and satellites offer greater security from sabotage. Other independent users, transmitting data over long distances, are the electricity distribution companies and railways. The noise immunity of optical transmission is a further advantage for these operators. Heavy data users such as financial institutions are also showing an interest in having their own dedicated optical networks.

The next level of telecommunication link, is between local exchanges and is referred to as the junction network. This area is now becoming cost competitive as component costs fall, and significant optical penetration can be expected in the 1990s. The final level of telecommunication link is between the local exchange and the

subscriber, and is referred to as the local loop network. Apart from a few pilot experiments in selected towns and cities, optical penetration has not yet taken place in the local loop network. Complete penetration of the optical network would allow the transmission of high quality digital data, giving better quality voice circuits, faster and more widespread computer communication, and more widespread use of ISDN services. A variety of new services would also result, such as access to large information and video data bases, remote metering and control of for example gas meters, electronic mail, and a more integrated approach to the financial services of banks and payment by automatic debiting of accounts whilst shopping. These types of communication are of the traditional point to point variety. It is envisaged that cable television companies may wish to utilise the unused band-width of optical fibres, by overlaying multi-channel video data onto the local networks using different transmission wavelengths to the telecommunications operators.

Slow scan video links are presently available via special arrangements with the telecommunications operators. The high band-width of optical fibres, makes possible the replacement of the telephone by the video-phone for all users prepared to pay for the service. However, the capability to switch the high data rate signals in the same flexible manner as achieved in conventional telephone exchanges has first to be demonstrated. It is interesting to consider the social implications of being able view one's conversation partner as well as to hear them!

The practical realisation of local loop communications to the business customer is presently being investigated by British Telecom using the TEPON system [3]. This comprises the splitting of light from a distributed feedback laser through a 128 way passive splitter to 128 locations. Low cost receiver and transmitter technology is used within the customers premises, and a 20Mb/s data rate envisaged. The system is designed to be a first stage implementation of the present data quality and service range obtained from System-X facilities. With the fibre installed to the customer, a future increase in the use of the fibre band-width can be envisaged, as and when services become available and customer needs develop. This could be implemented at the customer and exchange ends by upgrading of transmitter and receiver modules. An overlay at a different operating wavelength of a cable

television system may bring the system cost down such that private customers may be interested in the services available, in addition to business users.

Scaling down communication distances further, optical links within buildings, offices and between computers are of interest. Such links are often referred to as local area networks, allowing communications between many users, peripherals and computers. Trends in information technology and computer speeds are requiring transmission of data at high rates. Cost is important however, so largely passive optical networks of either ring or star configuration are being considered. The important components for this application are multi-point passive couplers, taps, modulators, transmitters and receivers. The large volume of users make sale of such systems and associated components attractive to some companies.

At further lower communication distances, computer performance is becoming limited by the speed at which data can be moved from chip to chip and even across large integrated circuits. This is due to resistance-capacitance time constants of the electronic connectors and cables. The problem can be circumvented by the use of parallel data transmission, but pin counts of chips are consequently higher, which increases costs and poses problems during manufacture. Application of short distance, high bit-rate serial optical data links to this problem is being considered, as is the multi-processor computer communicating optically through free space using opto-electronic components.

The other advantages of optical fibres, other than band-width; such as immunity to electromagnetic interference and low weight, has led to optical systems of data transmission being adopted in military arenas such as aircraft data buses and in phased array radars. The dielectric nature of fibres also make the application of this technology attractive in explosive environments and in high voltage areas.

All of the above systems have relied upon simple on-off modulation of the light sources, with a maximum band-width of 2.4Gb/s being achieved. Slower rate data streams are time division multiplexed to make up the higher rate data stream. The small size of optical fibres also allows system capacity to be expanded by increasing the number of fibres used in existing ducts compared with conventional

cables.

Consideration of the actual band-width available in an optical fibre gives a value of ≃100THz. Clearly the medium is not being exploited to the fullest extent in conventional systems. Usage of fibre band-width can be increased by simultaneously using emitting devices with very narrow spectral line-widths of differing wavelengths. Such systems are frequency division multiplexed, and require receiver demultiplexing components that can separate out the different wavelengths transmitted through the fibre.

Finally, it is worth mentioning an alternative to direct digital pulse code modulation; the technique of coherent optical data transmission. This method requires that a modulated signal is allowed to beat against a local oscillator to give a modulated carrier signal. This is the same technique as used in conventional radio transmission with the electromagnetic wavelengths changed to optical wavelengths. The use of many carrier frequencies, each separately heterodyned in a similar manner to radio signals, would greatly increase the usage of the available optical band-width. Other advantages include the ability to tune through many channels, and higher receiver sensitivity, since the method allows operation closer to the quantum detection limit.

Opto-Electronic Devices

The systems discussed above require devices that can transmit, receive and modulate light, so that optical systems can interact with the normal electronic methods of data generation, processing, transmission and storage. The requirement for low cost, small size and high reliability has resulted in solid state components being adopted for most applications. Detectors are constructed from III/V semiconductors, germanium or silicon rather than using photo-multiplier tubes, and light sources are semiconductor lasers rather than lasers requiring flash-lamp stimulation. Direct modulation of the source is normal, though much work has been undertaken upon non linear optical materials such as lithium niobate which can be used to modulate laser sources externally.

Optical sources fall into two categories, light emitting diodes (LEDs) and lasers, and for the applications considered above, both are solid state semiconductor devices. Both rely upon electron-hole

recombination in a p-n junction within a direct energy band-gap material, resulting in the generation of photons of energy equivalent to the material's band-gap energy. LEDs rely principally upon this mechanism, whilst semiconductor lasers require carrier population inversion, generated by high levels of carrier injection at the p-n junction, and upon light fed back from the laser facets. Lasers are detailed in greater depth in a later chapter of this thesis.

The detectors presently used in systems are of the p-i-n type and comprise a p-doped region, a low doped "i" region, and an n-doped region, which is reverse biased. Incident photons are absorbed by the material and create electron hole pairs which are subsequently separated by the electric field across the device to give a detectable current. The magnitude of the current is proportional to the flux of incident photons. The photogenerated current is subsequently amplified, often using a high speed GaAs FET. For short wavelength detection such as at 0.85μm, silicon and germanium implanted detectors are adequate. For low noise performance at longer wavelengths such as 1.3μm and 1.55μm, III/V heterostructure devices such as n-InP/(GaIn)As/p-InP devices are used. Much developmental effort is being concentrated upon the integration of p-i-n diodes and FETS into the same chip, and the (GaIn)As/InP alloy system appears well suited to this application [4].

Avalanche photodiodes are a further high performance variant upon p-i-n detectors, where amplification occurs internally by secondary generation of carriers due to high reverse bias voltages. Avalanche photodiodes are not yet commonly available in III/V materials.

Other opto-electronic components that may have a future rôle in optical systems are devices that can be inserted into local area network fibres to allow data to be added and subtracted to that already travelling along the fibre. Of particular interest is a component termed a transmissive detector and modulator (TDAM) [5]. Such devices are now being developed in quantum well constructions of (GaIn)(AsP)/InP materials.

There is current interest in the direct amplification of light in fibre optical systems without the need to convert the light back into an electrical signal as an intermediate step. A suitable amplifier is a semiconductor laser structure, pumped to maintain a population inversion, but with non reflective facets to prevent optical feedback

and lasing occurring. The device then preferentially gives out light in a coherent manner, in phase and proportional to an input flux of photons.

III/V Semiconductors

The semiconductor GaAs, has been used for many years for the manufacture of electronic devices, exploiting identical fabrication technology to that used in the silicon industry. Early examples of devices are Gunn diodes, and discrete FET transistors. More recently, GaAs has been used to fabricate fast, radiation hard integrated circuits of both analogue and digital type. The high electron mobility of GaAs when compared with silicon, has resulted in many attempts to use the material for advanced, high speed devices, and many circuits are in commercial production. Advances in silicon technology have always maintained silicon integrated circuit performance at only slightly reduced levels with respect to GaAs integrated circuits, and at a cheaper fabrication cost. As a result, GaAs electronic devices have, to date, been applied to a few high cost, high performance applications.

The III/V semiconductors GaAs and InP and their alloys, differ considerably from silicon in that they possess a direct band gap energy transition between the valence and the conduction bands, whereas silicon possesses an indirect band-gap. The direct band-gap of many III/V semiconductors can be exploited to give radiative electron-hole recombination, whereas such devices cannot be fabricated using silicon technology.

The earliest examples of GaAs opto-electronic light emitters were originally used as proximity fuses for military applications. GaAs emitters have continued to be produced for other military products such as range finding and target illumination. More familiar are the red, green and yellow LEDs found in many commercial and domestic products and which are made from the semiconductors GaP or Ga(AsP).

Light emitting devices based upon epitaxial crystal growth, were first fabricated from the GaAs/(GaAl)As alloy material system, and operated at a wavelength of 0.85μm. In order to address longer wavelengths that match the low loss windows of optical fibres at 1.3μm and 1.55μm, a narrower band-gap alloy system has to be used. Suitable

materials are (GaIn)(AsP) and (GaInAl)(As), grown upon InP substrates. (GaIn)(AsP)/InP epitaxy is the more frequently used material system, and the MOVPE of this alloy is covered in depth in chapter (4).

It is along with the invention of fibre optic communication systems, that more sophisticated III/V opto-electronic semiconductor components have been developed. In parallel with these applications, optical read and write memory systems, which contain opto-electronic components have been developed. An example of this technology is the compact disc player.

Device Fabrication

Figure (1.3) illustrates the series of processes required to produce a packaged III/V semiconductor opto-electronic component. In most laboratories, the process starts with procurement of substrates and epitaxial growth materials. Epitaxial layers are grown upon the substrate to varying thicknesses and compositions. The sandwiches of materials are subjected to processing stages whereby they are coated with oxide and photo-resist, and shaped into structures using conventional photolithography, which are then suitable for the confinement of light and electricity. A series of metal layers such as titanium, platinum and gold are electron beam evaporated onto the top surface of the material to act ultimately as a contact. The substrate is thinned typically from a thickness of 300μm to 100μm using a polishing technique, and an etch, such as bromine methanol for InP. The wafers are metallised on the substrate side of the device, following which an alloying step may take place to form an ohmic contact. The processed wafers are scribed and cleaved into individual chips for testing and visual inspection. The above process is largely common to all device structures with only the epitaxial growth sequence, the physical shape, and the method of electrical contact to the device varying. The device chips are soldered onto a small submount to allow easy handling at the next stage which is package assembly.

A typical trunk application laser package will contain the laser on its submount, a Peltier cooler to control the temperature of the device, and a monitor photodiode which detects light from the rear facet of the laser and sends electrical signals to a control circuit

monitoring the performance of the laser. An optical fibre pigtail is carefully aligned to the front facet of the laser chip, and the whole of the package is hermetically sealed. Many manufacturers are automating the above process to maximise yield and reduce high labour costs. There is now a tendency to add other components to the package such as silicon integrated circuits to provide value added products which the customer can treat as normal electronic components. An example is a product which requires only a power supply and a TTL drive signal, and which provides a modulated optical light output. The early sophisticated hermetically sealed packages intended for low volume, high cost applications such as submarine communication lasers, are being complemented by low cost, high volume products which are plastic encapsulated for local loop applications.

Epitaxial Layer Growth

All of the above electro-optic devices require semiconductor layers of differing compositions of III/V elemental alloys to be grown upon a single crystal wafer or substrate. In this thesis, the focus is mainly upon the growth of the alloys of gallium, indium, arsenic and phosphorus grown upon InP substrates. The growth of crystalline layers of the order of a few microns thickness upon crystalline substrates, with the short and long range order of the crystal structure remaining preserved, is referred to as epitaxial layer growth.

There is a variety of techniques available to grow these layers, of which MOVPE is the subject of this thesis. In each case the objective is to grow crystalline layers with an average lattice parameter which usually matches that of the substrate, and with a controlled composition to give material of an appropriate band-gap. The different refractive indexes of differing materials are used to affect the way in which light is guided in the final structure. In addition, impurity doping of the different layers is controlled to achieve the desired electrical and optical behaviour of the final device. Many of the following techniques can be used also to grow II/VI epitaxial material such as zinc sulphide, zinc selenide and cadmium mercury telluride, but the details of these processes are beyond the scope of this work.

Liquid Phase Epitaxy (LPE)

Liquid phase epitaxy is still the most commonly used method of III/V epitaxial growth, and was the earliest successful technique [2]. The method consists of dissolving a mixture of the elements required for the epitaxial layer in a liquid metal, which is also required in the final layer. An example is the addition of small amounts of indium phosphide, gallium arsenide and indium arsenide to molten indium to grow a layer of (GaIn)(AsP). The liquid charge is then solidified and transferred to the LPE reactor, along with a carefully sized substrate. The whole furnace or reactor is then heated for some time, following which the temperature is gradually decreased. The solutions of III/V elements become supersaturated at specific temperatures, and the substrate is then moved to beneath the liquid solutions, following which crystal growth occurs at a rapid rate with the substrate acting as a seed for the supersaturated solution to nucleate upon. Growth is fast, of the order of several microns in tens of seconds, and proceeds for as long as the melt remains supersaturated. The melts and substrate are all held in a graphite arrangement, termed a boat. Purified hydrogen is passed through the reactor to prevent ingress of water and air, and to sweep out vapours from the melts. The growth is terminated by removing the substrate from beneath the final melt. The earliest type of reactor was a tipping furnace, where gravity was used to tip the melt over the substrate and then off again. The most modern LPE reactors have several separate melts contained in separate wells in the graphite boat to allow different compositions of materials to be grown. Wafers of up to 1.5cm by 3cm are grown upon. The graphite is heated radiantly by carefully positioned resistance elements, outside a quartz glass tube surrounding the boat. It is necessary to provide an over pressure of the group V elements to prevent surface erosion of the substrate during the heat up phase. This over pressure is usually provided by a crystalline cover slice coated with a layer of the necessary group V element. An alternative method is to use phosphine to provide phosphorus to prevent thermal erosion of an InP substrate.

The main advantages of the LPE technique, are simplicity, low cost and a fairly safe process, the only significant hazard being the presence of hydrogen at high temperatures. These advantages have led to its widespread use as a production technique, however it has

several disadvantages. Great control is required over the temperature of the furnace since this controls the supersaturation of the melts. Too high a temperature results in the substrate or previously grown layers dissolving into the melt rather than the growth of further layers, since the technique is close to equilibrium. Even with good control it is not possible to grow certain layer combinations, such as InP upon (GaIn)As, and in order to grow InP upon 1.55µm emission (GaIn)(AsP), an intermediate higher band-gap quaternary layer is required as an anti-melt-back buffer layer. It has proved difficult to reduce background carrier concentrations of layers to below 10^{17} cm^{-3} for InP based materials, causing problems with the performance of devices such as detectors. Scaling up of the technique to larger wafer sizes has proved difficult as has the growth of quantum well layers of ~100Å or less due to the high growth rates encountered.

Vapour Phase Epitaxy (VPE)

There are two non metal-organic methods of vapour phase epitaxy in common use, chloride VPE and hydride VPE [6]. Both are equilibrium crystal growth techniques requiring a high degree of temperature control. In III/V chloride VPE reactors, gaseous arsenic trichloride or phosphorus trichloride, is passed over molten gallium or indium melts. Gaseous mixtures of the group III and V chlorides are then passed over the substrate in a separate heated zone, and III/V alloy epitaxy takes place.

The hydride VPE technique utilises a gas stream of hydrogen chloride passing over molten group III elements to produce metal chlorides, and the group V elements are provided by pyrolysis of arsine and phosphine. The hydride technique is the more commonly used. Substrate erosion has to be prevented prior to crystal growth since the substrate is at a high temperature prior to introduction of the reactants.

The highly corrosive nature of the gases used has resulted in reactors being fabricated largely from quartz glass. Separate regions of the reactor are often used to grow different layers in order to improve interface abruptness. This however requires complex substrate movements.

High quality material has been grown using VPE techniques, and

some companies use this method in a two inch production environment. The fragility of the glassware, and the toxic nature of the reactants have prevented widespread use of the technique.

Metal Organic Vapour Phase Epitaxy (MOVPE)

There are several alternative titles to the MOVPE technique, including MOVPE and OMVPE (organo-metallic vapour phase epitaxy). A further variation is MOCVD (metal organic chemical vapour deposition). The first two titles emphasise the crystallographic nature of the grown films, whereas MOCVD infers a cruder deposition technique which does not give ordered crystallographic films. The latter term can also be applied to depositing polycrystalline layers such as metal films from metal alkyl vapours.

MOVPE was first established as a crystal growth technique by Manasevit et al in 1968, during investigations upon the growth of GaAs upon insulators such as sapphire [7]. Over the years the technique has developed as a result of improvements in reactor design and starting chemicals, and established credibility in 1981 with the first of a now regular biennial series of conferences dedicated to the field. It is clear that the technique is well established due to the number of companies that are using it as a production process. Substitution of the hazardous hydrides with safer chemicals which are presently under investigation, will further enhance the long term life-span of the technique.

In contrast to liquid and conventional vapour phase epitaxy, MOVPE is a non equilibrium process whereby metered amounts of metal organic reactants such as trimethylindium and trimethylgallium, along with metered amounts of the hydrides arsine and phosphine are supplied to a heated reaction zone, whereby pyrolysis of the reactants occurs and epitaxial growth takes place. It is a hydrodynamic technique, and many aspects of the epitaxy are controlled by the conventional constraints of fluid dynamics.

Advantages of the technique include a robust, albeit complex stainless steel gas delivery system, with only the reaction chamber being constructed from quartz glass. High levels of epitaxial composition and thickness control have been demonstrated, along with low carrier concentrations and high mobilities. Many different devices

have been fabricated using the technique. The large number of commercial companies supplying chemical sources and complete reactors, has ensured a widespread and growing application of the technique to research, development and production rôles. The economic advantages of the technique centre around the ability to grow upon two inch wafers, with high levels of compositional uniformity, along with a high degree of flexibility of the apparatus, allowing different devices to be fabricated in consecutive growth runs. The use of a standard wafer size of two inches, allows established wafer handling and processing machines to be used for automated production, so lowering overheads. Growth rates are typically of the order of a few microns per hour, allowing thin quantum well layers and sharp interfaces to be achieved. The capabilities of MOVPE are catching up with MBE. The non equilibrium nature of the chemistry permits most combinations of materials to be grown upon each other.

There are several disadvantages of MOVPE, namely a significantly increased capital cost with respect to liquid phase epitaxy, along with the use of highly toxic gases. The latter subject is considered in a later chapter of this thesis, however it is worth noting that only highly trained people can operate the apparatus, and the machine integrity, extraction plant, and toxic gas monitoring apparatus, contribute to high overheads. In common with other vapour phase epitaxial techniques, pollution control and monitoring form a further part of the overall facility and raise costs.

Molecular Beam Epitaxy (MBE)

Molecular beam epitaxy is an entirely different type of growth technique [8]. A heated substrate is located in a high vacuum chamber and beams of atoms which are constituents of the epitaxial layer are directed towards the substrate. The method is ballistic rather than hydrodynamic, the incident beams are derived from elemental sources such as gallium and arsenic, the latter providing a source of As_2 and As_4 molecules. The beams are turned on and off using mechanical shutters. Growth proceeds according to the number of free atoms that stick to the growing surface. Advantages of the technique include a capability for very slow growth rates and consequently a high degree of low dimensional structure control. The technique is extensively

used in research laboratories and universities throughout the world to grow superlattices and novel materials. There are however several disadvantages, including high capital expense due to use of a large amount of high vacuum apparatus, and long down times when sources require replacement, or machines require cleaning, due to a need to expel all traces of water and oxygen prior to resuming growth. Excess deposits of arsenic are collected upon cryogenic panels. Phosphorus compounds are difficult to grow due to debilitating effects upon vacuum pumps, and the presence of large quantities of pyrophoric deposits upon opening machines for servicing and cleaning. MBE has however proved to be a valuable research tool and in some cases a production method for the fabrication of GaAs FETs.

Metal Organic Molecular Beam Epitaxy (MOMBE)

There is a variety of epitaxial growth methods which span the range from conventional atmospheric pressure and low pressure MOVPE through to MBE type growth according to the pressure used within the growth chamber. A hybrid technique is MOMBE [9], whereby metal-organic and group V hydride sources are fed to a high vacuum MBE chamber via high impedance orifices. The vacuum chamber is of a similar design to that used in MBE, although the reaction chemistry is different. The technique appears to eliminate many of the source problems encountered using MBE, and also allows phosphorus compounds to be grown. However the equipment is expensive, essentially combining the gas handling apparatus of an MOVPE reactor, with the high vacuum components of an MBE facility. The use of toxic hydrides also makes MOMBE unattractive, but many workers perceive it as the growth technique of the future.

Summary

The above introduction has attempted to provide a background setting of crystal growth techniques and components, through to systems concepts and engineering that have driven III/V component technology forward, and hence research and development into MOVPE of InP and (GaIn)(AsP) alloys. The following chapters of this thesis deal specifically with different aspects of the MOVPE growth technique.

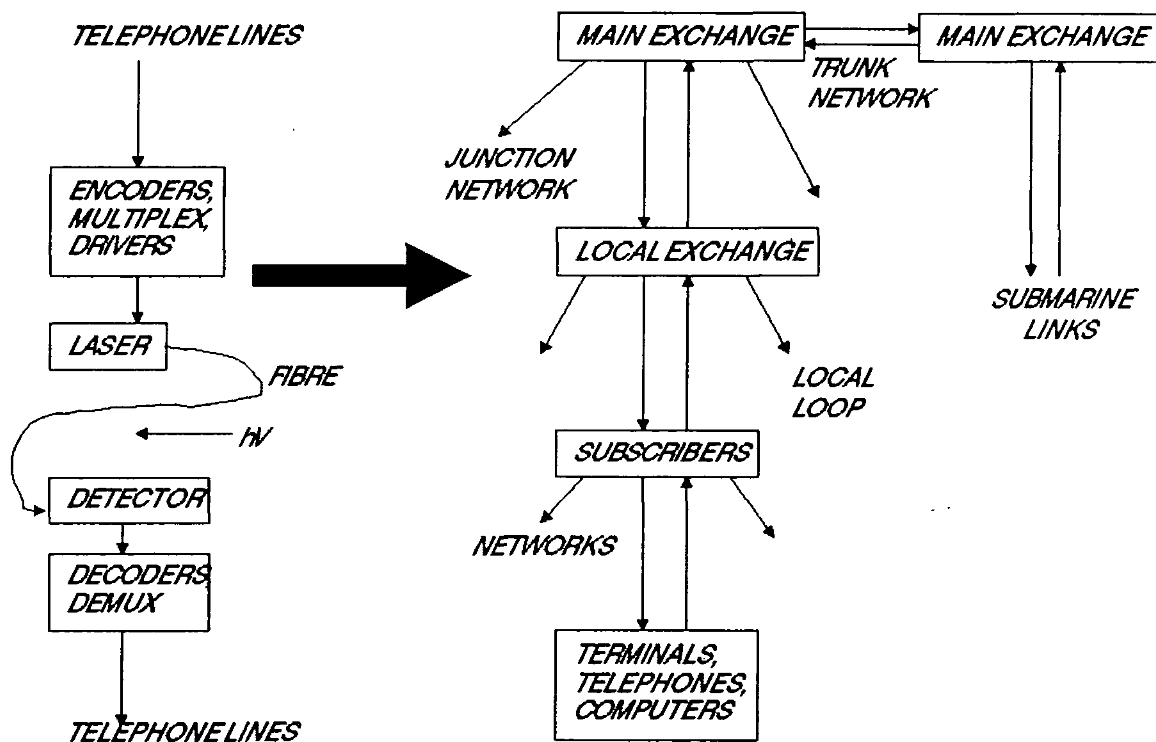

Figure (1.1): Summary of the layers of telecommunication systems and the rôle of optical and opto-electronic components.

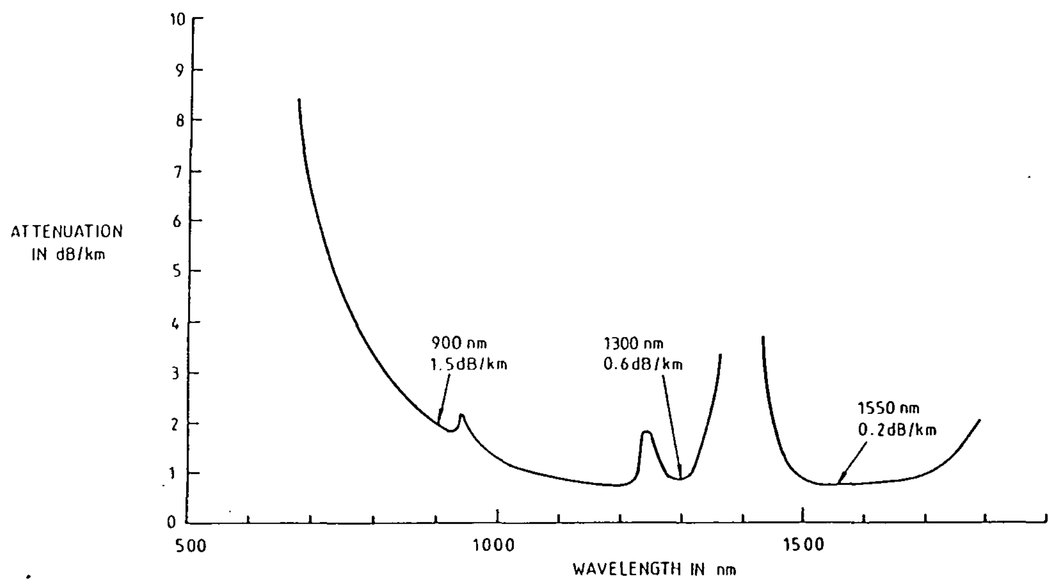

Figure (1.2): Attenuation as a function of optical wavelength in silica optical fibres, showing the low loss windows at 1.3μm and 1.55μm wavelength.

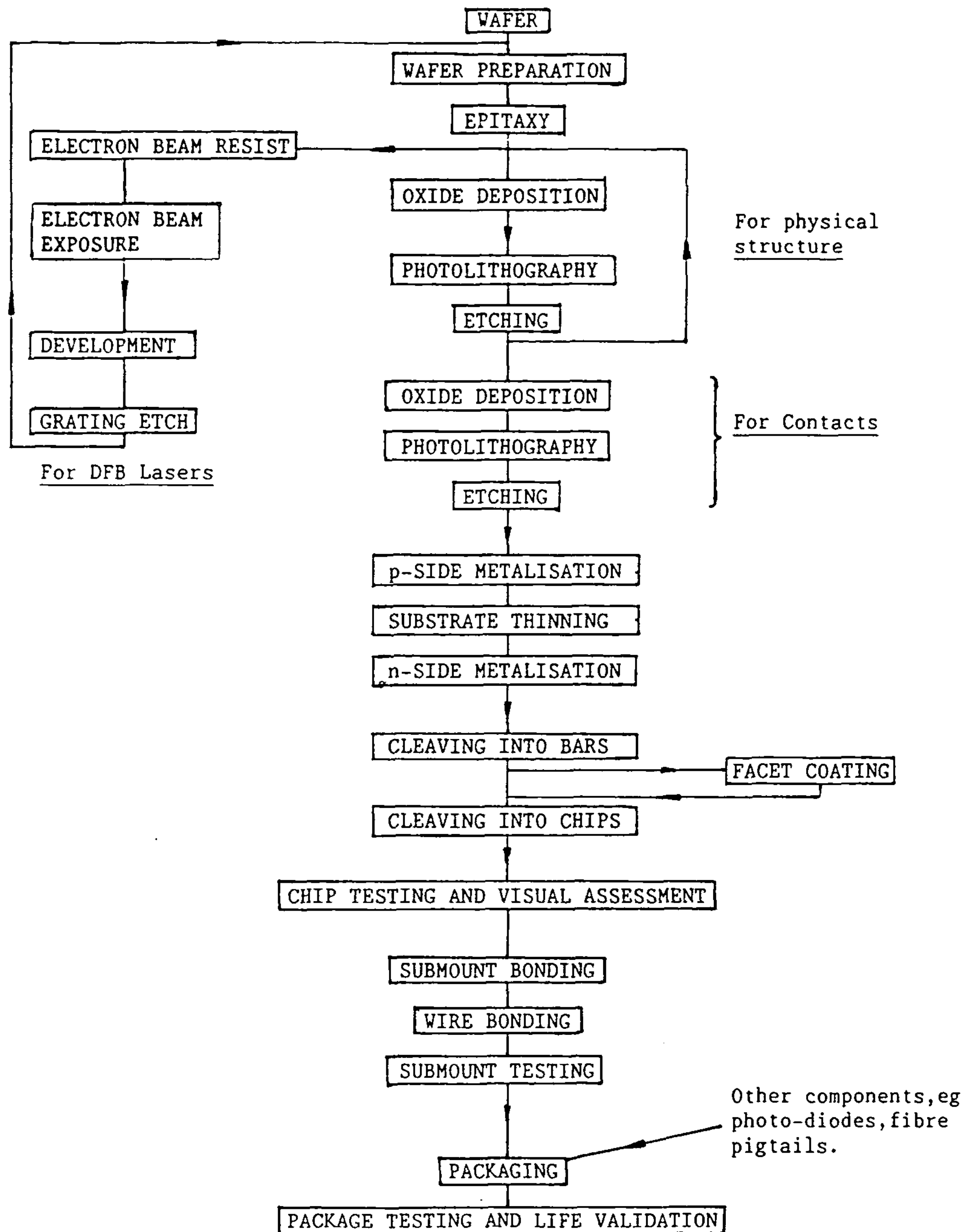

Figure (1.3): Semiconductor laser fabrication steps.

Chapter 2

MOVPE Chemistry

In this chapter the reaction mechanisms of MOVPE are discussed, the choice of the various source chemicals considered and the methods of preparation of the alkyl sources outlined.

Reaction Mechanism for MOVPE

MOVPE was originally proposed on the basis that the simple reaction of the type:

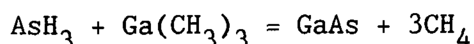

$$AsH_3 + Ga(CH_3)_3 = GaAs + 3CH_4$$

was possible. It is a non equilibrium process carried out at elevated temperatures of 550°C to greater than 1000°C. The upper temperature limit is partially based upon the temperature that the reaction vessel can withstand, the melting points of the crystal substrates, and the temperature at which the GaAs fails to be deposited and starts to evaporate or dissociates to Ga and As. Preferred growth temperatures tend to be around 650°C for InP and (GaIn)As based materials, and around 750°C for aluminium containing compounds. The growth rate of the compound always appears to be a linear function of the group III metal molecules arriving at the growth zone, and normally is independent of the excess of group V gases.

The exact reaction process, namely the order in which the hydrocarbon groups are removed from the metal alkyls, the rôle the hydrides play in the process and the position in the reactor where these processes take place is not well understood. Different reaction paths may exist for different starting materials and for different growth conditions. Whilst these areas are not understood, MOVPE has acquired the mark of maturity of being used as a production technique, but a more complete understanding will help to obtain better transport

properties and to exploit the different growth habits available, so advancing device design.

At a recent conference [10], a consensus emerged upon a probable reaction route. The hydride and metal-organic molecules once introduced into the hot reaction zone are heated in the gas stream and boundary layer above the susceptor by radiant heat. Some of the hydrocarbon groups may be removed from the metal-organic molecule whilst still in the gas stream, leaving a highly reactive metal-methyl radical to be adsorbed onto the surface of the hot substrate. The hydride reacts with the metal-methyl radical on the surface of the material, liberating an alkane and hydrogen. Both the group III and the group V atoms then accommodate themselves in appropriate positions in the semiconductor crystal lattice, forming an epitaxial layer.

Suitable reactions for InP may be:

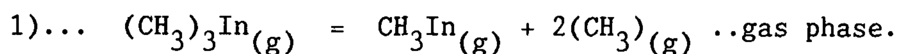

1)... $(CH_3)_3In_{(g)} \;=\; CH_3In_{(g)} + 2(CH_3)_{(g)}$ ..gas phase.

2)... Adsorption of $(CH_3)In$ onto the crystal surface

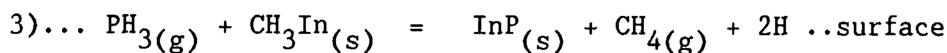

3)... $PH_{3(g)} + CH_3In_{(s)} \;=\; InP_{(s)} + CH_{4(g)} + 2H$ ..surface

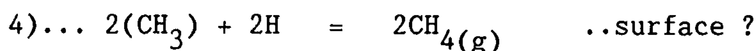

4)... $2(CH_3) + 2H \;=\; 2CH_{4(g)}$ ..surface ?

5)... $2H \;=\; H_{2(g)}$ ..excess hydrogen liberated from PH_3

The law of mass action applied overall to these reactions gives:

$$\frac{[(CH_3)_3In].[PH_3]}{[InP].[CH_4]^3} = \text{constant} \qquad (2.2)$$

Evidence for the above reaction mechanism has been compiled from a variety of sources. Stringfellow et al have undertaken optical absorption and time of flight mass spectrometry measurements upon hydride and metal-organic mixtures, and have determined that no reactions occur at room temperatures to form adducts [11]. This

indicates that the MOVPE reaction most likely takes place close to the hot epitaxial layer.

An excess of the group V species is always required to produce epitaxial material. This may be due to the fact that considerable amounts of arsenic and phosphorus are deposited onto the reactor walls wherever the quartz is cool enough to allow condensation. It is not clear if all the group V pyrolysis takes place close to the substrate, however the author has observed increased phosphorus deposits upon the quartz reactor tube if the substrate is present, or if an InP coated susceptor is used compared with using a new virgin susceptor.

A large amount of evidence indicates that the hydrogen released from the excess of the group V compounds has an important rôle to play in combining with the methyl or ethyl groups from the group III compounds to form alkanes. Failure to provide hydrogen such as when using arsenic vapour, or group V compounds where the hydrogen has been fully replaced by organic groups, appears to lead to carbon incorporation in the epitaxy [12,13].

Lum et al have identified carbon 13 (^{13}C) in GaAs layers grown using trimethylarsenic with labelled alkyl groups. Further, addition of ^{13}C labelled methane to the carrier gas did not result in ^{13}C being incorporated into the epitaxial layers [14]. This indicates that any carbon incorporation must occur prior to formation of the methane molecules and that methyl radicals must exist at the epitaxial surface.

The possibility of hydrogen from the carrier gas being involved in the reaction, is unlikely since epitaxial growth of good quality has been reported when using nitrogen and helium as carrier gases [15,16]. The fluid dynamic behaviour of the reactor was however modified. Deuterium has also been used as a carrier gas when studying MOVPE. Mass spectrometer analysis of reaction products has indicated that methane was still formed, but that neither ethane or CH_3D were detected [17].

Evidence that atomic hydrogen, liberated from the hydrides is present at the growing surface, is also provided by work upon hydrogen passivation of p-type InP detailed in the doping chapter of this thesis.

It is the author's opinion that MOVPE chemistry is predominantly

a surface reaction upon the epitaxial layer, and that the removal of the last hydrogen atoms from the group V compounds, and the alkyl groups from the group III compounds takes place simultaneously.

Metal-Organic Compounds

The choice of metal-organic compounds available to grow a specific material is usually limited. For gallium compounds, either trimethylgallium (TMGa) or triethylgallium (TEGa) have been successfully used, the major difference being the vapour pressures. Similarly trimethylaluminium (TMAl) and triethylaluminium (TEAl) are used for growing aluminium containing compounds. There is a tendency to avoid mixing ethyl and methyl compounds to avoid carbon group exchange reactions taking place en route to the reaction chamber, however evidence that this a real problem in modern reactors is not available.

The choice of indium precursor is more difficult, and the subject of continuing research. Originally only triethylindium (TEIn) was available as a pure indium precursor, and this material whilst a liquid at room temperature, has a low vapour pressure compared to trimethylgallium. To obtain epitaxial growth from this compound it is necessary either to supply very high flow rates through the bubbler, or to heat the source and subsequent pipework. It also tends to form an aerosol over the susceptor giving rise to dust and poor growth. When used at low pressure ($\simeq$ 76 torr), and when well purified, it can be used for the growth of high quality InP.

The group III metal alkyls and group V hydrides are respectively Lewis acids and Lewis bases and it is the formation of an adduct between the indium compounds and the hydrides, particularly arsine, that is believed to cause problems when mixed at atmospheric pressure. It is believed that the indium alkyls and the hydrides, after forming an adduct, then irreversibly polymerise to form a stable compound that no longer takes part in the epitaxy [18].

For atmospheric pressure growth, the preferred precursor is trimethylindium (TMIn). Whilst still having a low vapour pressure compared to trimethylgallium, by heating the source to around 50°C, reasonable flows of trimethylindium can be supplied to the reaction

chamber. It is more stable than triethylindium in the presence of hydrides at one atmosphere pressure, but still undergoes a reaction with arsine. This phenomenon has been seen on a variety of reactors including the author's [21], a brown deposit in the vent line where the group III and group V gases mixed, was chemically analysed and found to consist mainly of indium and arsenic. Whilst this does not appear to interfere to any major extent with the main high temperature reaction, it poses sufficient concern to avoid mixing of the group III and V compounds until just before the reaction chamber.

The major problem with the use of trimethylindium is that it is a solid at room temperature, and using it above the melting point of 87°C results in too high a vapour pressure and pipework has to be heated to high temperatures to avoid condensation. The solid is believed to be a polymeric tetramer but the vapour is monomeric [22]. The use of trimethylindium is dealt with in greater depth in a later chapter.

A method that has been used to avoid polymeric adduct formation is to deliberately adduct the Lewis acid indium alkyl with a stable group V Lewis base. Moss et al have successfully used trimethylindium-trimethylphosphorus and trimethylgallium-trimethylphosphorus adducts to grow InP and (GaIn)As of high quality [18]. The adduct has been formed either as an in-situ reaction product in the gas handling areas of an MOVPE reactor, or from a pre-formed adduct. The adduct, formed at room temperature, is returned to the original two compounds when raised to epitaxial growth temperatures. The base part of the adduct does not take part in the MOVPE reaction. Bass et al have also grown (GaIn)As by the adduct route using a pre-formed trimethylindium-trimethylamine adduct [23].

A further advantage of adducts is that since the electron affinity of the metal alkyl is satisfied by the presence of the group V compound, the adduct is more stable than the pyrophoric metal organic compounds. This in turn eases handling and purification. Many of the adduct sources are liquids at room temperature.

An alternative to the above indium precursors is dimethylethylindium. This is a liquid at room temperature and has an

acceptable vapour pressure. However recent studies at Queen Mary College, London, have revealed that the compound undergoes carbon group exchange reactions resulting in a mixture of trimethylindium, dimethylethylindium, diethylmethylindium and triethylindium [24]. If used as an MOVPE precursor, the most volatile compound would evaporate more quickly than the least volatile, causing the overall mole fraction of indium compound reaching the growth chamber to vary through the life of the source. This is unacceptable for alloy growth, however Fry et al have used this material successfully to grow InP and (GaIn)As of reasonable quality and claim from mass spectrometer studies that only one indium compound is present [25].

Table (2.1) summarises data upon commonly used metal-organic compounds.

Group V Precursors

Other new materials being developed are the alternative alkyl precursors to arsine and phosphine. The impetus for this work is mainly based upon safety and a desire to avoid the use of high pressure toxic gases. Toxic limit values for arsine and phosphine are 0.05 and 0.3 ppm respectively. Some successful work has been achieved with the growth of InP and GaAs but problems remain with the cost of materials and with carbon incorporation. However local resident resistance and new legislation in the U.S.A. is forcing companies to look carefully at developments in this field.

A further problem with arsine and phosphine is the disparate cracking rates of the two gases at 650°C [26]. The extent of this problem will become clear later, but it is an additional drive towards finding arsenic and phosphorus compounds that have more equal cracking rates. The use of higher order, and less stable compounds of phosphorus, eg. P_2H_4 has been considered but has met with low enthusiasm from manufacturers since these compounds have an even higher level of toxicity.

Lum has reported the growth of GaAs using arsine, trimethylarsenic, triethylarsenic, diethylarsine and tertiarybutylarsine (t-Bu-AsH_2) [14]. In general it was found that the more hydrogen bonded directly to the arsenic atoms, the better the epitaxy in terms of morphology, luminescence and low carrier concentration. Many of the layers were carbon contaminated from the alkyl radicals, such as CH_3 from the trimethylarsenic. Unfortunately the toxicity of the compounds is also believed to increase with more hydrogen bonded to the arsenic, however the toxicity of tertiarybutylarsine is still believed to be lower than that of arsine, and it is also used as a liquid at atmospheric pressure rather than as a high pressure gas.

Growth from a pure arsenic vapour source has yielded poor epitaxy and high levels of carbon incorporation [12].

Attempts to use trimethylphosphorus and triethylphosphorus as starting materials failed due to the stability of these compounds. Indeed high quality (GaIn)As has been grown using the trimethylindium-trimethylphosphorus adduct implying that the triethylphosphorus remains unpyrolysed [18]. Liquid group V sources that have given good epitaxial growth include diethylarsine [27], tertiarybutylphosphine and isobutyl-phosphine [28]. Chen et al have reported the growth of high quality InP using tertiarybutylphosphine at 600°C when using a V/III ratio of as low as 3:1 [29]. During the pyrolysis of each of these compounds, hydrogen is released which has been bonded directly to the group V atoms.

An interesting alternative to using phosphine, is to use red phosphorus evaporated from a furnace in a hydrogen gas flow. Naitoh et al have shown that InP free of carbon contamination can be grown using this method [13]. Phosphine is produced by passing the phosphorus-hydrogen mixture through a hydrogen plasma generated by microwaves. When using this process without the plasma, carbon contamination was found to occur.

Preparation of Metal-Organic Compounds

Metal organic compounds have been available for a considerable time. Trimethylaluminium for example was first prepared in 1865 [22], however it is only during the latter half of this century that large quantities of the materials have become available. One of the main starting routes for the compounds is from trimethylaluminium, which is used in large quantities as a catalyst in the manufacture of polymers. There are several methods of preparing the various compounds, a simple route being to heat the metallic metal with dimethylmercury:

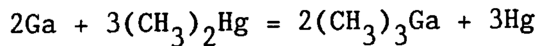

$$2Ga + 3(CH_3)_2Hg = 2(CH_3)_3Ga + 3Hg$$

Dimethylmercury in turn is readily synthesised via reaction with alkyl halides. Trimethylaluminium can be synthesised by the exothermic reaction of aluminium with an alkyl halide to give a sesquihalide which in turn is reduced to the aluminium alkyl by reaction with an alkali metal:

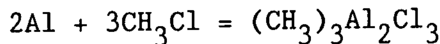

$$2Al + 3CH_3Cl = (CH_3)_3Al_2Cl_3$$

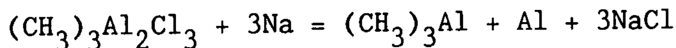

$$(CH_3)_3Al_2Cl_3 + 3Na = (CH_3)_3Al + Al + 3NaCl$$

Another route for metal-organic preparation is to use Grignard reagents, magnesium compounds formed readily by the reaction of magnesium with an alkyl halide. The Grignard reagent is reacted with indiumtrichloride in ether:

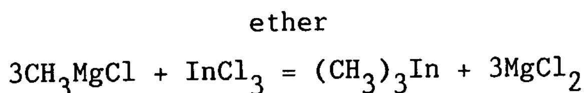

$$3CH_3MgCl + InCl_3 \overset{\text{ether}}{=} (CH_3)_3In + 3MgCl_2$$

A third route is to react the metal chloride with methyl lithium in ether:

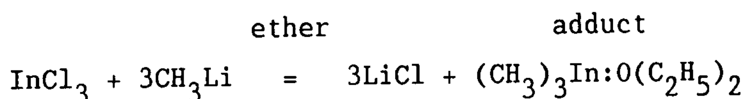

$$InCl_3 + 3CH_3Li \overset{\text{ether}}{=} 3LiCl + \overset{\text{adduct}}{(CH_3)_3In{:}O(C_2H_5)_2}$$

The very high purity precursors required for MOVPE, place stringent demands upon the preparation routes for the metal alkyls. To

obtain doping levels of 10^{14} cm^{-3} for example, it is necessary to purify source materials to part per billion levels of compounds that can be easily incorporated during epitaxy. It is necessary to remove obvious dopants such as zinc and silicon, deep level dopants such as transition elements and oxygen, and also to remove organic contaminants which may catalyse undesirable reactions such as between trimethylindium and arsine at room temperature [30].

The methyl lithium preparation route has been shown to be good for removal of transition elements. Distillation of the etherate removes non volatile impurities. For trimethylindium, a further purification step has been used to reduce zinc, cadmium and silicon to very low concentrations.

This process, called the "diphos" process uses the Lewis acid-Lewis base adduct of trimethylindium with the compound 1,2 bis(diphenyl phosphino) ethane ("diphos") [30]. Benzene is added to the etherate along with diphos. The volatile ether group is displaced, and a new 2:1 adduct is formed between the trimethylindium and the diphos:

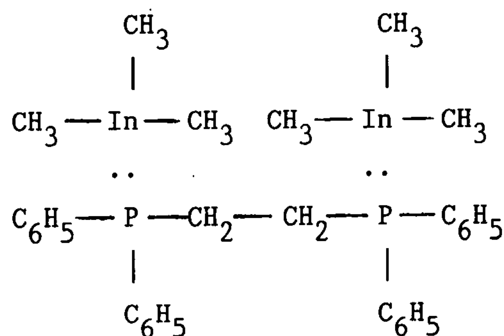

Zinc, cadmium and hydrogen selenide do not form diphos adducts and so are eliminated at this stage. Silicon contamination of sources is heavily reduced using this purification technique.

Once synthesised, the metal-organic materials are transferred to stainless steel all-welded bubblers. The bubblers are cleaned, etched and chemically passivated, and finally leak tested before use. These sources are then suitable for surface shipment, storage and can be directly and quickly plumbed onto MOVPE reactors. Whilst the liquid

compounds can be decanted into the bubblers under oxygen and water free conditions, trimethylindium has either to be shovelled or recrystallised into place by subliming the vapour into a cooled bubbler. The former method, though easier, tends to give more contaminated material due to exposure to trace gases in the dry-box.

Table (2.1) Properties of metal-organic compounds:

Compound	Melting Point °C	Boiling Point °C	Association	Reaction in air	Reaction in water	Vapour Pressure Eqn (mm Hg)
$(C_2H_5)_3In$	-32	184	Monomeric	Pyrophoric	Hydrolysis	
$(CH_3)_3In$	88	135	Monomeric in vapour	Pyrophoric	Explosive hydrolysis	$Log_{10}P=11.2-3261/T(K)$
$(C_2H_5)_3Ga$	-82.3	143	Monomeric	Pyrophoric	Violent hydrolysis	$Log_{10}P=8.224-222/T(K)$
$(CH_3)_3Ga$	-15.8	92	Monomeric	Pyrophoric	Violent hydrolysis	$Log_{10}P=8.07-1703/T(K)$
$(C_2H_5)_3Al$	-52.5	185.6	Unstable dimer	Pyrophoric	?	$Log_{10}P=10.78-3625/T(K)$
$(CH_3)_3Al$	15	126	Dimeric vapour	Pyrophoric	Explosive hydrolysis	$Log_{10}P=7.315-1534/(T-53)$
$(CH_3)_2Zn$	-29.2	44	Monomeric	Pyrophoric		$Log_{10}P=7.802-1560/T(K)$
$(CH_3)_2Cd$	-2.4	105.5	Monomeric	Pyrophoric		$Log_{10}P=7.764-1850/T(K)$
$(C_5H_5)_2Fe$	173	249	Monomeric	Stable	Stable	$Log_{10}P=28.17-4581/T(K)-6.04Log_{10}T$

Chapter 3

InP Epitaxy

In this chapter we will first consider the crystal structure of InP and other III/V semiconductor compounds, then the various regimes of crystal growth, and finally report upon the effect of changing the growth conditions on the epitaxial layer properties.

Crystal Structure of InP

The crystal structure of InP consists of two intersecting crystal networks of face centred cubic atoms, one network consisting of indium atoms and the other of phosphorus, displaced by a quarter of the body diagonal.

The lattice parameter of InP is 5.8688Å and the band gap energy is 1.35eV. Further data upon InP and other III/V semiconductor materials are available from the paper by Adachi et al [31].

The planes of easiest cleavage of the material are the {110} type and it is these planes that are used as cleavage planes when fabricating devices.

Closer consideration of the crystal structure of the material shows that the {111} type planes can consist of a surface layer of either indium atoms bonded to the adjacent structure by 3 bonds or conversely phosphorus atoms bonded by three bonds. One remaining bond is left dangling in each case. Careful selection of chemical etches can allow material to be removed with the etching stopping at the appropriate {111} face, so allowing 'v' grooves and dovetails to be etched in {100} surfaces.

Epitaxial Crystal Growth

The model often used to simulate the epitaxial growth upon a substrate is to consider a surface with defects or an atomic step present. Atoms or molecules containing indium and phosphorus arrive at

the surface during growth and move over the surface, sometimes evaporating again until they find an energetically favourable site upon which to settle. This usually means a position where the largest number of atomic bonds can be satisfied. Once a few atoms have successfully bonded into position, further atoms will prefer to bond alongside the first arrivals to maximise the number of satisfied bonds. In this way the crystal growth tends to spread sideways and can be seen to be largely two dimensional, each individual crystal plane being completed before growth on the next plane is energetically favourable to the influx of atoms. Failure to provide adequate surface mobility for the reactants leads to three dimensional growth and the formation of hillocks and inclusion of crystal defects in the epitaxy.

The surface mobility may be enhanced by increasing the growth temperature, i.e. the velocity of the reactants over the surface of the material, decreasing the pressure in the reactor, i.e. increasing the mean free path, and possibly by modifying the chemistry of the surface reactions. It has been found that hillock formation is certainly enhanced at low growth temperatures, and that at a low growth temperature the morphology of InP grown using trimethylindium is inferior to that grown using triethylindium [32].

The likelihood of introducing three dimensional growth is enhanced if too many atoms are trying to coalesce upon the surface at the same time and for this reason it is important to ensure that growth rate effects are carefully studied and that the growth rate is not too high.

It is interesting to compare the growth upon {100} and {111} faces. The following photograph (figure 3.1) illustrates that if a {111} face is introduced into the growth environment, this forms the slowest growth plane, giving rise to pyramidal and triangular features nearby. This can be explained by the {111} faces having only one free bond available, and alternate layers of indium and phosphorus being required to build up the crystal structure. This is an energetically less favourable occurrence than crystal growth on the {100} planes.

The technique of atomic layer epitaxy that has been promoted in recent years is worth considering here. The technique, whether applied via MBE, VPE or MOVPE consists of allowing the group V atoms to arrive

at the crystal surface, followed by the arrival of group III atoms in separate rapidly repeating pulses of gas. It is hoped that this technique will allow precise atomic control of epitaxial layers to be achieved, though the practical realisation of this technique has yet to be attained.

Substrates

Substrates of InP are usually sawn from ingots of the material grown by the liquid encapsulated Czochralski method under a high partial pressure of phosphorus. Substrates are available with dislocation densities of less than 1000 cm^{-3} for sulphur doped material. Whilst this dislocation density is high compared to silicon wafers, it ensures fairly high discrete device yields since the active layer of many devices constitutes only a small part of the total chip area. Iron doped substrates with higher dislocation densities are used for structures that require an insulating substrate.

The substrates are subsequently polished to a thickness of 300-350μm using an abrasive method along with a bromine methanol etch. The final orientation of the substrates is determined by the customer, but most workers are tending to use substrates with (100) orientation surfaces. This aids advanced device fabrication. Also the morphology of the epilayers grown upon this orientation appears to be of a higher specular quality than epilayers grown on 2° off (100) substrates. The latter is the preferred substrate orientation for epitaxial growth of GaAs.

Substrate Preparation

Prior to loading in an MOVPE reactor, substrates are usually cleaned by one method or another. Several techniques exist, and in some cases the chemistry is obscure. The wafers are usually unpacked from the suppliers' containers, and then degreased using a solvent clean of 1,1,1,trichloroethane and also, perhaps, a fluorinated hydrocarbon. If surface damage resulting from the polishing process is not of major concern, then a soak in nitric acid, forming a surface oxide layer, followed by oxide removal using buffered hydrofluoric acid can be used. This is similar to the process used for preparing

silicon wafers prior to processing. The use of a weak solution of bromine in methanol is often used to remove the top surface of the InP and therefore the polishing damage. The etching mechanism of this process is not known. For GaAs, nitric acid can not be used since it dissolves the wafer rapidly (hydrochloric acid similarly dissolves InP rapidly). The normal cleaning process used is a $H_2SO_4:H_2O_2:H_2O$ mixture to etch the surface. This etch has also been used to etch the surface of InP successfully. Following etching, rinsing in de-ionised water followed by blow drying or spinning in iso-propyl-alchohol completes the preparation. The wafers are then rapidly transferred to the growth chamber where they are retained under a hydrogen ambient prior to growth.

Another method of preparing substrates prior to epitaxy is to load the wafers into the reaction chamber and use a flux of hydrogen chloride gas to etch the wafers in-situ. Whilst this uses the versatility of the vapour transport system and reduces the likelihood of oxide formation compared with processes that use wet etching; the added complexity of hydrogen chloride in a steel gas system has so far resulted in it not being universally used. Ethylenedibromide may be a suitable alternative for in-situ wafer preparation [33].

InP Growth Conditions

The usual growth conditions for InP used by the author are fairly standard with a growth temperature of around 650°C. A trimethylindium molar flow rate of $2.5.10^{-5}$ mol.min^{-1} and a phosphine molar flow rate of $1.3.10^{-3}$ mol.min^{-1} has generally yielded epitaxial InP with specular morphology. These flow rates correspond to a V/III ratio of 50 and a growth rate of about 4μm hour^{-1}. The ability to vary reactor pressure was not available for early experiments. The variation of growth of InP with reactor pressure has been studied by Clawson [34]. He showed that increasing the reactor pressure lowered the growth rate and also lowered the background doping level. Further, the growth rate was seen to be inversely proportional to the input gas velocity, and inversely proportional to the substrate area used. Whilst there is certainly a growth rate dependence upon the size of substrate used, it is the author's experience that it does not have such a strong dependence as Clawson has stated.

Background Doping of InP

The electron mobility of InP is directly related to the background carrier concentration, and a large amount of work was undertaken to reduce this to a minimum level in an uncompensated form [35].

The trimethylindium used had been purified via thermal dissociation of the recrystallised trimethylindium-1,2-bis(diphenyl phosphino)ethane ("diphos") adduct as described in chapter (2).

Prior to optimising the growth conditions, InP epitaxial layers with carrier concentrations in the range $1\text{-}2\times10^{15}$ cm^{-3} were achieved. Comparison of the 77K mobility of this material with the best reported values [36], and the theoretical data of Walukiewicz et al [37], indicated that the material was not heavily compensated. Accordingly it was reasoned that it would be sufficient to establish the growth conditions necessary to produce material with the smallest possible carrier concentration and that this could be achieved very rapidly by the growth of appropriate stepped layer structures.

Epilayers were routinely assessed using the Polaron PN4200 electrochemical carrier concentration profiler. During the growth of a single epilayer, the growth conditions were varied at intervals to produce a series of steps in the carrier concentration profile. These steps were then measured using the PN4200. This enabled the effect of varying one of the growth parameters, such as growth temperature, to be measured with a single growth run and a single measurement. This minimised any uncertainties due to operating parameters which could not be controlled. For example it had been suggested that common contaminants of trimethylindium tend to be relatively volatile so the degree of contamination of a trimethylindium source would decrease with use. The greatest source of uncertainty in the carrier concentration profile measurements arises from the difficulty in exactly defining the area of the Schottky contact, and the slightly smaller area etched for n-type material [38]. By using single epilayer, stepped structures, any uncertainty due to irreproducibility between successive measurements was eliminated. To minimise

uncertainties due to the difference between the contacted and the etched areas, the growth parameters were varied in such a way that the carrier concentration increased with profile depth.

Variation of InP Background Doping Level with Growth Conditions

Figures (3.2) and (3.3) show the carrier concentration profile and SIMS profile for silicon for a structure in which the growth temperature was stepped while the gas flow rates were held constant. Because the SIMS apparatus used for this study was used routinely to profile silicon semiconductor structures, the background count rate was high for this element, equivalent to a concentration of approximately 10^{15} cm^{-3}. However, if this is taken into account there is a close correspondence between the silicon concentration profile and the measured carrier concentration profile. SIMS profiles of selenium and sulphur were also examined as other possible donor impurities. No selenium was detected and the sulphur count showed no variation with growth temperature and was slightly lower for the epilayer than for the iron doped substrate. The concentration of silicon or of free carriers increases with increasing growth temperature. The behaviour appeared to follow an Arrhenius law, the apparent activation energy being ≃ 2.2 eV.

Figures (3.4) and (3.5) show the carrier concentration and SIMS silicon profile for a structure in which the growth temperature and V/III ratio were held constant and the growth rate increased by increasing the group V hydride and group III alkyl flow rates. In fact the growth rate is controlled by the trimethylindium flow and increases in proportion to the flow rate. Thus at each step the flow rates were increased and the growth time decreased. The carrier concentration decreased with increasing growth rate and again the silicon concentration appeared to decrease although the smaller steps were difficult to resolve by SIMS. To within the limits of experimental accuracy, the carrier concentration varied in inverse proportion to the growth rate. This indicates that the silicon which was incorporated into the InP during these growth experiments did not originate from contamination of either the trimethylindium or phosphine sources, unless the incorporation rate is affected by the

growth rate.

Figure (3.6) shows the carrier concentration profile for a structure in which the growth temperature and trimethylindium flow rates were held constant and the phosphine flow rate was varied. While the phosphine flow rate was adjusted between each step the growth was interrupted for 5 minutes by switching the trimethylindium flow to vent. The measured carrier concentration was found to be independent of the V/III ratio but interrupting the growth resulted in a small increase in carrier concentration in the vicinity of each interface. Figure (3.7) shows the SIMS silicon profile for the same structure to a depth of ≃ 8μm. An increase in the silicon count was observed corresponding to the outermost and largest increase in the carrier concentration but the increase at the second pause, resolved in the carrier concentration profile, could not be detected in the SIMS profile. Other authors [39,40], have also reported that the InP carrier concentration is independent of V/III ratio using trimethylindium and phosphine, however for triethylindium and phosphine the InP carrier level has been shown to decrease with increasing V/III ratio [41].

Interface Carrier Concentration Spikes

Figure (3.8) shows a carrier concentration profile for a thick layer of InP grown under the optimum conditions. The carrier concentration is constant through the bulk of the epilayer but shows a spike at the interface to the iron-doped substrate. Routine carrier concentration profiles were performed on the InP growths and an interfacial carrier concentration spike was almost always found, although the total number of carriers within the spike was very variable. As a general trend it was found that the height of the spike increased with growth temperature so it always remained greater than the background carrier concentration. A similar phenomenon has been reported by Bass and co-workers [39,42]. It was also observed that the SIMS profiles always revealed a spike in the silicon concentration at the interface to the substrate. Such spikes may be observed in the SIMS profiles of figures (3.3) and (3.5). Huber et al reported a similar silicon spike in the SIMS profile for InP grown by MOVPE [43].

The spike was observed not only at the interface to the substrate, where other contaminants were found, but also at the interface created by stopping epitaxial growth, removing the specimen from the reactor and then replacing it and continuing growth. Silicon was in fact the only impurity reported to have been found at this interface. It is likely that silicon is responsible for the carrier concentration "spikes" which we observed on interrupting growth (figure 3.6), although the correlation between the SIMS and carrier concentration profiles is insufficient to establish this conclusively. It has been observed that the presence of this spike is mainly a function of substrate cleaning and not substrate orientation or substrate dopant [43].

Source of Background Doping

The previous experiments have established that silicon is the major background impurity which, acting as a donor, controls the electrical carrier concentration. The carrier concentration exhibits an Arrhenius relationship to the growth temperature, is independent of V/III ratio and varies in inverse proportion to the growth rate. Spikes are observed in the carrier concentration when the growth is paused or at the interface to the substrate and it is inferred that these are due to the increase in the silicon concentration in these regions.

Silane is widely used as a source of n-type dopant for MOVPE GaAs and (GaAl)As and its doping characteristics are well known. Bass [44] showed that for a constant silane flow the resultant electron concentration was related to the growth temperature by an Arrhenius law. He also observed that if silane was allowed to flow over the substrates prior to growth (i.e. at the growth temperature in the absence of organo-metallics) this gave rise to a spike in the carrier concentration at the substrate epilayer interface. The spike persisted even after prolonged flushing following an initial exposure to silane, indicating that the silicon becomes very strongly bound to the surface. Veuhoff et al [45], noted that for a constant flux of either silane or disilane the carrier concentration varied in inverse proportion to the growth rate. They proposed a model for silicon

doping in which the rate determining step is the decomposition of silane to form an adsorbed species. This model was later extended to the case of unintentional doping by a silicon-containing impurity [46]. The model predicts that the concentration of silicon incorporated into the epilayer at constant total pressure, is proportional to the gas phase concentration of the silicon-containing species multiplied by a Boltzmann factor and inversely proportional to the growth rate. In this case the predictions are:

$$[Si]_{InP} \propto \frac{[Si]_g \, e^{-E_a/kt}}{GR} \qquad (3.1)$$

Where: $[Si]_{InP}$ = the concentration of silicon in the epilayer.
$[Si]g$ = concentration of gaseous silicon species.
GR = growth rate.

For the STL observations to be consistent with the predictions of this model, the gas phase concentration of the silicon-containing species needed to remain constant when the trimethylindium and phosphine flow rates were changed. It was also seen that silicon appeared to accumulate in the absence of any trimethylindium flow. This suggests that the source of the silicon contamination must be the MOVPE reactor. If so, the likely origin of the silicon was the reduction of the quartz-ware in the reactor cell.
Although the walls of the reactor vessel are cooled, the susceptor is mounted on a silica boat and the parts close to the susceptor are radiantly heated to a similar temperature to the substrates. The most likely mechanism by which silicon is transported is

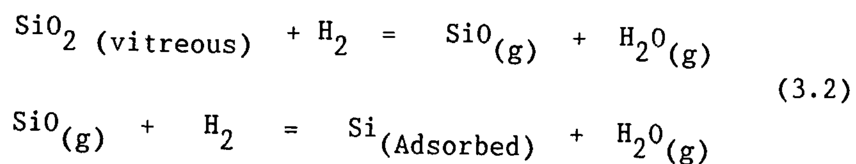

$$SiO_{2\ (vitreous)} + H_2 = SiO_{(g)} + H_2O_{(g)}$$
$$SiO_{(g)} + H_2 = Si_{(Adsorbed)} + H_2O_{(g)} \qquad (3.2)$$

Silicon contamination by reduction of quartz vessels has been shown to take place in LPE [47], and the above mechanism of gas transport was proposed by Weiner [48]. The reduction will be suppressed by the presence of water (or oxygen which will react to

form water) in the gas phase mixture [47].

The apparent activation energy from the Arrhenius plot was 2.2eV. By comparison a value of 1.5eV has been reported for silicon doping from silane [45]. An experimental value of 2.9eV was reported for silicon contamination due to reduction of quartz [47], although in this case it was thought that thermodynamic equilibrium had not been achieved. A second trimethylindium source from Sumitomo was also examined. Qualitatively this showed very similar doping levels and characteristics, however the fit to an Arrhenius plot and the linear dependence of carrier concentration with the reciprocal of the growth rate were markedly inferior to those achieved with the purified trimethylindium source. Using the Sumitomo source the best mobility at 77K for optimum growth conditions of single epilayers was 75,000 $cm^2V^{-1}s^{-1}$. It appeared that the Sumitomo source contained a small concentration of impurities, giving rise to both donor and acceptor levels.

Single Epilayer Mobilities

These experiments suggest that the lowest carrier concentrations may be achieved using the lowest practicable growth temperature and the largest growth rate. A large V/III ratio may be employed to optimise the morphology, since decreased growth temperature and increased growth rate both tend to impair morphology. It was found that the highest purity material could be grown at 600°C with a hydrogen flow through the trimethylindium bubbler of 60 cm^3min^{-1} and 300 cm^3min^{-1} of 10% phosphine. This gave a V/III ratio of 25:1. To achieve satisfactory morphology under these conditions it was necessary to place the substrates towards the back (i.e. downstream) position on the susceptor. It was found that a small increase in growth temperature (to 605°C) could be compensated for by an increase in growth rate to achieve a similar mobility.

A number of authors have reported MOVPE growth of InP with 77K mobility > 100,000 $cm^2\ V^{-1}\ s^{-1}$ [49,50,51,52]. These results are comparable to, or better than the highest reported purity for LPE or chloride and hydride VPE. It appears that these results have been achieved as a result of improvements in the purity of the group III

alkyl sources.

The epilayers, grown to a thickness of 8-10μm, were routinely examined by making Van der Pauw Hall effect measurements at room temperature and 77K. Large area specimens were used, ≃ 1 cm square, with small indium contacts made at each corner. Figure (3.8) shows the carrier concentration profile of a layer grown under the optimum conditions described. The bulk carrier concentration and mobility measured at room temperature were $n=3.3.10^{14}cm^{-3}$, $\mu=5160cm^2v^{-1}s^{-1}$ and at 77K, $n=3.0.10^{14}cm^{-3}$, $\mu=119,000cm^2v^{-1}s^{-1}$. It seemed likely that the carrier concentration spike at the interface to the substrate would impair the results, so a chemical etch was used to remove portions of the epilayer. The sample was then remeasured, and the carrier concentration and mobility of the material removed was calculated. These values are shown in figure (3.8). The mobility appears to increase slightly towards the epilayer surface. The best mobility values are slightly better than those calculated by Walukiewicz et al for uncompensated material [37]; an observation also reported by other authors [52]. The optical quality of this material is also extremely good as shown by the presence of the free exciton and two neutral donor-bound exciton (D°,X) peaks in the photoluminescence spectra of figure (3.9). A sample of this high purity material was sent to the University of Illinois for magneto photoluminescence and photothermal ionisation spectroscopy measurements. The results indicated that the residual remaining donor was silicon.

More recent work on a low pressure MOVPE reactor at STL, also using the diphos purified trimethylindium as the indium source, has yielded material with 77K electron mobilities of up to 300,000 $cm^2V^{-1}s^{-1}$, and a peak electron mobility of 400,000 $cm^2V^{-1}s^{-1}$ at 45K [32,53]. The use of a low growth pressure of 150 torr, and a high phosphine flux compared to that available in the author's reactor, allowed the growth temperature to be reduced to 570°C. The low carrier levels obtained were presumably the result of low silicon incorporation at this low growth temperature.

To obtain such material it has been necessary to remove all traces of the interface spike of donor carrier concentration as shown in the sample of figure (3.8). This interface spike has proved difficult to eradicate consistently, but one InP growth run undertaken

using substrates cleaned via a number of processes has indicated that a likely source of the impurities is the bromine-methanol etch, since substrates cleaned either without this etch, or ones which have subsequently been exposed to a 5:1:1 $H_2SO_4:H_2O_2:H_2O$ etch have not shown this spike.

It is interesting to note that silicon is an amphoteric dopant in III/V semiconductors. Whilst high purity InP is always n-type, GaAs epilayers can be grown either n or p-type corresponding to high or low arsine fluxes into the reactor chamber respectively. It is not clear whether for GaAs the change in doping is due to the silicon appearing on an arsenic site or gallium site, or if it is due to other dopants such as carbon or is due to variations in stochiometry relating to the arsine flow into the reactor. A higher arsenic vacancy density will occur for low arsine flows and a higher gallium vacancy density will occur for high arsine flows. InP and GaAs further differ in the relative amount of silicon incorporated into the material for the same flux of silane introduced into the reactor.

B337

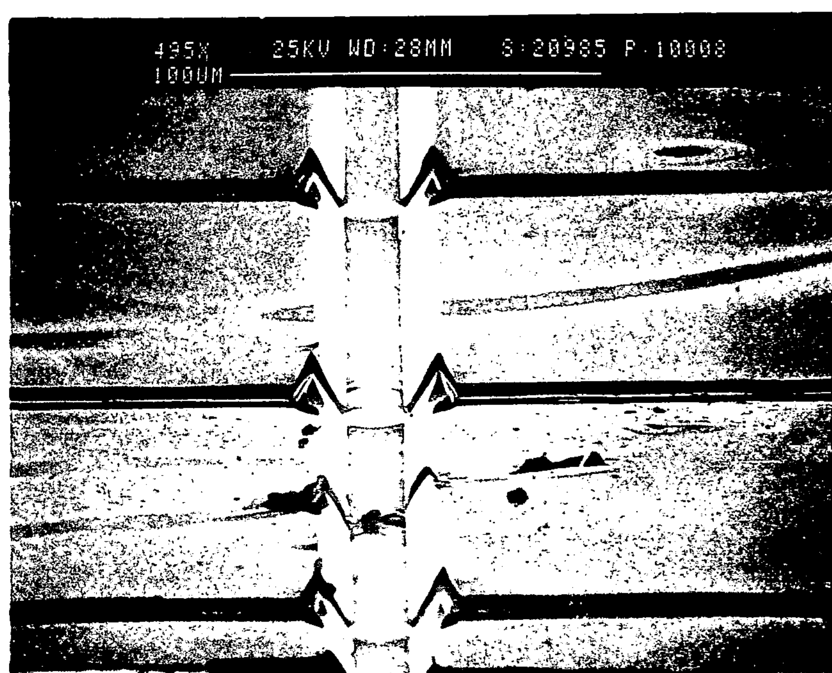

Figure (3.1): Scanning electron microscope image of non planar InP growth on a channelled substrate of InP. The slow growing {111} planes give rise to triangular and pyramidal type features at the edge of the {110} channels.

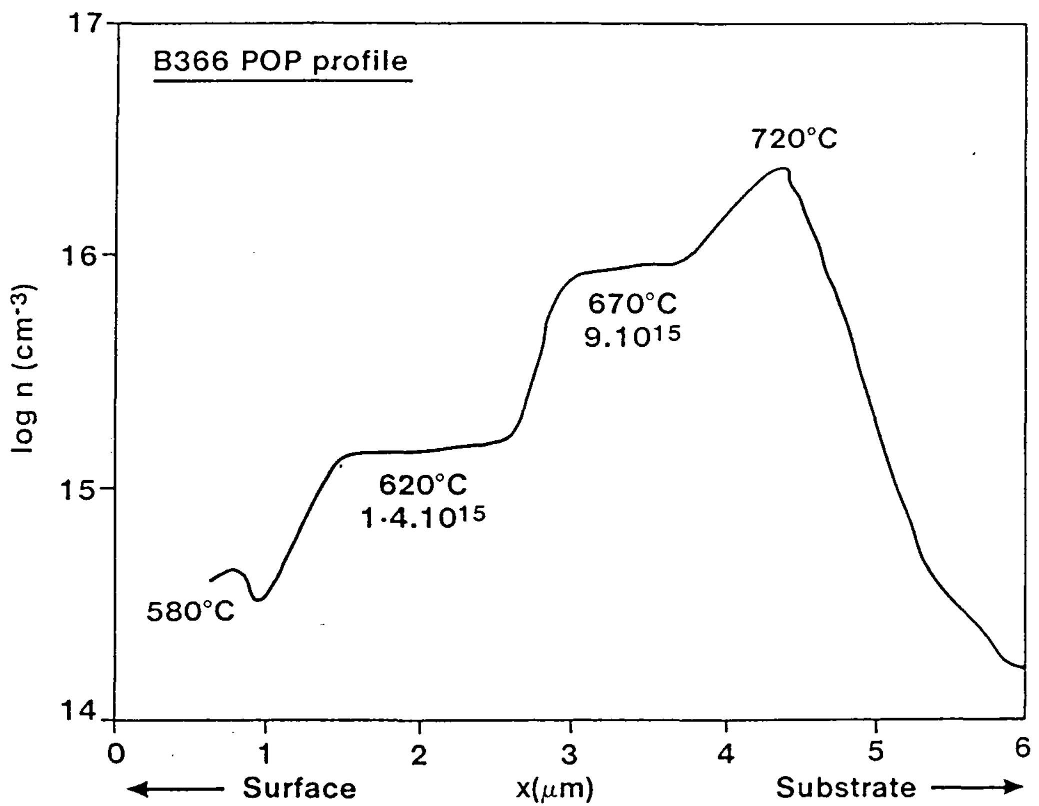

Figure (3.2): Electrochemical profile through undoped InP showing the variation in background doping as a function of growth temperature, for four InP layers grown consecutively at 720°C, 670°C, 620°C and 580°C.

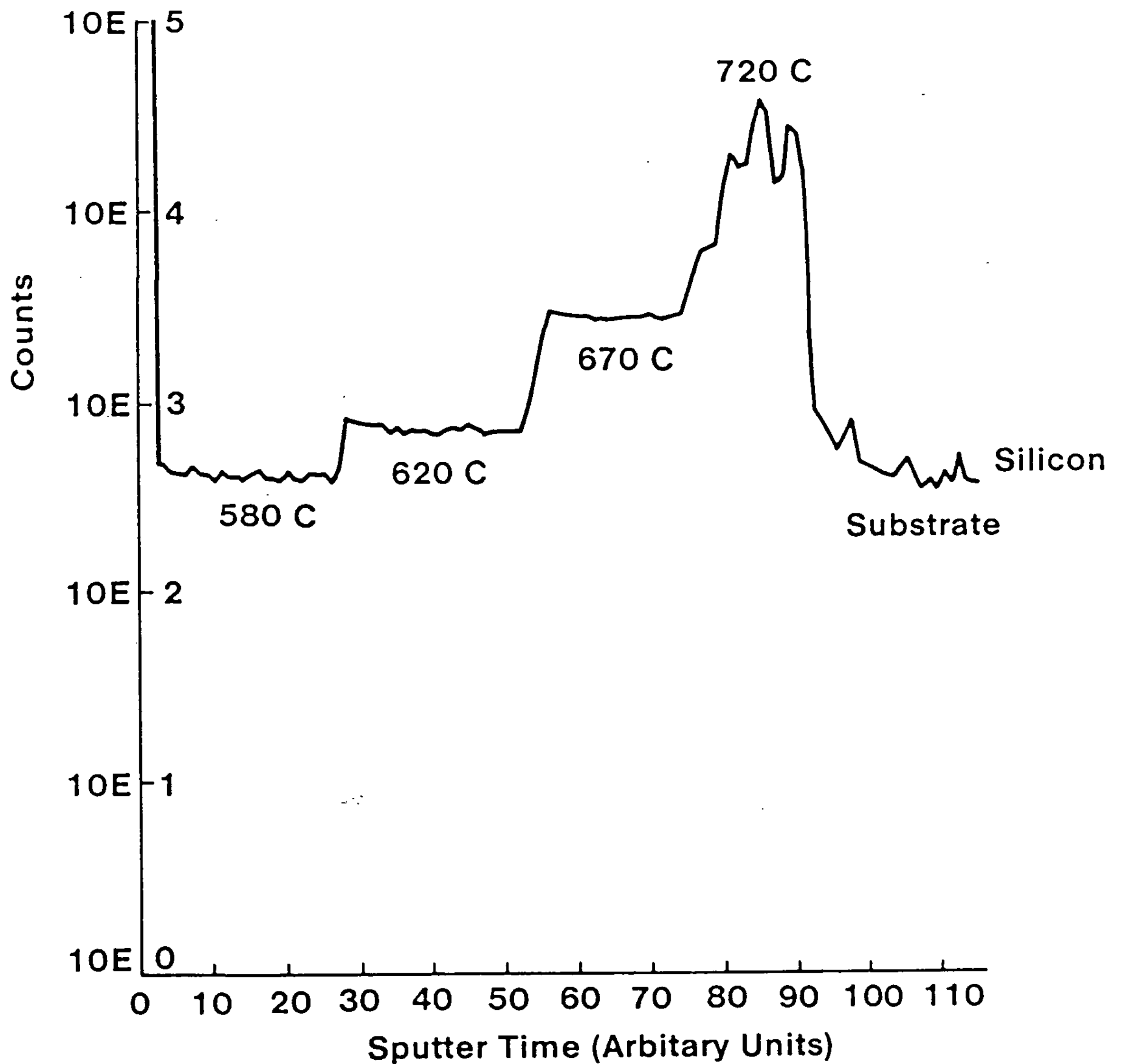

Figure (3.3): SIMS depth profile through the same four layer InP sample as shown in figure (3.2). The silicon content varies with growth temperature in the same manner as the electron concentration, confirming that silicon is primarily responsible for the background doping of InP.

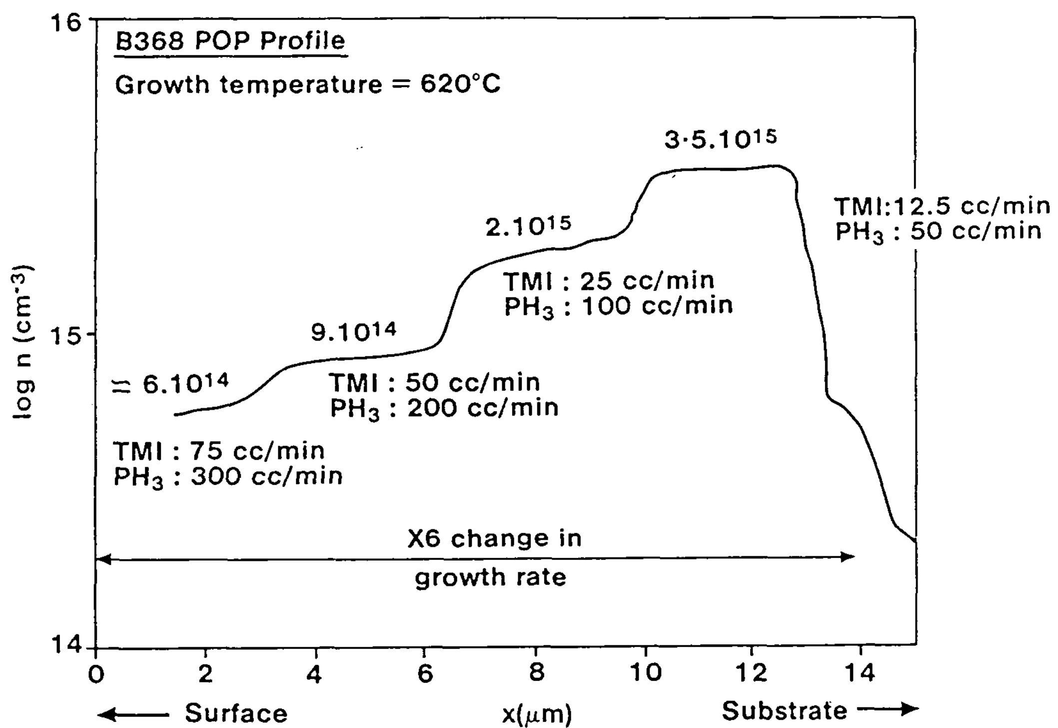

Figure (3.4): Electrochemical depth profile through four layers of InP showing the dependence of background doping upon growth rate. The layers were grown upon the substrate at ≃ 1.25, 2.5, 5, and 7.5μmhr^{-1} respectively and the V/III ratio was maintained constant.

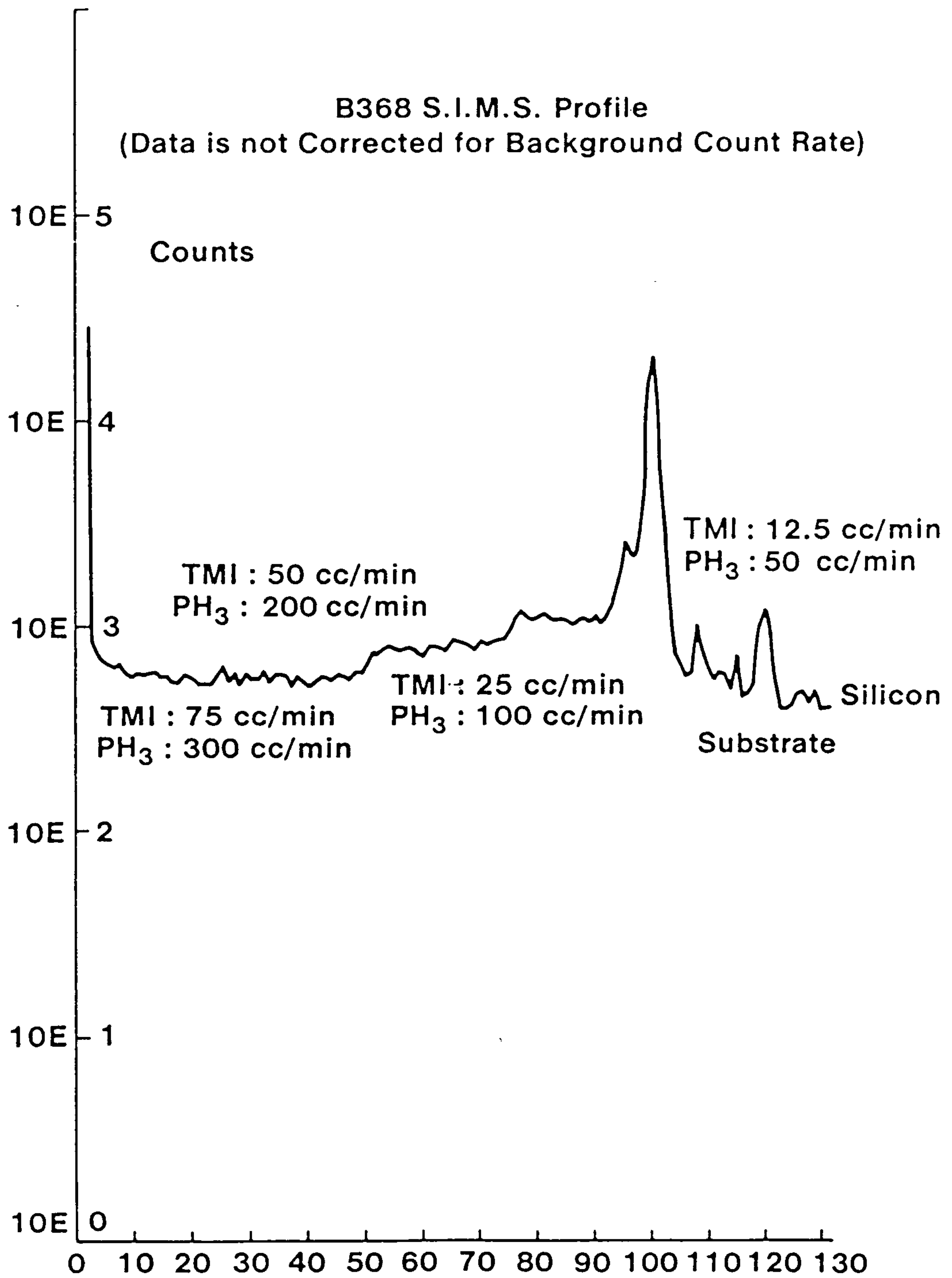

Figure (3.5): SIMS depth profile through the same four layer InP structure as shown in figure (3.4); the dependence of silicon content upon growth rate is the same as that observed for background electron concentration.

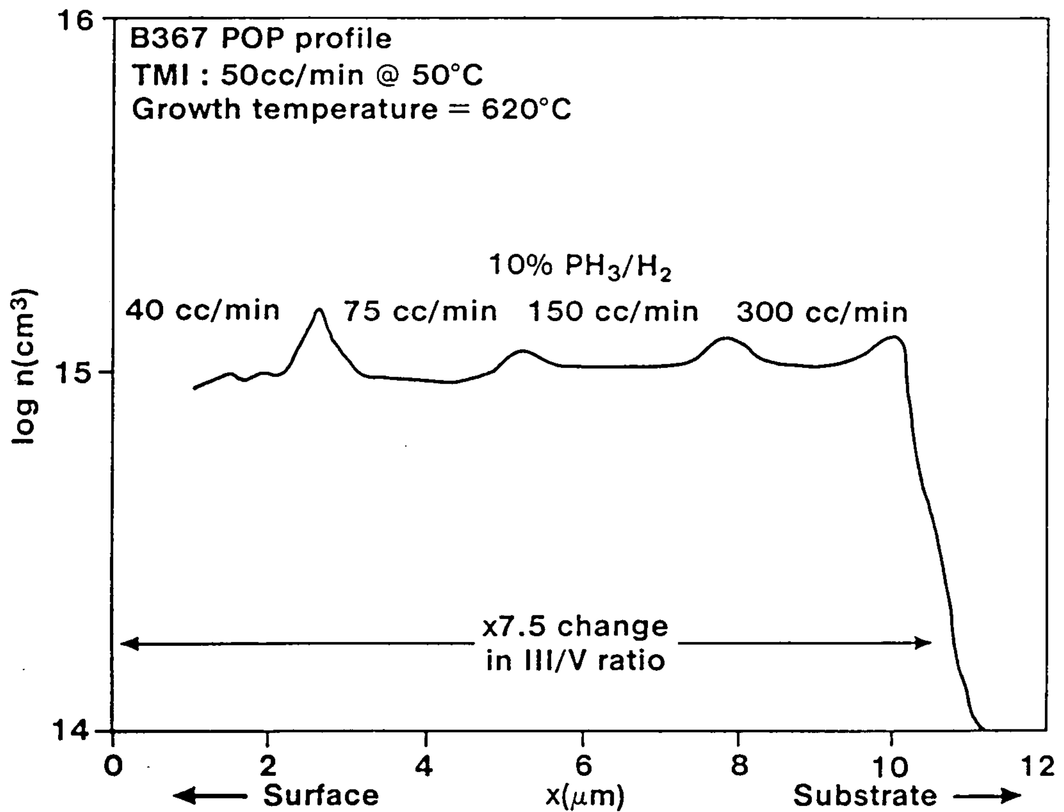

Figure (3.6): Electrochemical depth profile through four consecutive InP layers grown under different V/III ratios by varying the phosphine flow. The background doping level is independent of V/III ratio, but deliberate growth pauses between layers caused carrier concentration spikes to be incorporated into the material.

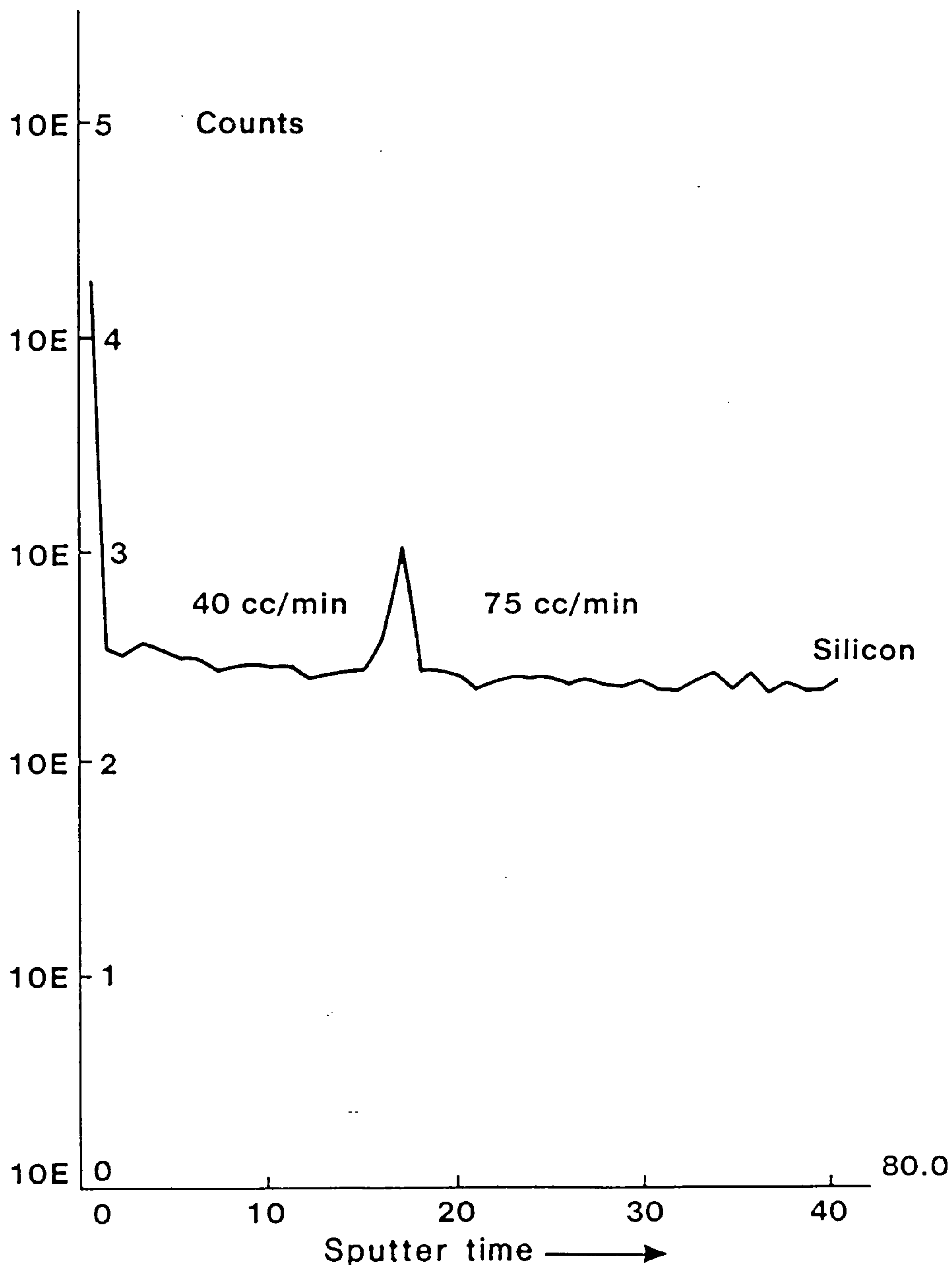

Figure (3.7): SIMS depth profile through the first two layers of the same sample as shown in figure (3.6), showing the presence of a silicon spike between the two layers.

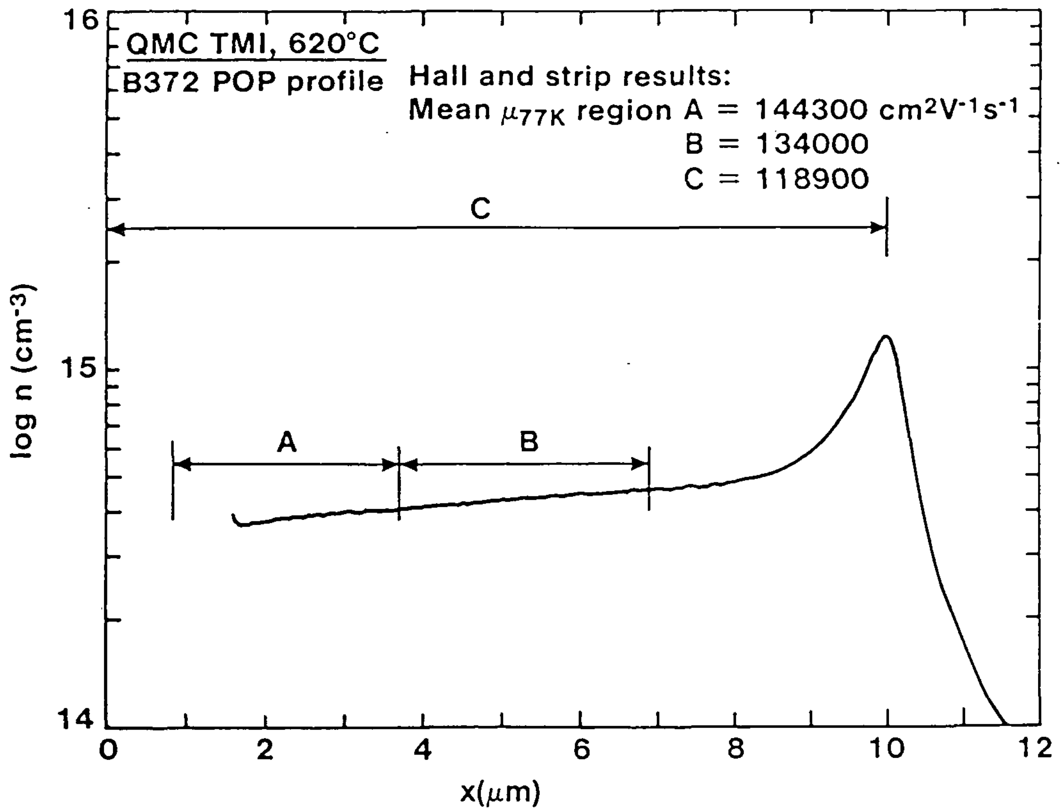

Figure (3.8): Electrochemical depth profile through a single layer of undoped InP grown under optimised conditions, showing a carrier concentration spike at the substrate-epilayer interface. The mobilities in areas "A" and "B" were obtained by Hall and strip measurements.

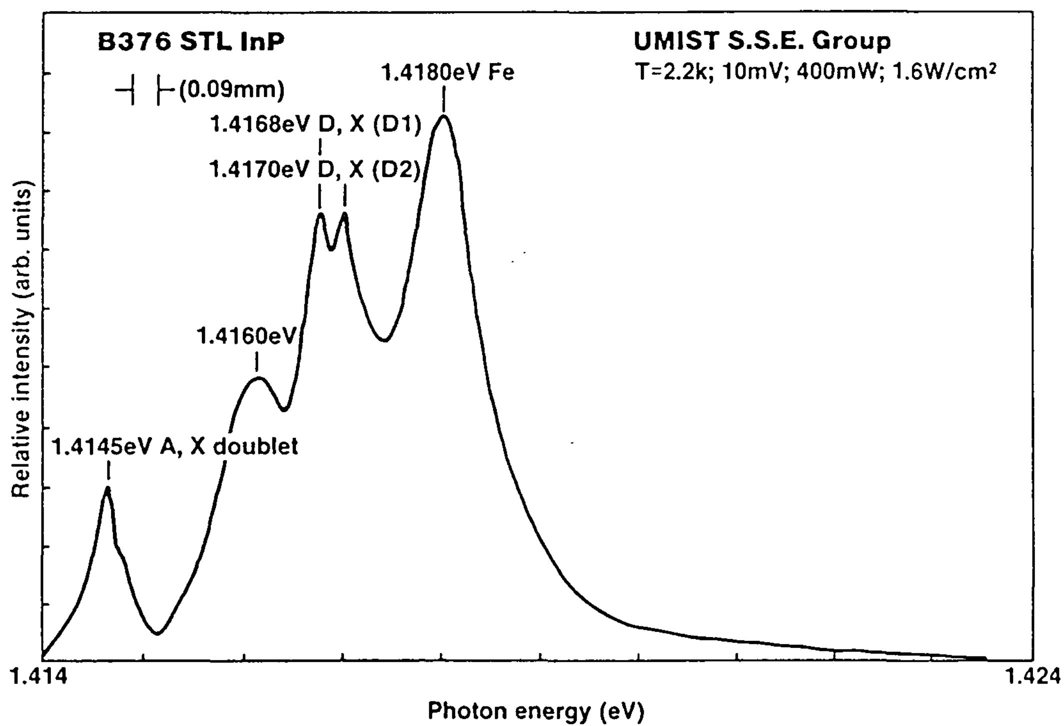

Figure (3.9): Low temperature photoluminescence spectrum for a high purity layer of InP, showing strong free exciton luminescence.

Chapter 4

(GaIn)(AsP) Alloy Epitaxy

The growth of (GaIn)(AsP) alloys is described in terms of crystal perfection, luminescence, and transport properties. Compositional uniformity of the alloys is discussed and a novel vapour measurement technique detailed.

III/V Alloy Systems

Epitaxial layers of InP grown upon InP substrates can be used for the fabrication of FETs. However, alloys with differing band-gaps and lattice matched to InP are more relevant to the construction of opto-electronic devices. Figure (4.1) shows the band-gap against lattice parameter for different alloys and illustrates that (GaIn)(AsP) alloys can be lattice matched to both InP and GaAs substrates. The alloy composition lattice matched to GaAs covers a similar band-gap range to (GaAl)As alloys. Lasers fabricated at 0.85μm wavelength have a reputation for being less reliable than those emitting at the longer 1.3-1.55μm wavelengths. It is not known whether this degradation is due to the aluminium content, or if it is due to the higher energy photons of the shorter wavelength material lubricating movement of dislocations or causing other debilitating effects. Some work has therefore been undertaken to study the (GaIn)(AsP) alloy matched to GaAs, especially in Japan, for optical disc applications. A disadvantage of this system is that the majority of the epitaxial structure has to be made of the difficult to control quaternary alloy, rather than from (GaAl)As which is easier to lattice match.

For emission of light at 1.3-1.55μm wavelengths, there are two contenders, (GaIn)(AsP) and (GaInAl)(As). The former has a more established growth history, being commonly used in liquid phase epitaxy. Concern over device reliability still surrounds the use of the aluminium compound, but the conduction band offsets of the alloy may lead to better carrier confinement in laser structures than available from the phosphorus alloy, and so to improved device

performance. The author has largely worked on the (GaIn)(AsP) alloys and it is these that are now described. The accepted method of defining the composition of this alloy, is to refer to the formula $Ga_xIn_{(1-x)}As_yP_{(1-y)}$; where x and y denote the amount of gallium and arsenic in the alloy respectively.

Lattice Matching of Alloys

The need to lattice match epitaxial layers to the substrate is not readily apparent. Lattice matching essentially requires that the average lattice parameter of the epitaxial layer is the same as the substrate lattice parameter. Whilst gallium and arsenic are very different in size and bond lengths from indium and phosphorus, in a well lattice matched layer an increase in the average lattice parameter due to the incorporation of arsenic into InP, is compensated for by an equivalent increase of gallium. If the average lattice parameter of the epitaxial layer is greater than the substrate, then the epilayer will be compressed laterally and will expand vertically to retain the same density. The converse applies if the average lattice parameter of the epilayer is less than the substrate. It is the change in vertical lattice parameter that is exploited by the various x-ray Bragg reflection techniques to determine material composition.

If the epitaxial layer is grown with an average lattice parameter sufficiently far from that of the substrate that the strain can no longer be accommodated elastically, then the strain will be relieved by formation of edge dislocations starting at the epitaxial interface, with Burgers vectors parallel to the growth plane. If the strain is severe, microcracks will appear which prevent conduction parallel to the growth plane and render the whole structure fragile. Lattice mismatch of thick layers also causes the substrate to bend, this in turn prevents photolithography upon the wafer. A pronounced cross hatch pattern is usually seen on poorly matched layers. The point at which dislocations are introduced into the material is dependent upon alloy composition and epilayer thickness [54]. It is far more difficult to grow thick alloy layers than the thin active layers of (GaIn)(AsP) lasers or quantum well structures. The formation of dislocations during growth may lead to sites of non radiative

recombination in laser structures and so reduce performance. Such defects are also able to move and grow under the influence of electric fields and high optical power densities, changing the device performance and causing degradation of critical parameters [55]. For these reasons, an as measured lattice matching specification of $\Delta a/a = \pm 4.10^{-4}$ is often imposed on device structures. This tolerance requires the gallium and indium contents of (GaIn)As to be controlled within ±0.6%, and imposes a similar tolerance to the input flows of gases into the MOVPE reactor.

<u>(GaIn)As</u>

The relationship between lattice parameter and the composition of an alloy is given by Vegard's law, and for (GaIn)As is a linear interpolation between the lattice parameters of GaAs and InAs. The relationship between band-gap (E_g), and alloy composition is given by equation (4.1):

$$E_g(\mathrm{eV}) = A_0 x + A_1(1-x) + A_2 x(1-x) \qquad (4.1)$$

Where: $A_0 = E_g$ (GaAs) = 1.425 eV
$A_1 = E_g$ (InAs) = 0.36 eV
A_2 = bowing parameter

Equation (4.1) describes a line upon the band-gap-composition graph for (GaIn)As drawn between the values for InAs and GaAs. The line has a slight curvature or "bow"; a bowing parameter of -0.475 and a lattice match band-gap of 0.74 eV have been used at STL.

The band-gap of the material is related to the photoluminescence emission wavelength by:

$$\text{PL wavelength } (\mu\text{m}) = 1.24/E_g \text{ (eV)} \qquad (4.2)$$

Suitable stimulation of the alloy by a light source of shorter wavelength energy than the alloy band-gap results in photoluminescence emission of light characteristic of the material, provided that the band gap is direct, and that there are few non radiative recombination centres in the material.

Recent studies within STC to compare composition measured from x-ray data with that from photoluminescence data, have shown that equation (4.1) does not always apply. A similar effect has been reported by Olsen et al [59]. It is inferred that strain within the lattice may affect the band-gap, and epitaxial layer thicknesses may further complicate the amount of strain present. This may account for the large scatter in the literature of bowing parameters and photoluminescence wavelengths at lattice match [56,57,58].

The normal growth rate conditions used on the author's reactor are a growth rate of 0.1μm min^{-1}, a growth temperature of 650°C, input flow rates of $10cm^3min^{-1}$ for trimethylgallium, $33.8cm^3min^{-1}$ for trimethylindium and $150cm^3min^{-1}$ of 10% arsine in hydrogen. The growth rate appeared to be an important factor limiting the crystallinity of the epitaxial layers. Figure (4.2) shows optical micrographs of two epitaxial layers grown under similar conditions and at similar times. The first exhibits a very smooth texture, has strong photoluminescence emission and double crystal x-ray rocking curve half-widths of around 50 arc seconds. The second layer has a rough texture, negligible photoluminescence emission, extremely broad x-ray half widths, and 300K electron mobilities of $3000cm^2V^{-1}s^{-1}$ falling to lower values at 77K. This type of growth may consist of clusters of islands of (GaIn)As caused by growth in three instead of two dimensions. The phenomenon has been seen on several different reactors and has disappeared sometimes spontaneously, inferring machine malfunction. The problem has also been overcome by reducing the growth rate, or by re-timing the arrival of the group III and group V species at the substrate.

(GaIn)As lies at the edge of a miscibility gap in the (GaIn)(AsP) phase diagram, and there has been speculation by some workers that spinodal decomposition of epilayers has occurred [61,62].

A further factor affecting the crystal quality of (GaIn)As epilayers is the regularity of flow of the group III sources into the reaction chamber [60]. Any event which causes a variation in these flows will be reflected in the composition of the material being grown. This in turn will induce mismatch and strain, possibly induce

growth of a different form, and change transport properties. A particularly easy method of introducing flow variations is to use unstable mass flow controllers, and cause transient changes in mass flow controller output due to their sensitivity to upstream and downstream pressure fluctuations. Downstream pressure fluctuations are often caused by the MOVPE reactor exhaust blocking, and careful attention has to be given to the design of this component.

The author has grown specular epitaxial layers of (GaIn)As with x-ray rocking curve full width half maxima as low as 22 arc seconds and with high photoluminescent properties. Background doping levels for material grown at 650°C are n-type = $2\text{-}5.10^{14}cm^{-3}$. It is common practice to quote mobilities in the literature for epitaxial layers of (GaIn)As grown upon an InP buffer layer [63]. The author's best results are 300K electron mobilities of $11{,}500cm^2V^{-1}s^{-1}$ and 77K electron mobilities of $75{,}000\ cm^2V^{-1}s^{-1}$. The possibility exists of growing a highly doped region next to the substrate as detailed in the previous chapter. The donors so formed are likely to fall into the lower band-gap (GaIn)As and due to band bending at the heterojunction, become confined and form a two dimensional electron gas. This in turn leads to enhanced mobilities which may not be a true reflection of the material quality. This phenomenon has also been reported by Zhu et al [64], and the existence of a two dimensional electron gas has been confirmed by Shubnikov-De Haas measurements. Several workers have exploited this effect by deliberately growing a highly doped InP layer close to an undoped (GaIn)As layer and achieving electron mobilities of $100{,}000cm^2V^{-1}s^{-1}$ [63,65,66,67,68,26].

The arsine over-pressure during growth of (GaIn)As is also of importance. The two micrographs of figure (4.3) illustrate two (GaIn)As epitaxial layers grown respectively with high and low arsine flow rates. Small pin-holes can be seen in the sample grown using a low arsine flux, and these defects have completely disappeared upon use of a high arsine flux. The transport properties of these layers were identical.

(GaIn)(AsP)

Alloy growth was extended from the ternary alloy to the quaternary alloy by the addition of phosphine. The distribution coefficient for the group III metals is near to unity, and so flows of trimethylindium and trimethylgallium were interpolated from those used for (GaIn)As.

The ratio of arsine to phosphine required to grow a particular (GaIn)(AsP) alloy bears no resemblance to the solid arsenic to phosphorus ratio due to the different pyrolysis rates of the two gases. There are several references in the literature stating the arsine to phosphine ratios needed to grow a particular alloy [26,69,70]. Theoretical studies based upon diffusion, pyrolysis rates and the thermodynamics of the reactions of the two gases have also been undertaken [71,72]. This data, applied at 650°C, was used to obtain the correct flow rates for initial attempts at the growth of the quaternary alloy. Assessment of these often poor layers, using energy dispersive x-ray analysis then allowed corrections to the gas flow rates to be made. Growth of layers of sufficient quality for photoluminescence and double crystal x-ray rocking curves were then achieved.

Lattice parameter data for the quaternary alloy was again obtained by Vegard's law [31]:

$$a = 0.1894y - 0.4184x + 0.0130xy + A(InP) \quad (4.3)$$

where x and y are the relative amounts of gallium and arsenic in the alloy, a is the measured lattice parameter, and A(InP) is the lattice parameter of InP in ångstroms.

The most up to date references [73,74] for the relationship between quaternary alloy composition and band-gap (E_g) in eV gives:

$$Eg(x,y) = 1.35 + 0.668x - 1.068y + 0.758x^2 + 0.078y^2 - 0.069xy - 0.322x^2y + 0.03xy^2 \quad (4.4)$$

By solving the above two equations simultaneously using a graphical computer solution, more precise compositions of the alloys could be obtained. Since strain is likely to affect the band-gap of this material in the same manner as for (GaIn)As, caution has to be exercised when using these equations. Inevitably, final approach to lattice matching and correct photoluminescence emission wavelengths is obtained by an iterative growth and measuring cycle. The final accuracy of material grown is dependent upon the run to run stability of the MOVPE reactor and upon uniformity of the epitaxial layers.

The growth conditions finally established are given in table (4.1) and the disparity between the amount of arsine and phosphine required to grow a particular quaternary layer is clear. It is postulated from these results that the pyrolysis rate of arsine is 20-40 times faster than that of phosphine at 650°C.

Specular, highly luminescent layers of (GaIn)(AsP) were grown with 1.18, 1.3 and 1.55μm emission wavelengths. Doping levels appeared to follow those of InP at 650°C and be around $n = 1\text{-}2.10^{15}cm^{-3}$. Hall measurements obtained on 2-3μm thick 1.3μm emission samples gave 300K electron mobilities of $4000\text{-}4700 cm^2V^{-1}s^{-1}$ and 77K electron mobilities of $20{,}400\ cm^2V^{-1}s^{-1}$. These values compare well with data upon LPE samples [75], although a 0.6μm thick InP buffer layer was used next to the substrate, and this may have given rise to a two dimensional electron gas at the hetero-interface in a similar manner to (GaIn)As. X-ray rocking curve half-widths as low as 34 arc seconds were obtained indicating a high level of epitaxial quality. Figure (4.4) shows a 77K photoluminescence spectrum for 1.3μm epitaxial quaternary, figures (4.5) and (4.6) show double crystal x-ray rocking curves for 1.18 and 1.3μm quaternary layers respectively.

The quaternary layers used in the active and guide layers of semiconductor lasers, normally have a total thickness of less than 0.5μm. It was easier to achieve the growth of these thin layers than thicker layers, since any dislocations present due to lattice mismatch or other effects, tend to worsen the quality of the epitaxy as the thickness of the layer is increased.

The low flow rate ratio of trimethylgallium to trimethylindium needed for the shorter wavelength quaternary alloys tended to require

very low and therefore unstable flow rates of trimethylgallium. To compensate for this, the flow rates of both the group III alkyls were increased which in turn led to a high growth rate of approximately $0.13\mu m\ min^{-1}$.

Apart from this requirement, and the similarly low flow rates of arsine needed, the growth of the quaternary alloys appeared quite straightforward. Table (4.2) shows the permissible variation of each of the four matrix element flow rates needed to keep the solid alloy composition within an as measured value of $\Delta a/a = \pm 4.10^{-4}$. These tolerances are a key to good quality epitaxial growth and to good device reliability, and so are used as a guide to mass flow controller sizing and to general reactor design.

Alloy Uniformity

Epitaxial alloy layers exhibit compositional non uniformity of varying scales in the growth direction, and also in the plane of the substrate both perpendicular and parallel to the gas flow direction. Equipment factors such as mass flow controller stability, pressure transients, exhaust blockage, and temperature fluctuations will affect the small scale uniformity in the direction of growth. Banding often seen in transmission electron micrographs of alloy layers has also been seen and ascribed to compositional changes, and sometimes explained in terms of segregation due to spinodal decomposition [62].

In the following sections, the different causes of compositional non uniformity, using equipment known to be functioning well, are discussed.

Non Uniformity due to Slow Arrival of Reactants

It might be expected that as soon as hydrogen gas is routed through an alkyl source, a flow of gas saturated to the required amount would reach the reactor chamber, delayed only by the transit time of the pipework separating the reactor chamber and the source. In fact the gas develops a parabolic velocity profile and so some of the saturated gas reaches the reaction chamber earlier than expected, and the reactant concentration asymptotes towards the expected

concentration. It is also possible that adsorption and desorption of metal-organic compounds onto the stainless steel pipework slows the time response of the gas packet reaching the growth chamber.

For these reasons, the vent-run design of reactor was introduced. A stable flow of gas was allowed to pass through the alkyl sources until it was believed that the actual molar flux of metal-organic reaching the vent-run manifold was also stable. This flow of gas was then switched to and from the growth chamber as needed for epitaxial growth.

The required flushing times before stable concentrations were obtained were not known, so concentration-time profiles for trimethylgallium and trimethylindium were measured using a membrane sampling probe and mass spectrometer [32]. This work established that a time of 5 minutes was needed to stabilise the trimethylgallium flux, and for trimethylindium a period of 20 minutes was needed despite the higher flow rates used. The above method of gas sampling was found not to be suited to continuous use and an alternative method of metal-organic vapour pressure measurement was sought. It was also observed that the run to run compositional repeatability of alloys was not as good as expected. Furthermore, there have been observations that more than one phase of trimethylindium crystal might exist [76], and that these in turn might have different rates of sublimation and even different partial pressures. These factors led to the development of an ultrasonic technique of vapour pressure measurement.

Ultrasonic Binary Gas Composition Monitoring

Stagg at STL developed the ultrasonic cell, the detailed construction along with vapour pressure measurements upon trimethylindium and trimethylgallium are discussed in reference [77]. The ultrasonic cell forms a direct method of source monitoring, rather than relying on the normal slow method of growing layers, measuring alloy composition, and from that inferring the behaviour of the source.

The principle of operation is that the velocity of sound in a gas mixture is proportional to the mean density of the gas, all other conditions remaining the same:

$$v = (\gamma RT/M)^{0.5} \qquad (4.5)$$

where: M is the mean gram molecular mass of the gas mixture (kg),
v is the velocity of sound in the gas mixture (ms^{-1}),
R is the universal gas constant (8.3143 $JK^{-1}mol^{-1}$),
T is the cell temperature (K).
γ is the ratio of specific heats for the measured gas($\approx$1.4).

Since trimethylindium is believed to be a monomeric vapour from vapour density measurements, M relates to the concentration of vapour in hydrogen passing through the ultrasonic cell.

The practical realisation of this theory used a pair of ultrasonic transducers at either end of a stainless steel chamber, transmitting ultra-sound pulses at a frequency of 1MHz. The temperature was carefully measured using a platinum resistance thermometer. Once the equipment was proven, it was installed in the trimethylindium line of the author's MOVPE reactor.

The reactor and the ultrasonic reagent monitor are illustrated in figure (4.7). Under normal conditions, the trimethylindium source was submerged in an oil bath heated to 50°C and, when required, a flow of purified hydrogen was passed through the source to collect the trimethylindium vapour at a flow rate of 10-70cm^3min^{-1}. The output from the source was joined by an additional flow of up to 50cm^3min^{-1} of hydrogen, to provide some gas dilution before passing to the ultrasonic reagent monitor. It was then passed to the reaction zone via a fast gas switching manifold. All of the pipework downstream of the source, along with the valves and the gas switching manifold was heated to 70-80°C, and the ultrasonic cell was heated to 100°C.

Assuming ideal gas behaviour, the steady state trimethylindium concentration (x) in the cell is related to flow rates, atmospheric pressure and trimethylindium partial pressure in the source by:-

$$x = \frac{Vp(TMIn).F(TMIn)}{P(Total).F(Cell)} \quad . . (4.6)$$

where: Vp(TMIn) is the trimethylindium partial pressure in the trimethylindium source,
P(Total) is the total pressure of the gas in the ultrasonic cell,
F(Cell) is the total hydrogen mass flow rate through the ultrasonic cell,
F(TMIn) is the hydrogen mass flow rate through the trimethylindium source.

The molar flow rate of trimethylindium reaching the reaction zone is inversely proportional to the total pressure and therefore atmospheric pressure. This results in the growth rate varying by ±3% with atmospheric pressure variations, and the values of vapour concentration displayed by the ultrasonic system varying similarly. However these changes should not alter dramatically the composition of alloys since each of the metal-organic sources is affected in the same way.

The ultrasonic cell was fitted with a flow and by-pass valve arrangement to determine the effect upon epitaxy purity, and to observe time constants for vapour adsorption and desorption onto the materials within the cell. The use and proximity of RF heating during epitaxial growth required careful attention to be applied to screening of the signal paths, and notch filters were required in the RF amplifier to achieve an adequate signal-to-noise ratio.

InP epitaxial layers with 77K mobilities as high as 130,000$cm^2V^{-1}s^{-1}$ were grown shortly after installation of the ultrasonic cell, indicating that the reactor performance had not been compromised by the addition of the system.

The ultrasonic measurement apparatus collected data for every

growth run following installation, in order to establish trends in partial pressure, and to establish run to run vapour pressure variations.

Trimethylindium Vapour Pressure Rise Time Measurements

Figure (4.8) shows a plot of trimethylindium concentration in hydrogen against time for a typical growth run. It should be noted that the vertical axis has a heavily suppressed zero to increase the resolution of the plot in the region of interest. This plot was characteristic of growth runs where the source was held at 50°C and when the source was either full or a long time from exhaustion. The vertical bar represents the range of variation of trimethylindium concentration that translates to an unstrained lattice mismatch of $\pm 2.10^{-4}$ for $Ga_{0.468}In_{0.532}As$. Quantifying the shape of the curve in figure (4.8), a time of 16 minutes was needed for the variation in concentration to fall below the value required to achieve this lattice matching criterion. In practice, growth of an alloy such as (GaIn)As would not be started until about twice this time was reached, and then only if the data indicated that the trimethylindium source was behaving as expected. This long time to reach stability required the trimethylindium to be flushed to vent for some time prior to growth, which was wasteful in terms of consumption of trimethylindium and of reactor time.

Efforts were made to determine the cause of the long time to reach a stabile concentration. Figure (4.9) shows a similar plot to figure (4.8) where the trimethylindium had first been flushed to vent for 85 minutes though by-passing the ultrasonic cell. The cell was then placed in circuit and the measured concentration of trimethylindium rose rapidly, with a time constant of better than 3 minutes. This result indicates that adsorption and desorption of trimethylindium on or from the surfaces of the ultrasonic cell, is not the cause of the long time required to reach a stable concentration.

Since the surface area of pipework from the trimethylindium source to the reactor is similar to the surface area of the ultrasonic cell, then the adsorption and desorption of vapour onto the stainless steel pipework is also eliminated as a cause. Heating of a single

known cold spot in the reactor pipework had no significant effect upon the time constant. It is concluded that the large time constant is related to changes occurring within the trimethylindium source such as variations in the temperature, or crystal structure of the trimethylindium.

Figure (4.10) shows a trimethylindium concentration against time plot where the experimental conditions were a trimethylindium source temperature of 40°C and all other conditions the same as those of figure (4.8). The temperature control of the trimethylindium bath was not optimised for this lower temperature and resulted in the temperature hunting by ±2°C. This variation was reflected in the trimethylindium partial pressure oscillating as illustrated by figure (4.10), and is further evidence of the fast response of the overall system to changes in trimethylindium partial pressure. The time constant for the average concentration to be stable within the lattice match criterion was determined to be 6 minutes, a major reduction to that required at 50°C. The exact explanation for the change in time constant, and the slow rise to stability of partial pressure at 50°C is not fully understood. However Kayser et al have reported that the vapour pressure of trimethylindium, measured under static conditions, rose slowly with time after an initial sharp increase in pressure [78]. The explanation given for this effect was that the trimethylindium was slowly dissociating. This does not however explain why growth of InP was still possible with low trimethylindium vapour pressures in the author's reactor.

Run to Run Vapour Pressure Stability

Equally important for alloy growth, is run to run repeatability of partial pressure. By determining the final concentration of trimethylindium in the gas stream, and correcting for the total pressure, the absolute partial pressure of the trimethylindium source can be determined for the end of each growth run, using equation (4.6). Figure (4.11) shows the variation of this partial pressure as a function of run number. All the points relate to similar flow rate and temperature conditions, and the plot was started from the installation of a new source of trimethylindium. A gradual fall in the partial

pressure is observed with consumption of the source, but the trend is for stability to be reached with the majority of the curve lying within the lattice match criterion stated earlier.

Trimethylindium Source Exhaustion Characteristics

It is interesting to observe the effect on the trimethylindium partial pressure as the source becomes depleted. Figure (4.12) shows a series of concentration against time curves for the last few growth runs prior to a trimethylindium source being totally exhausted. The amount of trimethylindium left in the source bottle once removed from the reactor was determined by radiography to be negligible. Curve (1) is a concentration curve representative of a source nearing exhaustion, characterised by a 10% lower partial pressure than expected and a peak in concentration rather than a curve tending to stability. This behaviour can be explained by the volume in the source being fully saturated before a gas flow is started through it, so giving gas with a normal concentration; followed by a decrease in concentration caused by insufficient surface area of crystals of trimethylindium being available to evaporate and saturate the gas flowing through the cylinder.

A technique that has been used recently to recover the performance of a trimethylindium source is to raise the source temperature above the melting point of trimethylindium and then cool and recrystallise the trimethylindium under a slow gas flow [79]. The source on the author's MOVPE reactor was heated to 95°C, then cooled rapidly with a flow of hydrogen being maintained through the source. Concentration curves (2) and (3) illustrate the recovery of the source to its original performance following the recrystallisation process. However a few growth runs later the ability to maintain saturation of the vapour was again lost (curve 4), and the three curves (5,6 & 7) show the final drop in partial pressure during growth runs before the source was removed.

A consequence of identifying the exhaustion characteristics of a trimethylindium source, is that the event can be predicted by observing the onset of droop of the concentration curve. This is

preferable to discovering exhaustion from composition and growth rate changes, which may be due to other factors, and are somewhat 'after the event' methods. It is also preferable to predicting the amount of alkyl used from run times, partial pressures and flow rates since an error in any one of these, or in the weight of the trimethylindium originally placed in the source by the manufacturer, will result in confusion.

Mircea et al [80] have noted that the partial pressure of trimethylindium sublimed at 25°C decreases with increasing flow rate through the source, the lack of saturation of the vapour being most marked above $100cm^3min^{-1}$. This effect may be expected to become worse with consumption of the trimethylindium source, and indicates that it is better to use a combination of low flow rates and a heated source rather than a cold source with high gas flow rates.

Gas Mixing

To obtain epitaxial layers that are compositionally uniform in the plane of the substrate, it is essential that the constituents of the gas stream arriving at the substrate are thoroughly mixed. Varying gas concentrations measured across the cross section of the gas stream and induced in the gas switching manifold, will be reflected in epitaxial compositional variations, unless the gas stream has had sufficient time to inter-diffuse into a homogeneous mixture on the way to the reaction chamber. The present interest in low dimensional structures and highly abrupt interfaces has resulted in the vent-run gas switching manifolds being positioned very close to the reaction chamber. Failure to do this results in grading of epitaxial interfaces. A severe criterion is therefore imposed: in order to grow low dimensional structures and uniform layers it is necessary to site the switching manifold close to the reaction chamber and mix the gases without introducing any recirculation or static volumes that would store gas. As an example, Thrush at S.T.L. tried to use glass wool at the reaction tube inlet to improve mixing. This was achieved, but T.E.M. cross sections of low dimensional epitaxial structures revealed that the interface quality had been degraded.

The author's reactor is so designed to provide good low dimensional capability, but yields epitaxial layers of poor uniformity. Figure (4.13) illustrates a typical (GaIn)As epilayer compositional cross section perpendicular to the gas flow over the substrate. A fairly linear change in gallium content can be seen. It was suspected that this non uniformity was associated with the proximity of the switching manifold to the reaction zone. An improvement in uniformity from 6% gallium content (figure 4.13), to 3% was obtained by moving the trimethylgallium input port to the same side as the trimethylindium input port in the gas switching manifold (figure 4.14). The area of maximum gallium content in the epitaxial layer also changed from one side to the other.

The flow rates of trimethylgallium and trimethylindium used were carefully considered and it was decided that injection of $5cm^3min^{-1}$ of trimethylgallium into a hydrogen flow of 4 $lmin^{-1}$ was resulting in the vapour creeping along the edge of the pipework in the slowest moving part of the gas stream. In an attempt to improve the gas mixing, further hydrogen was added to the trimethylgallium line downstream of the source, the increased gas velocity causing injection of gas into the centre of the switching manifold. The result of this modification can be seen in figure (4.15). The slope of the composition relative to the gas stream has reversed and worsened for a maximum extra flow of hydrogen added to the trimethylgallium line of 200 cm^3min^{-1}. Some reduction of this additional flow provided an improvement in epitaxial uniformity, presumably due to the trimethylindium and trimethylgallium gas clouds being injected into closer range of each other. However the required uniformity target of 2% total variation in gallium content was not achieved.

A further modification to the reactor gas switching manifold, was to add small pipes onto the ends of each injection port to a depth of 1.5mm, equivalent to a quarter of the diameter of the manifold bore. The vapours of trimethylgallium and trimethylindium were then injected into the central, high velocity part of the gas stream, rather than into the slow moving side-wall flows. This change resulted in an improvement of the lateral compositional uniformity to a total of 1.25% gallium variation, or a lattice mismatch of $\pm 4.10^{-4}$. A composition map of a typical epitaxial layer is shown in figure

(4.16). It is evident that there is as much compositional variation in the direction of gas flow, as there is perpendicular. This is probably due to increasing depletion of trimethylindium from the gas phase along the length of the susceptor.

Consideration of the mechanisms available for the mixing of the gases gives three possibilities. The first, injection of the gases to be mixed into exactly the same position in the carrier gas stream, was not pursued due to engineering constraints and because the above experiments indicated that different flow rates needed for different growth conditions would affect the gas mixing. The possibility of distancing the manifold further from the growth tube, and of inducing mixing by turbulence or diffusion was investigated in greater depth.

Turbulent Mixing

The likelihood of inducing turbulence in a gas stream is given by equation (4.7), when for a given geometry, the Reynold's number (R_e) exceeds a certain value [81]:

$$R_e = \frac{\rho d v}{\eta} \qquad (4.7)$$

where for hydrogen at S.T.P,

R_e = Reynold's number,
ρ = gas density = $0.09 kgm^{-3}$,
η = gas viscosity = $8.35.10^{-6} Nsm^{-2}$,
v = gas velocity,
d = tube diameter.

For the case of a cylindrical pipe, R_e is approximately 2000, and additionally some discontinuity is needed to start turbulence in the pipe in the first instance.

For the author's reactor, with a hydrogen flow rate of 4 $lmin^{-1}$ and a switching manifold bore diameter of 6mm, the value of R_e is calculated to be 152, far short of the value needed to sustain

turbulence. If the gas pressure is reduced, for the same mass flow rates, the gas velocity is increased proportionally and the density is decreased. The viscosity of a gas does not change significantly with pressure and so no change in R_e results from reducing the reactor pressure. For the same flow rate (F), R_e can only exceed 2000 if the tube diameter is below 0.45mm, from:

$$d = \frac{4\rho F}{\eta \pi R_e} \qquad (4.8)$$

Hydrogen has a comparatively low value of kinematic viscosity (ρ/η), and so is a particularly difficult gas to mix.

By scaling of flow rates and using dyed water in a mock up scale model of an MOVPE reactor, the lack of turbulent mixing was observed along with creeping of low injected flows along the side-walls of the reactor [82].

Further efforts to induce turbulent mixing in the MOVPE reactor were made using a mixing nozzle consisting of a plug that fitted into the output of the gas switching manifold with a 0.2mm hole in the centre. Figure (4.17) shows the uniformity of a (GaIn)As epitaxial layer grown using this device. Although the uniformity dramatically improved, the quality of the epilayers was considerably poorer than layers grown without the mixing nozzle. This was determined to be due to the nozzle introducing a 60 mBar pressure rise into the alkyl manifold and subsequently affecting the pressure balancing of the arsine-phosphine manifold. Attempts were made to improve the epitaxial quality by reducing the nozzle impedance by drilling the hole larger, but it was found that when a hole large enough to allow specular epitaxy was used, the epitaxial layers had returned to the original non-uniform state.

The above experimental data and calculations were given further support by a publication a few months later by Blaauw et al detailing similar experiments and results [83].

Diffusion Mixing of Gases

The second method of thoroughly mixing gases injected into a gas stream is to allow sufficient time for the gases to inter-diffuse. This occurs in reactors where the gas injection point is remote from the reaction chamber.

To calculate how long is required for a gas stream to mix adequately, the following approximate model was considered. A column of gas diffuses sideways, and the concentrations at the centre of the column, and at a point away from the centre of the column were compared as a function of time. When the two concentrations are similar to within ~ 1.5%, the gas is considered to be mixed. The model is illustrated in figure (4.18). An error function diffusion equation applies:

$$C(x,t) = \frac{1}{2}C_o\left(\mathrm{erf}\left(\frac{(h-x)}{\sqrt{(Dt)}}\right) + \mathrm{erf}\left(\frac{(h+x)}{\sqrt{(Dt)}}\right)\right) \qquad (4.9) \quad [84]$$

where: C = the gas concentration,
t = time,
x = radius from the centre of the column,
D = diffusion coefficient for the gas,
h = radius of the gas column at zero time,
C_o = initial concentration of gas, (100%).

The diffusion coefficient for trimethylindium and trimethylgallium was determined to lie between 0.4 and $0.5cm^2s^{-1}$ at STP from comparison with data on gases with similar molecular weights, and to be $0.2cm^2s^{-1}$ from diffusion studies [85]. The diffusion coefficient is also a function of temperature ($D \sim T^{1.75}$). The temperature of the gas whilst being mixed was around 60°C in the author's reactor and so a value of D of $0.4cm^2s^{-1}$ was considered appropriate for use in calculations.

The above diffusion equation was solved and tabulated using an initial gas column diameter of 0.5mm, and observing the concentration of gas at the centre of the column and at a radius of 1.5mm. It was calculated that the difference between the two concentrations would be

16.7% after 0.01s, 1.3% after 0.1s and 0.5% after 1s had elapsed. The value of 1.3% is acceptable for the growth of uniform material and this diffusion time then allows the necessary length of pipe to be determined. For a 4 $lmin^{-1}$ flow of gas through a 6mm diameter pipe, a distance of 23.5cm is required. This is considerably further than the available distance on the author's reactor and it is therefore not surprising that non-uniform epitaxy results.

An alternative method of ensuring complete mixing of gases by the time the growth zone has been reached, is to pre-mix the gases remotely. The various mixtures are then either switched close to the reactor, or the substrate is passed to and from two separate gas streams in the reactor by mechanical means. Figure (4.19) illustrates the uniformity obtained for (GaIn)As grown by Antell at STL, using a reactor that switched gas mixtures close to the reaction cell. The maximum spread of photoluminescence wavelengths obtained upon two half two-inch diameter wafers grown in two consecutive growth runs was 13nm and 6nm. The standard deviation of photoluminescence wavelength over the total area was 4.2nm, well within the uniformity requirements for many applications.

Interface Abruptness: The Effect of Gas Diffusion

The above results indicate that it is preferable to distance the gas switching manifold from the reaction chamber, at least when using a conventional fast gas switching reactor. Applying diffusion theory again, this time to two packets of gas passing from gas manifold to reaction zone, it is possible to determine the amount of inter-diffusion that will have taken place between the two gas packets at the entrance to the reaction zone. A complementary error function equation is used:

$$C(x,t) = \frac{C_0}{2}.\mathrm{erfc}\left(\frac{x}{2\sqrt{(Dt)}}\right) \qquad (4.10) \quad [84]$$

where: $D = 0.4cm^2s^{-1}$,
C_0=initial gas concentration at the packet interface (100%),
C = gas concentration after time (t) and at a distance (x) from from the gas packet interface.

For the previously calculated time of t = 0.1s, the distance over which the gas packet has spread to the range of 5 - 95% of its original value can be determined. The 5 - 95% range is chosen as that compositional fluctuation that would appear in cross sectional TEM micrographs of the epitaxy.

The value calculated is ±0.46cm, from the original interface, and in a 6mm diameter pipe with 4 $lmin^{-1}$ of gas flowing, this distance corresponds to a time of 3.9ms. During this time, even at the highest envisaged growth rates, only an average thickness of 0.1Å epitaxial layer will have been grown, and so mono-layer sharp interfaces should be possible. However diffusion is not the only factor causing smearing together of gas packets and poor epitaxial interfaces.

Interface Abruptness: Effect of Parabolic Velocity Profile.

Since the gas flow between the switching manifold and the reactor chamber is laminar, the gas stream develops a three dimensional parabolic velocity profile. The peak velocity of the gas is at the centre of the tube, and is twice the average gas flow velocity.

Starting from a parallel profile, the full parabolic velocity profile is attained at a length L_e along the pipe:

$$L_e = 0.0288.R_e.d \quad (4.11) \quad [86]$$

where: R_e = the Reynold's number,
d = the tube diameter.

Using the previously calculated value of R_e of 152, L_e is calculated to be 4 diameters. In a 6mm bore tube, this corresponds to a distance of 2.4cm, so the full parabolic profile will have evolved after a transit time of 0.01s. It is interesting to calculate the average gas concentration that exists at the entrance of the growth

zone at various times after the gas composition has been switched. It takes a certain time before any change is seen at all, and after this the parabolic interface between the two packets of gas will gradually cross into the growth zone.

By considering the cross sectional area of the pipe occupied by the new gas packet, the average concentration of new gas type can be calculated:

$$C=C_o.\frac{t.v(p) - L}{t.v(p)} \qquad (4.12)$$

where: t = time,
C_o = initial concentration (100%),
C = measured concentration,
$v(p)$ = peak gas velocity,
L = distance from the start of the pipe.

For a 6mm diameter pipe and a flow rate of 4 $lmin^{-1}$, at a distance of 23.5cm, 1 second is required for the gas concentration to reach 95%, from a value of 0% at 0.05s. In the intervening time, at a growth rate of 0.05$\mu mmin^{-1}$, an interface width of 8Å would be obtained. This is adequate for many applications.

Another effect that limits interface abruptness is adsorption and desorption of gases from the pipe walls. The extent of this is difficult to determine, but the effect will scale with surface area and therefore with pipe length and diameter.

Entrance Effects

A further factor that affects both compositional uniformity and gas switching abruptness is the manner in which gas leaves the gas handling pipework and enters the larger diameter reaction tube. If the diameter change is too abrupt, the original narrow stream of gas will break away from the tube walls and continue into the wider tube areas as a gas plume. Recirculating stagnant gas zones are then left behind at the start of the reaction tube, and this leads to poorer interface abruptness. The plume of gas in the reaction zone may give rise to

localised cooling of the substrate, and also to an area of different compositional uniformity to the rest of the substrate.

Johnson et al have further shown that argon and nitrogen carrier gases exacerbate these effects due to their higher kinematic viscosities (ρ/η), compared to hydrogen and helium [87]. More recently, Mason et al have used titanium dioxide smoke studies to demonstrate that the angle of divergence between the small and large areas of the reaction tube should be less than 10° to avoid the above effects [88,89]. They have further shown that the length of glassware required can be reduced by using a curved cross sectional change of area with a parabolic profile.

Longitudinal Compositional Uniformity

The compositional uniformity of wafers parallel to the gas stream (longitudinal uniformity) is of equal importance to that obtained laterally. Some workers have reported very uniform epitaxy in this direction [90,91], whilst others have reported significant variations [69]. Figure (4.20) illustrates the photoluminescence uniformity obtained for a wafer of 1.55µm quaternary grown in the author's reactor. A wavelength range of 15nm is observed, comparable to other data in the literature [90]. Further studies of composition variations were undertaken upon epitaxial quaternary material of 1.3µm wavelength. Figures (4.21) and (4.22) show gallium (x) and arsenic (y) content, against distance along a wafer in the direction of gas flow. The temperature of the growth tube was varied from a water cooled 13°C, to an uncooled and therefore hot walled tube. The most uniform epitaxy was obtained for the coldest tube temperature, the trend in each case being an increase in phosphorus incorporation in the gas flow direction. The colder tube may result in a more uniform susceptor temperature so improving the uniformity of cracking ratio of arsine to phosphine. The sensitivity of growth to reactor temperature demonstrates a need to formulate group V precursors that have similar cracking efficiencies.

The gallium content of this epilayer appeared to peak at the edges of the wafer, this is often found to be the case. The reason for this effect is not clear, but the proximity of the reactor walls may

affect the substrate temperature and therefore influence the epitaxial growth or cause reactant depletion. Haspekto et al have demonstrated that reactor wall temperature significantly affects both the absolute composition and the uniformity of (GaIn)As epitaxy [92]. This was ascribed to vapour phase depletion of indium due to formation of a parasitic compound at an enhanced rate due to the warm reactor walls. The same authors reported that lowering the growth pressure drastically improved the compositional uniformity of their epitaxy.

Thickness Uniformity

The quaternary layer epitaxial thickness variation was ≃7% over a wafer width of 20mm for a 1μm thick layer. Since this appeared to be adequate for many applications, no research was undertaken into the factors affecting thickness uniformity when using the Bass cell.

Small samples of less than 5mm by 5mm often showed growth rates higher than larger areas of material from the same growth run. Care was therefore taken to avoid the use of small samples when investigating laser structures. This effect was probably due to localised preference for growth to take place upon substrates rather than exposed susceptor surfaces.

Table (4.1)... Growth conditions for $Ga_x In_{1-x} As_y P_{1-y}$ alloys

Alloy composition and wavelength	TMGa flow ($cm^3 min^{-1}$) (Bath temp = -7°C)	TMIn flow ($cm^3 min^{-1}$) (Bath temp = 50°C)	AsH_3 flow ($cm^3 min^{-1}$) (10% in H_2)	PH_3 flow ($cm^3 min^{-1}$) (10% in H_2)
x=.202 y=.440 λ = 1.18μm	5.1	66.4	9	300
x=.280 y=.607 λ = 1.3μm	7.5	66.4	16	300
x=.408 y=.880 λ = 1.55μm	5	16	104	300
x=.468 Ga(InAs)	10.4	33.8	80-200	-

Table (4.2): Mass flow rate tolerances required to achieve lattice matching as measured of $\Delta a/a = \pm 4.10^{-4}$ for (GaIn)(AsP) alloys.

Alloy	Ga ±%	Ga $\pm cm^3 min^{-1}$	In ±%	In $\pm cm^3 min^{-1}$	As ±%	As $\pm cm^3 min^{-1}$	P ±%	P $\pm cm^3 min^{-1}$
λ=1.18μm	2.5	5.1 ±0.13	0.6	66.4 ±0.4	1.1	9 ±0.1	0.8	300 ±2.4
λ=1.3μm	1.7	7.5 ±0.13	0.7	66.4 ±0.46	0.74	16 ±0.11	1.1	300 ±3.3
λ=1.55μm	1.4	5 ±0.07	0.95	10 ±0.095	0.72	104 ±0.75	6.2	300 ±18.6
(GaIn)As	1.1	10.4 ±0.114	0.94	33.8 ±0.318	-	-	-	-

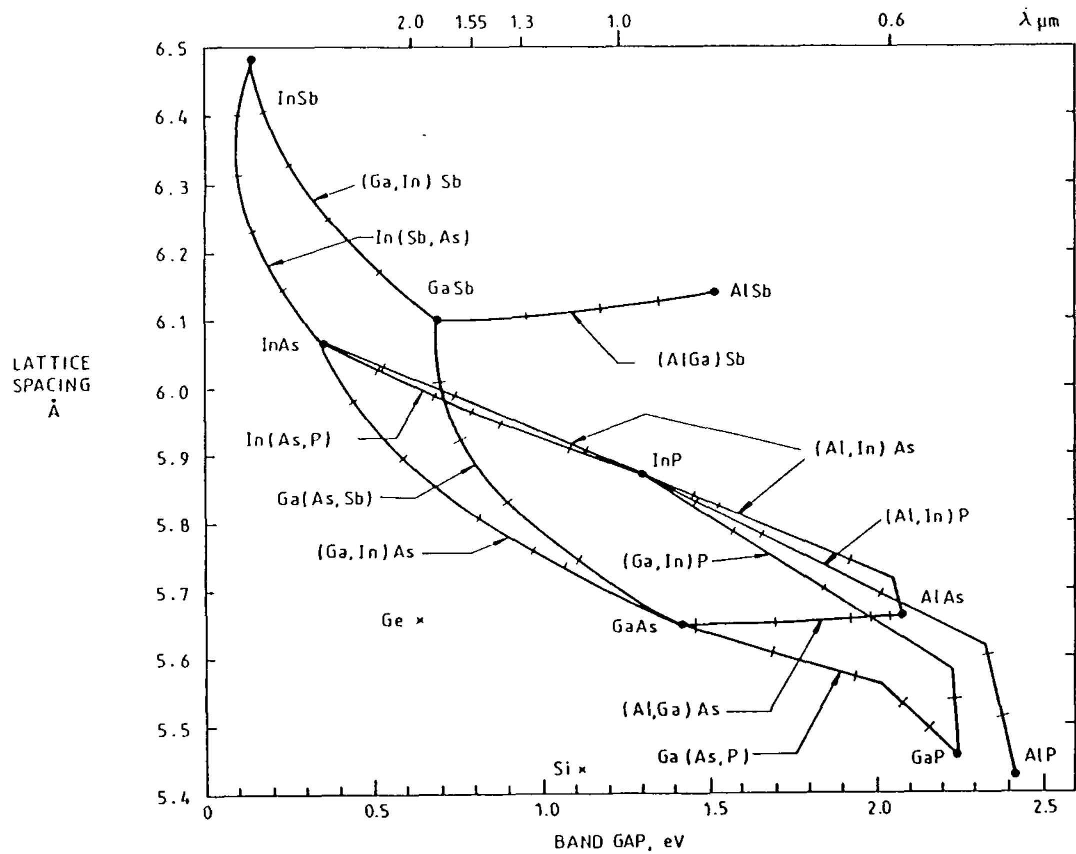

Figure (4.1): Composition contours as a function of band-gap, wavelength, and lattice spacing for III/V compounds. The areas bounded by ternary contours represent compositions of quaternary compounds.

X 800

Optical micrograph of good quality epitaxial (GaIn)As.

Figure (4.2)

Optical micrograph of poor quality epitaxial (GaIn)As.

X 800

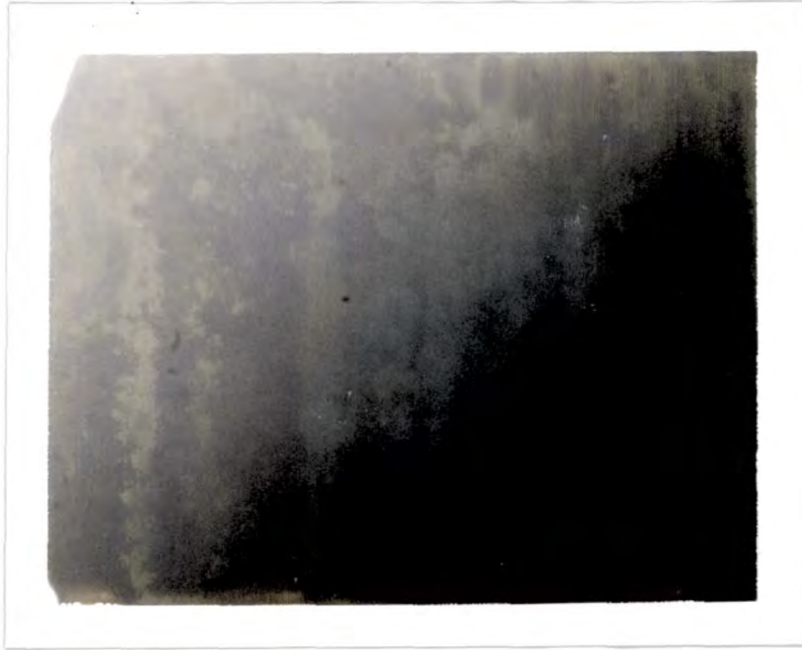

X 800

Normal arsine over-pressure.

Figure (4.3) Optical micrographs of epitaxial layers of (GaIn)As.

Reduced arsine over-pressure.

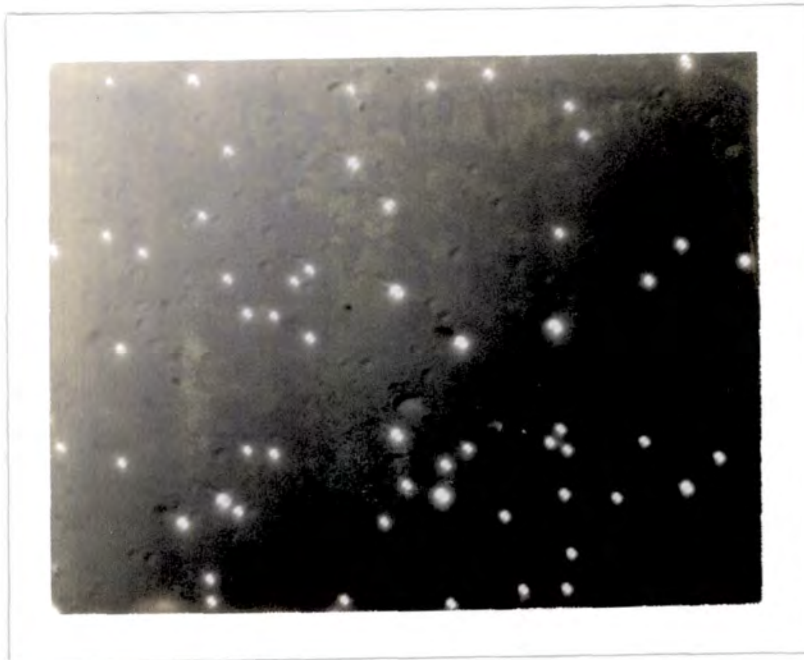

X 800

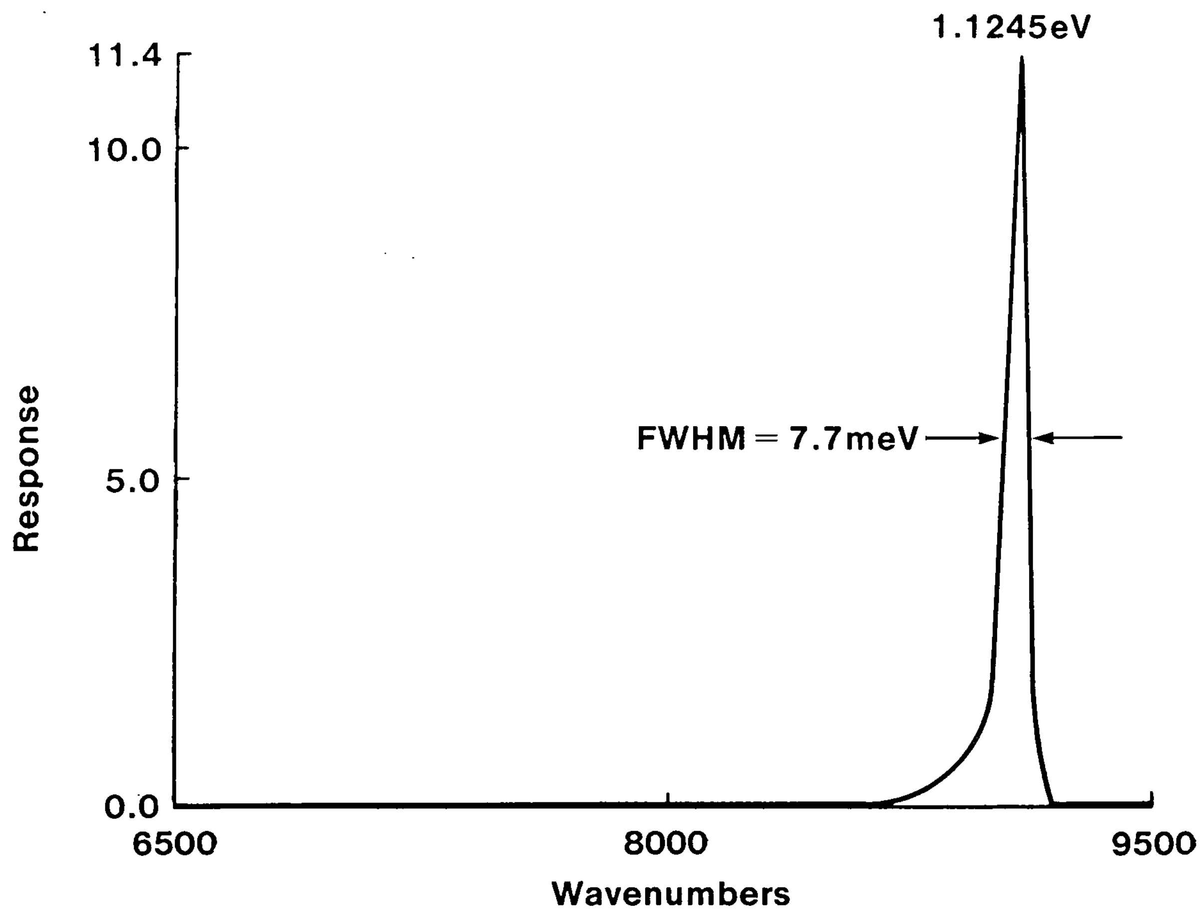

Figure (4.4): 77K photoluminescence emission from a 1.3μm quaternary layer.

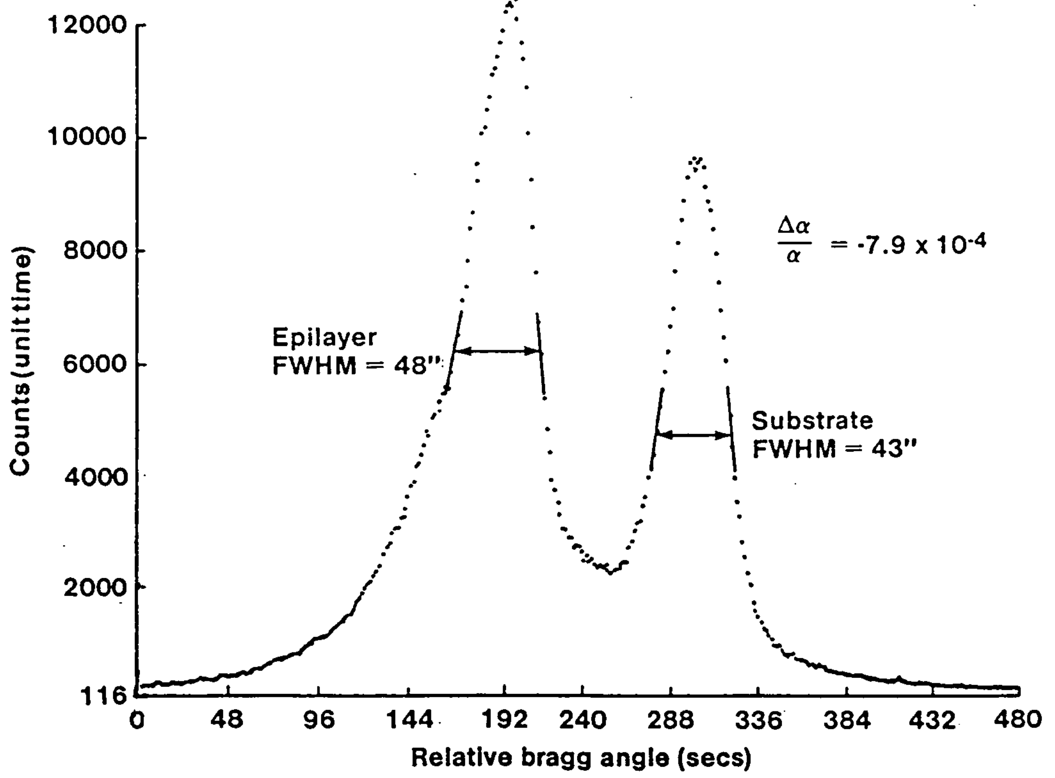

Figure (4.5): Double crystal x-ray rocking curve on a 1.18μm emission quaternary layer.

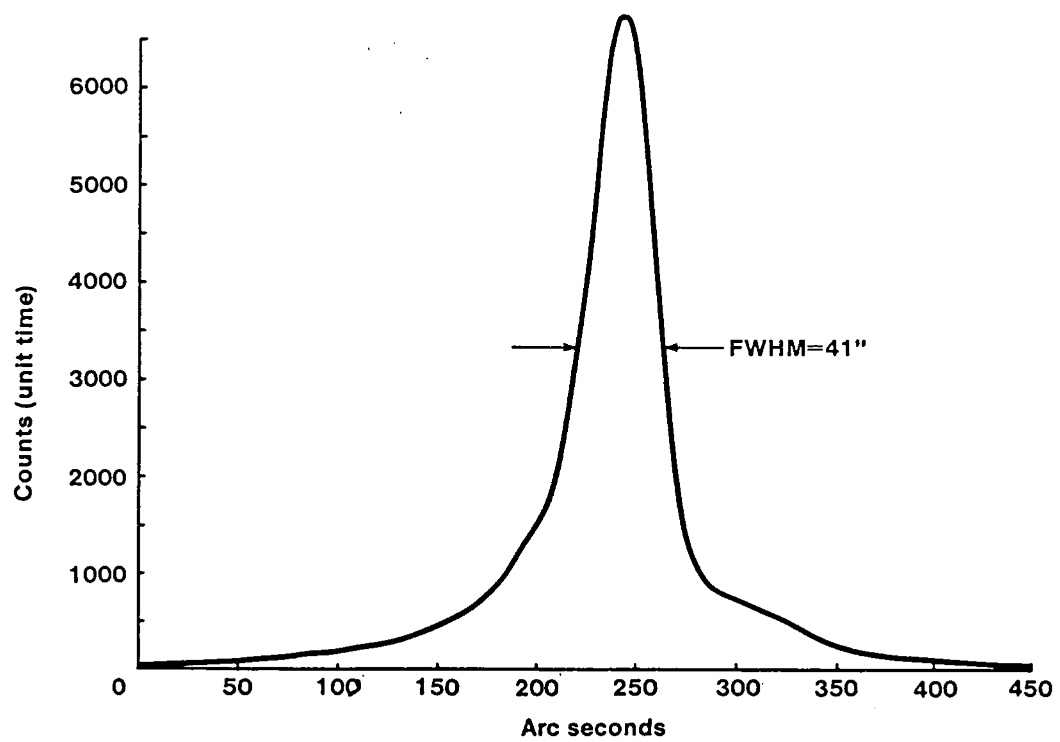

Figure (4.6): Double crystal x-ray rocking curve on a 1.3μm emission quaternary layer.

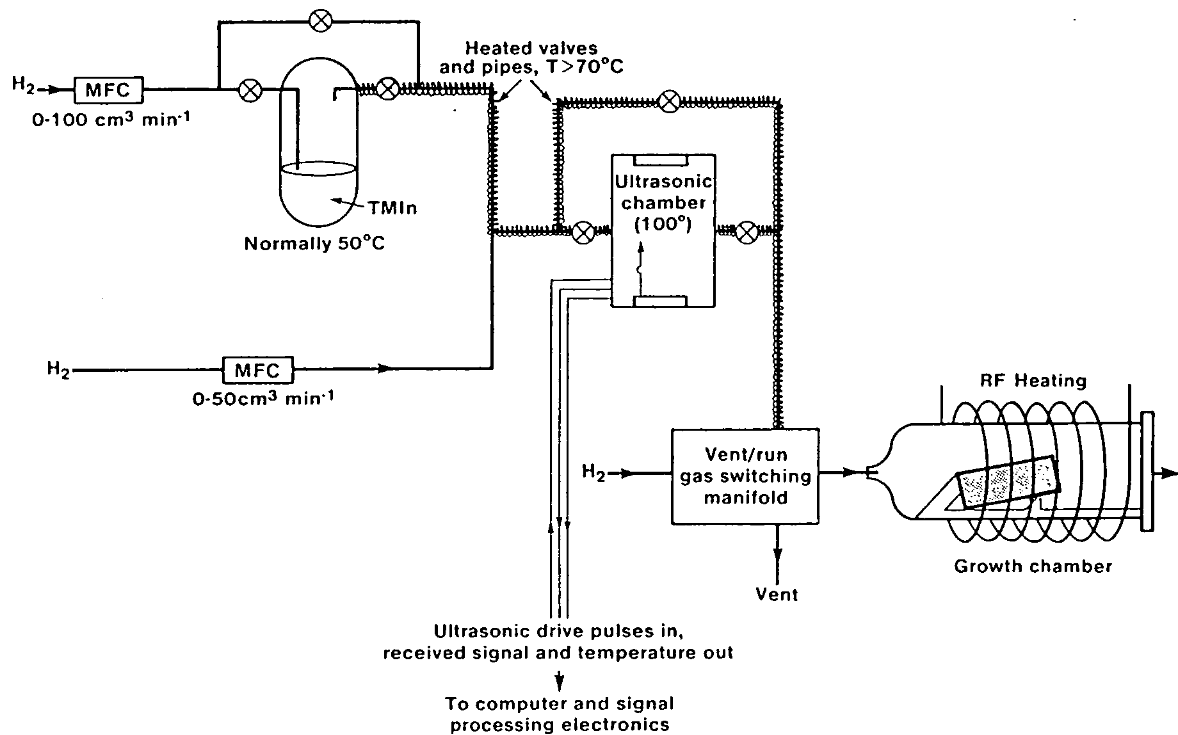

Figure (4.7): Layout of the trimethylindium line, incorporating an ultrasonic reagent concentration monitor, on the author's reactor.

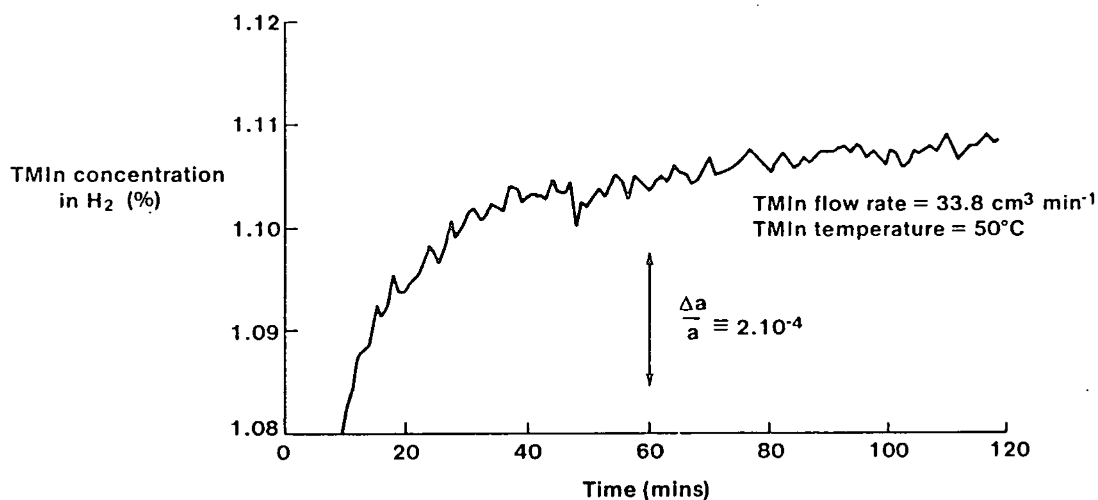

Figure (4.8): Time response of trimethylindium vapour pressure as measured through the ultrasonic monitor with a source temperature of 50°C. The hydrogen flow was switched through the trimethylindium source at 0 minutes. Note the heavily offset origin on the vertical axis.

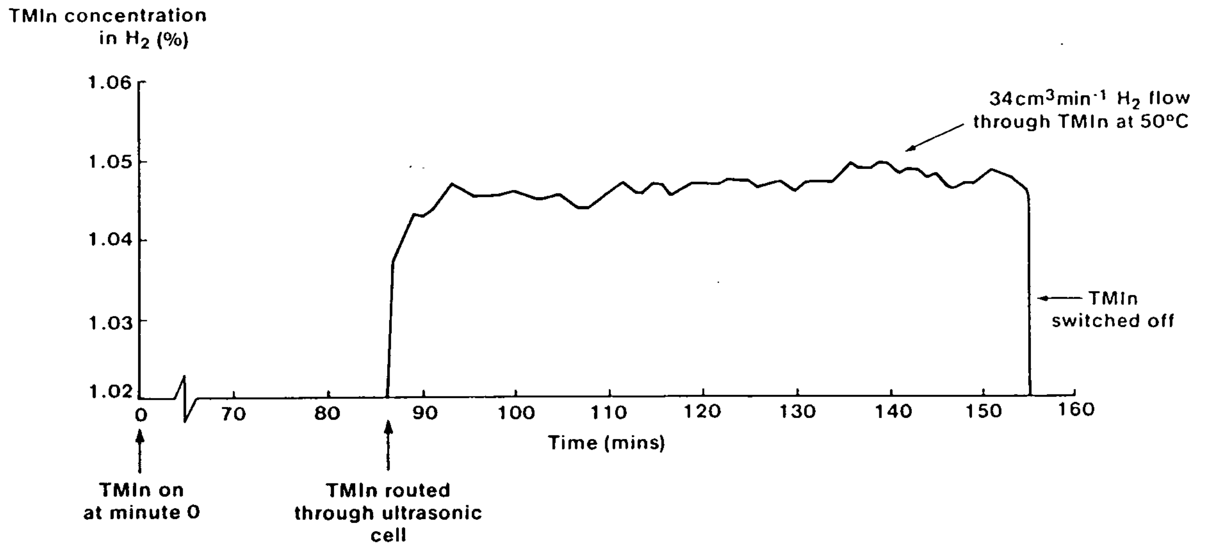

Figure (4.9): Time response of the ultrasonic cell to a flux of trimethylindium that had already reached equilibrium within the source and with the reactor pipework.

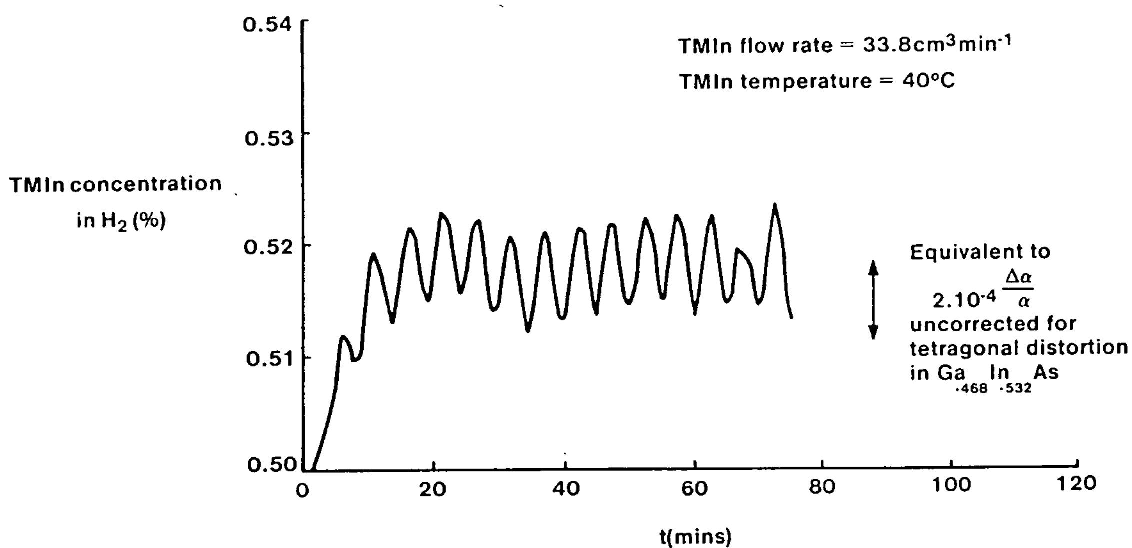

Figure (4.10): Time response of trimethylindium vapour pressure as measured through the ultrasonic monitor with an unstable source temperature of 40°C. The hydrogen flow through the trimethylindium source was switched on at 0 minutes.

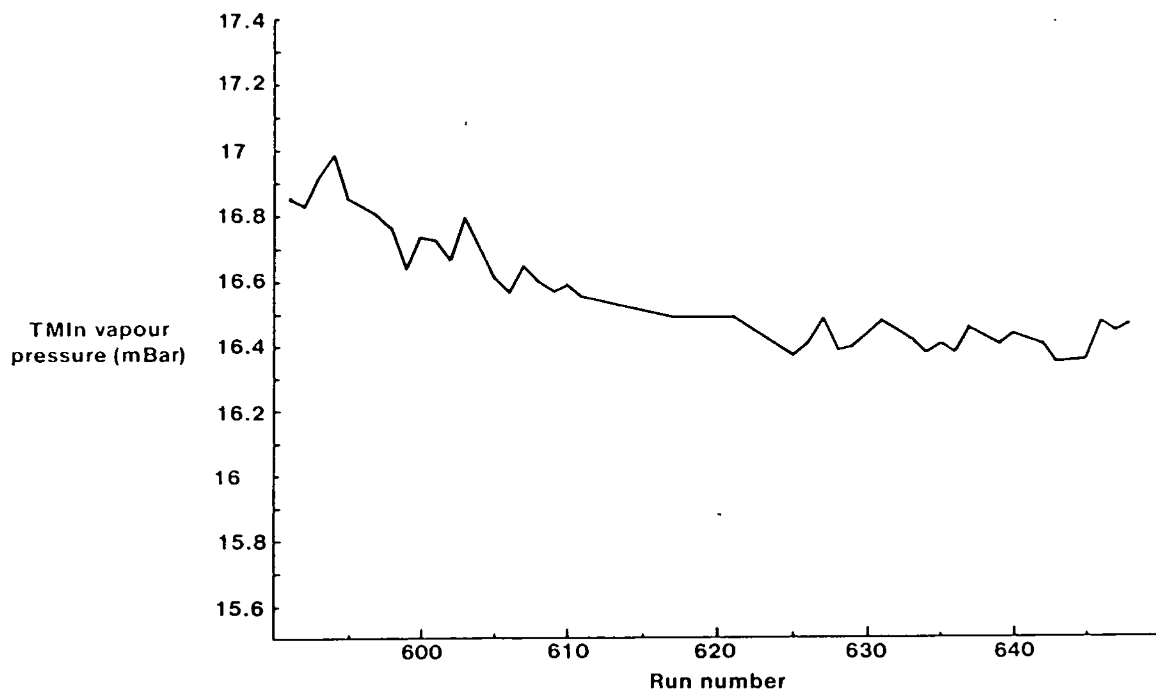

Figure (4.11): Variation of trimethylindium vapour pressure as measured through the ultrasonic chamber, from growth run to growth run for the same source. The vapour pressure values were corrected for variations in atmospheric pressure.

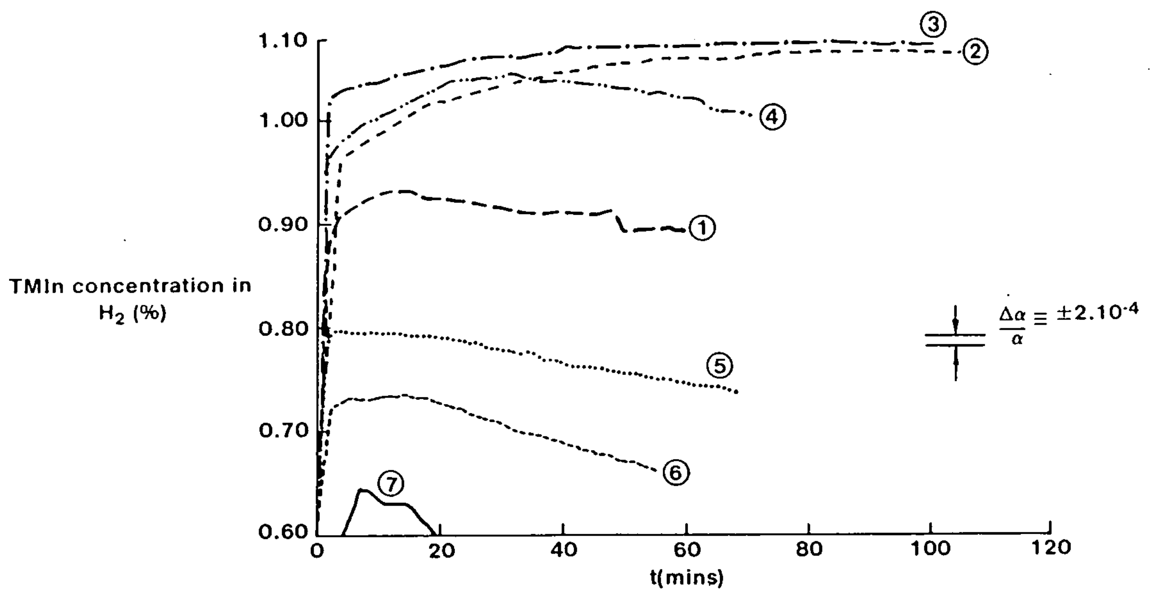

Figure (4.12): Time response of trimethylindium vapour pressure for consecutive growth runs prior to total exhaustion of the source:

(1): low vapour pressure giving rise to suspicion of the state of the source.

(2)(3): response after melting and recrystallising the trimethylindium.

(4)(5)(6): return to low vapour pressures.

(7): total collapse of output vapour concentration. The source was weighed subsequently and found to be empty.

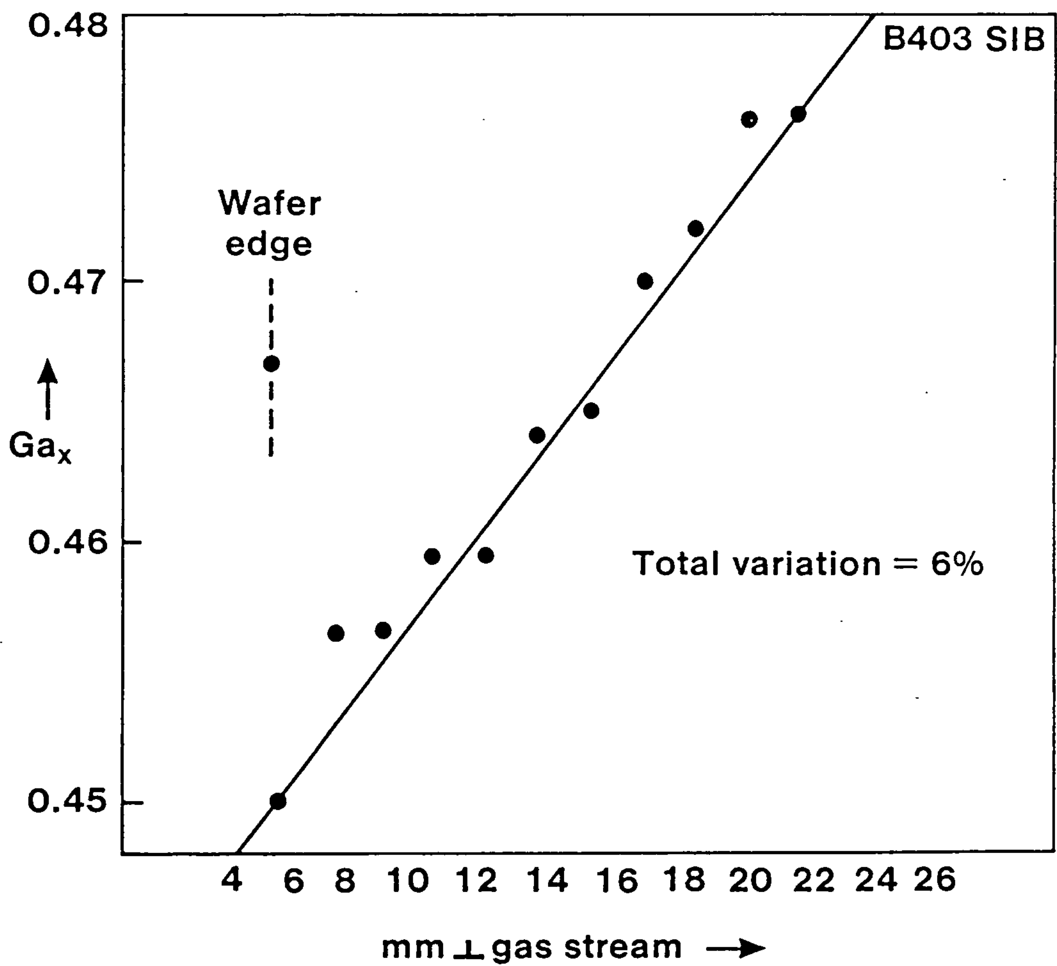

Figure (4.13): Composition of (GaIn)As as a function of position across the gas stream.

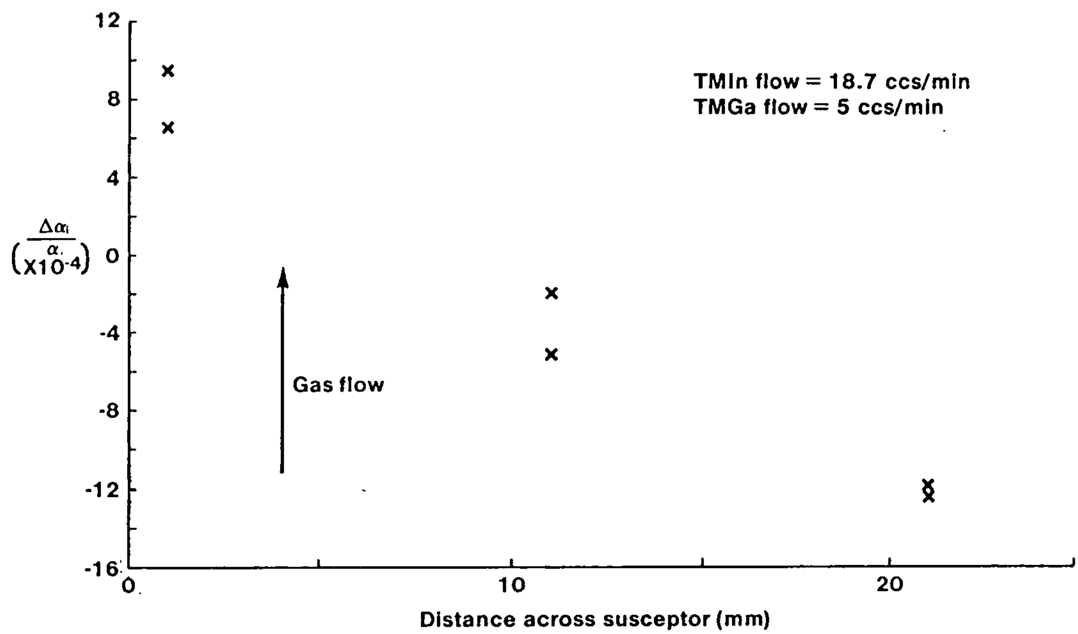

Figure (4.14): Lattice mismatch of (GaIn)As as a function of position across the gas stream, as determined by x-ray measurements. The position of the trimethylgallium inlet to the switching manifold was moved with respect to the growth run used for figure (4.13).

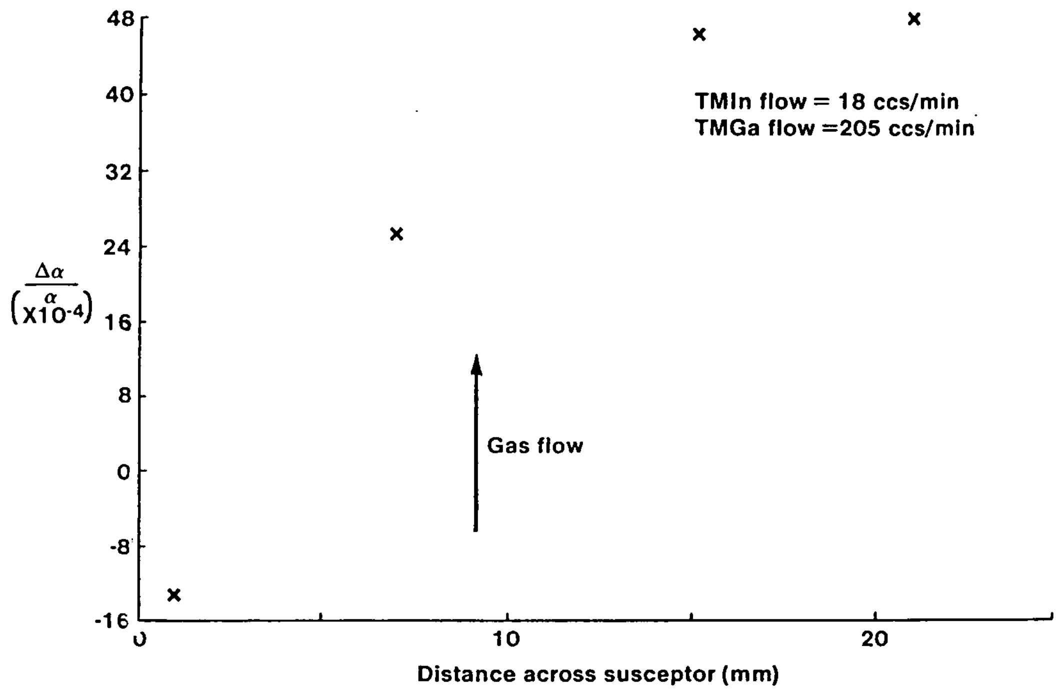

Figure (4.15): Lattice mismatch of (GaIn)As as a function of position across the gas stream with an increased injection velocity of trimethylgallium vapour.

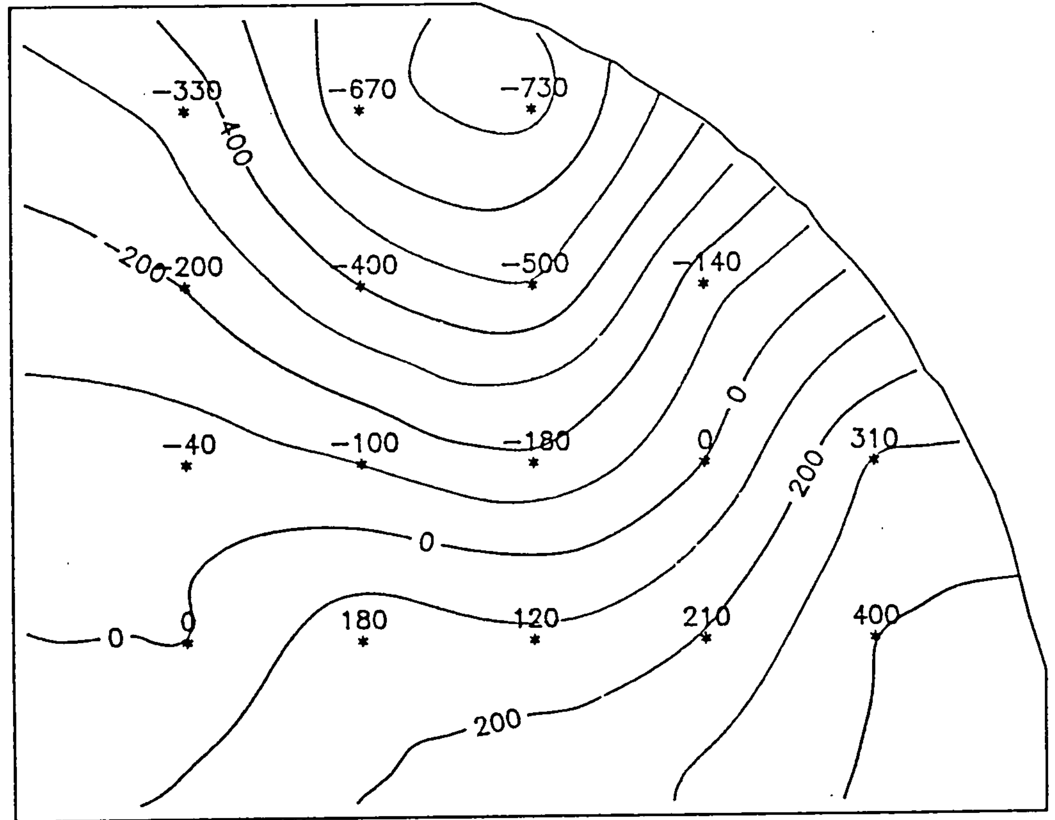

Figure (4.16): Lattice mismatch (ppm) contour map for a layer of (GaIn)As grown using a new gas injection manifold with protruding inlet pipes.

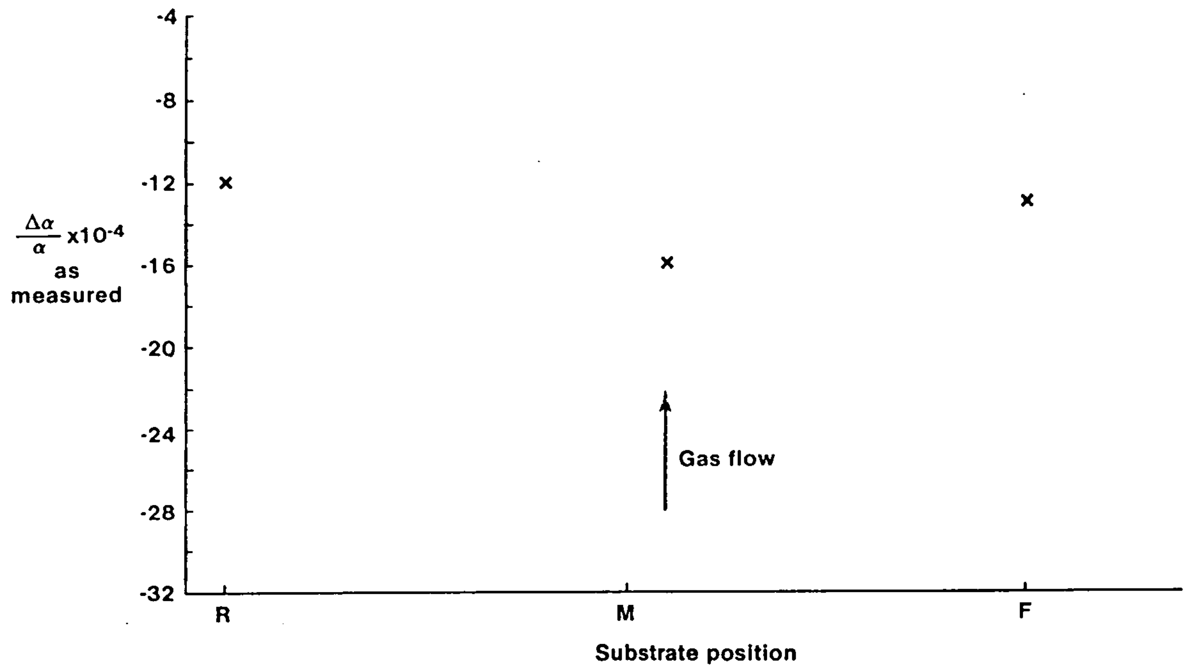

Figure (4.17): Lattice mismatch as a function of position across the gas stream for a layer of (GaIn)As grown using a high impedance gas mixing nozzle.

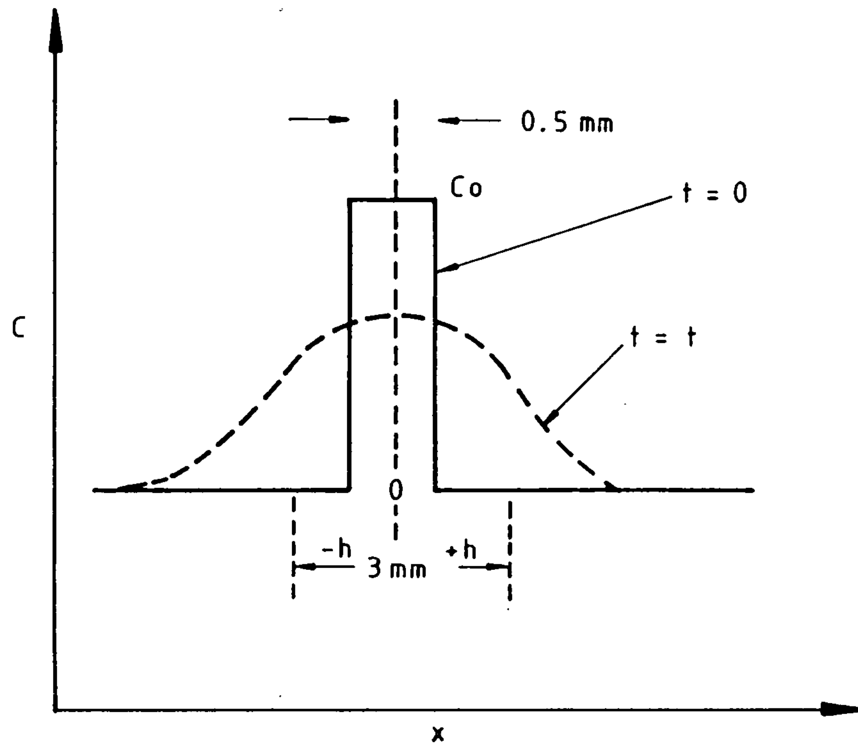

Figure (4.18): Approximated sideways diffusion of trimethylgallium in hydrogen across the diameter of a pipe. D is $\approx 0.4 cm^2 s^{-1}$ for trimethylgallium, based upon similar molecular structures and weights. Only after 0.1s will the concentration C at x=0 and at x=±1.5mm, vary by less than 1.5%. In a 6mm diameter tube, with a gas flow rate of 3.5l/min, a segment of gas will have travelled 20cm in 0.1s.

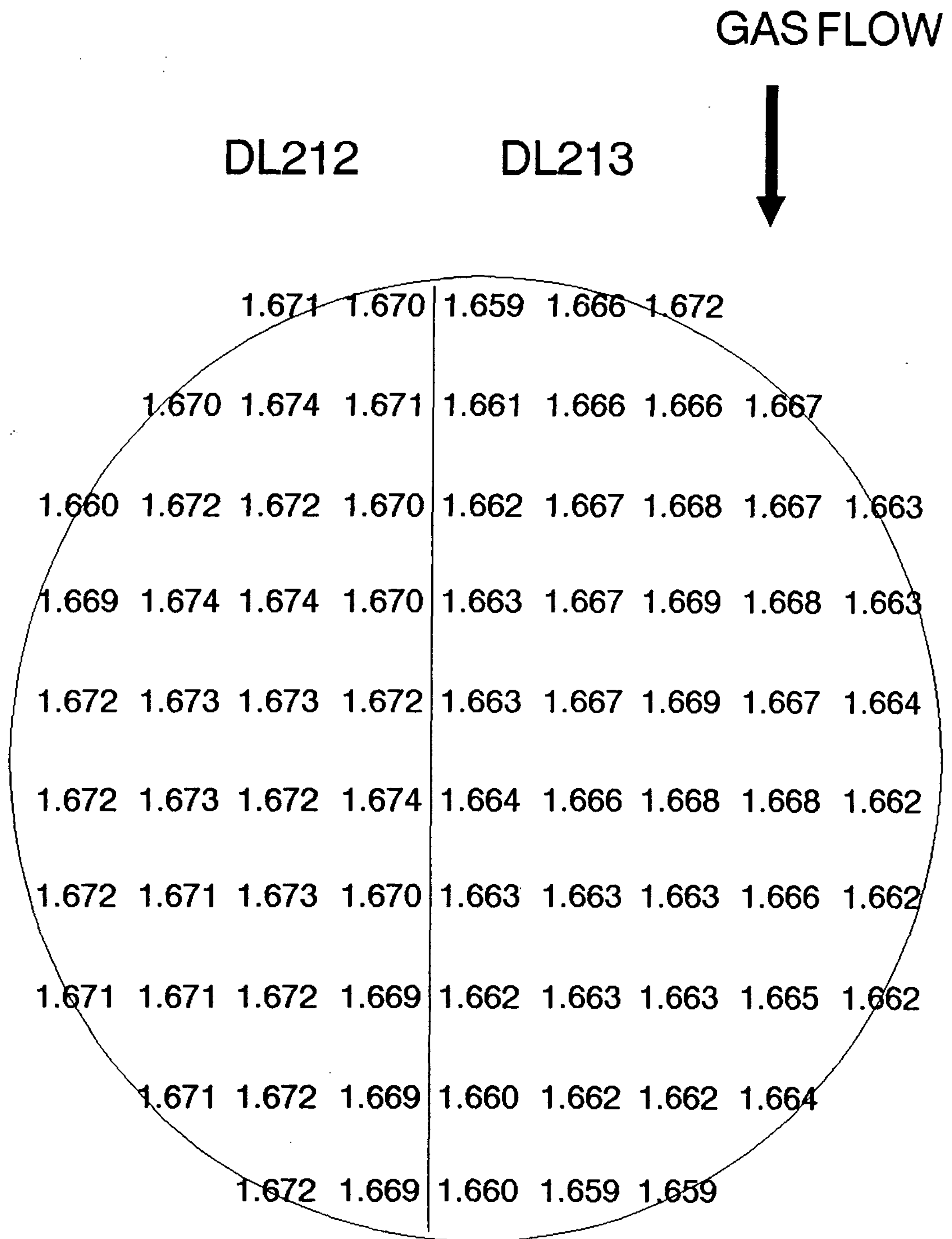

Figure (4.19): Photoluminescence map of two half two inch diameter wafers of epitaxial (GaIn)As grown in a dual line MOVPE reactor.

Chapter 5

Impurity doping of InP and (GaIn)As

The doping of InP and (GaIn)As using hydrogen selenide, silane and dimethylzinc is described and the use of other dopants is reviewed. The rôle of atomic hydrogen in InP is discussed.

The majority of practical electronic and opto-electronic semiconductor devices require either p or n-type doping of the various semiconductor layers. Depending upon the overall technique, doping may occur as part of the growth process, or by subsequent diffusion or ion implantation into the structure after growth. MOVPE has the advantage that a wide variety of dopants can be grown into the epitaxial layers, and a wide range of carrier concentrations obtained.

For example, semiconductor lasers grown by MOVPE usually incorporate a highly p-doped capping layer which when metallised gives a low resistance contact. However, for the growth of such structures by LPE, a highly doped cap can only be obtained by a post growth zinc diffusion stage, an extra process is therefore needed with its consequent effect upon reproducibility and yield.

n-type Dopants

The elements available for the n-type doping of III-V materials are those in group VI of the periodic table (sulphur, selenium, tellurium) which are incorporated onto the group V lattice sites; and those in group IV (silicon, tin) which are incorporated onto the group III metal sites. Carbon is considered to be both a p and an n-type dopant in GaAs but in InP it does not usually feature highly as an impurity. The exact choice of dopant is dependent upon the doping level required, its diffusion coefficient in the material, and its ease of pyrolysis during MOVPE growth.

Silane

Silane is a pyrophoric gas when mixed with air. It also forms white silica dust when in contact with water. It is essential therefore, when using this particular dopant, to ensure that the apparatus is leak tight and dry. Failure to do this leads to silica dust coating pipework and valves, and eventually leads to component malfunction. For these reasons many workers have preferred to use other dopant sources, however silicon has the advantage of having a low diffusion coefficient and the ability to grow layers with sharply graded doping profiles. Although silicon should be able to be incorporated as an acceptor upon the group V lattice site, there are no such reports in the literature of any such behaviour in InP and (GaIn)As.

The author has undertaken doping studies of InP and (GaIn)As using a 400vpm mixture of silane in hydrogen. Figure (5.1) shows the log(carrier concentration) against log(dopant flow rate) curves for the incorporation of silicon into InP and (GaIn)As. The graph slopes are close to unity within experimental error for both materials, and agree with data obtained by other workers [93,94,95,96]. The silicon is incorporated much more easily into InP than (GaIn)As. This is a general trend for n-type dopants, (GaIn)As behaving in a similar manner to GaAs. An electrochemical profile of a (GaIn)As layer grown using different fluxes of silane is shown in figure (5.2), each of the different doping fluxes are clearly resolved. The final part of the epitaxial structure was grown with no silane present and was fully depleted during the electrochemical profiler measurement. This indicates that a low doping level was rapidly obtained upon switching off the dopant flow, and further illustrates the low diffusion levels obtained when using silane as a dopant.

The uniformity of doping level obtained using silane appears to be reasonable, very flat doping profiles through the material were obtained, and a series of measurements upon a 2cm square layer of InP doped to $n=1.17cm^{-3}$ had only a 7% variation in doping level. The variation that does occur may be due to fluctuations in susceptor temperature.

Figure (5.3) shows an electrochemical profile through an InP epitaxial layer grown with a constant flux of silane flowing, and with the growth temperature varying in four steps from 600°C to 750°C. The doping level increases markedly with temperature and further, the growth rate at 750°C has diminished to half that at the normal growth temperature of 650°C. A strong feature of this profile is the sharply defined steps in doping level, again indicating a low level of silicon diffusion during subsequent growth.

The doping behaviour has also been investigated as a function of growth rate. Figure (5.4) shows an electrochemical profile through an epitaxial layer of InP where the silane flux was kept constant, and the trimethylindium flux stepped to change the growth rate. The doping behaviour was found to be inversely proportional to the growth rate.

Finally the effect of varying the V/III ratio was investigated. A change of V/III ratio of x4 produced a doping level change of only 40%. The growth of InP at low V/III ratios tended to yield poor quality material due to phosphorus loss, and it is not clear to what extent this affected the doping levels in the material. Clawson [96] found that the doping level obtained when using silane in InP is independent of the V/III ratio. The above experiments indicated that many of the silicon atoms reaching the growth interface were incorporated into the epitaxial layer. The rate limiting step in the doping of InP using silane appeared to be the pyrolysis of the silane.

The incorporation of silicon can therefore be described by the equation:

$$n = C.F^{1} .V/III^{\sim 0}.GR^{-1}.e^{-E_a/kT_g} \qquad (5.1)$$

where: n = donor concentration in the epitaxial layer,
C = constant,
F = flow rate of silane
V/III = V/III gas phase ratio,
GR = growth rate,
E_a = activation energy,
k = Boltzman's constant,
T_g = growth temperature (K).

The equation is of the same form as that derived for the background impurity doping of InP in chapter (3). In this case, the value of E_a is 1.8-2.2eV, depending upon whether the results from the electrochemical profiles are corrected for the observed variations in growth rate. This compares with an activation energy of 2.2eV for silicon background doping of InP determined in chapter (3).

Disilane

As a result of the temperature sensitivity of doping using silane, Kuech et al proposed the use of disilane, Si_2H_6, as a silicon source [97]. This gas has a lower pyrolysis temperature than silane, and Kuech obtained temperature invariant doping of GaAs and (GaAl)As. Woelk et al however, did not find temperature invariant behaviour when doping InP using disilane, and obtained an activation energy of 1.2 $\pm$0.4eV [98]. All of the above workers found the growth rate dependence using disilane to be similar to silane, and the dependence of doping level upon disilane flux for GaAs was found to be linear. However for the doping of InP and (GaIn)As a log(n) - log(flow) slope of 0.75 and 1 were found respectively [98]. It is therefore not clear whether disilane offers any advantages over silane for the doping of InP and its alloys.

Hydrogen selenide

There is little in the literature regarding the doping of InP using hydrogen selenide. Kawabata et al have reported its use in low pressure MOVPE and found high doping efficiencies in InP with respect to silane [99]. The author has used a nominally 50vpm concentration of the gas in hydrogen to dope InP. An electrochemical profile through a layer where the dopant flux was varied is shown in figure (5.5). Very high concentrations ($n > 10^{19}cm^{-3}$), were obtained. It is not clear in retrospect whether this unexpected result was due to the gas company supplying the wrong gas concentration, or if the relevant mass flow controller was faulty. The presence of structure in the electrochemical profile at such high doping levels, may indicate that hydrogen selenide, when used correctly, may be a suitable dopant for InP.

There are some opinions that the gas exhibits a memory effect and can cause unwanted doping after use. This problem may be eliminated with the modern use of vent run switching manifolds which have low surface areas onto which the gas can adsorb.

Hydrogen sulphide

Hydrogen sulphide is another commonly used MOVPE n-dopant, though little is published in the literature. Spier et al have reported that a 10% mixture of hydrogen sulphide in hydrogen gave satisfactory doping of InP, when a growth temperature of 650°C was used [100]. Extremely low flow rates were used ($< 1\ cm^3min^{-1}$), and more accurate control may be obtained with the use of a more dilute gas mixture. The doping level was found to decrease with growth temperature due to the volatility of sulphur.

Nelson et al have reported hydrogen sulphide doping with donor concentrations of $n=1.10^{16}-1.10^{18}cm^{-3}$ [101]. A linear relationship for the incorporation of sulphur as a function of hydrogen sulphide flow was found.

Diethyltelluride

Diethyltelluride has been used for the n-type doping of InP [94,96], and for the doping of $Ga_{0.5}In_{0.5}P$ [95]. The results from these workers are contradictory for the doping of InP, Hsu et al indicating super-linear doping dependence upon dopant flow rate [94], and Clawson indicating a linear dependence [96]. Interestingly Clawson has also reported that the incorporation of tellurium increases with growth temperature, and is inversely proportional to both the growth rate of InP and the phosphine flow rate. It appears from these results that the incorporation mechanism may relate to the number of phosphorus vacancies available.

Tetraethyllead

Tetraethyllead - $Pb(C_2H_5)_4$ has been used as an n-type dopant for DX centre investigations of (AlGa)As [102].

p-type Dopants

p-type doping of InP is usually achieved using the group IIb elements zinc or cadmium. The group IIa elements magnesium and beryllium, and also manganese have been used, though not extensively. Beryllium and its compounds are highly toxic and so are unlikely to become widely used. In each case, substitution of a group III lattice atom takes place to give an acceptor.

Dimethylzinc and diethylzinc

Zinc is the most commonly used MOVPE p-type dopant. Either dimethylzinc or diethylzinc are normally used, the alkyl group being chosen to match the other metal sources being used. Dimethylzinc has the higher vapour pressure, and is normally obtained as a high pressure vapour mixture in hydrogen. Diethylzinc is usually used in a conventional bubbler arrangement. The few workers that have compared both zinc alkyls, have reported similar incorporation data for the two sources. Zinc has many undesirable features as a p-type dopant, notably its high diffusion coefficient in InP, however no other element has yet been proved to be as versatile.

The author has used dimethylzinc exclusively. A low pressure mixture of the alkyl in hydrogen was prepared by subliming vapour from a cooled, solid source into an evacuated cylinder, which was subsequently back-filled with purified hydrogen. Since vapour pressure data upon solid dimethylzinc was unavailable, the concentration of the mixture was estimated to be 750vpm by comparison with a commercially prepared mixture. Mass flow rates from 1 to $100cm^3min^{-1}$ were used. Due to the importance of hole concentrations to device performance, it was decided to study p-type doping of InP in depth. Unfortunately, it was soon realised that the stepped doping structures successfully used to speed the study of silane doping of InP, could not be used with dimethylzinc due to the high diffusion coefficient of zinc causing smearing of the profiles. Some attempts were made to prevent zinc diffusing by the use of buffer layers of undoped InP, silicon doped InP or (GaIn)As. However this approach was unreliable due to difficulties encountered with the electrochemical profiling of

multiple p-n structures. It was therefore necessary to grow many individual layers of p-type InP which were subsequently assessed by electrochemical profiling and by Hall measurements. All of the epitaxial layers were cooled to ~100°C under an atmosphere of hydrogen, phosphine and dimethylzinc.

Figure (5.6) illustrates the variation of hole concentration as a function of normalised dimethylzinc flow into the reactor, all other growth conditions remaining constant. Saturation can be seen to occur at $p=10^{18}cm^{-3}$ for growth at 650°C. This value is lower than expected for InP, and is probably due to the hole concentrations sloping convexly downwards from the substrate interface to the surface. The Hall measurements will have averaged the overall hole concentration, and the electrochemical profile values were taken from the middle of the plots. The reason for the surface drop in hole concentration remained unknown for several years, but is explained in a later section.

The gradient of the unsaturated log(hole concentration) - log(dopant flux) curve of figure (5.6) is 0.5. This indicates that the hole concentration $\propto$ dopant flux$^{1/2}$. This data agrees with the early data of Nelson et al who were also able to confirm that the atomic zinc level as assessed by SIMS, was related to the dopant flux$^{1/2}$ [103]. A similar relationship was found by Rose et al [104]. However Hsu et al noted a super-linear dependence of hole concentration upon dopant flux [94].

More recently the author has noted that the relationship has changed to a linear one following major reactor modifications. Attempts to find the reason for this have been unsuccessful, however a similar change has been noted by other workers and is not understood.

Figure (5.7) shows the hole mobility as a function of hole concentration for the above samples. The results compare well with the data compiled by Wiley [105], except at low doping levels where the layers were compensated. This was due to the n-type background doping level in these early epitaxial layers being > $10^{16}cm^{-3}$ as a result of the quality of the trimethylindium then available.

A further series of zinc doped layers was grown to evaluate the effect of growth rate upon dopant incorporation. Figure (5.8)

indicates that the hole concentration as measured by Hall and electrochemical profiler, was invariant with growth rate change. However the growth rate was altered by varying the trimethylindium flux and therefore the V/III ratio will also have varied. This result indicates that the incorporation mechanism for zinc into InP is different from that of silicon.

There have been suggestions that the presence of zinc during the growth of InP layers increases the growth rate, though no data on this effect has been published. Figure (5.9) shows a plot of growth rate for samples grown with different amounts of dimethylzinc flux. No trend can be observed, and it is concluded that the growth rate is not influenced by the presence of the dopant.

Figure (5.10) shows the relationship between the log(hole concentration) and reciprocal growth temperature, all other growth conditions remaining constant. A linear fit and an activation energy of -1.55eV was obtained. The lower levels of zinc incorporated at high temperatures indicate that the zinc readily evaporates from the surface. It is concluded that the majority of the dimethylzinc reaching the hot zone above the susceptor is cracked, and the limiting factor controlling doping levels, is the vapour pressure of zinc needed to maintain equilibrium over the growing surface. The growth rate was found to be a factor of two lower for growth at 750°C compared to that at 650°C. Since the growth rate did not appear to influence the doping level, this effect could be ignored when determining the activation energy.

Dimethylcadmium

The high diffusion coefficient of zinc in InP has led to studies of other p-type dopants with lower diffusion coefficients, the most promising of which is cadmium. Nelson et al, Blaauw et al, and Spier et al have all reported cadmium doping of InP using dimethylcadmium [100,103,106]. Controllable doping was achieved in the range $p=10^{17}$-$10^{18}cm^{-3}$, and a linear relationship between dimethylcadmium flux and hole concentration was reported [103,106]. When used at low pressures, the dopant flow had to be increased in proportion to the change in pressure, and the hole concentration was found to decrease with growth

temperature [106]. This indicated that cadmium is a volatile dopant in the same manner as zinc. However, for high doping levels and for use at low pressure, degradation of surface morphology occurred. Blaauw has indicated that CdP particle formation may have taken place, and examination of the data shows that a 5:1 cadmium : indium mole fraction ratio was necessary for the high doping levels. This data infers that whilst cadmium may be of use as a dopant at low levels, at higher doping levels zinc remains preferable.

Magnesium doping

Magnesium has been considered as a possible p-type dopant. Both Blaauw et al and Nelson et al have reported a super-linear dependence of hole concentration upon the flow rate of bis(methylcyclopentadienyl) magnesium - MCp_2Mg, and (bis)cyclopentadienylmagnesium - Cp_2Mg respectively [103,107]. Blaauw also found that at high doping levels, $>10^{18}cm^{-3}$, the magnesium became electrically inactive. Further, the magnesium was seen to diffuse up to 40µm deep into iron doped substrates. These factors indicate the unsuitability of magnesium as a p-type dopant for InP.

Manganese doping

Manganese doping of InP was reported by Huang et al, using tricarbonyl(methyl cyclopentadienyl)manganese - $(CO)3CH_3C_5H_4Mn$ [108]. Doping levels of $p=7.10^{14}-2.10^{16}cm^{-3}$ were achieved for growth at 600°C, and a linear relationship between hole concentration and doping flux found. However a high ionisation energy was reported, with the manganese giving rise to a deep acceptor level, with only 25% of the atoms being electrically active. Spier et al have reported very sharp doping profiles using manganese [100].

Hydrogen passivation of acceptors in p-type InP

During the course of doping and device studies using zinc doped III-V compounds, it was found that atomic hydrogen could cause passivation of acceptors in InP, and this resulted in a reduced electrical activity of the layers. These phenomena are described in more detail in the following sections.

Hydrogen Incorporation in p-InP/p+(GaIn)As Structures

An essential step in the fabrication of semiconductor laser structures is the provision of a p-passive InP layer followed by a contacting layer. The latter is necessary because it is difficult to form a low resistance metal contact to p-type InP. LPE grown structures normally use a quaternary alloy contact layer that is subsequently doped highly p-type during a zinc diffusion stage prior to metallisation. This diffusion step can be eliminated when growing structures by MOVPE since (GaIn)As can be doped p-type with hole concentrations as high as $10^{20}cm^{-3}$. Material doped above $p=10^{19}cm^{-3}$ can be used to form excellent low resistance contacts following metallisation.

The zinc doping of InP and (GaIn)As has been previously described (figure 5.6), and these doping level calibrations were used to grow heterostructures consisting of 2μm thick zinc doped InP layers followed by 0.2μm thick highly zinc doped (GaIn)As layers (figure 5.11). Whilst the doping of the ternary layer was satisfactory, the hole concentration in the p-InP layer was found to be markedly lower in the heterostructure when compared to the level expected from the doping calibration obtained upon simple p-InP layers; conditions of growth rate, temperature and doping flux being identical. This result is illustrated in the electrochemical profile of figure (5.12). Early suspicions that the electrochemical profiler was giving erroneous results due to the presence of the p^+(GaIn)As layer, were dispelled by re-measuring the samples once the (GaIn)As layer had been removed using nitric acid. The results were further confirmed by making Hall measurements upon the combined structures, and with the (GaIn)As removed. An unusual effect had therefore been uncovered - the disappearance of zinc dopant in InP, caused by the addition of a

p^+(GaIn)As layer.

Zinc was known to have a high diffusion rate in p-type materials, diffusing by the substitutional-interstitial diffusion mechanism [109]. For a while it was considered that the zinc was moving out of the InP layer and into the (GaIn)As layer during the growth of the latter. However this mechanism was thought to be unlikely due to the concentration gradient of zinc between the two layers being in the opposite direction to this movement. SIMS analysis upon these layers revealed that the zinc concentration in the p-InP parts of the heterostructures was around $10^{18}cm^{-3}$, this value being slightly higher than that expected from the calibration experiments. It was therefore concluded that out-diffusion of the zinc had not occurred, but instead that the hole concentration had fallen to the $1\text{-}3.10^{17}cm^{-3}$ level, due to reduced electrical activity of the zinc in the InP. The SIMS levels were carefully compared against zinc implanted p-InP standards.

Reduced electrical activity of the material could either have been caused by compensation of the acceptors with a donor species, or by the zinc atoms residing upon lattice sites other than indium sites. It was thought that interstitial zinc could act as a donor and additionally cause compensation [110]. The presence of known donor species such as silicon and sulphur which could cause compensation was eliminated by further SIMS analysis. It was decided that the zinc was somehow the cause of the compensation, and that redistribution of the zinc in the lattice might be achieved by annealing the layers after growth.

Heterostructures were thermal pulse annealed at 800°C for 5s, a silicon nitride cap was used to prevent phosphorus loss from the surface of the material. Figure (5.13) shows an electrochemical profile of such an annealed sample, and indicates that the electrical activity of the zinc doped InP layer had recovered to the same level as that obtained during the SIMS analysis, and to a slightly higher level than expected from the calibration experiments. It therefore became clear that the zinc was either being displaced within the InP layer during the growth of the (GaIn)As cap layer, and that the material was being reordered during the anneal stage, or that some unknown donor was being incorporated during the growth process and expelled during the anneal stage. The former was thought less likely

since devices fabricated from this material worked well, with excellent reliability, implying that no significant crystal imperfections existed within the InP.

A search for possible compensating donors which had not previously been considered, gave rise to the suggestion by Antell at STL of attempting to observe hydrogen in the form of protons in the epitaxial layers. SIMS analysis of samples using caesium ion sputtering, revealed the presence of atomic hydrogen at levels just above the background count. The atomic hydrogen was found only in the p-InP layer, and the concentrations observed correlated well with the number of donors required to compensate the zinc [110]. The presence of atomic hydrogen was further proven by the growth of a series of epitaxial layers consisting of p-InP, n-InP, p-InP, p^+(GaIn)As layers, the structures finally being cooled under arsine. The electrochemical profile of this structure is shown in figure (5.14), and the doping level of the InP close to the surface is markedly lower than that of the InP next to the substrate. The SIMS profile of the layer (figure 5.15), indicated that the zinc levels in the two layers were identical, and the hydrogen levels in the two InP layers complemented the doping level observed in the electrochemical profile. In each case, the amount of hydrogen detected was only slightly above the background level of the SIMS apparatus, however sufficient data was amassed to confirm the conclusion that atomic hydrogen was responsible for the drop in doping level in the structures. Other workers have subsequently observed similar effects [111,112,113].

Further experiments were undertaken to understand the behaviour of the atomic hydrogen in InP. Figure (5.16) shows electrochemical profiles through two structures. The first consisted of p-InP, p^+(GaIn)As cooled under arsine, and the other of p-InP, p^+(GaIn)As, n-(GaIn)As cooled under arsine. In the latter sample the presence of the n-type layer on the surface, eliminated the deactivation effect. This inferred that atomic hydrogen could not diffuse through n-type material, and that most of the atomic hydrogen was produced and adsorbed into the structures during cooling under arsine after growth.

Figure (5.17) shows electrochemical profiles of a series of pieces of material from the same epitaxial slice, which were thermal pulse annealed at different temperatures. The electrical activity of the layers was progressively recovered by increasing the annealing

temperature or the annealing time. It was observed that temperatures of above 400°C were sufficient to cause the atomic hydrogen to be mobile in the layers, and to be completely driven out to give activated material. It was further shown that material which was activated could be deactivated by heating to 650°C in the MOVPE reactor, followed by cooling under an ambient arsine and hydrogen atmosphere. Conversely, samples which were deactivated could be returned to high doping levels if heated to 650°C and cooled under phosphine and hydrogen. This gave further evidence for the source of the atomic hydrogen being the pyrolysis of arsine during post growth cooling, and that the hydrogen could be driven in and out of the material according to the surface concentration of atomic hydrogen.

It is useful to summarise the findings upon these phenomena. It appears that during the pyrolysis of arsine, atomic hydrogen is produced which is incorporated into epitaxial layers whilst at, or close to the growth temperature. Upon cooling, the arsine pyrolysis must eventually cease, however prior to this occurring, the atomic hydrogen in the epitaxial layers becomes immobile, and within p-InP, acts to reduce the electrical activity of the material. Movement of atomic hydrogen also appears to be blocked by n-type material, inferring that atomic hydrogen is only soluble in p-type material. This is further substantiated by the fact that attempts to implant n-InP with protons resulted in no detectable hydrogen being observed. The ability to reactivate samples by heating above 400°C, no hydrogen subsequently being found by SIMS analysis, indicates the atomic hydrogen is mobile and can be expelled from p-type material in the absence of a high concentration of hydrogen. There appears to be no evidence of atomic hydrogen incorporation in (GaIn)As layers.

Many of these observations are consistent with the behaviour of atomic hydrogen in silicon [114], and it is interesting to note that hydrogen can also be introduced into p-InP by exposure to a methane-hydrogen plasma such as that used in dry etching processes [115].

Hydrogen Incorporation into p-InP Layers

The experiments detailed above, were extended to single epitaxial layers of p-InP. Early work using dimethylzinc included cooling the epitaxial layer after growth under a phosphine-hydrogen-dimethylzinc gas mixture. This was done to maintain an over-pressure of zinc, since it was known that zinc could easily be lost from the material due to its high vapour pressure. It was found that electrochemical profiles of the p-InP layers displayed a reduction in hole concentration at the surface of the material. This reduction and the consequent concave profile, was not found in p-InP cooled under a phosphine-hydrogen mixture. It was postulated that atomic hydrogen was again responsible for de-activation of the p-InP, with the hydrogen source being either the phosphine or the dimethylzinc.

Figure (5.18) shows electrochemical profiles through three p-InP layers. Two of the curves are as described above for p-InP cooled under phosphine-hydrogen and phosphine-hydrogen-dimethylzinc mixtures. The third profile is through a p-InP layer that was cooled under a phosphine-hydrogen-dimethylzinc mixture to 600°C, and then to room temperature under a dimethylzinc-hydrogen mixture. Each layer had been grown using identical phosphine, trimethylindium and dimethylzinc flow rates. It was necessary to cool the InP to 600°C before switching out the phosphine flow to avoid deterioration of the surface due to phosphorus loss. It was reasoned that atomic hydrogen present in the material would still be mobile between 600°C and 500°C. The electrochemical profile of this last layer indicated that no deactivation of the zinc had occurred, and that the hole concentration was higher than that of the sample cooled under the normally used phosphine-hydrogen atmosphere. It was therefore concluded that atomic hydrogen was being produced from phosphine in the same manner as from arsine, but to a lesser extent due to the higher thermal stability of phosphine. Moreover, it appeared that dimethylzinc was able to enhance the production of atomic hydrogen from the phosphine.

It was necessary to confirm that atomic hydrogen was responsible for the deactivation of the p-InP. A first step in this direction was to subject samples to thermal pulse annealing, and observe if similar behaviour occurred, compared with that exhibited in p+(GaIn)As/pInP heterostructures. Each of the three layers described above were

thermal pulse annealed at 800°C for 5s. Figure (5.19) shows the results of this experiment, with the electrochemical profiles through the three layers indicating near identical hole concentrations deep within the structures. The sample cooled under a gas mixture of phosphine-hydrogen-dimethylzinc to room temperature, exhibited an increased hole concentration close to the surface. This implies that further zinc in-diffused into the structure during the cooling period. However, indiffusion of zinc did not take place into the sample cooled under a dimethylzinc-hydrogen mixture, indicating that free zinc atoms were not available at the surface of the epitaxial layer.

SIMS measurements were undertaken upon the layers to confirm the presence of hydrogen in the samples. A decreasing trend in the amount of hydrogen in the three layers was observed in order of the samples cooled under: phosphine-hydrogen-dimethylzinc, phosphine-hydrogen and hydrogen-dimethylzinc. However the background concentration of hydrogen in the apparatus contributed sufficient noise to the measurements to make them unreliable.

A further sample was therefore grown consisting of p-n-p InP layers using dimethylzinc and silane as p and n dopants, which was cooled under a gas mixture of phosphine-dimethylzinc and hydrogen. An electrochemical profile of this layer is shown in figure (5.20), and it can be seen that the surface layer of p-InP exhibits a drop in hole concentration, with the maximum level being lower than that in the inner p-InP layer. This structure was then analysed by SIMS (figure 5.21), and the presence of hydrogen confirmed. The zinc levels in the two p-InP layers were found to be nearly identical, with a slightly higher level close to the surface of the structure, probably due to indiffusion of zinc during cooling. Deuterium implants of p-InP provided SIMS calibration of the hydrogen levels. The above experiments indicated that phosphine could provide atomic hydrogen in a similar manner to arsine in MOVPE.

Relevance of Hydrogen Incorporation to Reaction Mechanism

The above results are also important to obtaining a more complete understanding of the reaction mechanism of MOVPE.

The presence of the dimethylzinc and phosphine together when cooling p-InP caused increased amounts of hydrogen to be incorporated

compared with cooling under phosphine alone. There was also an indication that the dimethylzinc was able to provide more atomic zinc during cooling if phosphine was also present, compared with no phosphine being available. It is therefore concluded that the presence of phosphine and dimethylzinc together causes enhanced pyrolysis of each of the reactants. This behaviour may be reasonably extended to other phosphine-metal-organic compound combinations, such as phosphine-trimethylindium. Further, for the atomic hydrogen to be adsorbed onto the epitaxial layer, the reactions must take place upon or very close to the crystal surface since hydrogen is highly reactive in its monatomic form, readily combining with itself to form hydrogen (H_2), or with alkyl radicals to form alkanes.

As indicated in the chapter upon MOVPE chemistry, it is concluded that the MOVPE process involves reactions of the alkyls and hydrides together upon the epitaxial surface, and not in the gas phase.

Bonding Mechanism for Hydrogen in p-InP

It is interesting to consider the manner in which the hydrogen passivates the p-InP layers. For the acceptor concentration introduced by the zinc to decrease, the hydrogen must donate electrons to the lattice. The region around a zinc atom that is substituted onto an indium lattice site, is surrounded by the de-localised negative charge caused by acceptance of an electron from the lattice to locally satisfy the bonding requirements of the III-V crystal structure. It is postulated that the positively charged protons are attracted to the negatively charged area, and a further bond is developed, trapping the protons in the lattice at low temperatures.

Pajot et al have undertaken infra-red absorption spectroscopy and identified the position of the proton as being between the zinc atom and a phosphorus atom [116].

The lattice is then slightly relaxed compared with the distortion introduced originally by the zinc atom. Since the negative charge on the zinc atom has been cancelled by the presence of the proton, the amount of ionised impurity scattering should be reduced, and so the sample is said to be passivated rather than compensated.

The hydrogen-arsenic bond is weaker than the hydrogen-phosphorus bond. For p-type GaAs or (GaIn)As, the lack of observed passivation by

atomic hydrogen can be explained by the protons still being mobile when with decreasing temperature, the pyrolysis of the arsine has ceased to provide an over-pressure of atomic hydrogen to the epitaxial slice.

Rare Earth Element Doping

Doping of epitaxial layers using rare earth elements has recently been proposed. Uwai et al reported the use of ytterbium doping of MOVPE grown InP [117]. The inner electron transitions within the rare earth elements are used to radiate light at single frequencies. The inner electron energies are relatively unaffected by the presence of the atom in the bulk crystal field. In the case of ytterbium, intra 4f electron shell transitions radiate light at ~1.5μm, suitable for optical communication applications. Uwai used tris-cyclopentadienyl ytterbium - $Yb(C_5H_5)_3$, and obtained doping to $3.10^{18}cm^{-3}$ as measured by SIMS with n-type conductivity. The 4f transitions are caused by excitation of electrons within these levels by optical absorption from a pumping light source. In a semiconductor laser the light would originate from the normal band-gap transitions. However it is not clear whether sufficient ytterbium atoms can be incorporated to adsorb and generate the required amount of light.

Iron Doping of InP

There are many applications in the fabrication of opto-electronic devices where it is desirable to incorporate a crystalline but non conducting layer during the growth phase. Examples are isolation layers between epilayers of integrated devices, or to surround the active layer of a laser in a non conducting media to restrict current flow to the active layer alone.

Devices of the latter form would conventionally be grown using reverse biased p-n blocking layers in the structure. The use of insulating isolation layers reduces capacitance, and may prove easier to use in a production environment. To achieve this end, InP has been doped with a variety of elements that introduce deep level traps to remove carriers and form highly resistive layers. Such an element is iron, however when growing by liquid phase epitaxy, the solubility

limit of iron in InP causes the layers to be insufficiently resistive. More recently the application of iron doping in InP by MOVPE has been considered, and appears to be promising.

Long et al first reported the growth of iron doped InP by MOVPE [118]. Iron pentacarbonyl - $Fe(CO)_5$, was found to be too volatile, and so ferrocene - $Fe(C_5H_5)_2$ was investigated. This metal alkyl is solid to 450°C, and, unlike many other metal organic compounds used in MOVPE, is stable in air. The material is commonly available, however supplies of electronic grade purity material are still expensive. Long et al were able to grow iron doped layers with room temperature resistivities of 1.10^6-2.10^8 Ωcm, and further were able to construct 5mm diameter Schottky diodes from the material [119]. These devices, with iron doped epilayers up to 9μm thick, gave currents of 0.5μA when biased at 75V. This indicated the suitability of the material as a current blocking media. It is thought that the iron forms a deep level acceptor near the middle of the band gap. Emission of carriers at room temperature is considered to be negligible [119].

The same group examined MOVPE grown iron doped material in more detail and discovered precipitates of FeP and FeP_2, mainly upon the surface [120]. Huang et al have demonstrated that low level doping of InP using iron does not appreciably affect the mobility of the material [121]. This indicates that no additional ionised impurity scattering takes place and that all the deep level traps introduced are full. 10K photoluminescence measurements have indicated that the iron introduces a 1.07eV deep radiative transition into the InP.

Sugawara at al have also indicated that iron introduces a mid gap state, but that only ~1% of the iron atoms are electrically active [122]. Takanohashi et al have doped InP with ferrocene held at 20°C and using a flow of $100cm^3min^{-1}$ to obtain iron concentrations of $2.10^{18}cm^{-3}$ [123]. However only 10% of the iron atoms were concluded to be electrically active from comparison of SIMS and DLTS measurements. The remainder of the iron was thought to be incorporated in the form of FeP precipitates, and unlike Long et al, the precipitates were evenly distributed throughout the epilayer. It would appear from Sugawara's work that whilst the iron appears to be fully active at low doping levels, beyond a ~ mid $10^{16}cm^{-3}$ concentration, precipitates are formed and electrical saturation occurs. This solubility limit is

thought to be a function of the growth temperature, with somewhat higher doping levels being obtained at higher growth temperatures [124].

Hess et al have demonstrated the fabrication of buried crescent 1.5μm lasers using iron doped InP blocking layers, and obtained 12mA threshold currents [125]. Tell et al have demonstrated the growth of iron doped layers of (GaIn)As using ferrocene in the same manner as for InP [126]. An acceptor ionisation energy of 0.35eV was obtained, placing the level in the middle of the 0.74eV (GaIn)As band gap. These workers found that a deficiency of iron in the epilayers led to n-type conductivity, and an excess of iron gave p-type conductivity.

Zah et al have fabricated buried crescent lasers on p-type substrates, using MOVPE grown blocking layers co-doped with titanium and iron [127]. The titanium was used to provide a deep donor level to complement the deep acceptor level introduced by the iron. The deep donors were needed to prevent p-type conduction caused by indiffusion of zinc from the p-type substrates.

In summary, it appears that iron doping of these materials is possible provided that the concentration of iron is kept to around $\sim 5.10^{16}cm^{-3}$ in both InP and (GaIn)As. This behaviour may be reasonably extrapolated to quaternary alloys.

The author has grown ferrocene doped InP layers which when measured by SIMS, had an iron concentration of $8.10^{16}cm^{-3}$. 4μm thick layers were fully depleted of carriers when measured using a mercury probe. Iron doped layers were grown directly upon undoped (GaIn)As and 1.3μm emission (GaIn)(AsP) layers. SIMS analysis showed that little indiffusion of iron had taken place into the alloy layers.

An electrochemical profile through an InP multi-layer doped with silane and ferrocene is shown in figure (5.22). Four InP layers, each of 2μm thickness were grown and comprised: ferrocene doped InP, ferrocene and silane doped InP, silane doped InP, and finally undoped InP. The electrochemical profile indicated a background carrier concentration of $n=4.10^{15}cm^{-3}$, and an intentionally silicon doped layer of $n=5.10^{16}cm^{-3}$. The addition of the iron to the layer also doped with silicon, caused the electron concentration to fall to below

the background doping level. The layer doped solely with iron could not be etched using the electrochemical profiler, though the profile of figure (5.22) indicates that depletion of the layer occurred along with evidence of p-type conductivity at the interface.

Cobalt Doping

As an alternative to doping with iron to obtain semi-insulating layers, Hess et al have reported the use of cobalt from a source $Co(NO)(CO)_3$. The cobalt was found to be a deep acceptor and a greater amount of dopant flux was needed to give semi-insulating layers, compared to the use of iron [128].

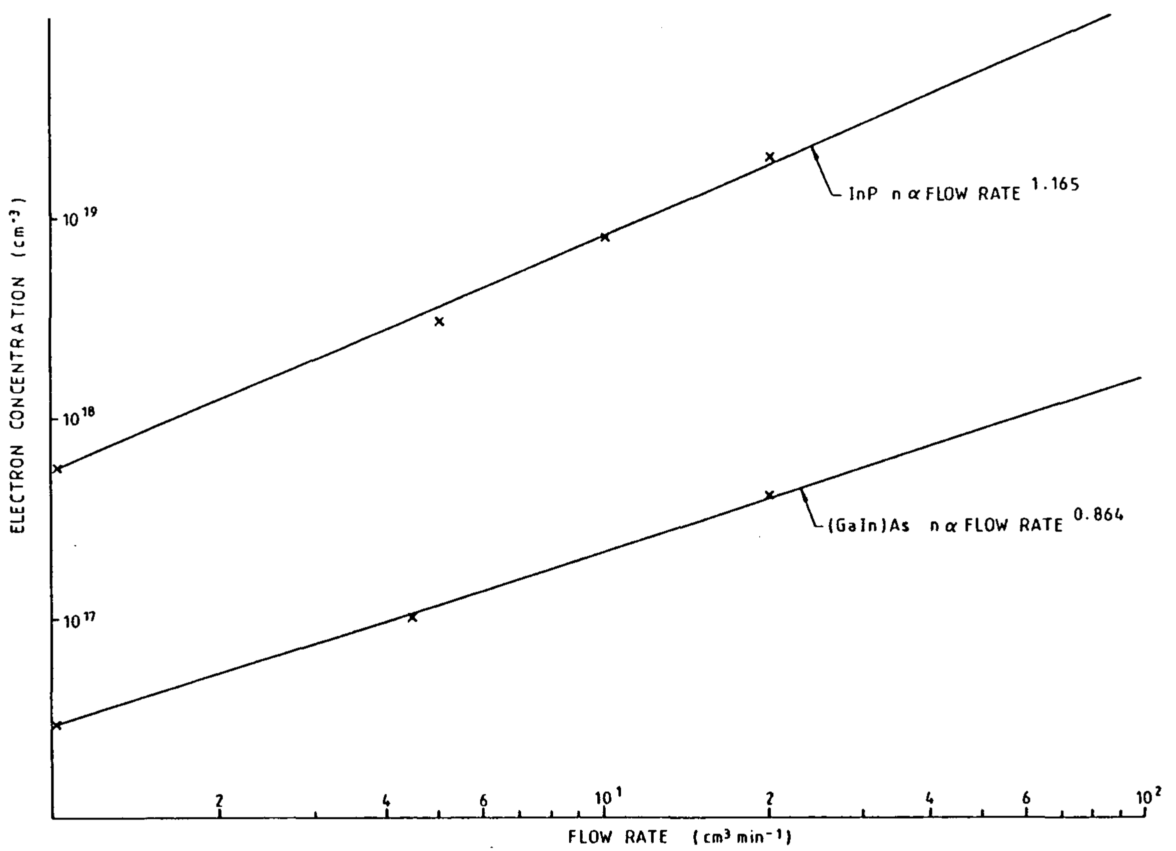

Figure (5.1): Electron concentration as a function of SiH_4 flow-rate for (GaIn)As and InP. The values were determined using an electrochemical profiler.

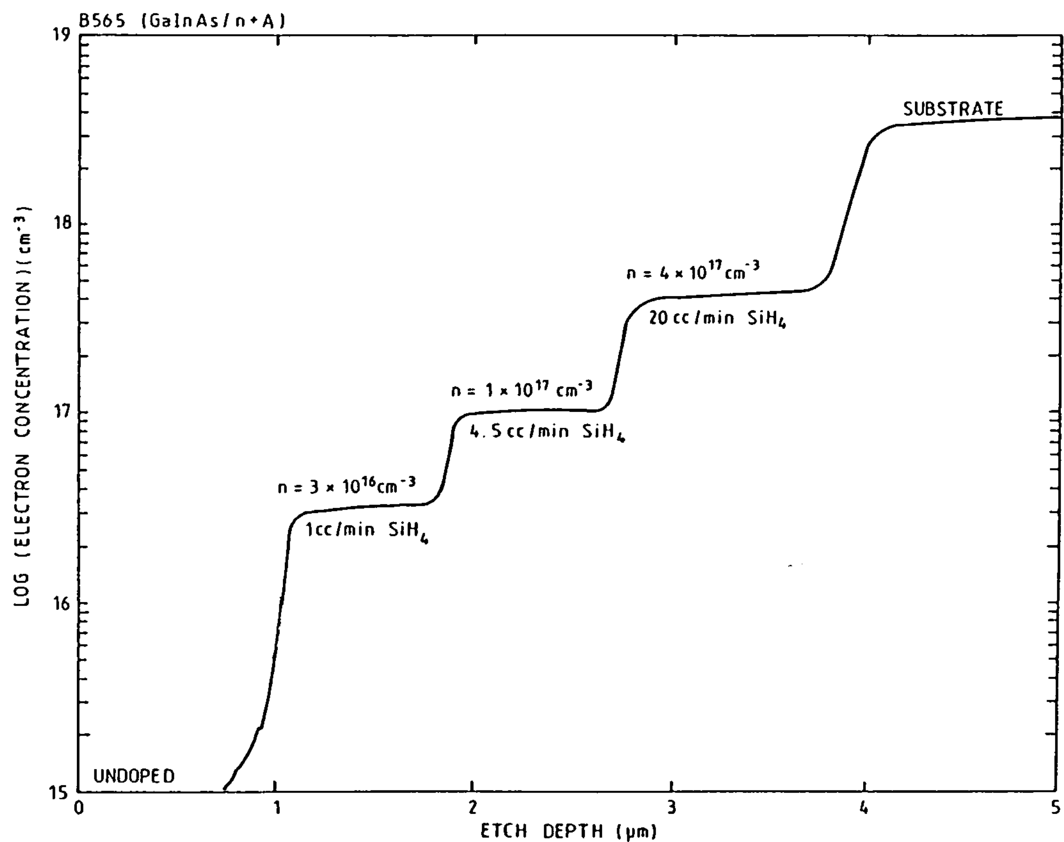

Figure (5.2): Electrochemical depth profile showing the variation of electron concentration with input flow rate of SiH_4 for InP. The abruptness of the interfaces indicates that silicon does not diffuse quickly in InP.

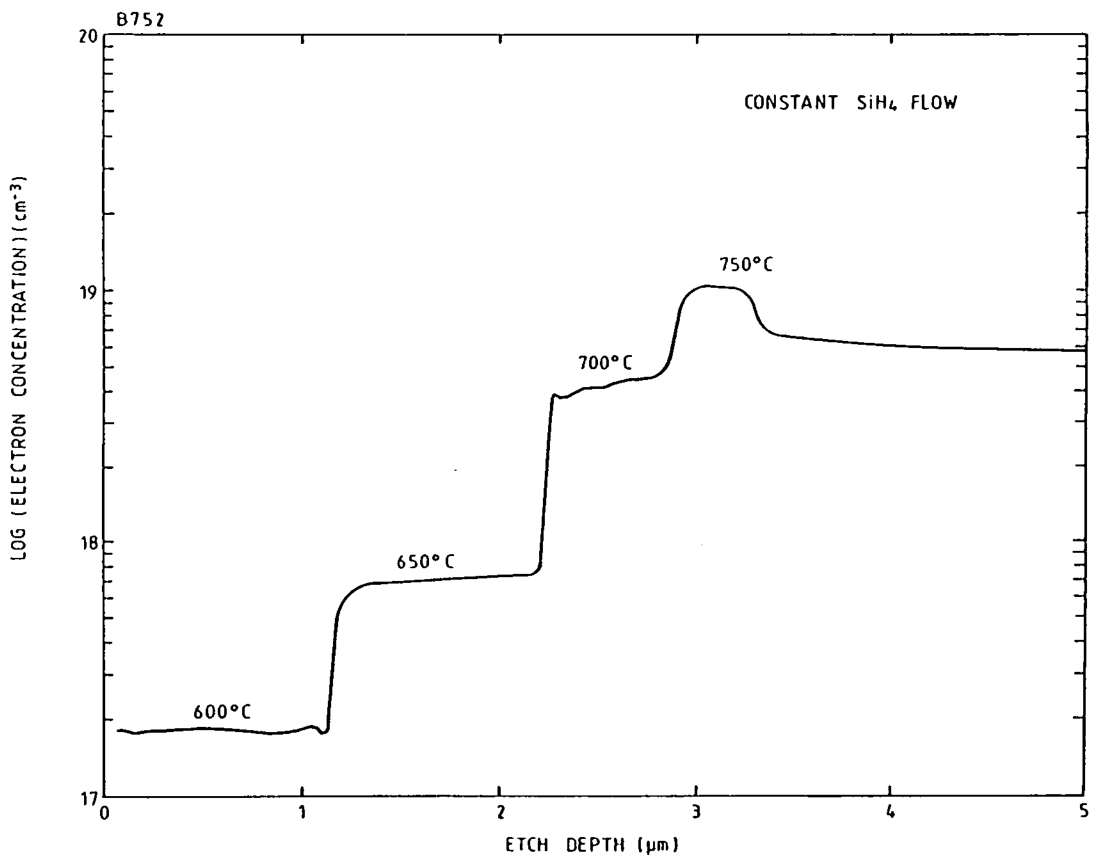

Figure (5.3): Electrochemical depth profile showing the variation in electron concentration for a layer of silicon doped InP which was grown whilst stepping the growth temperature. All other growth parameters remained constant.

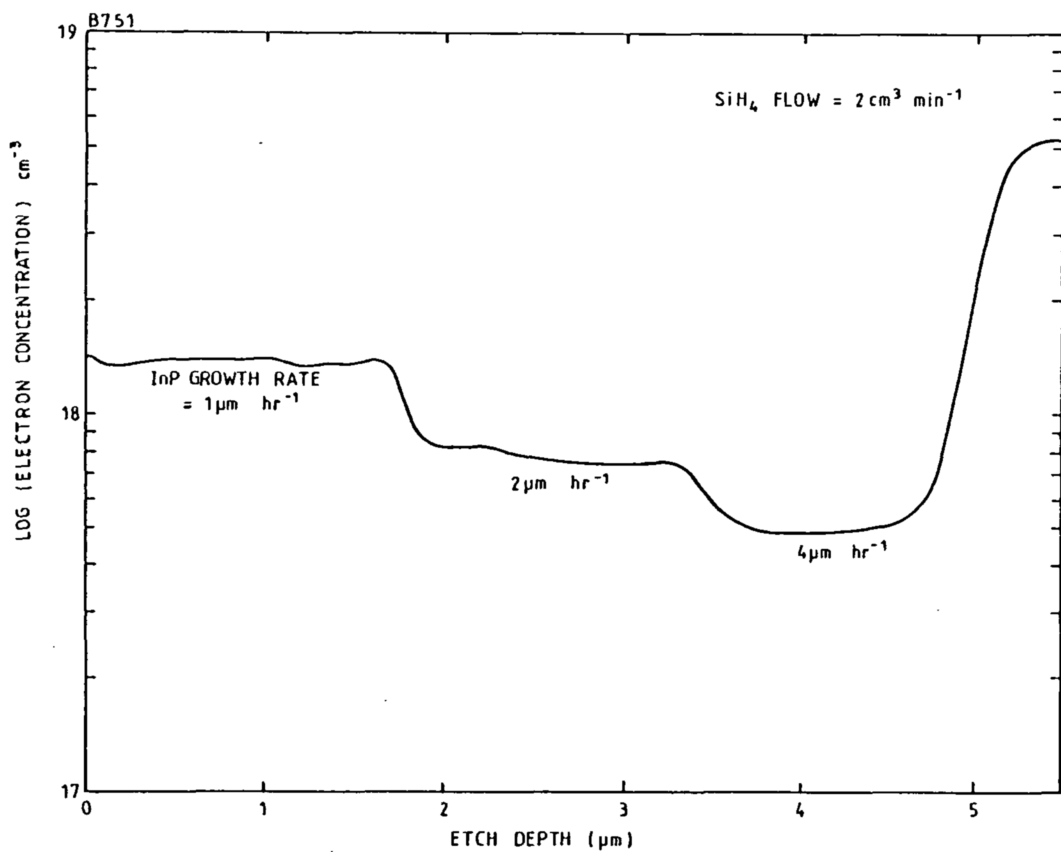

Figure (5.4): Electrochemical depth profile showing the variation of electron concentration for a layer of silicon doped InP which was grown at three different growth rates. All other growth parameters remained constant, except for the V/III ratio.

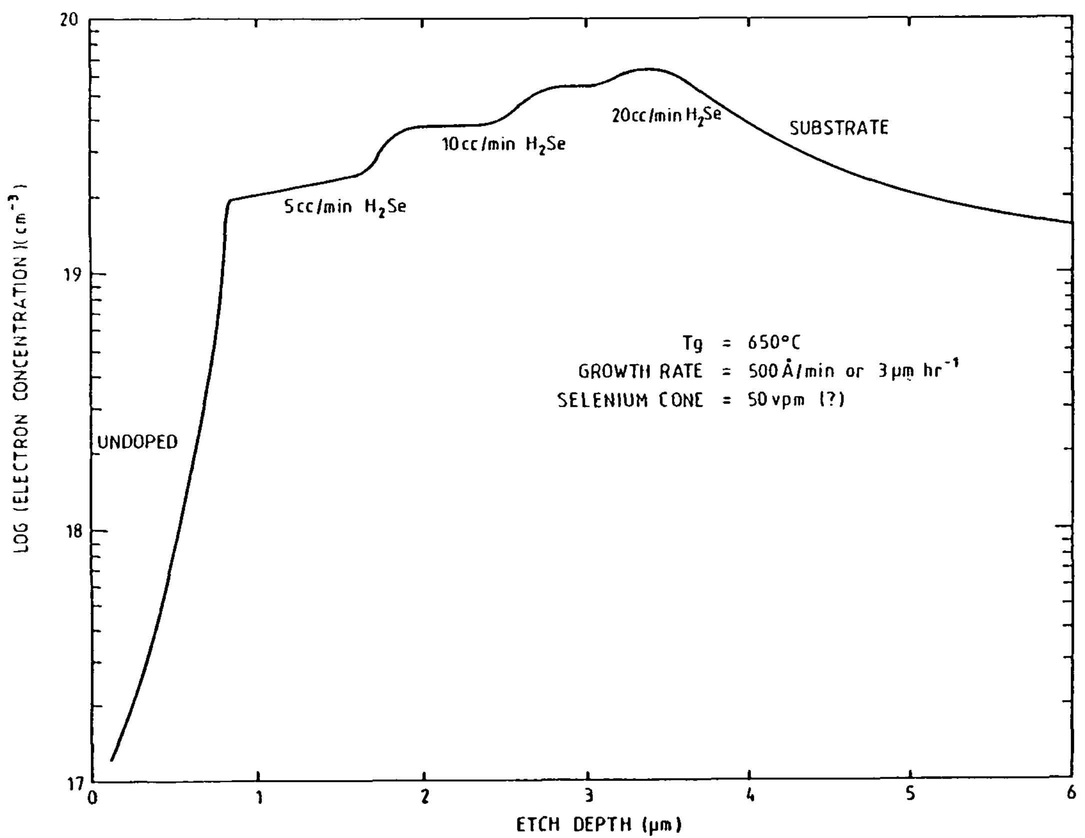

Figure (5.5): Electrochemical depth profile showing the variation of electron concentration with input flow rate of H_2Se for InP.

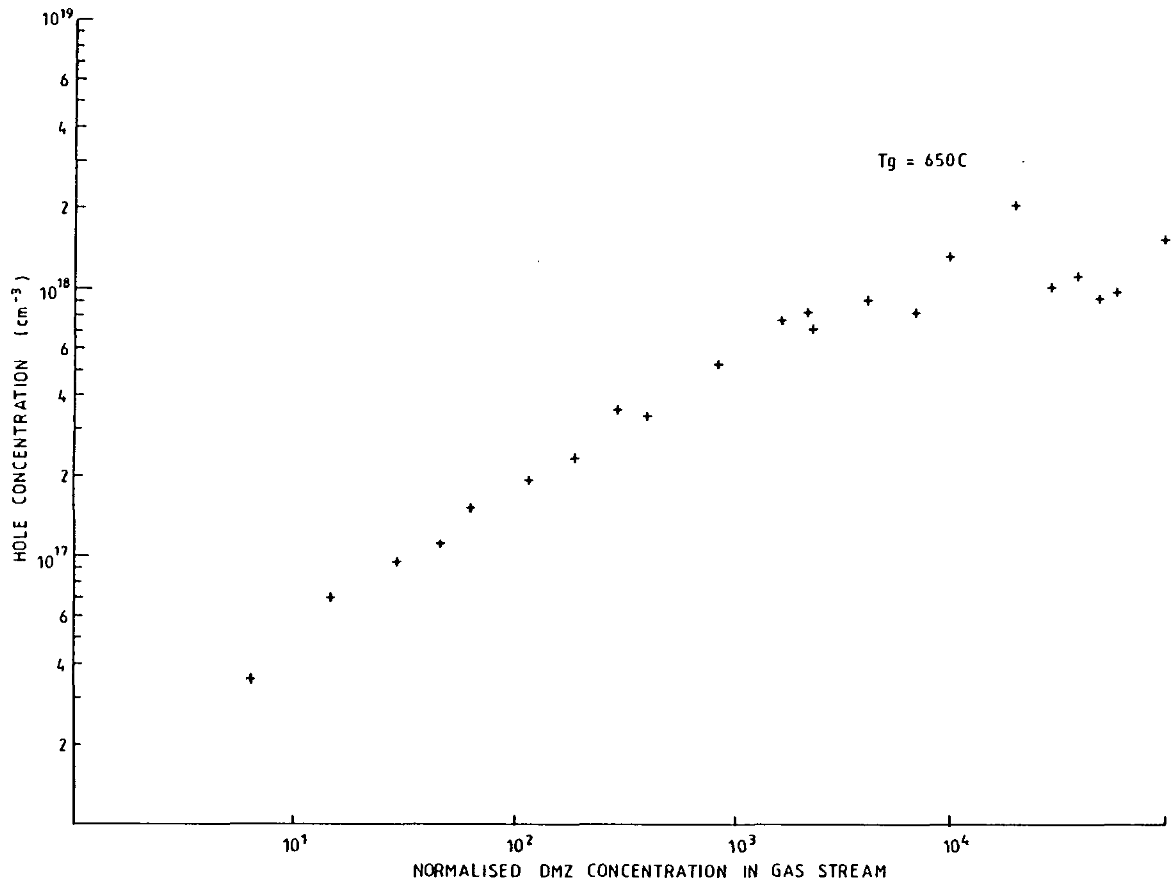

Figure (5.6): Variation of hole concentration in InP as a function of dimethylzinc input flux. The slope of the graph is ≃ 0.5 and saturation occurs at ≃ $1\text{-}2.10^{18} cm^{-3}$.

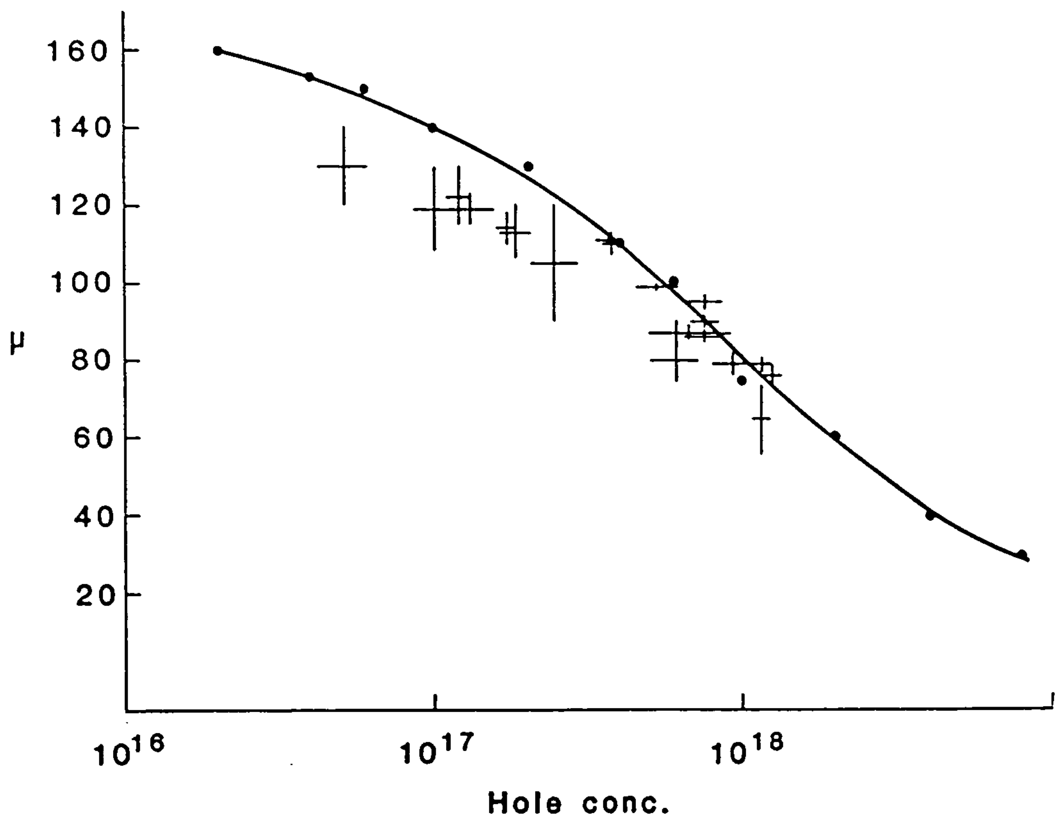

Figure (5.7): Hole mobility in p-InP doped using dimethylzinc as a function of hole concentration. The solid line and points represent data obtained by liquid phase epitaxy [Reference 105]. The crosses and error bars are from measurements upon the author's MOVPE material.

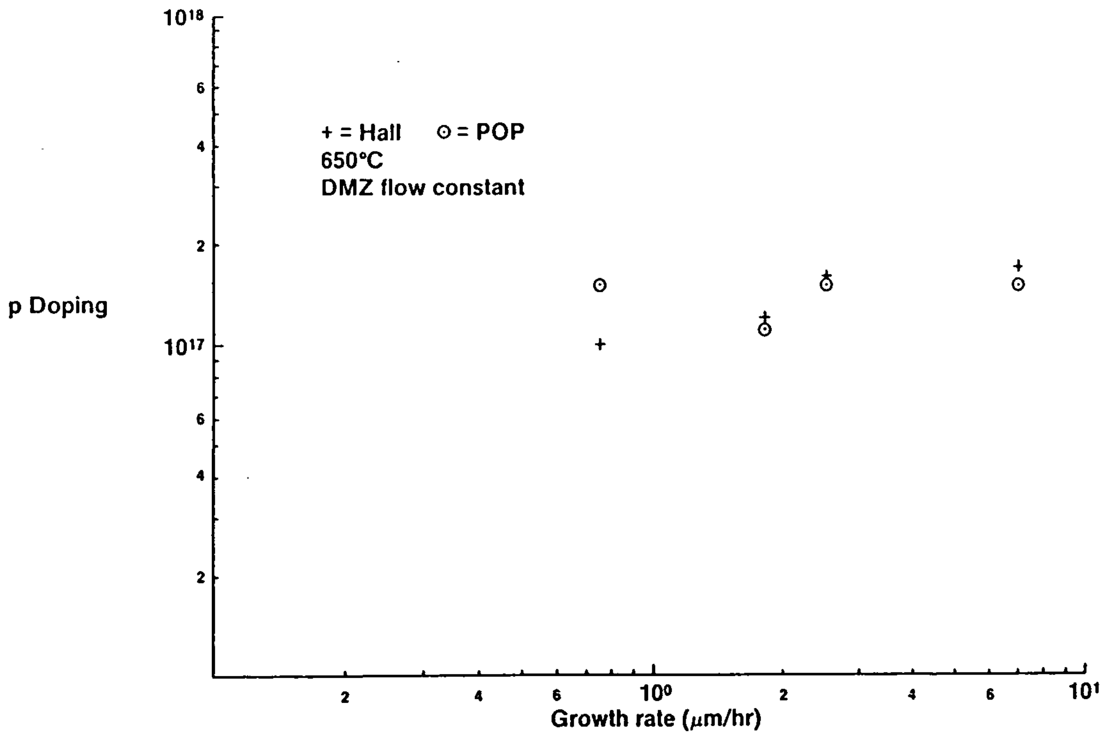

Figure (5.8): Hole concentrations in p-InP doped using dimethylzinc, showing an approximately invariant behaviour with growth rate.

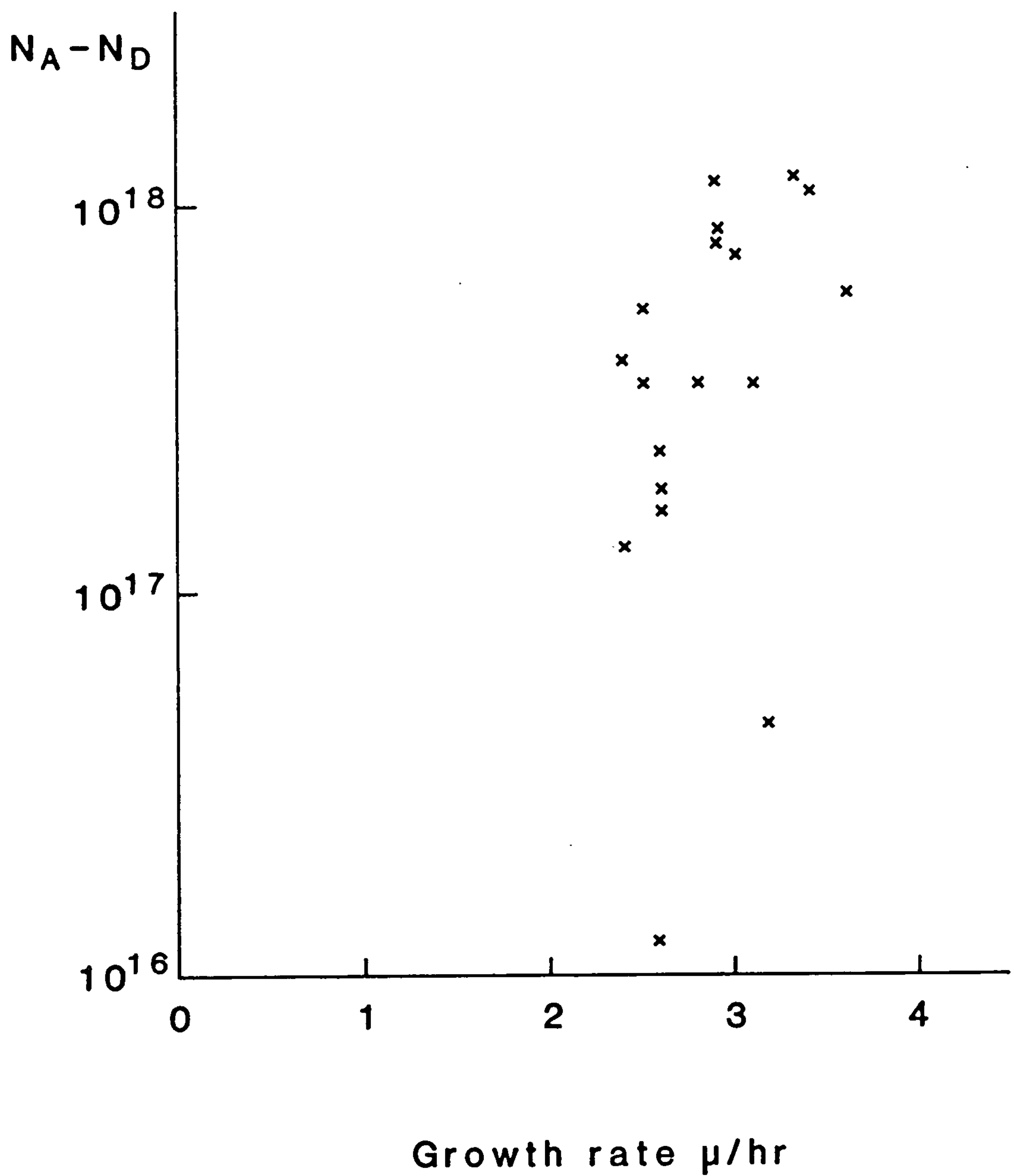

Figure (5.9): Growth rate measured upon p-InP layers doped using dimethylzinc, showing little correlation upon carrier concentration and dopant flux into the reactor.

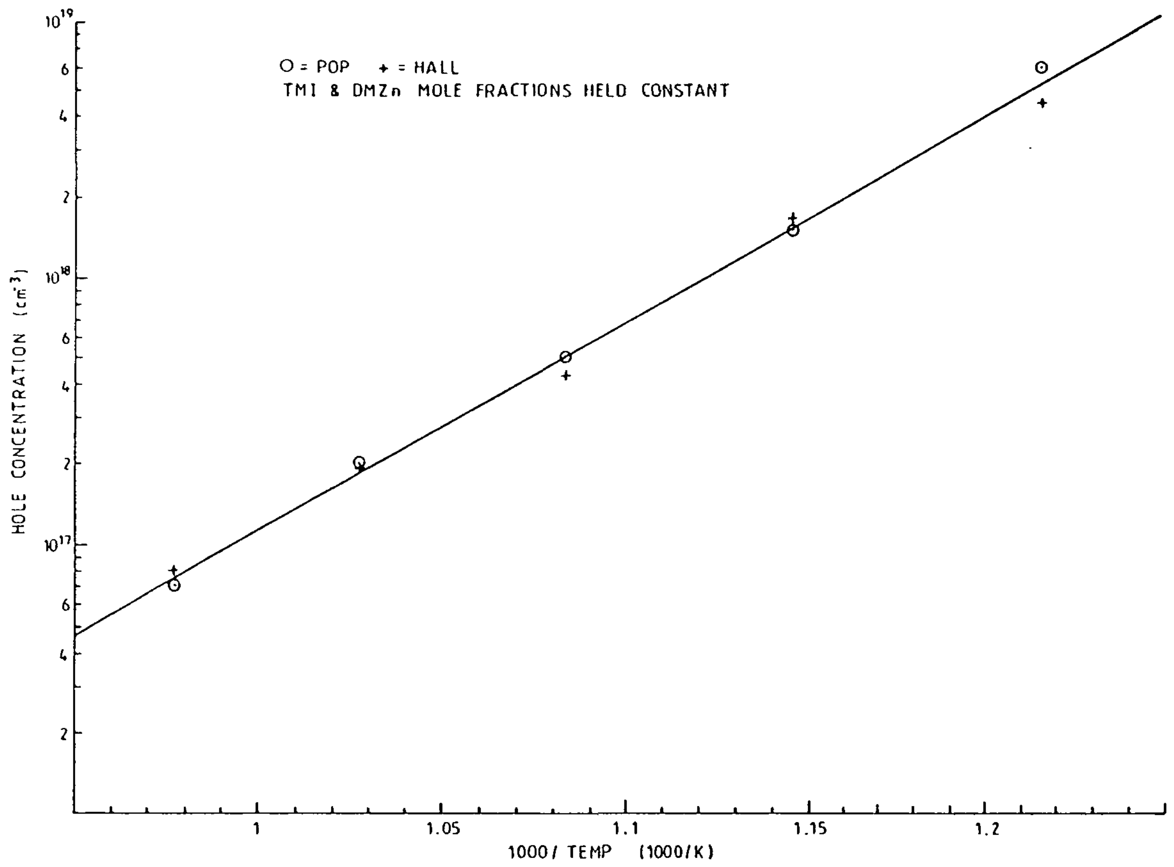

Figure (5.10): Variation of hole concentration for p-InP layers doped using dimethylzinc, as a function of growth temperature. All other growth conditions were maintained constant.

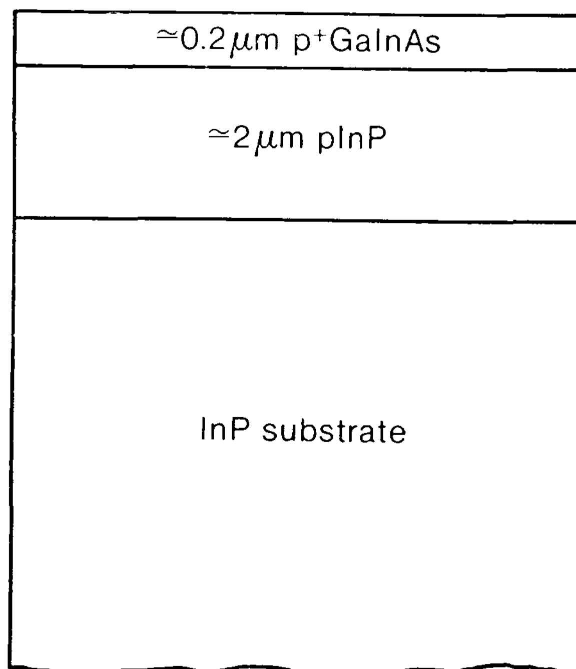

Figure (5.11): p^+(GaIn)As/p-InP structure used to study hydrogen passivation in InP.

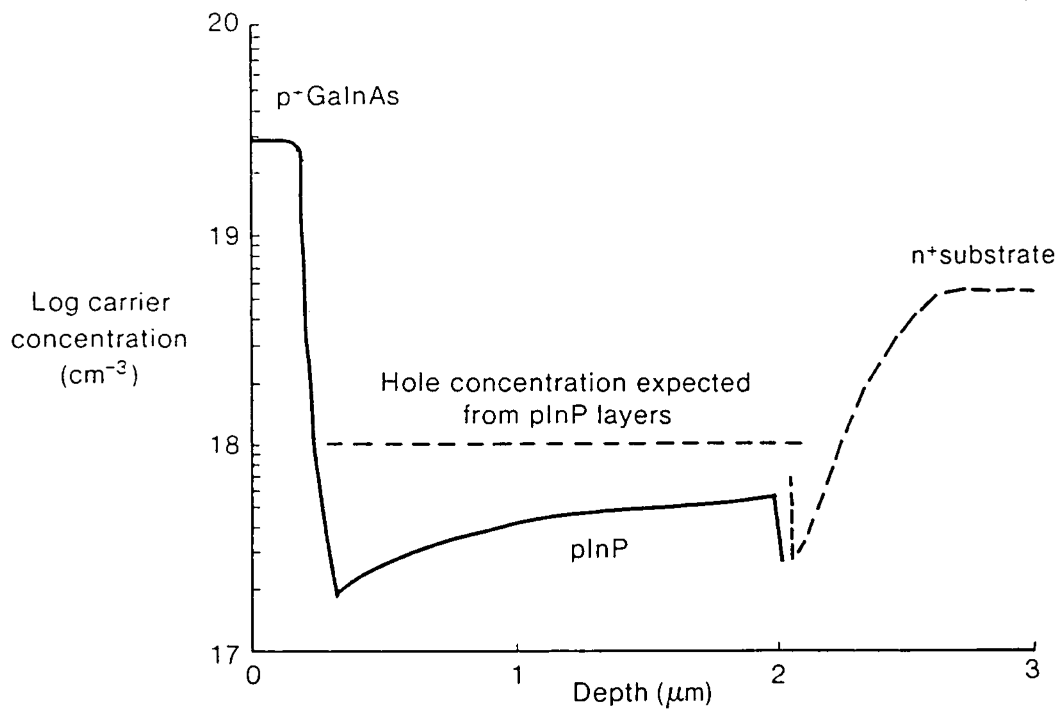

Figure (5.12): Electrochemical profile through the structure shown in figure (5.11), showing the expected and real InP hole concentrations.

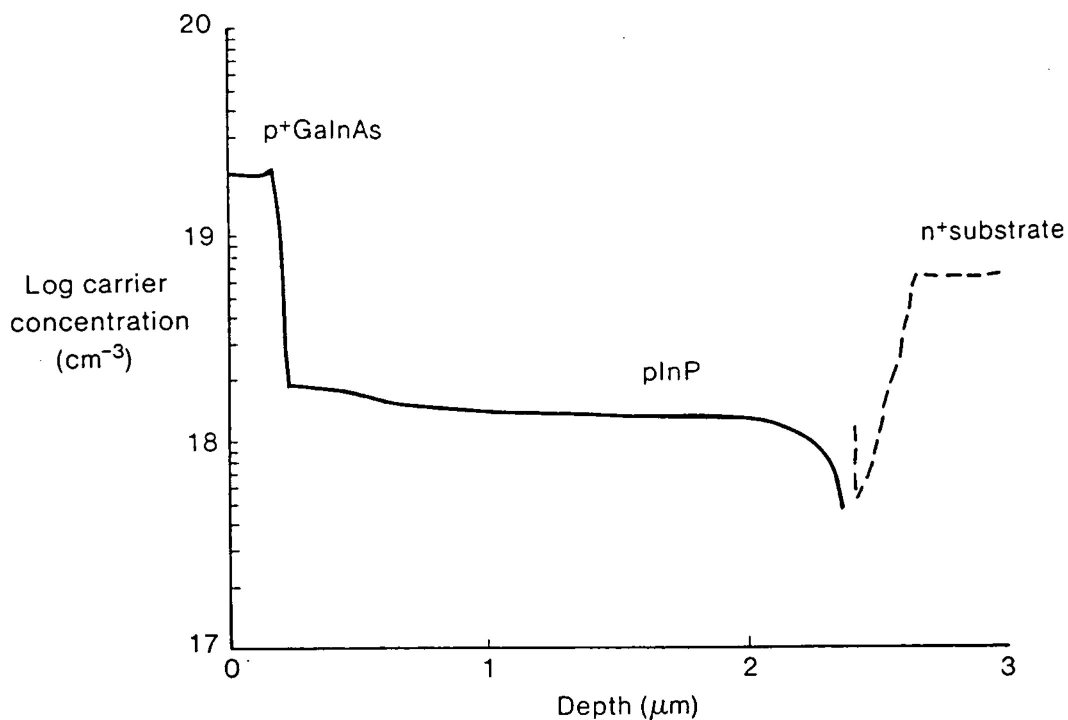

Figure (5.13): Electrochemical profile through the structure shown in figure (5.11), following thermal pulse annealing. The hole concentration rose to higher than the values expected originally.

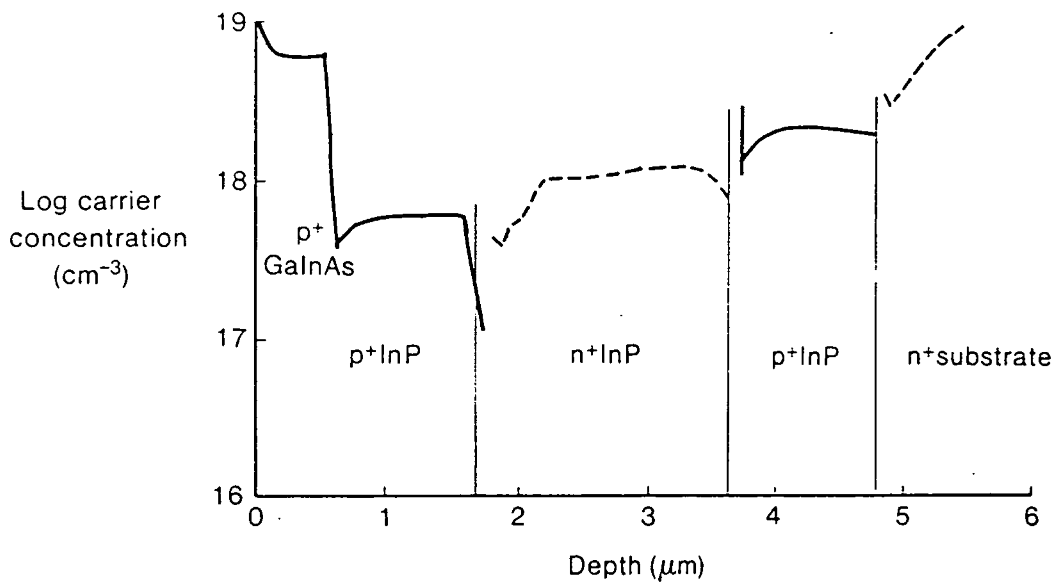

Figure (5.14): Electrochemical profile through a p^+(GaIn)As /p-InP/n-InP/p-InP structure, showing suppression of the hole concentration in the layer closest to the surface of the material.

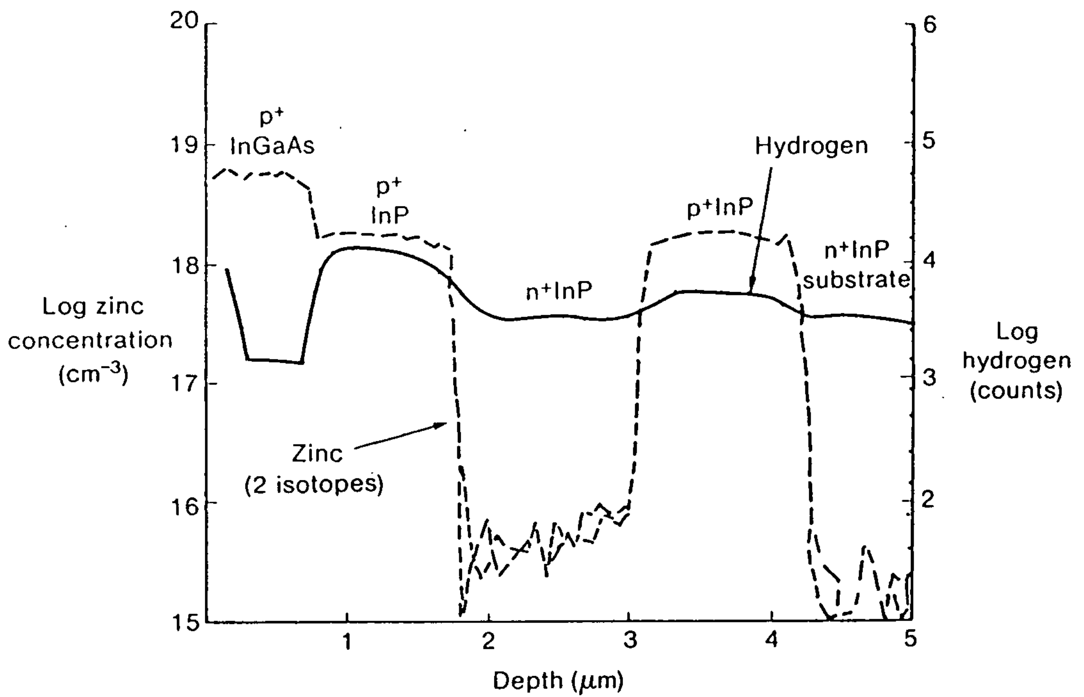

Figure (5.15): Zinc and hydrogen SIMS depth profile through the same structure as that used for figure (5.14). A noticeable hydrogen presence was detected in the p-InP layers, with the highest signal being obtained from the layer closest to the surface of the sample.

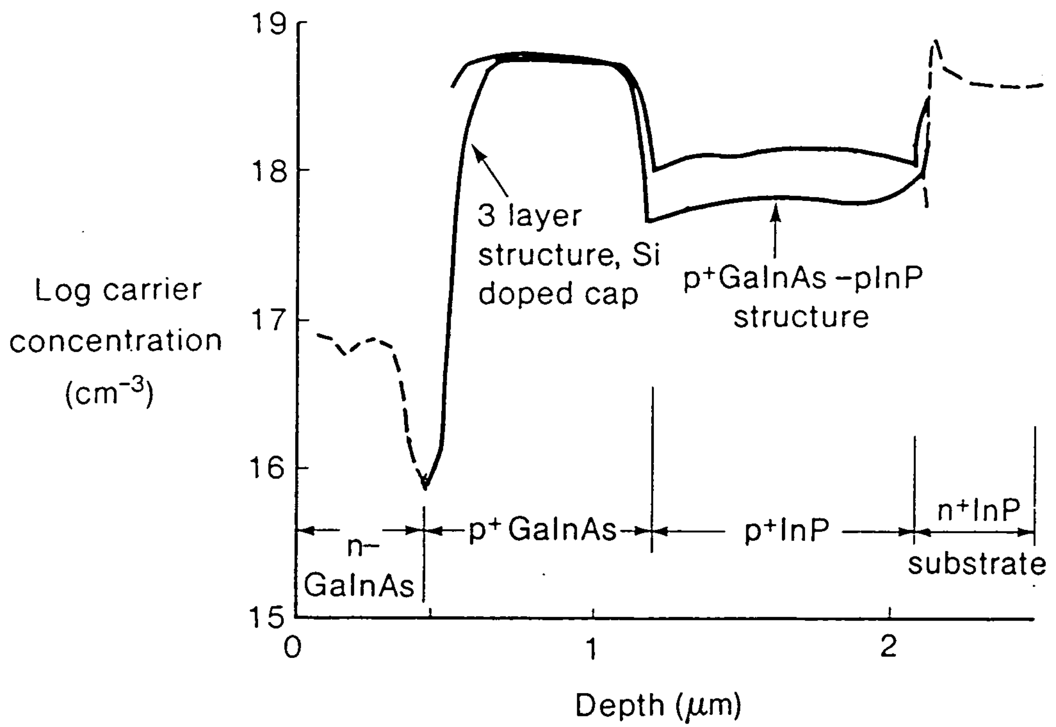

Figure (5.16): Electrochemical profiles through an n-(GaIn)As/p^+(GaIn)As/p-InP structure, and (offset) a p^+(GaIn)As/p-InP structure. The layer capped with silicon doped material shows a higher hole concentration in the p-InP.

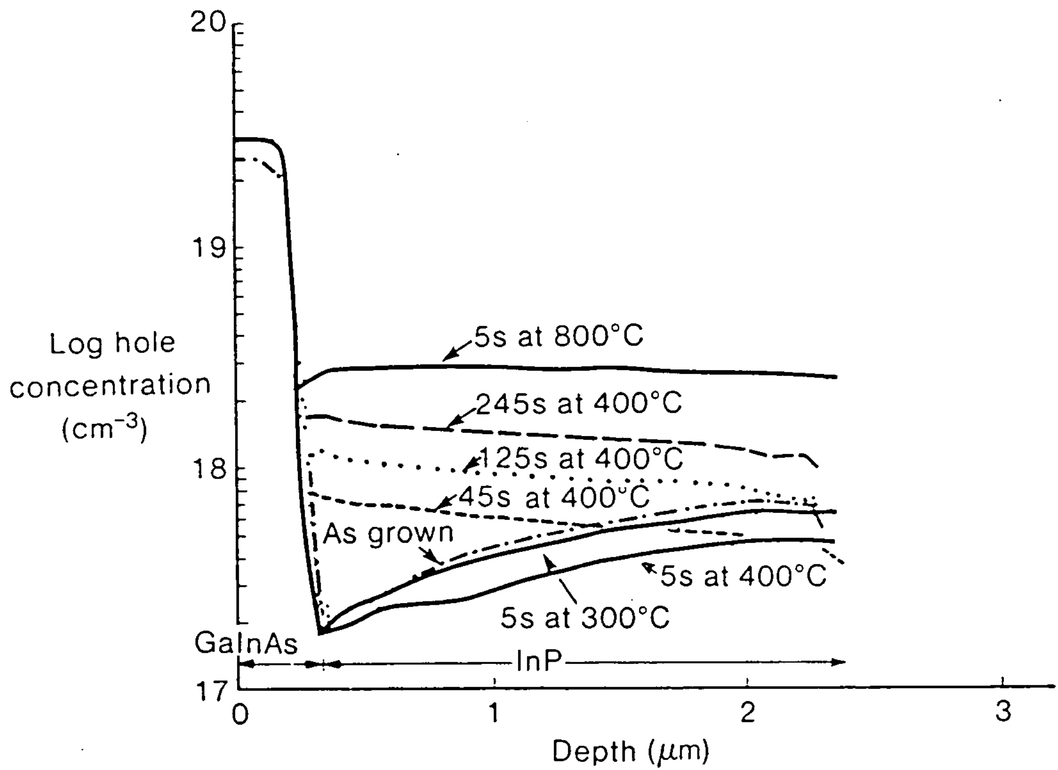

Figure (5.17): Electrochemical profiles through several p+(GaIn)As /p-InP samples from the same epitaxial layer, which were thermal pulse annealed at different temperatures and for different times.

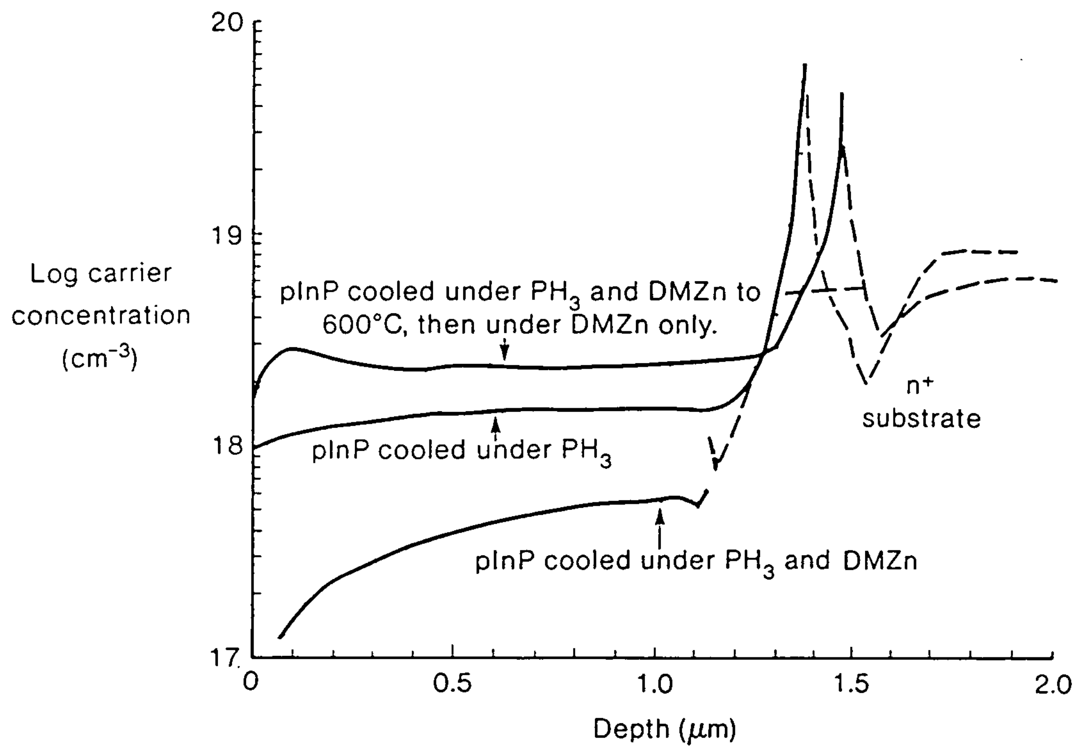

Figure (5.18): Electrochemical profiles through three zinc doped p-InP layers which were cooled from the growth temperature under different conditions.

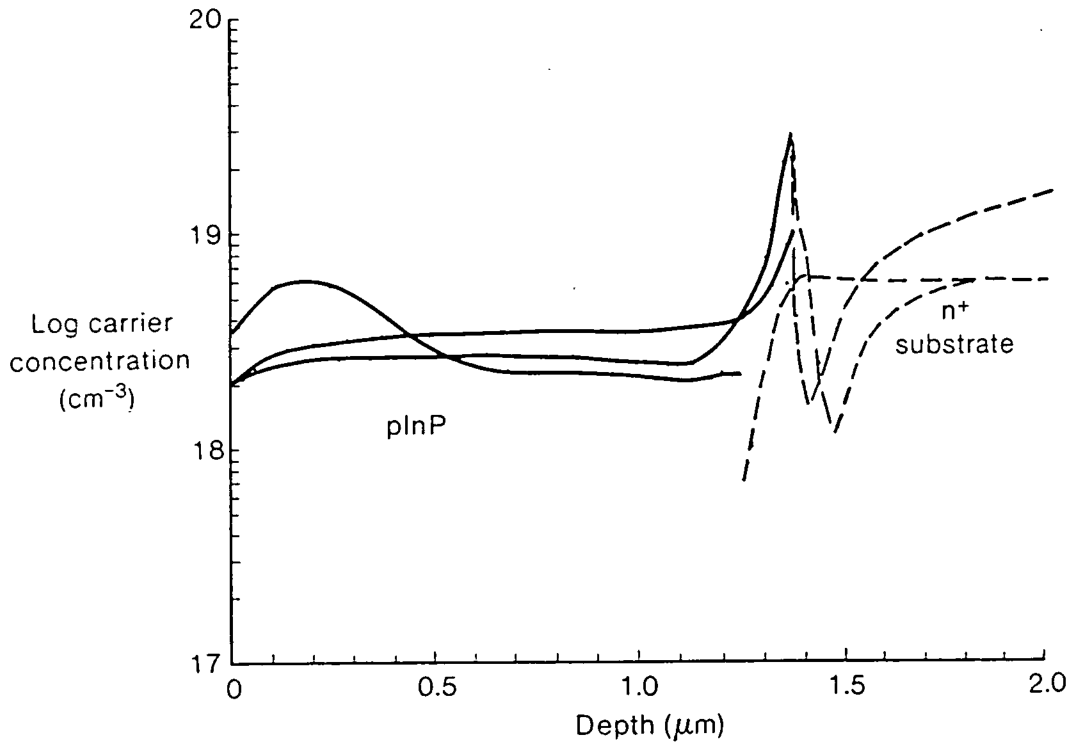

Figure (5.19): Electrochemical profiles through the same samples as used for figure (5.18), but after being thermal pulsed annealed at 800°C for 5s. The hole concentrations have risen, and a surface accumulation of holes has appeared for the layer cooled under dimethylzinc, hydrogen and phosphine.

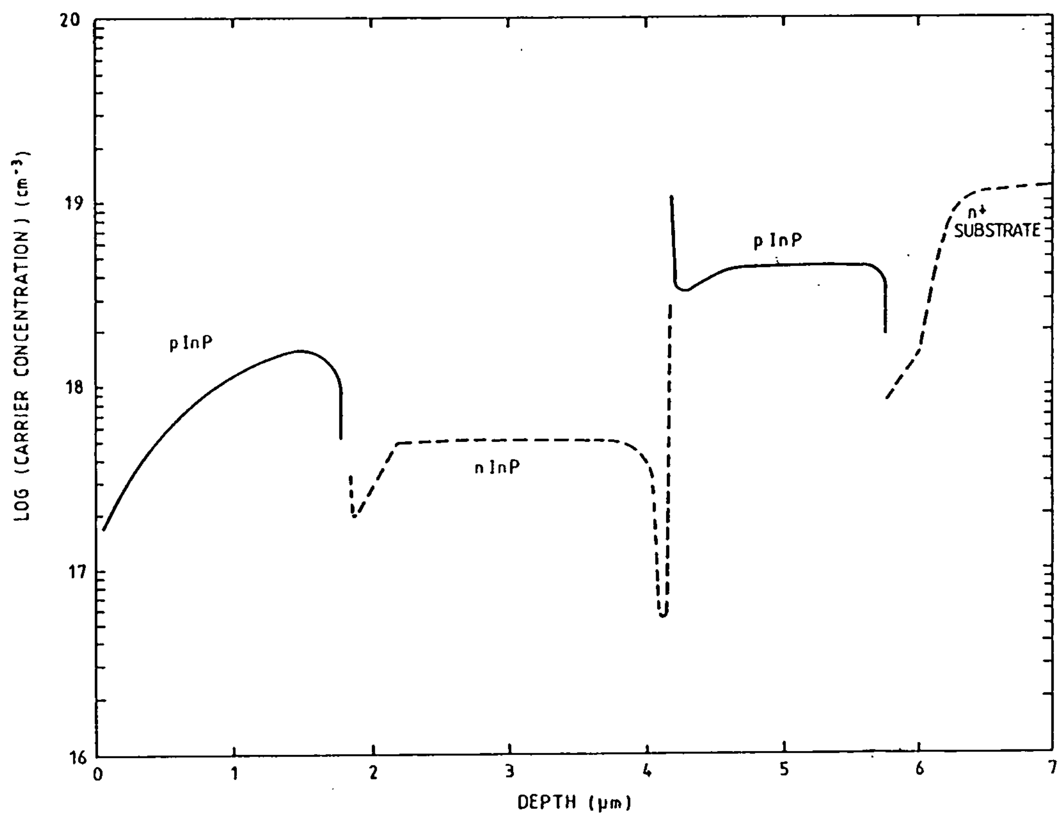

Figure (5.20): Electrochemical profile through a p-InP/n-InP/p-InP zinc and silicon doped structure, where the last InP layer was cooled under a gas mixture of hydrogen, phosphine and dimethylzinc.

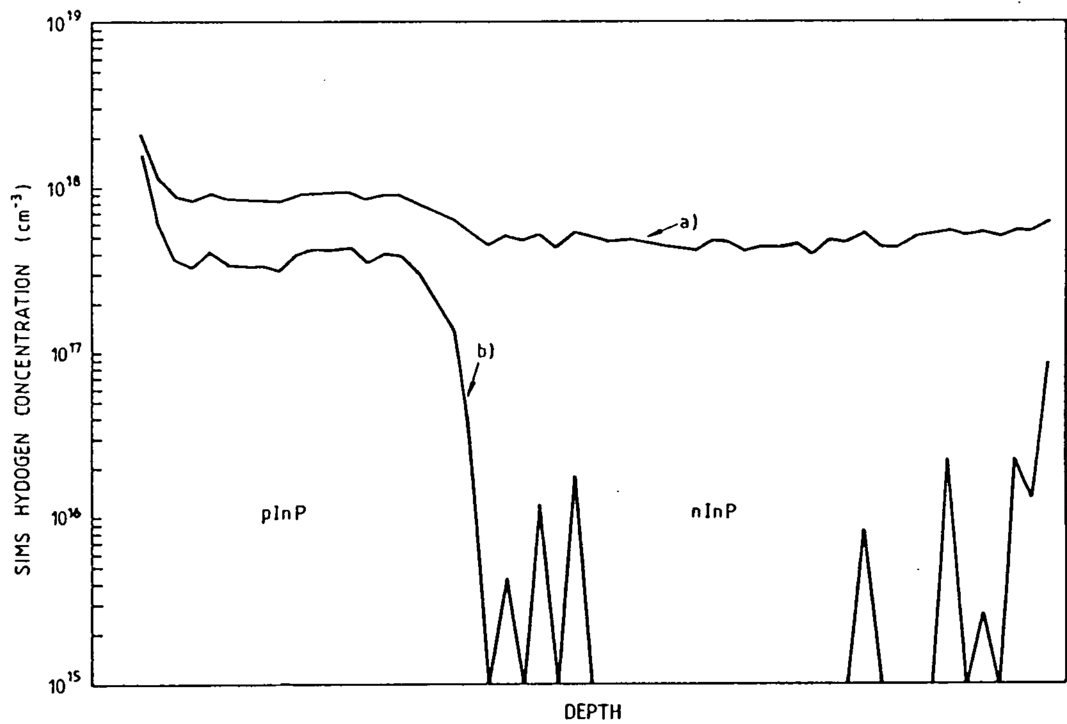

Figure (5.21): SIMS depth profile through the sample used for the results of figure (5.20), showing the presence of hydrogen in the surface layer of p-InP. Curves (a) and (b) give respectively the hydrogen concentration before and after correction for the background level of hydrogen in the SIMS apparatus.

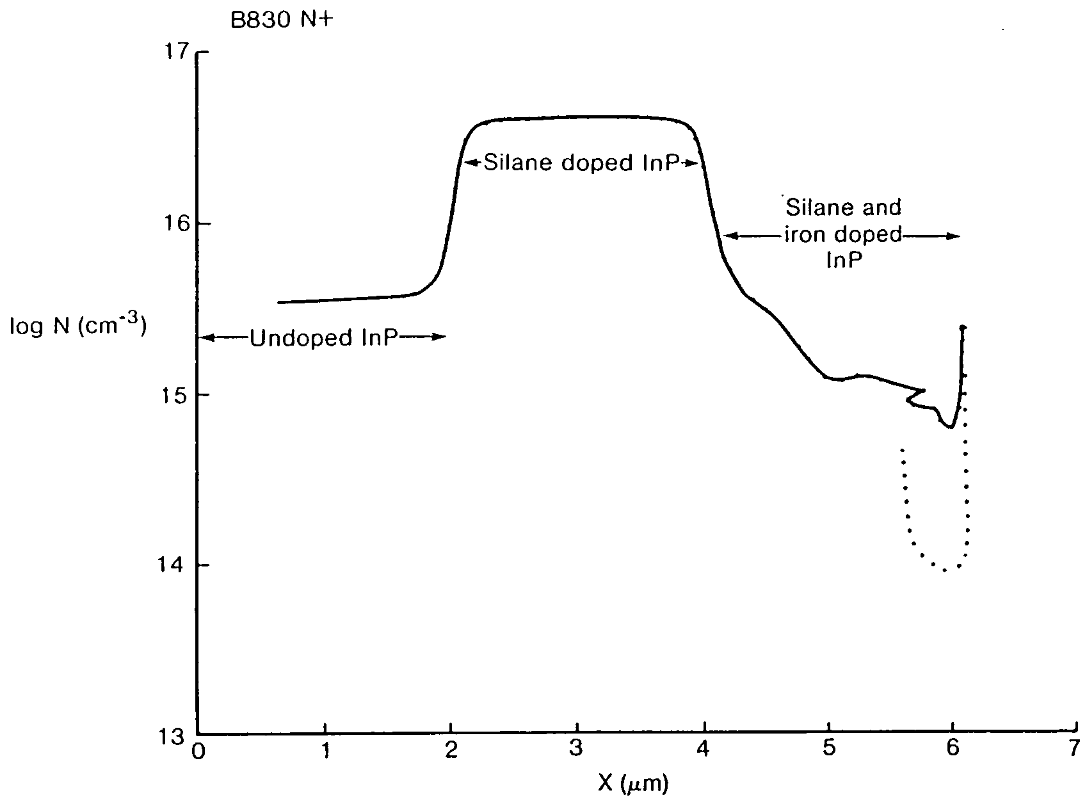

Figure (5.22) Electrochemical profile through a structure consisting of undoped InP, silicon doped InP, silicon and iron doped InP, and iron doped InP. The layer doped with both iron and silicon, gave an electron concentration less than the layer doped only with silicon. The material doped only with iron would not etch, though a p-type trace was obtained (dotted line).

Chapter 6

Low Dimensional Structures

A brief outline of low dimensional structures along with device applications is given. Experimental results are presented upon (GaIn)As/InP and (GaIn)(AsP)/InP multi-quantum well structures.

Background

The term low dimensional structures, refers to structures and devices where the dimensions of epitaxial layers, are reduced to less than a few hundred Ångstroms thickness. Due to quantum confinement effects, a layer of (GaIn)As of 100Å thickness for example, sandwiched between InP layers, will exhibit a higher energy radiative transition than a thick 1000Å layer of (GaIn)As. Such thin layers are normally referred to as quantum wells.

A simple model for explaining the quantisation of energy levels within the quantum well, is to consider the converse situation to that normally applied via the Kronig Penney model for band structure in crystalline solids. As the number of energy levels available reduces as the number of atoms reduce, the band structure of the material, normally smeared together to form a continuous band, begins to resolve into individual energy levels. The individual energy levels are of a higher energy in the conduction band compared with bulk material, and of a lower energy compared with bulk material in the valence band. The radiative transition equivalent to that from the conduction to valence band, is then of a higher energy and shorter wavelength than the bulk material. The quantum well energy level distribution can be modelled from the hydrogen atom model, allowing for the different materials and surrounding crystal fields.

For the energy levels in the quantised region to be occupied by carriers, the surrounding material must have a larger band gap and so donate electrons and holes to the well material. Examples of suitable material combinations are GaAs quantum wells surrounded by (GaAl)As, and (GaIn)As quantum wells surrounded by (GaIn)(AsP) material.

Quantum wells refer normally to structures where quantisation has

taken place in one dimension only, and solely by manipulation of the crystal growth technique. Quantisation can be taken further by confining the low band-gap material in two dimensions - quantum wires, and completely surrounding the low band-gap material in three dimensions - quantum boxes [129,130]. The latter two structures are achieved by sub-micron lithographic techniques, usually involving the use of electron beam lithography and epitaxial re-growth.

Most structures fabricated to date usually consist of a series of quantum wells of different thicknesses plus a thick reference layer of the same material, separated by thicker layers of the wider band gap material. The different layer thicknesses result in different energy gaps, and hence in different photoluminescence emission wavelengths when the material is pumped by a laser beam. The luminescence intensity and the sharpness of the emission peaks, give an indication of the quality of the quantum wells in terms of compositional uniformity, spatial planarity and interface abruptness. It is difficult however, to de-convolve the effects due to each of the above causes, without additional information gained from other experimental techniques, such as transmission electron microscopy (TEM).

Many of the papers written upon low dimensional structures and MOVPE, refer to theoretical models of the variation of energy level and photoluminescence wavelength as a function of well width. Experimental data often lies at shorter wavelengths than predicted, and it is clear that progress is still required before quantisation in quantum wells is correctly modelled and understood.

An alternative structure that is often grown, consists of multiple quantum wells of equal thickness, separated by barrier layers thick enough to isolate the quantum wells from each other. Structures consisting of many repeats of quantum wells of the same thickness, separated by barrier material of similar thickness are termed superlattices. These latter structures exhibit electronic properties that are different from either of the constituent materials, and it is predicted that new materials and devices will result from superlattice development.

Device Applications

Single and multiquantum well structures are used in laser applications with GaAs quantum wells surrounded by (GaAl)As. Improved laser performance has been reported and will be elaborated upon in the next chapter. An advantage of quantum wells used in the (GaIn)As/InP system is that the full wavelength range from (GaIn)As bulk material at 1.67μm, through to 1μm wavelength can be addressed [131]. In principle it is easier to grow multiple ternary layers than the thicker quaternary layers needed to address the same wavelength range. However, there are few reports of good quality laser material being obtained using the (GaIn)As/InP quantum well arrangement. The GaAs/(GaAl)As quantum well emitters are able to emit in the red region of the visible spectrum due to the wavelength shift obtained by quantisation.

Superlattices, which exhibit high non-linear electro-optic properties have been exploited to fabricate optical modulators, and it has been predicted that the construction of optical switches may also be possible [132]. Another device is the Bloch oscillator for sub-millimetre microwave generation, which relies upon electron tunnelling through the barrier layers separating the quantum wells. Avalanche photodiodes have also been fabricated using periodic thin layers of materials [133].

The use of heterojunctions to induce two dimensional electron gases at interfaces, and consequently the realisation of high mobility material, has already been discussed in chapter (4)[134]. This concept can be extended further to multiple quantum wells of undoped high mobility (GaIn)As, surrounded by highly doped n-type InP layers which act as electron sources. Such structures are called modulation doped multi-quantum wells. Thin spacer layers of undoped InP are incorporated to prevent dopants diffusing into the (GaIn)As during growth, and cause the mobility of the two dimensional electron gas to reduce due to ionised impurity scattering [135]. Shubnikov de Haas measurements are used to confirm the two dimensionality of electron movement in such material, by measuring magneto resistance in a high magnetic field. When applied to the above structures, these measurements have indicated that only the outer two wells in repeated structures were contributing to the mobilities measured [136,137].

This was thought to be due to the barrier material being unable to supply sufficient electrons to the quantum well for the two dimensional electron gases to be formed. For the outer wells, much thicker layers of higher band-gap material are normally adjacent.

The two dimensional electron gas concept and structures may also be extended to p-type material, where hole mobilities of 10500 $cm^2V^{-1}s^{-1}$ have been reported for hole measurement in undoped thin layers of (GaIn)As adjacent to p-type InP [138].

An associated concept to superlattices is the formation of layered crystals. Fukui et al have reported the growth of alternate layers of GaAs-InAs upon InP substrates [139]. The crystal structure then consists of alternate sequences of gallium, arsenic, indium and arsenic atoms in the (100) growth direction. Such layers are expected to yield higher mobilities than conventional (GaIn)As layers which are less ordered, and suffer from alloy scattering.

Growth on Mismatched Substrates

There has been considerable interest in the growth of GaAs/(GaAl)As epitaxial layers upon silicon substrates, and of InP/(GaIn)(AsP) layers upon GaAs substrates. In each case the epitaxial layers are severely lattice mismatched to the substrate. The objective is to combine the cost effectiveness of silicon integrated circuits, the high speed of GaAs electronic devices, and the opto-electronic capability of the III/V alloy system.

The large lattice mismatch however in some cases prevents devices from working, and in other cases results in poor device reliability. The most frequently observed cause of poor reliability in (GaIn)(AsP) devices, is the formation of dark-line or dark-spot defects, which in lasers for example, give rise to non-radiative transitions. They can also act as fast recombination paths in devices. Dark-line or dark-spot defects are associated with single dislocations or dislocation clusters, usually threading through layers from interfaces. Mismatched structures introduce a profusion of dislocations. Superlattices are reported to have the property of turning dislocations away from the growth direction. Gourley et al have reported a reduction in the number of dark-line defects observed in strained epitaxial systems by using superlattices to prevent

propagation of defects [140].

Growth of Low Dimensional Structures

The growth of thin layers, of less that 1000Å, in principle requires that reactants are switched quickly in and out of the MOVPE growth zone, and that growth rates are sufficiently slow that valve switching delays have negligible effect, and the overall reactor control system is accurate and reproducible.

The growth rate is determined by the number of moles per second of group III elements, reaching the hot growth zone. These amounts are in turn dependent upon the metal alkyl vapour pressures, and flow rates through the bubblers. Since trimethylindium has a relatively low vapour pressure, there is no difficulty involved in reducing the growth rate of InP, since hydrogen flow rates through bubblers are normally in excess of $30cm^3min^{-1}$. However, trimethylgallium has a much higher vapour pressure, with flow rates through the bubbler of around $10cm^3min^{-1}$ normally being used. Flow rates below $2cm^3min^{-1}$ are usually considered unrepeatable and inaccurate for matrix elements. A normal epitaxial growth rate in an MOVPE reactor might be $0.05\mu m\ min^{-1}$ or $8Ås^{-1}$. The growth rate of gallium containing alloys can be lowered by diluting and discarding some of the trimethylgallium flow, a system that is used upon many modern MOVPE reactors. Alternatively a lower vapour pressure gallium source can be used such as a trimethylgallium - trimethylphosphorus adduct. The authors reactor had neither of the above features available, and so a minimum growth rate of $8Ås^{-1}$ was obtained for (GaIn)As.

It is necessary for the gas compositions entering the reaction zone to change abruptly, otherwise the resultant interface disturbance will constitute the whole extent of the quantum well. Most reactors that have successfully grown low dimensional structures have therefore utilised vent-run switching manifolds, with constant volume switching within the valves, and with pressures equalised between the vent and run lines. Even then, the change in viscosity resulting from switching from a flow of phosphine to a flow of arsine though the reactor, causes pressure transients and flow rate changes. To overcome this, further amounts of compensating flows of hydrogen gas can be toggled in and out of the reactor to maintain a constant pressure in the

growth tube. Control algorithms however become complicated. It is also essential that all of the reactant valves to be switched, are activated simultaneously to avoid for example, arsine appearing in InP barrier layers.

Any stagnant areas that might cause storage of gas between the switching valves and the growth zone also require reducing to a minimum. Reactor cells with transverse baffles are often used to induce a parallel gas velocity profile over the substrates, however, the risk of introducing a recirculating storing area between the baffles is enhanced. Even after all of the above precautions have been taken, it is common to find arsine in InP barrier layers grown directly after (GaIn)As quantum wells [131].

The problem of arsenic or arsine remaining at the growing interface long after the arsine flow has been switched out, has resulted in many MOVPE and MBE workers using growth pauses between the layers of quantum wells [131,133,135,141,142,143,144]. This technique allows sweeping away of residual reactants, but may result in surface degradation due to group V element loss, or to impurity contamination of interfaces. Barrett et al have demonstrated that the level of arsenic found in InP barrier layers was inversely proportional to the growth pause time [144].

Moss et al have pioneered a new approach that may avoid many of the above reactor complications, whereby the substrate is transferred from one gas stream to another by mechanical means [145]. Each flow is constant and would constitute the reactants needed to grow the different layers of superlattice structures.

The author has grown low dimensional structures in both the (GaIn)As/InP and (GaIn)(AsP)/InP systems. It is convenient to review results upon these structures in conjunction with data obtained from the literature. Periodic multi-quantum well structures are normally assessed by cross sectional TEM and double crystal X-ray diffractometer studies. Single quantum wells and multiple quantum wells, where the well width varies, are normally assessed using low temperature photoluminescence.

Photoluminescence Studies of (GaIn)As/InP Quantum Wells

Figure (6.1) shows a structure consisting of four quantum wells of (GaIn)As of 400Å, 200Å, 150Å and 86Å thickness. The growth conditions for the ternary layers were identical to those used for bulk (GaIn)As with a growth rate of 8Ås^{-1}. The InP barrier layers were 200Å thick, and were grown at a rate of 5Ås^{-1}. The photoluminescence spectrum at 4.5K from this sample is shown in figure (6.2). The emission from the thinner wells can be clearly distinguished, whilst emission from the 400Å and 200Å wells overlap each other. The narrowness of the photoluminescence peaks is used to ascertain the quality of the interfaces. An irregular interface will give rise to a variety of emission wavelengths, and a broad spectrum.

Figure (6.3) shows the structure of a multiquantum well sample with thinner quantum wells, along with a thick 1000Å ternary layer incorporated as a bulk material reference, against which the composition of the layers can be determined from the quantised energy shift. The InP barriers were again 200Å thick and the intended thicknesses of the quantum wells was 100Å, 50Å, 25Å and 10Å. The growth time of the thinnest layer was only two seconds.
A photoluminescence spectrum of this layer at 5K is shown in figure (6.4). The 100Å quantum well gave the narrowest full width at half maximum value for this series of layers, and a figure of 6.9meV was obtained. These results are compared with those of other workers in table (6.1) and figure (6.5).

There is a clear trend to narrower photoluminescence peaks with increasing well widths, almost regardless of worker. This may arise because a thickness variation due to gas switching, will constitute a greater proportion of a narrow quantum well compared with a thick quantum well.

The first reported MOVPE quantum wells grown by Kuo et al are included in table (6.1)[142]. The sharpest photoluminescence full width at half maximum value of 24 meV on 5Å thick quantum wells, was reported by Pannish et al using MBE growth [150]. It should be noted that the temperatures of the measurements in table (6.1) vary, though most are quoted as being between 4-6K. A further note of caution is that it is possible for sharper photoluminescence peaks to be obtained from the same sample if the incident laser beam power density is

Table (6.1): Comparison of Low Temperature Photoluminescence Results

Liquid helium photoluminescence energy, full width at half maximum (FWHM)(meV)	(GaIn)As well thickness (Å)	Literature reference
2.2	200	143
3	100	143
4.5	160	146
5.3	150	147
5.5	80	146
6	65	143
6.1	**150**	**This work**
6.9	**50**	**This work**
7.9-10	100	148
8	103	131
9	54	131
9	8	149
9.1	**86**	**This work**
10	30	150
10.7	35	142
14.5	**25**	**This work**
15	25	146
15	35	131
15	25	141
15.1	**100**	**This work**
21	25	143
21.5	125	142
24	5	150
25	19	131
26	15	146
26	10	131
30	20	141
32.7	**15**	**This work**
37	10	143
53	62	142

reduced.

Many of the results quoted in table (6.1) were from samples grown utilising pauses in the growth between the (GaIn)As and InP layers and vice versa. This was usually achieved by switching off the group III alkyl sources at the vent-run manifold of the reactor. The author's results were obtained by continuous growth at atmospheric pressure. It is expected that better interfaces are obtained at low growth pressure due to the shorter transit times of the gases.

TEM Studies of (GaIn)As quantum wells

A method of judging the quality of quantum wells, which is more appealing to the human eye than other techniques, is to cross section epitaxial slices and obtain transmission electron micrographs of the layers. Figure (6.6) shows a cross sectional micrograph through the four quantum well sample illustrated in figure (6.3). The lighter areas represent the (GaIn)As layers, each of which can be observed clearly, including the thinnest one which is only a few atoms thick. Each of the small spots observable on this high magnification lattice imaging TEM micrograph, represents a column of atoms running perpendicular to the plane of the paper. An idea of the interface abruptness, and of the number of misplaced atoms and edge dislocations, can be obtained upon closer examination. A disadvantage of TEM however, is that it is possible to produce a high contrast image, even for a poorly defined interface, which could be misleading.

A third structure is illustrated in figure (6.7). This consists of a repetition of ten 100Å (GaIn)As quantum wells, separated by nine 200Å InP barrier layers, along with an InP substrate buffer layer of 1000Å and an InP cap layer of 1μm thickness. The latter was grown to protect the quantum well structure during the delicate thinning operation required for TEM studies.

At first sight, the interfaces appear to be very sharp with no fuzziness, indicating that mixing of the InP and (GaIn)As layers had not occurred. However, whilst the interfaces between the (GaIn)As grown upon InP layers appear to be planar, the interfaces between the InP grown upon (GaIn)As layers undulates. It was unclear why this phenomenon occurred, however it has been observed in the TEM micrographs of other workers' layers, always with one planar and one

undulating interface [144]. It is also possible that the arsenic signals detected in InP layers discussed earlier are also related to this phenomenon. In all cases the growth of subsequent InP layers re-planarises the structure.

In order to gain a better understanding of the effect, similar quantum well structures were grown using different growth conditions. Initially it was believed that either growth temperature or growth rate was responsible for causing undulations in the (GaIn)As layers, which gradually worsened through the layer, the InP growth recovering the overall planarity of the epitaxy.

Epitaxial layers were grown consisting of groups of (GaIn)As/InP quantum wells, with each group being grown under different conditions. The first structure (figure 6.8) consisted of four groups of quantum wells, each containing eight wells of (GaIn)As, where the growth conditions were identical except that the growth temperature was changed from 600°C through to 700°C. A second similar structure was grown with the batches of wells grown under different V/III ratios, and with 6s pauses under the previous group V reactant also being present for two of the four batches (figure 6.9). A third structure was grown with different growth rates being used for each of the four batches of quantum wells, figure (6.10). When the above samples were thinned and examined using TEM, undulations were observed in most of the quantum wells, again at the InP upon (GaIn)As interface.

It was decided to determine whether the variability of well thickness was resulting specifically at the interface, or as originally thought, gradually throughout the growth of the (GaIn)As layer. A further structure was grown, figure (6.11), consisting of four groups of (GaIn)As/InP quantum wells, with the 100Å (GaIn)As layers being marked by very thin layers of (GaIn)(AsP) or InAs. One group of wells, each taking 6s to grow, was unmarked and used as a control for the experiment. Another two groups were marked with a 0.6s burst of either InAs or (GaIn)(AsP), two thirds of the way through the (GaIn)As layer. The InAs and (GaIn)(AsP) markers were grown simply by switching out the trimethylgallium flow or switching in a large phosphine flow respectively. No attempt was made to lattice match the marker layers to the surrounding crystal structure. A fourth group of 100Å thick quantum wells was grown, marked with three thinner (GaIn)(AsP) marker layers, each grown for 0.2s in the second half of

the quantum well. High magnification TEM images are shown in figures (6.12) and (6.13), firstly for quantum wells with single InAs marker layers, and secondly for quantum wells with triple (GaIn)(AsP) marker layers. In each case the wells and marker layers can be clearly seen. The (GaIn)As upon InP interfaces and all of the marker layers appear to be planar, whilst the InP on (GaIn)As interface appears irregular as observed in previous structures.

These results indicate that the growth of (GaIn)As quantum wells proceeds in a planar fashion, with the undulations in the InP on (GaIn)As interface appearing after completion of the (GaIn)As layer. The fact that the marker layers also appeared to be planar at both interfaces with the (GaIn)As, indicated that arsine, unswitched for growth of the markers but switched out to grow InP, may be instrumental in causing interface undulations.

A further structure was grown where attempts were made to improve interface planarity using growth pauses. This structure, shown in figure (6.14), consisted of three groups of 100Å thick (GaIn)As quantum wells, separated by 260Å thick InP barrier layers. The first group of wells was grown continuously, without pauses, to act as a control for the rest of the epilayer during TEM analysis. The second group of quantum wells were grown using 6s growth pauses at the interfaces. This was achieved by terminating growth by switching the group III reactants to vent, pausing the InP under a hydrogen and phosphine gas ambient, and pausing the (GaIn)As under an arsine and hydrogen gas ambient. The third set of quantum wells retained the same method of growth pause, using phosphine for the InP to (GaIn)As interface, but the (GaIn)As layers were paused for 12s under hydrogen alone, prior to resuming growth of InP.

The structure was analysed using cross sectional TEM. In each case the lower interfaces of (GaIn)As grown upon InP were sharp, as observed previously. For the first, unpaused group of wells, the second InP upon (GaIn)As interface exhibited undulations. The same interface for the second group of quantum wells, paused under arsine for 6s, exhibited far worse undulations (figure 6.15). The upper interface for the third group of wells, paused under hydrogen alone, appeared to be the flattest of the three groups of quantum wells grown (figure 6.16).

There is therefore a trend towards achieving better interfaces,

using growth pauses that allow sweeping away of excess arsine, and towards degraded interfaces when pausing under arsine. This conclusion is consistent with those of other workers. Miller et al have detected arsine in InP layers using auger sputtering techniques. It was inferred that the arsine was 100 times slower than phosphine in being swept out of the reaction zone [141].

MBE grown (GaIn)As/InP quantum well structures do not appear to exhibit the problem of undulating interfaces [150].

Double Crystal X-Ray Analysis of (GaIn)As Quantum Well Samples

Figure (6.17) shows a double crystal x-ray rocking curve from a ten period (GaIn)As quantum well structure. The gain of the x-ray detector was increased away from the main peak in order to detect satellite peaks due to the quantum wells. The spacing of the satellite peaks in this sample, 640 arc seconds, relates to a 290Å quantum well periodicity which agrees closely with the intended growth cycle of 100Å of (GaIn)As and 200Å of InP. Barnett et al have modelled the x-ray rocking curve from a similar structure, and determined that a low arsenic level within the start of the InP barrier layers was necessary to explain the experimental results [144]. These predictions were subsequently confirmed by SIMS analysis, with the level of arsenic detected in the InP being inversely proportional to the pause in growth after the Ga(InAs) epitaxy.

(GaIn)(AsP) Quantum Well Structures

Quantum well structures were also grown using 1.3μm emission (GaIn)(AsP) material surrounded by wider band-gap InP barrier layers. Figure (6.18) shows a ten quantum well repeat structure consisting of 100Å quaternary layers separated by 350Å InP layers. A 0.5μm substrate buffer and a cap layer was also grown. The last two (GaIn)(AsP) wells were grown without a barrier layer due to a computer fault. A cross sectional TEM micrograph of the above structure is shown in figure (6.19). The interfaces observed in this structure appear to be more planar than those obtained within (GaIn)As/InP quantum well structures. It was noted however that rippling of the InP upon (GaIn)(AsP) interface was observed for 1.55μm emission quaternary

material, grown upon a different reactor.

The above observations are consistent with disturbances at interfaces due to gas switching transients, or more likely, reluctance of arsine to be swept away from the substrate at the start of InP growth. 1.55μm emission quaternary bears more resemblance to (GaIn)As than to 1.3μm emission quaternary in terms of growth conditions, there being a 5 fold decrease in the amount of arsine required to grow the shorter wavelength material. The multiquantum well structure shown in figure (6.18) was also analysed using low temperature photoluminescence, and a full width at half maximum of 6.3 meV was obtained, indicating good reproducibility of one well with respect to another. A double crystal x-ray rocking curve taken upon the structure is shown in figure (6.20). The satellite peaks due to the quantum wells are visible, as are the substrate and main epilayer peaks.

The final quaternary quantum well structure grown is shown in figure (6.21), this consisted of four wells of 200Å, 100Å, 70Å and 35Å plus a bulk 2000Å quaternary layer. The epilayer was analysed using low temperature photoluminescence at 4.2K in a similar manner to that used for (GaIn)As quantum well samples. The spectrum is shown in figure (6.22), each of the layers being well resolved. The full width at half maxima appears to correlate well with the data upon (GaIn)As/InP quantum wells in table (6.1), despite the difference in materials.

There are relatively few literature references to quaternary quantum well results with which to compare the above data. There are a few references available on Shubnikov de Hass measurements undertaken upon (GaIn)(AsP) structures [136,137].

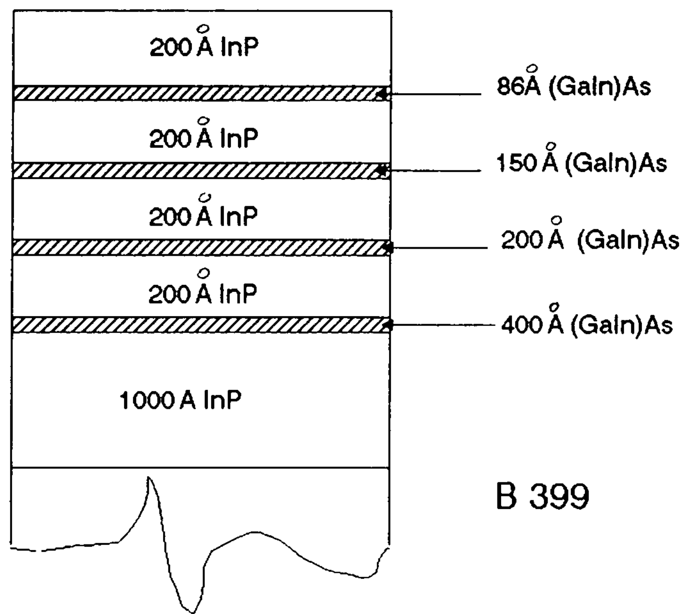

Figure (6.1): "Quantum well" structure consisting of (GaIn)As and InP layers.

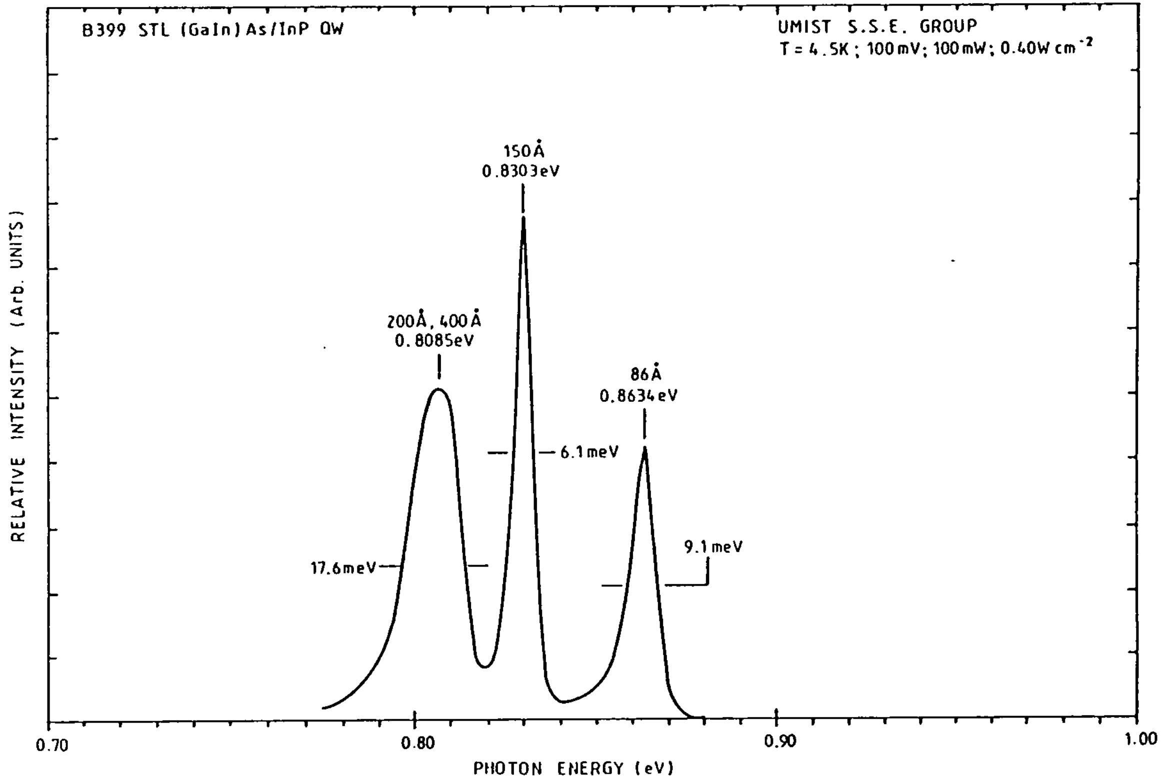

Figure (6.2): 4.5K photoluminescence spectrum from the structure illustrated in figure (6.1).

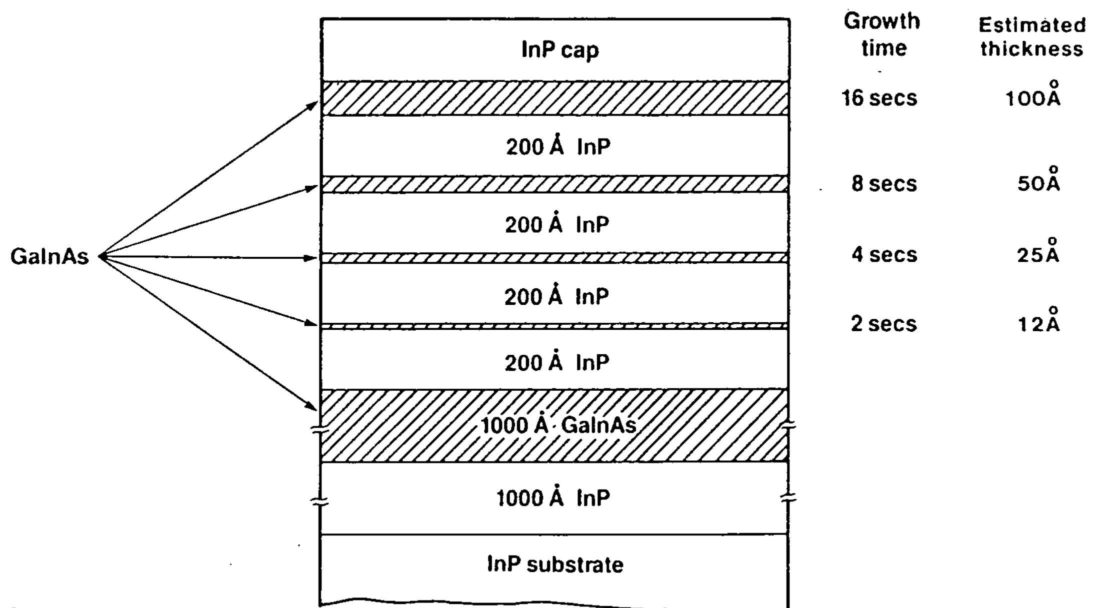

Figure (6.3): Quantum well structure consisting of four (GaIn)As wells surrounded by InP along with a thick reference layer of (GaIn)As.

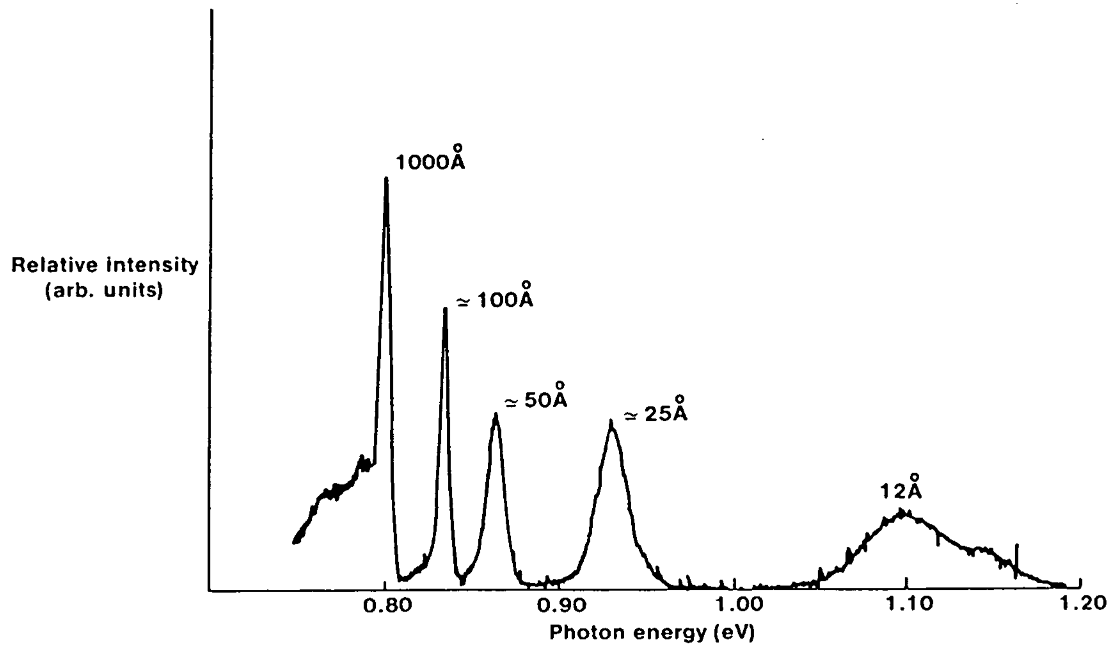

Figure (6.4): 5K photoluminescence spectrum for the structure illustrated in figure (6.3).

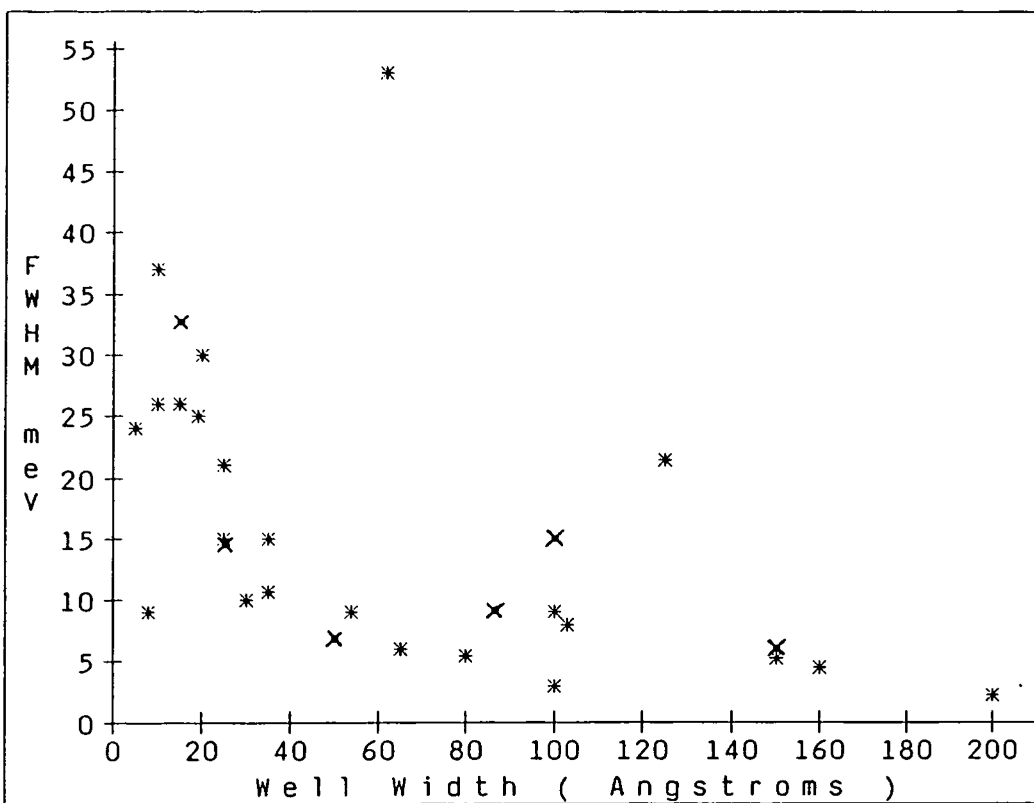

Figure (6.5): Variation of low temperature photoluminescence spectrum full-width-half-maxima, as a function of (GaIn)As/InP quantum well width; for data taken from the literature (*) and the author's work (x).

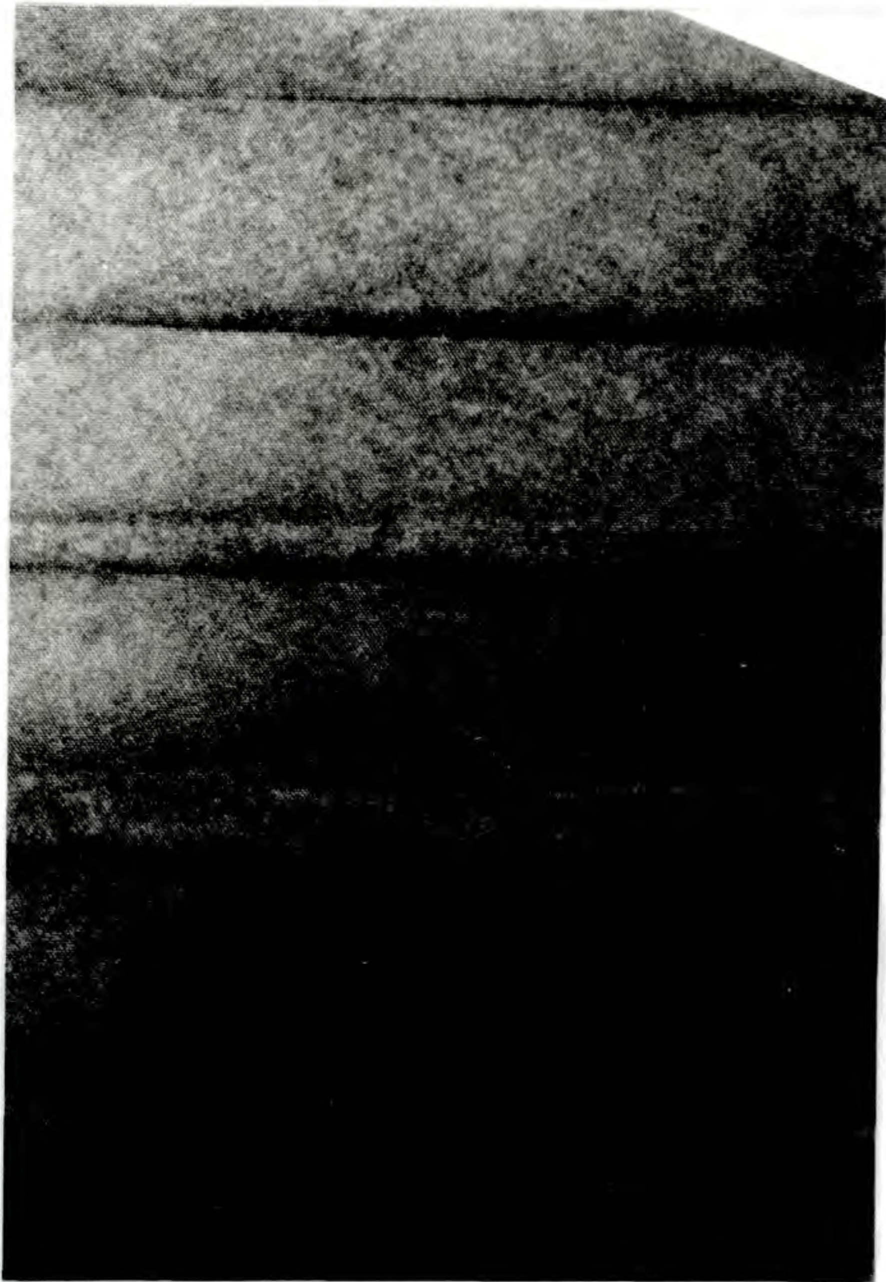

Figure (6.6): Transmission electron microscope high resolution lattice image through the structure illustrated in figure (6.3).

Magnification = X 1310000

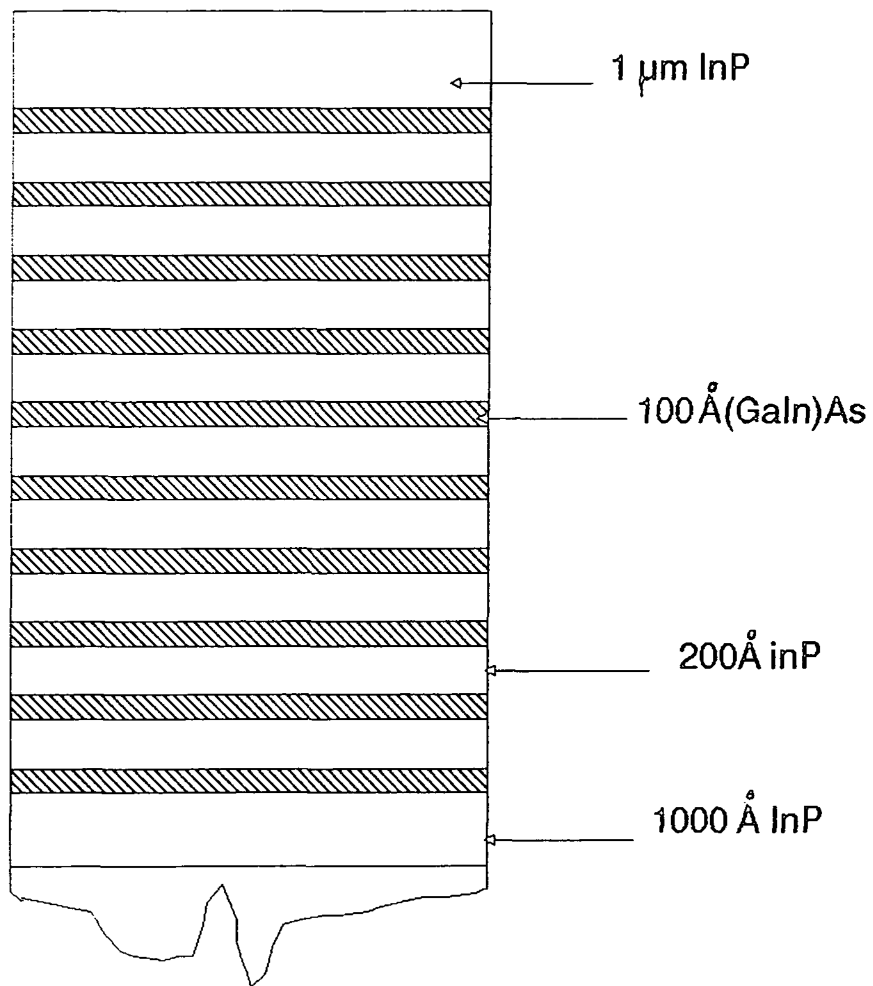

Figure (6.7): 10x (GaIn)As/InP repeated quantum well structure.

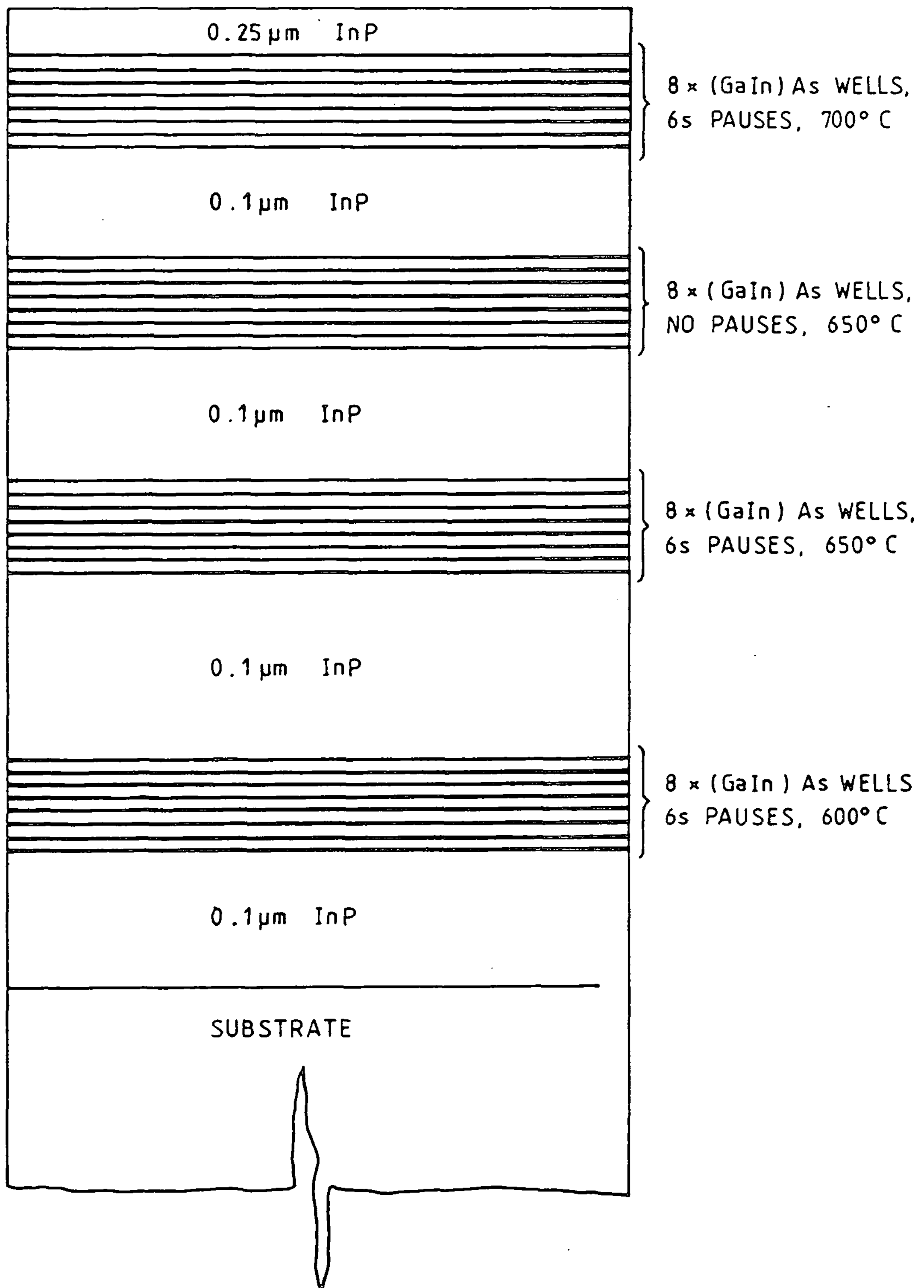

Figure (6.8): (GaIn)As/InP quantum well structure consisting of 4 groups of wells, each group being grown at different growth temperatures, with and without growth pauses. The (GaIn)As layers were ≈100Å thick, and the InP spacer layers were ≈250Å thick.

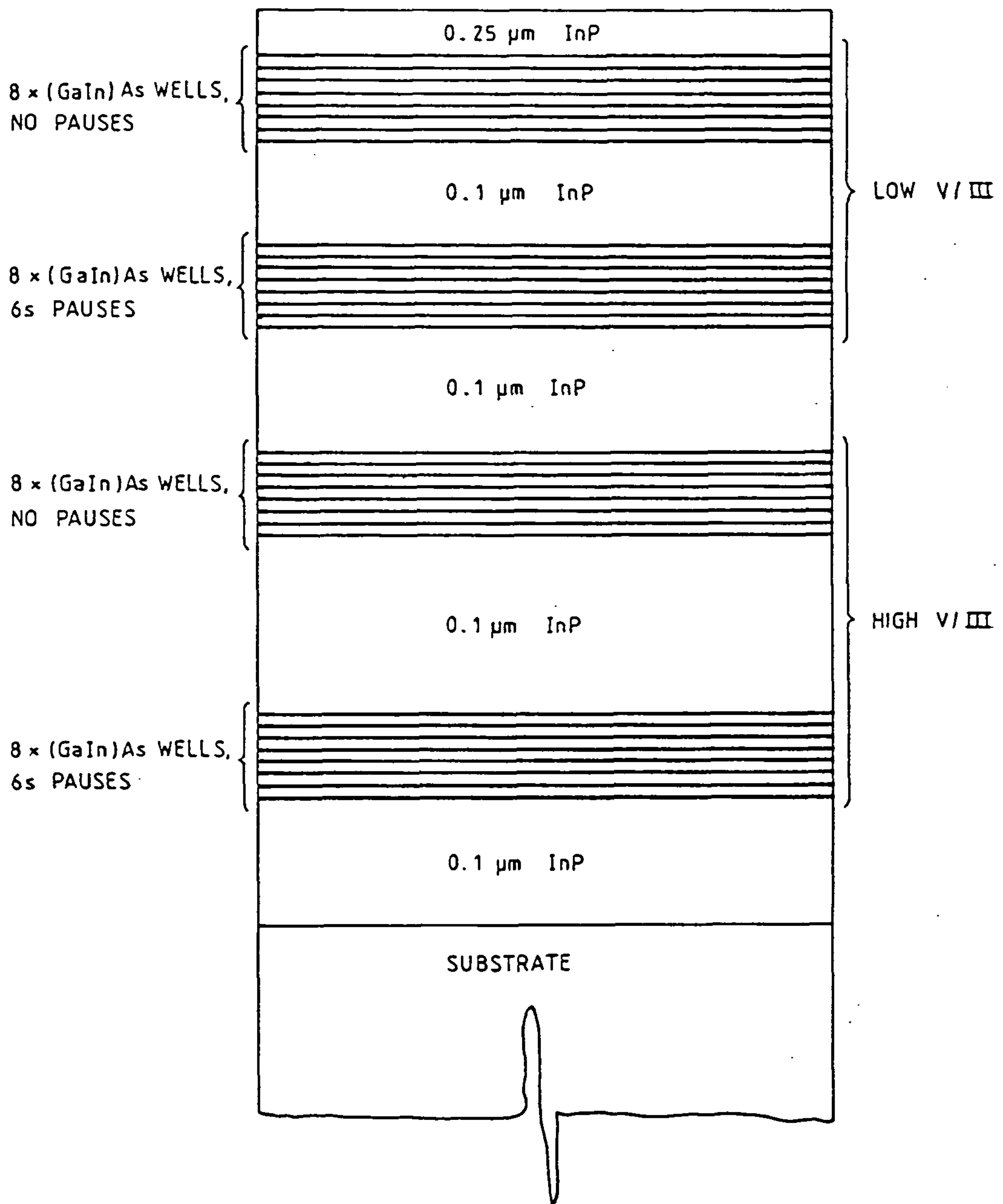

Figure (6.9): (GaIn)As/InP quantum well structure consisting of 4 groups of wells, each group being grown either with different V/III gas ratios, or with and without growth pauses. The (GaIn)As layers were ≈100Å thick, and the InP spacer layers were ≈250Å thick.

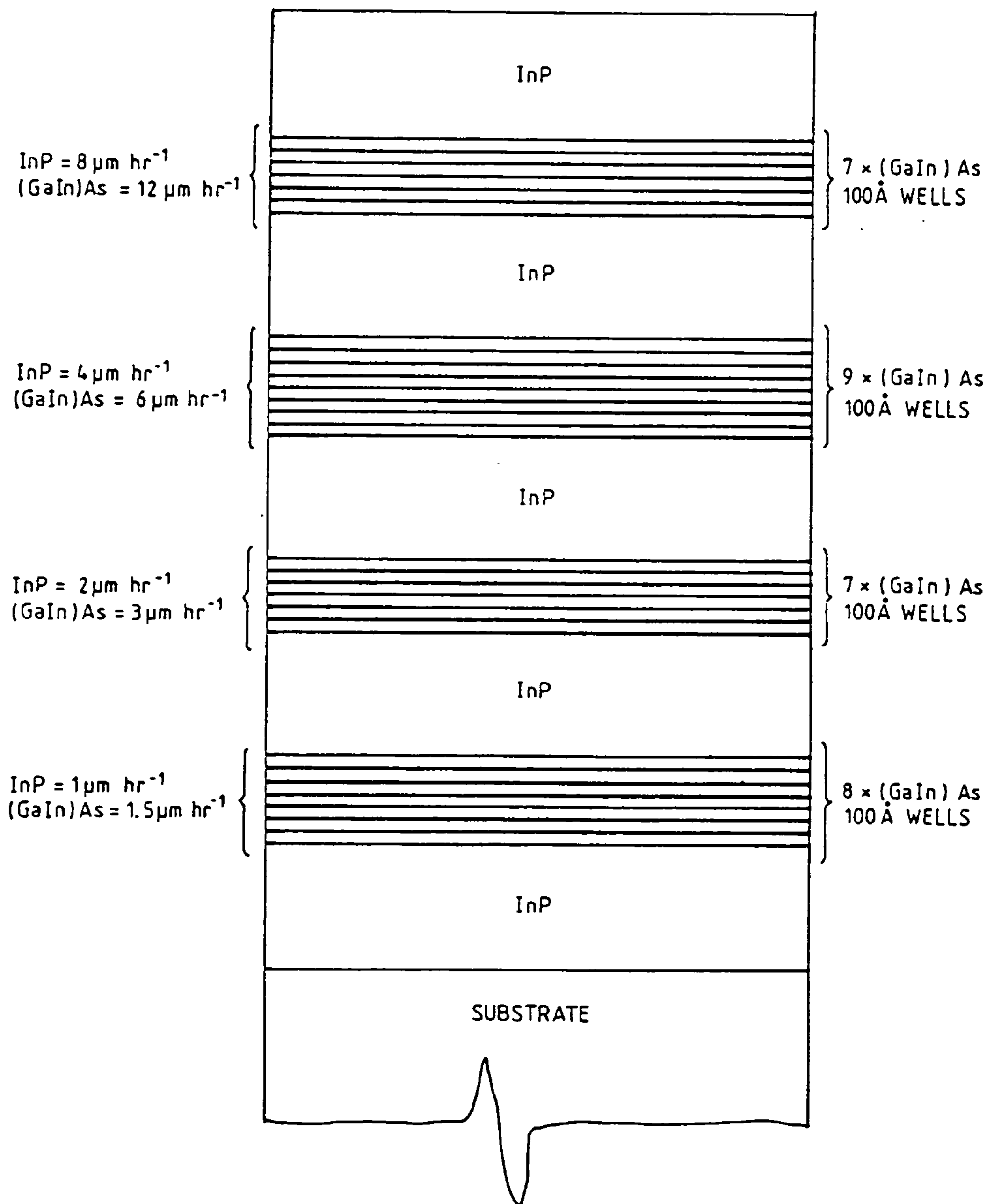

Figure (6.10): (GaIn)As/InP quantum well structure consisting of 4 groups of wells, each group grown using a different growth rate. The (GaIn)As layers were ≈100Å thick, and the InP spacer layers were ≈250Å thick.

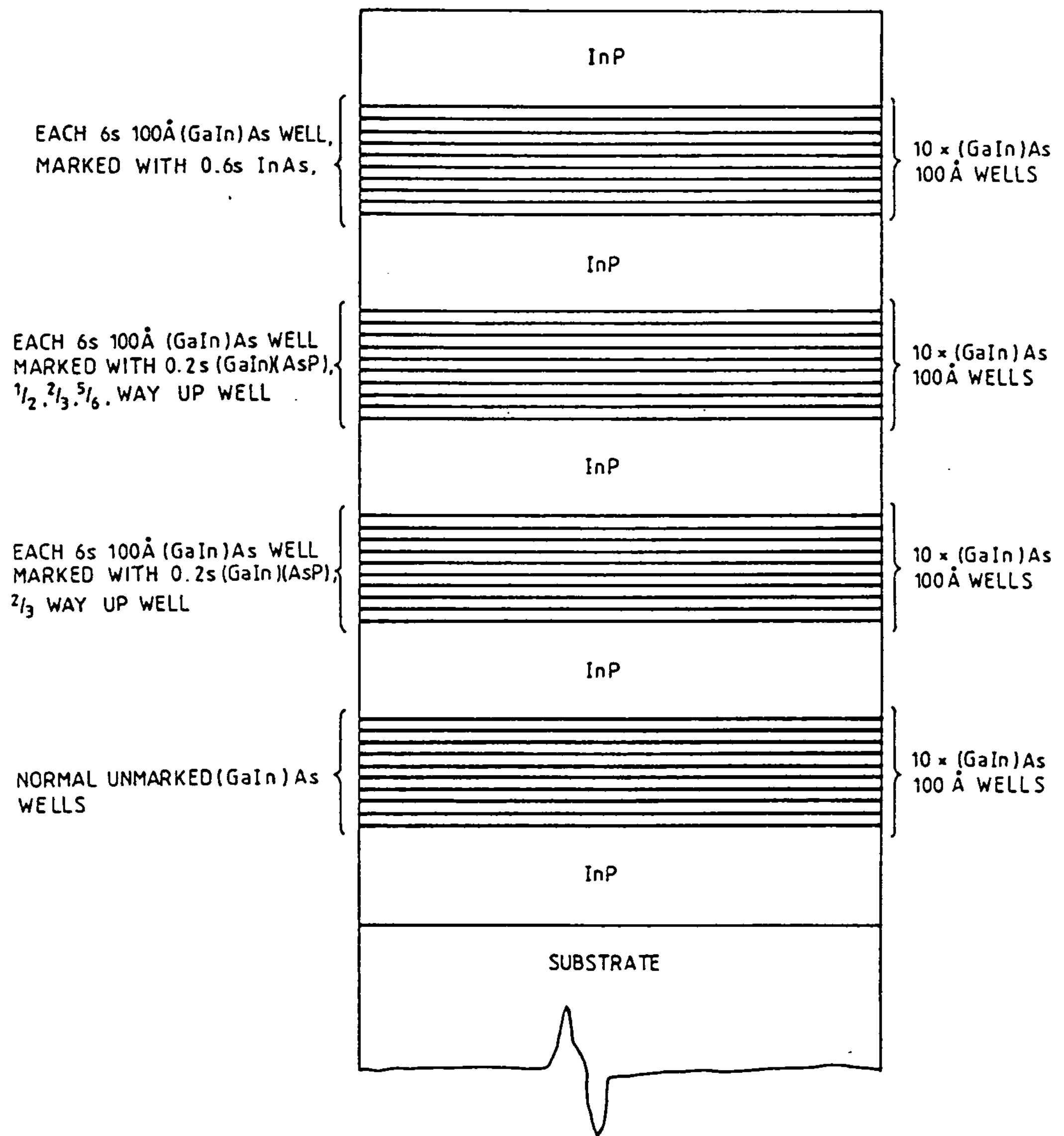

Figure (6.11) (GaIn)As/InP quantum well structure consisting of 4 groups of wells, the first group acting as a control group, and subsequent groups being marked with either (GaIn)(AsP) or InAs marker layers, to determine if interface irregularities are formed during growth, or at completion of the growth of each (GaIn)As well. The (GaIn)As layers were ≈100Å thick, and the InP spacer layers were ≈250Å thick.

Figure (6.12): Transmission electron micrograph of quantum wells marked with InAs layers, showing planarity of the layers during growth.

Figure (6.13): Transmission electron micrograph of quantum wells marked with 3 (GaIn)(AsP) layers. Each quaternary layer was grown for only 0.2s, and is <10Å thick.

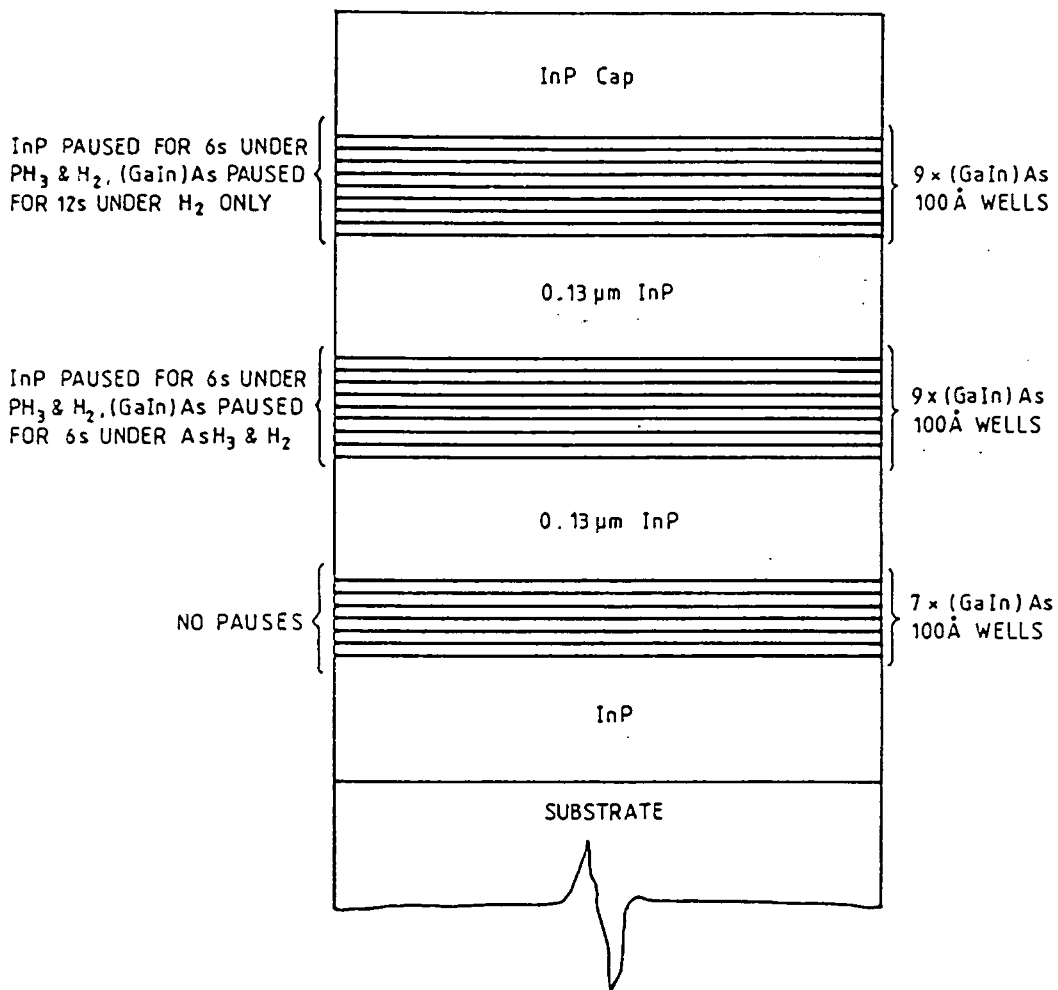

Figure (6.14): (GaIn)As/InP quantum well structure consisting of 3 groups of wells, each group grown using a different pause sequence. The (GaIn)As layers were ≈100Å thick, and the InP spacer layers were ≈250Å thick.

Figure (6.15): Transmission electron micrograph of the structure illustrated in figure (6.14), showing (GaIn)As surfaces paused under AsH_3 for 6s. The interfaces exhibit enhanced roughening.

Figure (6.16): Transmission electron micrograph of the structure illustrated in figure (6.14), showing (GaIn)As surfaces paused under H_2 for 12s. The interfaces exhibit reduced roughening.

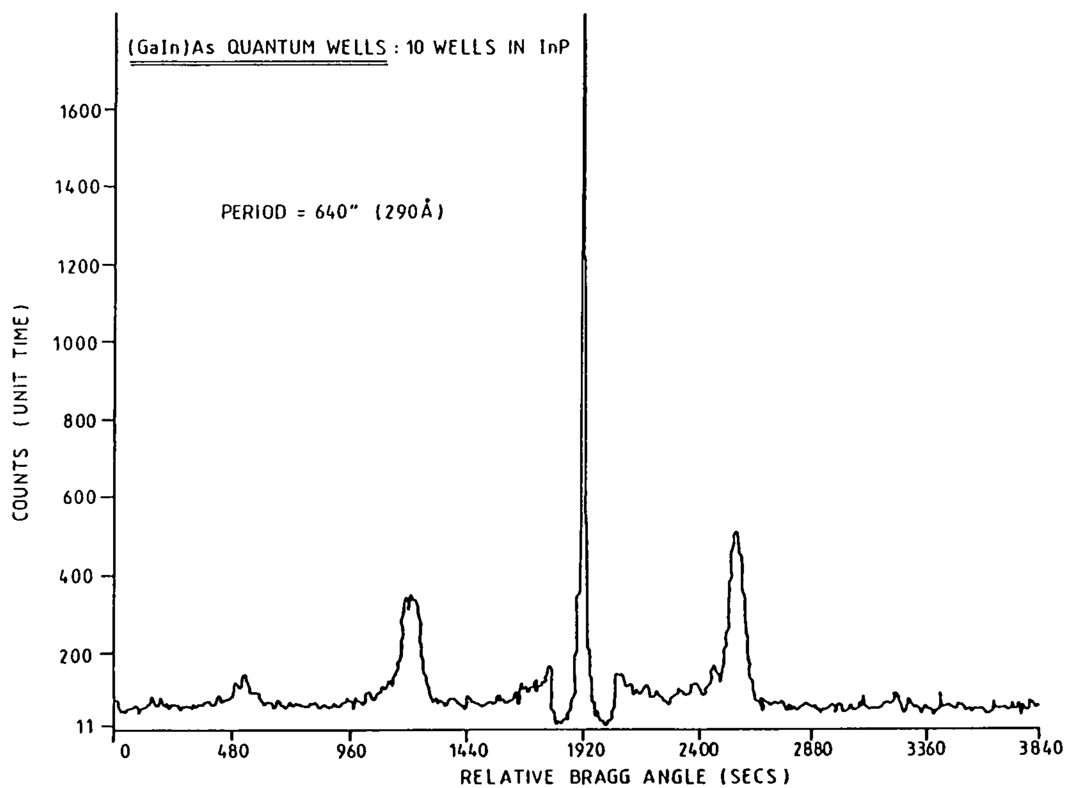

Figure (6.17): Double crystal x-ray rocking curve for the 10 period (GaIn)As/InP structure shown in figure (6.7). Satellite peaks can be observed.

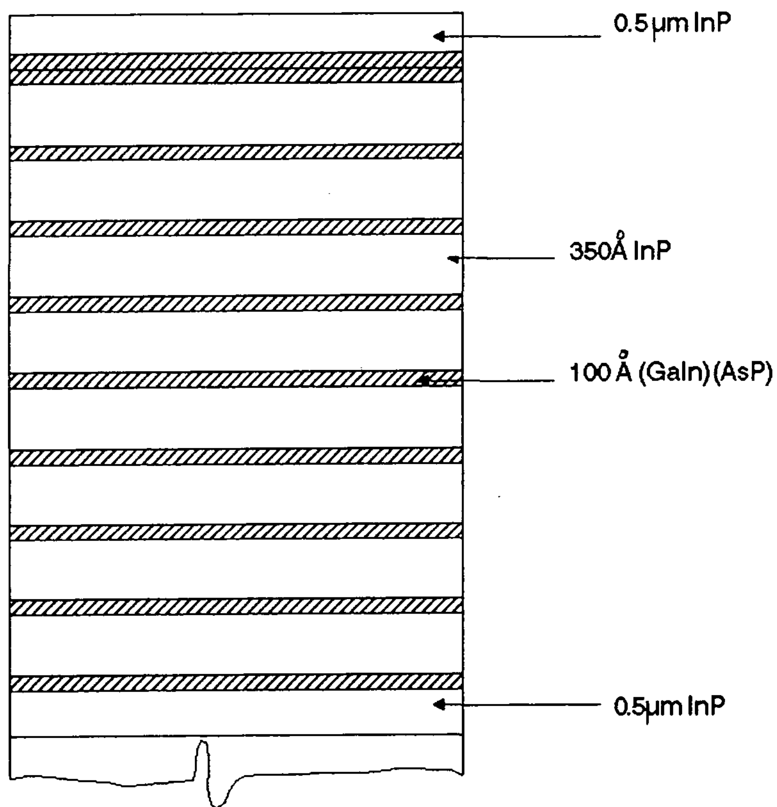

Figure (6.18): (GaIn)(AsP)/InP quantum well structure consisting of 10 repeated quaternary 100Å wells. The last two wells were grown next to one another due to a fault in the controlling computer.

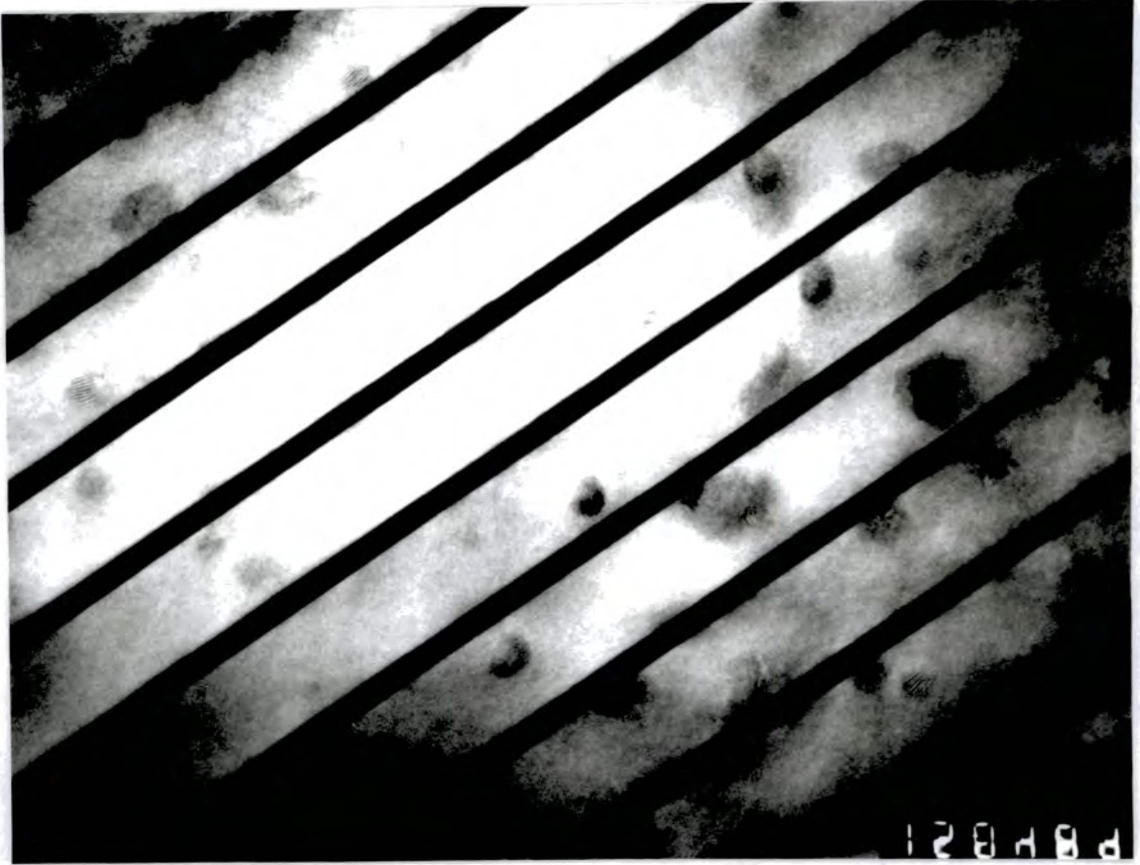

Figure (6.19): Transmission electron micrograph of the (GaIn)(AsP) structure illustrated in figure (6.18).

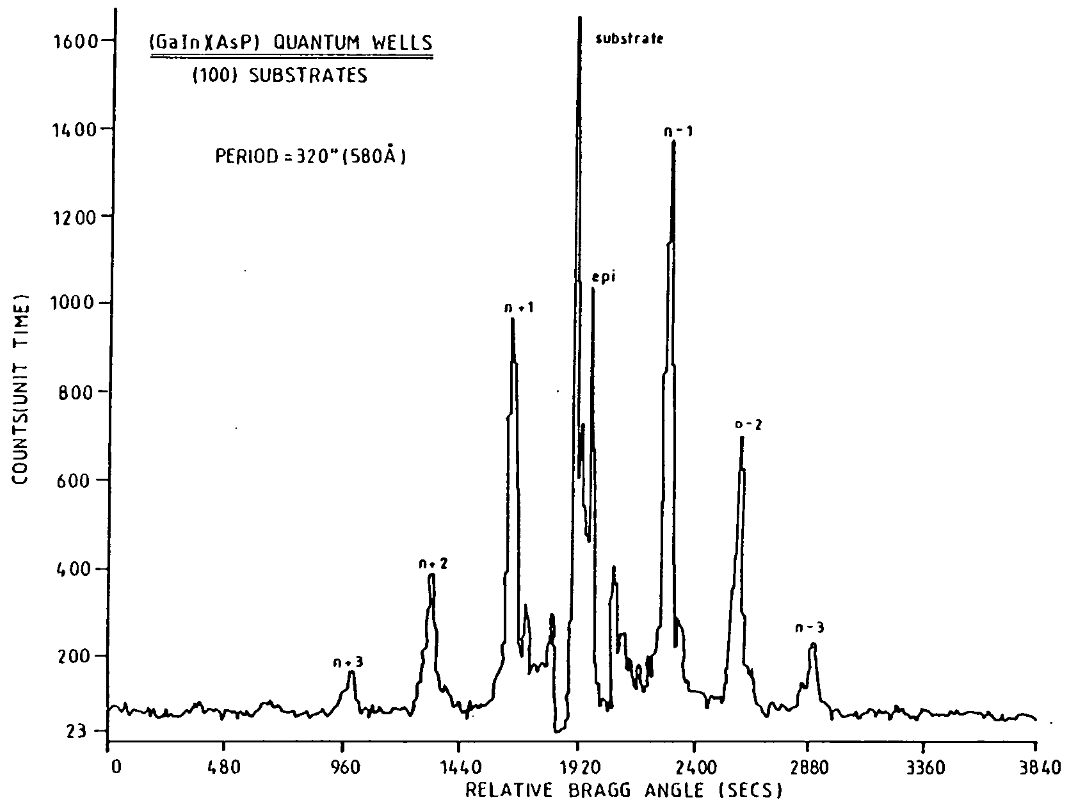

Figure (6.20): Double crystal x-ray rocking curve of the structure illustrated in figure (6.18), showing the presence of satellite peaks.

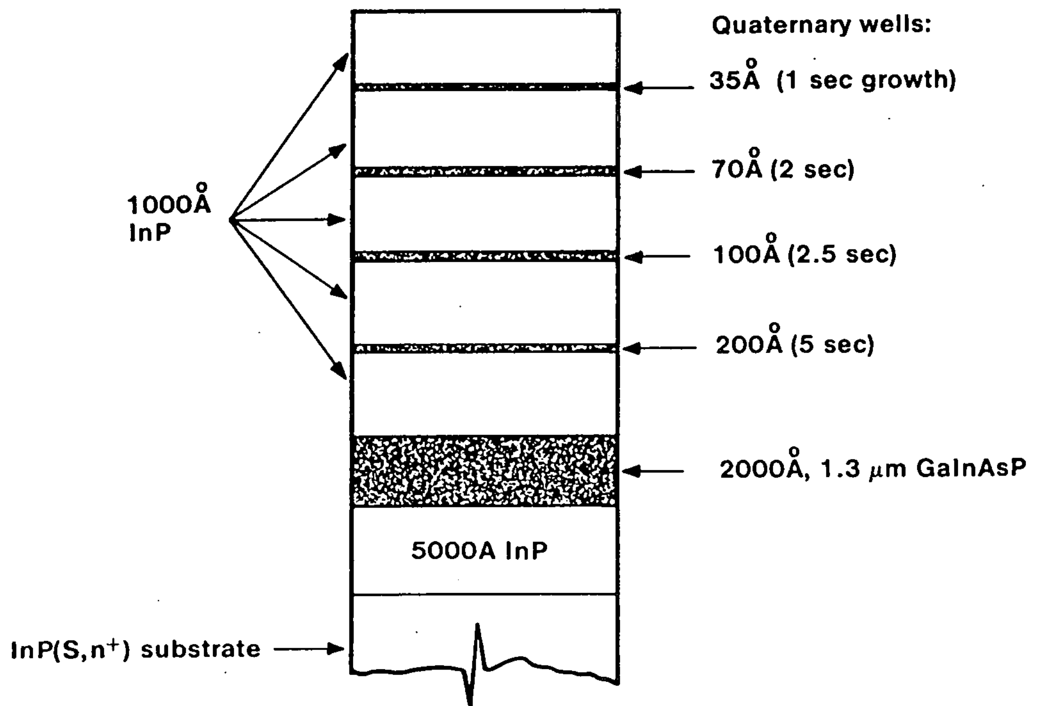

Figure (6.21): (GaIn)(AsP)/InP quantum well structure consisting of four quaternary wells of different thicknesses, and a thicker reference layer.

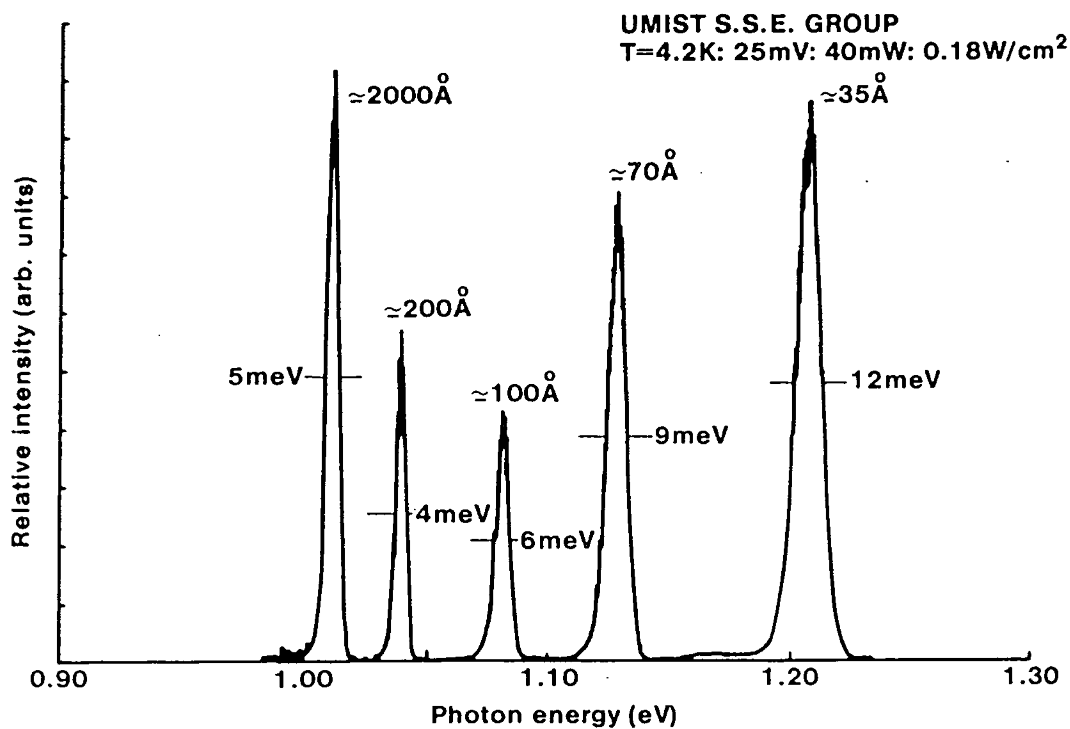

Figure (6.22): 4.2K photoluminescence spectrum on the (GaIn)(AsP)/InP structure illustrated in figure (6.21).

Chapter 7

Semiconductor Lasers Grown by MOVPE

A brief history of semiconductor lasers is given, followed by theoretical equations used to model the behaviour of the lasers. Details of the development along with experimental results are presented upon double heterostructure, ridge-waveguide, and distributed feedback lasers, fabricated using (GaIn)(AsP) based MOVPE technology. Future devices such as buried heterostructure and quantum well lasers are discussed.

History

The first semiconductor lasers were fabricated in 1962, and consisted of GaAs homo-junction devices that relied upon dopant diffusion to form a p-n junction. These devices had threshold current densities of 40kAcm^{-2}, and could only operate under pulsed conditions and at low temperatures. Reliability was a major problem, with devices living for only a few minutes. Improvements in performance were obtained with the development of the first single heterostructure lasers, and such devices are manufactured to this day. They are fabricated from consecutive layers of n-GaAs, p-GaAs and p-(GaAl)As, and threshold current densities of 10kAcm^{-2} are obtained.

In more general usage, are double heterostructure lasers fabricated using (GaAl)As-GaAs-(GaAl)As layers. Early devices still exhibited reliability problems, with devices failing after a few tens of hours. Improved devices are now commonly used in night vision torches, weapons simulation, high power arrays and other military applications.

The first successful communications demonstration carrying real data traffic, was the underground optical fibre link between Stevenage and Hitchin in 1977. This system used GaAs based double heterostructure 20μm stripe lasers. The initial application of semiconductor lasers to communications networks, was confined to long distance, costly, submarine and trunk land-line applications. This necessitated the maximisation of distance between repeaters, along

with high reliability. Further development was therefore mainly in the (GaIn)(AsP)/InP alloy system, which despite a higher degree of technological complexity, offered higher reliability, and emission wavelengths matched to the low loss windows of silica optical fibres.

The lasers deployed in the first undersea optical cable, were in part supplied by STC plc, and consisted of an inverted rib waveguide structure which combined current confinement to improve device performance, with a simple reliable structure (figure 7.1). The devices were fabricated using liquid phase epitaxy. The inverted rib waveguide laser has now been complemented by an equally reliable structure termed the ridge-waveguide laser, and is shown in figure (7.2). This structure has a lower threshold current than the inverted rib waveguide laser.

There are now many manufacturers developing laser structures with lower threshold current densities, and also distributed feedback lasers, which are detailed later in this chapter.

Because of the high powers and efficiencies that can be obtained from GaAs based lasers, these devices are finding applications in free space inter-satellite communications, and as light pumps for the rods of YAG lasers. The YAG lasers in turn may be used to heat plasmas in fusion reactors. Modern GaAs/(GaAl)As lasers are capable of emitting up to 2W of light continuously, 100W under pulsed conditions, and can have threshold current densities as low as $120Acm^{-2}$.

Theory of Operation

There are several texts detailing semiconductor laser theory [2,151], and only a few important aspects of theory are outlined in this section. In general, whilst theoretical models are able to provide early pointers towards correct research and development approaches, the complexity of solid state physics and quantum electronics prevents the accurate prediction of device performance. Much of the development work upon opto-electronic devices has been based upon iterative improvements upon structures until optimisation has been achieved. The device results are then fed back into the theoretical models, improving the accuracy of future predictions.

As explained in the introductory chapter, semiconductor lasers rely upon radiative electron-hole recombination occurring across the

direct band-gap of a semiconductor compound. The electrons and holes are injected from n and p-type material into a recombination region, referred to as the active layer of the laser. For lasing to take place, a population inversion is required, along with optical feedback of radiation to stimulate recombination of carriers. The population inversion is provided by a high level of carrier injection into the active layer. The radiation feedback is provided by light being reflected back off the two facets of the Fabry Perot laser cavity.

The equation describing the onset of laser action in a semiconductor laser is:

$$R.\exp\{(\Gamma g-\alpha)L\} > 1 \qquad (7.1)$$

Where: R is the facet reflectivity;
g is the gain coefficient of the material, and is related to the current density within the structure;
α is the scattering loss in the cavity per unit length;
L is the length of the cavity;
Γ is the confinement factor for light within the cavity.

Other important parameters are the internal quantum efficiency (η_{int}) which is the ratio of photons produced to electrons injected into the active layer, and the external quantum efficiency which is the ratio of the light power produced to the current supplied to the structure. The two are different due to shunting of current away from the active region of the laser, the light output being in the wrong direction to partake in laser action, reabsorption of light within the cavity, further reflection at the facets and reabsorption, and loss of light due to critical internal reflection at the material surfaces. The internal quantum efficiency is fundamental to the nature and quality of the material, and is limited by the amount of non-radiative recombination. For (GaIn)(AsP)/InP lasers, intervalence band absorption and Auger recombination are important fundamental physical factors that limit the performance of devices.

Lasing occurs when sufficient optical feedback is available to cause stimulated emission. The light can be concentrated by making the

active layer as thin as possible, until it ceases to confine light, whence the threshold current starts to rise again.

Thus another important relationship governing the onset of lasing is :

$$J_t \propto d/\eta_{int} \qquad (7.2)$$

where: d is the active layer thickness,
J_t is the threshold current density.

Whilst this relationship holds for double heterostructure lasers, quantum well lasers exhibit more complex behaviour.

Stimulated emission occurs when the electrical field of the stimulating radiation is strong enough to cause an inverted carrier population to recombine. Thus the lifetime of carriers in a laser is shorter than under normal conditions, such as during spontaneous emission. Lasers are able to operate at higher frequencies compared with light emitting diodes, which operate largely in the spontaneous mode.

Another effect of lasing, is to narrow significantly the number of modes supported by the cavity. The cavity tends to support only one transverse mode if the laser is of the heterostructure type, and lateral modes only tend to appear in well designed lasers when driven hard. However a significant number of longitudinal modes are supported in Fabry Perot lasers due to the long length of the laser cavity with respect to the wavelength of the light in the material. To cause lasers to operate in a truly single mode, and therefore to operate in a manner more similar to conventional radio and microwave sources, it is necessary to provide a grating in the lasing structure to allow feedback at only one wavelength. One such structure is the distributed feedback laser, which is elaborated upon later in this chapter.

The effect of further modes appearing in the laser output spectrum, is to cause non-linearity in the light-current characteristics of the device. This then limits device speed, increases bit error rates and causes information transmission to become noisy.

Heterostructures

Much of the complexity of laser fabrication arises from the need to use double heterostructures to improve the performance of devices. In turn, the problem of producing heterostructures has provided the focus of much of the work undertaken in the field of MOVPE. The heterostructure fulfils several rôles. Firstly, by choosing material of a suitable band-gap, the wavelength of the optical laser radiation is defined. Secondly the heterostructure material is chosen to have a lower band gap than the surrounding confining layers. When the confining layers are doped to form a p-n junction, with the low band-gap material in the middle of the p-n junction, potential barriers are formed such that it is difficult for electrons to traverse from the active layer into the p-layer, and for holes to traverse from the active layer into the n-layer. Under forward bias electrons and holes are injected respectively from the n and p-confining layers into the active layer, but can proceed no further. A high population of carriers is built up which provides one of the conditions needed for lasing action to occur. The active layer is then referred to as being pumped by the injected carriers. The heights of the barriers are key to the confinement of carriers. The difference between the conduction band levels either side of the heterojunctions, controls how well electrons are confined. Similarly the difference between the valence band levels either side of the heterojunctions, controls the confinement of holes. Generally the mobility of electrons is higher than that of holes, so that it is more important to have high conduction band offsets than valence band offsets.

One of the disadvantages of the (GaIn)(AsP)/InP alloy system, is that the ratio of conduction band offset to valence band offset is not as high as desired. This leads to electrons escaping over the heterojunction where they do not contribute to radiative recombination. The effect becomes worse as the junction temperature rises, causing a high degree of temperature sensitivity for (GaIn)(AsP)/InP lasers.

Therefore another important equation, which is determined empirically, is that defining the temperature sensitivity of lasing threshold:

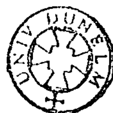

$$J_t = J_o exp(T/To) \qquad (7.3)$$

Where: J_o and T_o are constants; T_o is a commonly quoted laser parameter.

J_t is the threshold current density,

T is the junction temperature.

The second effect of the double heterostructure, is that the narrow layer of higher refractive index material acts a light guide in the same manner as the core of an optical fibre. Since one of the conditions that is important for good laser performance is a high concentration of light in the pumped region, then this feature is desirable.

Double Heterostructure Lasers

The simplest form of laser structure commonly fabricated, is the double heterostructure laser. A small amount of current confinement is provided by making contact to the epitaxial side of the laser, which is usually the p-side, by way of a small contact stripe. This is defined by photolithography, through a layer of insulating oxide. The injected current suffers from severe sideways spreading which in turn causes a large area of the active region to be pumped. Whilst stripe geometry lasers can produce high powers, the current spreading causes threshold current densities to be high. Although the lasers are particularly poor in this respect, they are used extensively to test out basic heterostructure performance, which in turn provides information upon alloy and interface quality. In this way, faults introduced during complex processing steps, do not confuse assessment of the epitaxy.

There are many papers in the literature reporting the threshold currents of (GaIn)(AsP)/InP lasers grown by MOVPE. In general, the lasing threshold current densities reported for broad stripe devices has reduced over recent years, values ranging from $8kAcm^{-2}$ to $1kAcm^{-2}$ being achieved. The technical detail enclosed in these papers appears to be sparse, the content mainly being centred upon the achievement of lasing.

The first reported all MOVPE lasers grown using (GaIn)(AsP)

active layers were fabricated at Thomson-CSF in France, using low pressure MOVPE, and publications date from 1981 [152,153,154,155, 156,157]. Growth at atmospheric pressure has also led to the fabrication of good quality devices [158,159,160,161]. It would appear that the pressure used for epitaxy, the choice of ethyl or methyl metal-organics, and a wide range of dopants do not have a significant effect upon the final double heterostructure device quality. The values often quoted in the literature, require careful examination, since it is possible to obtain low threshold current density lasers simply by cleaving the wafer into long cavity length devices.

The author has grown double heterostructure epitaxial layers, which have been processed subsequently into 50µm stripe lasers in order to determine the quality of the epitaxy. A typical epitaxial sequence is shown in figure (7.3). A buffer layer of n-InP, doped using hydrogen selenide or silane mixtures in hydrogen to $n=1.10^{18}cm^{-3}$, was first grown upon the highly sulphur doped (100) on-orientation substrate. This was followed by an undoped quaternary layer, of 0.1-0.2µm thickness, with an aimed-for emission composition of 1300nm. The p-side of the structure consisted of 1.5µm of InP doped using dimethylzinc to $p=1.10^{18}cm^{-3}$, followed by a p^{+} cap of (GaIn)As doped using dimethylzinc to $p=2.10^{19}cm^{-3}$. The p-side of the laser structure was copied from distributed feedback laser development, which was the subject of extensive research, and is discussed in a later section.

The first laser wafers grown had an active layer thickness of 0.17µm, and pulsed threshold current densities of $1.7kAcm^{-2}$ at 20°C. Figure (7.4) shows the light-current characteristics of such a laser operated under pulsed current conditions. Later structures achieved similar threshold current densities, provided the active layer thickness remained high. A structure grown with an active layer thickness of 0.12µm, showed an increased threshold current density of $2.7kAcm^{-2}$.

More recently, two stage buried heterostructures were grown by Jowett and the author at STL. These structures were grown with the intention of fabricating them into buried heterostructure lasers, and the first stage of growth was therefore the n-InP, followed by the active layer, and finished with a 0.25µm layer of p-InP. A further 1.5µm of p-InP and p+(GaIn)As contact layer was grown subsequently

upon part of the original wafer. The final structure differed from the earlier ones, by the p-doping level being reduced to $5.10^{17}cm^{-3}$, and with a 50Å undoped InP layer being included between the active layer and the p-InP layer. These two measures controlled the amount of zinc reaching the active layer of the laser, and limited the amount of non-radiative recombination that occurs when zinc is present in the active layer of devices. These devices were fabricated into 400μm long, 50μm stripe lasers, and a threshold current density of $1.1kAcm^{-2}$ was achieved. The T_o value was measured to be 75K.

Ideal Device Performance

The broad area double heterostructure devices detailed above are not suitable for system applications, due to the inefficient nature of the structure, and resultant poor electro-optic characteristics. Devices suited to commercial fibre-optic applications are required to have threshold currents of less than 50mA, and good high temperature performance with T_o levels of greater than 55K. To ease the complexity of the drive circuitry, which has to operate at very high speeds, the modulation currents also need to be kept as low as possible. Since lasers are usually biased at currents around the threshold values, an often quoted parameter is the extra current required to achieve a certain power. This is directly related to the external quantum efficiency of the laser. High speed operation is increasingly important, with systems operating to $2.4Gbs^{-1}$. The normal light-current curve for a laser is linear, provided extra transverse modes of radiation do not appear. This is best prevented by careful design of the optical and current confining structure. It is furthermore important that the effect of temperature upon these parameters is minimal under normal operating conditions. Many of the more expensive laser packages include peltier cooling units to maintain a stable operating temperature, when the surrounding ambient temperature is high. The lasers also need to be designed such that as much of the light as possible is coupled into the optical fibre.

The spectral width of the laser is also of importance. For wide diameter multi-mode fibres, a large number of longitudinal modes is desirable to avoid modal noise. Light emitting diodes are often used in these applications. For more demanding applications, single

longitudinal mode lasers, with narrow spectral line-widths are required. The stability of these lasers with output power and temperature is also of importance.

Ridge-Waveguide Lasers

The above text has indicated that in order for a semiconductor laser to function efficiently, it is necessary to guide the light into a small two dimensional region, coincident with the laser active layer, and to direct the electrical current to the same area. Any current outside of this region is effectively wasted and creates heat, which in turn is detrimental to device performance.

A structure that allows the epitaxial layers to be grown in a single growth run, but gives good current confinement, along with index guiding of light in the lateral mode, is the ridge-waveguide laser (figure 7.2). The structure is fabricated from a planar sequence of epitaxial layers, by etching grooves either side of a masked ridge, which becomes the guiding part of the laser. The active layer remains unbroken and unexposed, since the channels are selectively etched as far as a short wavelength quaternary layer, deliberately grown on top of the active layer to act as an etch stop layer. The ridge-waveguide laser is a highly reliable structure [162], and is manufactured by a large number of companies. There are no reports, to the author's knowledge of the fabrication of the structure entirely using MOVPE technology, though some workers have fabricated buried ridge lasers which include two different MOVPE grown quaternary layers next to one another [163,164].

The author has grown ridge-waveguide material consisting of 1.5µm of n-InP doped with silane to $n=5.10^{17}cm^{-3}$, a 1.3µm emission undoped quaternary layer of 0.16µm thickness, a 1.18µm emission undoped quaternary layer of 0.35µm thickness, a p-InP layer, 2µm thick doped to $p=1.10^{18}cm^{-3}$, and a p^{+}(GaIn)As contact layer doped to $p=2.10^{19}cm^{-3}$, of 0.27µm thickness (figure 7.5)[165]. The requirement to grow two critical lattice matched quaternary layers next to one another, required careful attention to be given to reactor control. A 5s pause in the growth, with the 1.3µm emission quaternary layer protected by arsine and phosphine was included prior to the growth of the second quaternary layer. During this pause, the trimethylgallium and arsine

flow rates were reduced to the flows needed for the shorter wavelength material, and growth was prevented by the group III alkyls being switched to vent.

A light-current curve for 400μm long, 3.3μm wide ridge lasers is shown in figure (7.6). CW threshold currents of 58mA at 23°C were achieved, along with a 6mW operating current of 110mA and a T_0 value of 57K.

Later experience has shown that the composition of the etch stop layer should have been ≈1.05μm, and that it should have been doped lightly p-type. More recently, Jowett at STL, using the same reactor has grown similar devices with threshold currents of 22mA at 20°C.

Distributed Feedback Lasers

The above lasers operate in single transverse and lateral modes, but give many longitudinal modes of light due to the number of modes that can be supported by the Fabry Perot cavity. In order to allow only one longitudinal mode to be supported, it is necessary to feedback light to the active layer, other than by way of the laser facets. To achieve this, a diffraction grating is formed between adjacent epitaxial layers of different compositions within the laser structure. The diffraction grating then provides distributed feedback, at a highly selective wavelength, so causing the device to operate in a single mode. Reflections from the laser facets are reduced by evaporating thin anti-reflection films, such as alumina, onto the facets during fabrication. The gratings are usually of a second order type, and are etched into the semiconductor via either electron beam lithographic or X-ray lithographic techniques.

The devices fabricated by the author involved two stages of epitaxy, the first by liquid phase epitaxy to grow the n-side and quaternary layers of the ridge laser structure, and a second stage using MOVPE to grow the p-InP and p^+(GaIn)(As) layers. The grating was etched approximately 0.2μm into the short wavelength etch stop layer of the liquid phase growth. A similar method of fabrication has been described by Nelson et al [158]. Other workers have etched gratings into InP substrates, followed by epitaxial growth of the complete structure [167,168]. This latter technique results in a grating that is coupled less efficiently to the light in the vicinity of the active

layer. It is also necessary to avoid thermal degradation of the grating by mass transport, which is more likely using an InP grating than an alloy grating, in which the presence of arsenic helps to stabilise the surface.

The fabrication steps for the DFB laser are illustrated in figure (7.7), and result in a ridge waveguide structure as described earlier, with the addition of the grating and anti-reflection facet coatings. Light current characteristics are illustrated in figure (7.8), and current thresholds achieved were 24mA at 25°C, and 43mA at 50°C for 300-400μm long devices. The output remained in a single mode in excess of 8mW, over a temperature range of 10-70°C, and linewidth-power products of 300MHzmW were obtained. The high speed performance of devices is often assessed by applying a pseudo-random pulse code modulated bit stream drive current, and detecting the output power and displaying the wave-form on an oscilloscope. The resultant wave-form is referred to as an eye diagram, and figure (7.9) shows the results obtained upon distributed feedback lasers operating at $2.4Gbs^{-1}$. The life of these devices was found to be good, extrapolated lifetimes of better than 10^5 hours being predicted at 50°C.

Whilst the MOVPE contribution to this device was limited to the p-type layers, many aspects of the growth were critical. The passivation of InP by hydrogen, explained in the doping chapter, was originally uncovered during this work. The exact amount of zinc in the vicinity of the active layer, and the position of the p-n junction proved to be critical. It was found necessary to distance the p-InP from the quaternary layer by a 0.1μm thick layer of undoped InP, which was subsequently doped p-type by diffusion during the growth of the rest of the structure. It was also found necessary to bake the susceptor at 650°C in phosphine, prior to loading the wafers, in order to drive off any traces of zinc left on the surface of the susceptor after growth of the previous p^+(GaIn)As layer. To prevent thermal degradation of the grating, the wafers were heated under phosphine to ≃615°C, and growth was then commenced by addition of trimethylindium before the reactor temperature stabilised at 650°C. Cleaved cross sections of epitaxial layers containing gratings, indicated that the original shape was retained. It was interesting to observe that the surface of the epitaxial layers, would become planar after only 0.2μm of InP had been grown.

Contact Layers

Devices grown by liquid phase epitaxy, usually have a p-doped quaternary capping layer of larger band gap than the active layer. This material requires further zinc diffusion to produce low resistance metal to semiconductor contacts. MOVPE grown contact layers can be of (GaIn)As, which can be doped to $p=10^{20}cm^{-3}$ during epitaxial growth. Low resistance contacts can be achieved immediately using this material, without the need for a diffusion stage. However, the (GaIn)As is a narrower band-gap material than the active layer of the lasers, and so will absorb light and cause poor device performance if it is not distanced to $\simeq$ 1.5µm from the active layer.

The growth of this contact layer by MOVPE, does suffer the problem of inducing hydrogen passivation of the underlying p-InP. It was found that the subsequent deposition of oxides during wafer processing, drove the hydrogen out of the epitaxial layers, depending upon the deposition temperature used. Whilst this effect fortuitously eliminated the problem in finished devices, the repeatability of the processing, and the need to measure doping levels in the p-InP after epitaxial growth, required a more elegant solution to be found. The approach finally adopted, was to grow an undoped layer of InP directly after the growth of the contact layer. This eliminated the ingress of atomic hydrogen during cooling, since arsine was no longer present in the growth environment. The InP layer also acted as a protective layer over the wafer, and was removed prior to processing using a 3:1 H_3PO_4:HCl etch.

p and n-Type Doping of InP Confining Layers

The doping level chosen for the n-InP layers of the lasers, appeared not to be critical. A value of $n \simeq 5.10^{17}cm^{-3}$ was settled upon.

However the doping level in the p-InP layers of the lasers was critical. Devices fabricated from layers with too much zinc in the active layers, exhibited high threshold currents. This is thought to be due to the introduction of non-radiative recombination centres by zinc atoms, a theory that is supported by the observation of reduced luminescence efficiency of layers depending upon the amount of zinc

incorporated into them. The temperature sensitivity of the devices was improved, and a trade-off has to be made between these two important parameters. The amount of zinc in the active layer of lasers could be controlled either by doping the p-InP layer to $p=5.10^{17}cm^{-3}$, or by using a higher doping level of $p=1-2.10^{18}cm^{-3}$, along with a 0.1-0.2μm thick undoped InP layer adjacent to the active layer of the device.

Sasaki et al have demonstrated similar results for the zinc doping of double heterostructure lasers, though the use of a diffused p-contact layer may have distorted their results in comparison to those above [168]. Miyamoto et al have grown lasers upon zinc doped substrates, and found that slow growth rates and therefore long growth times, gave rise to degradation of device performance, which was ascribed to out-diffusion of zinc from the substrate into the active layer [169].

In principal, a high doping level is desirable, since the conductivity of the material is also higher, giving less resistive heating of the devices. In later structures, the two doping levels were combined by changing from low to high dimethylzinc flow rates, in different stages of the p-side epitaxy.

Reliability of Lasers

Most lasers exhibit output power degradation with time, usually due to a rise in threshold current. For many devices this follows a law of the form:

$$\Delta I_t = At^n \qquad (7.4) \qquad [170]$$

where: I_t is the threshold current,
A is a constant,
n is a constant, and is 0.5 for many lasers.

However, it is equally important that other device parameters are also retained within specified limits. Extensive life testing arrangements have been developed for devices that are required to operate for tens of years. Paradoxically, the laser market is developing towards lower cost, less reliable lasers, for the shorter distances to customer premises, rather than the long trunk links where

the first lasers were used.

The factors that can influence device reliability as a result of epitaxial growth are epilayer strain, dislocations, and non-radiative recombination centres. The association between non-radiative recombination centres such as zinc atoms, and reliability, is not well understood. It has been firmly established that strain of the active layer, as a result of poor epitaxy, can lead to the formation of dislocations, which in turn act as non-radiative recombination centres, reducing the efficiency of the lasers [55]. Lattice matching of quaternary layers to InP is therefore required to be better than $\pm 2.10^{-4}$.

Buried Heterostructure Lasers

Whilst the ridge-waveguide laser can be described justifiably as a low threshold laser, there is an increasing number of applications where a device is required that has an even lower threshold of lasing, and better high temperature operation. One of the main advantages of this laser, is that it requires only a single stage of epitaxy. However this is counterbalanced by device performance, processing tolerances, and bonding difficulties caused by the use of a non-planar structure. The ridge-waveguide laser, which has an unbroken, broad active layer, suffers from poor lateral current confinement, and poor lateral optical confinement. The latter effect gives rise to asymmetric far fields, making launching of light into fibres difficult. This design of laser is, however, probably the most reliable in the world.

To obtain better lateral optical and current confinement, a structure is required that consists of a rod of active material, surrounded by material of higher resistivity and lower refractive index. Such a device is optically similar to an optical fibre. The many designs of buried heterostructure laser are of this form.

The earliest buried heterostructure lasers, were fabricated using liquid phase epitaxy. A planar sequence of epilayers was grown, and subsequently etched to form a mesa containing the active layer. The area surrounding the active layer was then re-grown using p-n InP blocking layers, followed by over-growing the top of the mesa with more p-type InP and a contact layer. This two stage growth process,

resulted in a structure which incorporated a reverse biased p-n junction, which effectively diverted injected current towards the low band-gap active layer. The liquid phase epitaxial buried heterostructure laser, has been successfully fabricated in many research laboratories world-wide, but has only been adopted for production by a few companies, due to the inherently difficult growth step involving precise positioning of the p-n blocking layers.

The first MOVPE grown buried heterostructure lasers, were buried ridge devices [171,172]. A planar sequence of layers, including the active layer, was formed into a mesa by etching through the active layer, as described for liquid phase epitaxial structures. The whole mesa was then buried in p-type InP followed by a suitable contact layer. Whilst this structure resulted in good optical confinement, current spreading and conduction through the p-InP was still a problem. Improved performance was obtained either by forming a narrow contact stripe, or by causing the material either side of the active layer to become resistive using proton bombardment. Threshold currents as low as 20mA at 20°C were obtained, but device reliability was poor.

The more commonly fabricated MOVPE buried heterostructure laser requires three stages of epitaxial growth, and was first demonstrated by Nelson et al [158,168]. Again this structure starts with a mesa of epitaxial layers in which the active layer has been cut. The oxide mask that is used to define the mesa, is retained during the second growth step which consists of the growth of p and n-type InP current blocking layers. The final growth step, undertaken once the oxide mask has been removed, is to cover the whole structure in p-type InP, followed by a p^+(GaIn)(As) contact layer. The structure is illustrated in figure (7.10). The position of the p-n blocking layers, again is important, but at least one major company has developed the technology to the point of putting the device into production.

Good reliability of this type of structure has been demonstrated with the best result giving a predicted life of $2.5.10^6$ hours at 25°C, defined by a 100% rise in threshold current [173]. Whilst this definition is more relaxed than that applied to the ridge-waveguide laser, the lower starting threshold current allows an increase in current to be accommodated. The most recently reported threshold current for this type of device is 8mA [174], and Kawabata et al have also demonstrated devices with threshold currents of 10mA and T_o

values of 59K [175].

Good buried heterostructure lasers have also been grown by vapour phase epitaxy, with threshold currents of 20mA at 25°C and T_0 values of 72K being obtained [176]. Mass transport has also been used in an MOVPE reactor to bury heterostructure mesas, by adjusting the over-pressure of phosphine to a level just above that needed to stop the material degrading [177].

Whilst the all MOVPE, p-n blocking layer buried heterostructure laser has found much favour with many companies, it has several disadvantages. The requirement for three stages of epitaxy is effort intensive. The reliability of the devices is not as good as structures in which the active layer is unbroken, though it is unclear whether this is an issue for low cost applications, where the devices are not required to last as long as those used in trunk telecommunication applications. The overall sequence of doped layers forms a p-n-p-n thyristor structure, which can conduct if turned on by a high voltage in the vicinity of the active layer. Any material problem which results in a high forward voltage, will therefore cause this structure to suffer from current leakage through the blocking layers.

Perhaps of greater concern, is the fact that the p-n blocking layers store charge, and so the devices exhibit a high capacitance. This limits the high frequency capability of the structures to less than 1GHz.

The use of Semi-Insulating materials in Buried Heterostructure Lasers

There have been many attempts to replace the p-n blocking layers in buried heterostructure lasers, with non-conducting materials. Silicon dioxide and polyamide have been used without great success. More recently, the ability to grow semi-insulating InP doped with iron, by both MOVPE and hydride vapour phase epitaxy, has allowed good quality devices to be fabricated. The crystalline nature of the iron doped InP contrasts with the polycrystalline nature of earlier materials. The use of a semi-insulating layer instead of p-n blocking layers to confine the current, results in reduced device capacitance, and improved high frequency performance.

The author has grown buried heterostructure lasers, using an iron doped blocking layer by MOVPE, however the threshold currents were

disappointingly high. It was found subsequently that the amount of iron in the InP blocking layer was far higher than required, and may have led to the formation of conducting paths via iron precipitates. Speier et al found it necessary to reduce the iron content of layers to obtain good device results [176].

The first iron doped buried heterostructure lasers were fabricated by etching a v-groove into an MOVPE grown epitaxial iron doped layer, followed by liquid phase epitaxial growth of a buried crescent laser structure into the v-groove [177]. Devices fabricated by this method have operated to 8.3GHz [178]. A similar liquid phase epitaxial structure was grown by Yamakoshi et al, in a recess etched into a layer of iron doped InP grown by vapour phase epitaxy [179]. This structure also gave good results, with a maximum frequency of operation of 6GHz.

All MOVPE structures grown using iron doped InP also have yielded good device results. Structures identical to the three step epitaxial structures described above, but with the p-n blocking layers replaced by iron doped InP, have yielded devices with threshold currents as low as 20mA, and -3dB frequency cut off values of greater than 10GHz [174,180].

A two-stage process using iron doped InP has also been developed, and consists of a mesa structure as described earlier being buried in iron doped InP as the final growth stage. The difference between this two-stage process and the three-stage process described above, is that the mesa structure consists of a full laser heterostructure, including a contact layer, from which a silicon dioxide mask is removed after the second epitaxial growth stage. Several groups of workers have used this process, and have obtained high frequency performance to 5.8GHz, with threshold currents as low as 20mA [181,176,182,183,184,185].

It is not clear whether the two or three stage structure is superior, nor is there any significant life-test data available upon iron doped blocking layer buried heterostructure lasers.

Quantum Well InP Based Lasers

The use of very thin laser active layers, of the order of 100Å, surrounded by guiding layers of intermediate refractive index to the active and confinement layers, has been exploited extensively in the

fabrication of GaAs/(GaAl)As lasers. These devices, commonly referred to as quantum well lasers, due to the quantisation of energy levels within the active layer, have exhibited lower thresholds, better reliability, narrower line-width, higher power and better temperature sensitivity than double heterostructure lasers.

The application of quantum well structures to longer wavelength light emitters has met with varying degrees of success. Miyamoto et al, fabricated a single quantum well structure consisting of a 150Å thick 1.66μm emission quaternary active layer, surrounded by 1.26μm emission quaternary layers [186]. Thin InP layers were incorporated to facilitate the growth of otherwise adjacent quaternary layers. High threshold current densities of $11kAcm^{-2}$ were obtained. Nelson et al, fabricated (GaIn)As/InP quantum well lasers which had threshold current densities of $7.5kAcm^{-2}$, and reported narrowing of the emission spectrum with respect to double heterostructure devices [187].

More recently, buried heterostructure multiple quantum well lasers have been fabricated using (GaIn)As active layers surrounded by (GaIn)(AsP) barrier layers [188,189,190]. These devices had threshold currents as low as 18mA, and when a grating was incorporated to form a distributed feedback laser, good TM mode suppression, low frequency chirp, enhanced T_o values, and line-width-power products of 28MHzmW were obtained [189,190]. The above devices, and also lasers fabricated using quaternary quantum well active layers and wider band-gap quaternary barrier layers, have not yielded lasers with improved threshold currents compared with quaternary double heterostructure devices [175,191]. A more complex structure, consisting of a series of graded quaternary layers, termed a "GRINSCH" laser, yielded threshold current densities of $1.4kAcm^{-2}$, which again is no better than double heterostructure lasers [192].

More promising results have been achieved by Glew et al, using four (GaIn)As quantum well active layers, surrounded by (GaInAl)As barrier material [193]. Threshold current densities of as low as $0.94kAcm^{-2}$, and T_o values of 61K were obtained.

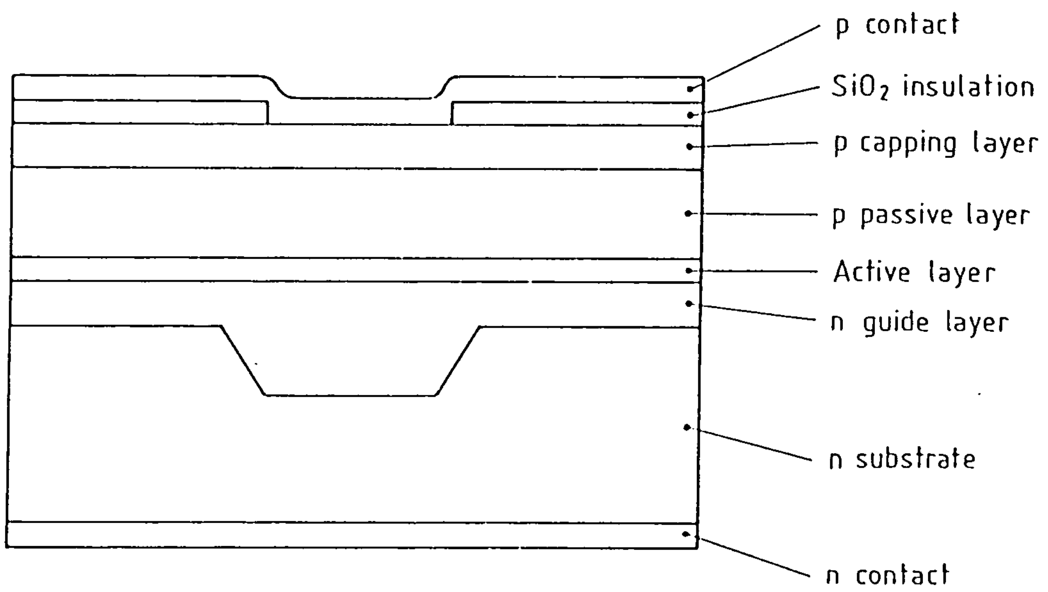

Figure (7.1): Cross section through the epitaxial structure of an inverted rib waveguide laser. (Not to scale.)

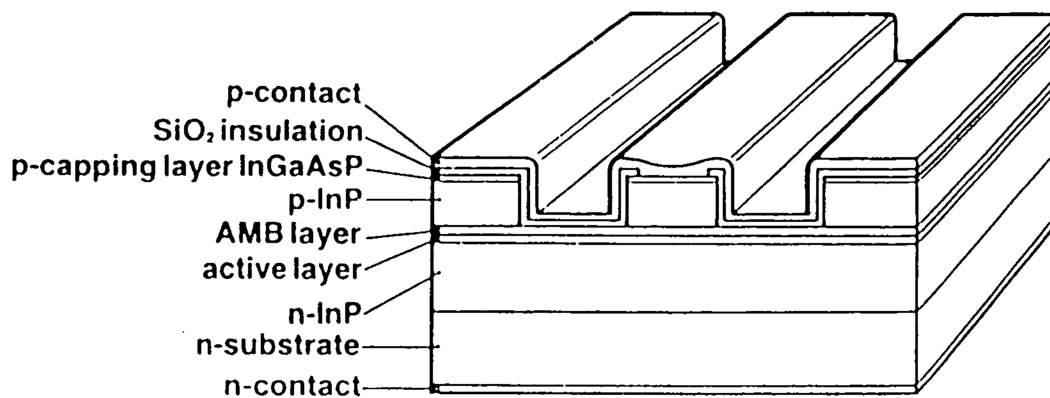

Figure (7.2): Schematic diagram of a ridge waveguide laser. (Not to scale.)

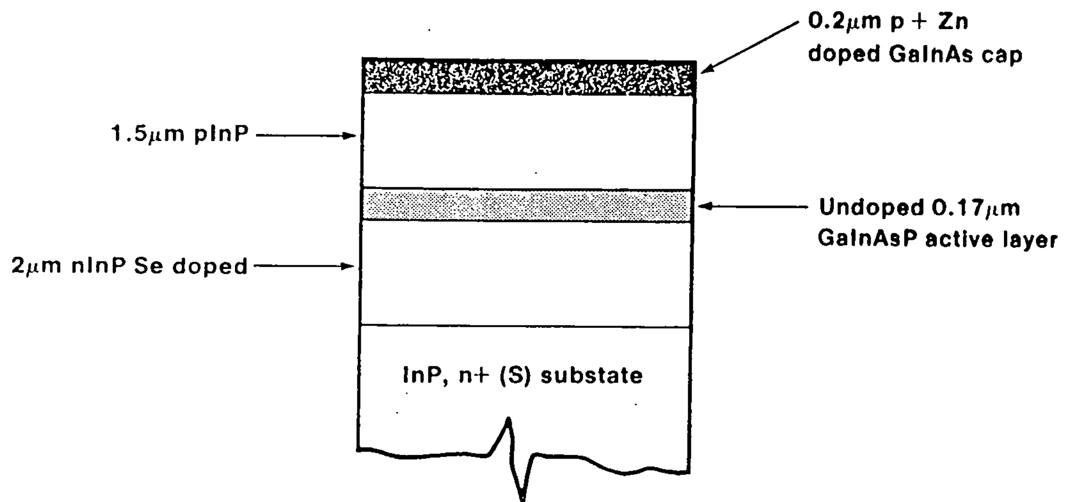

Figure (7.3): Schematic diagram of the sequence of epitaxial layers grown to produce broad area (50-80μm stripe) double heterostructure lasers.

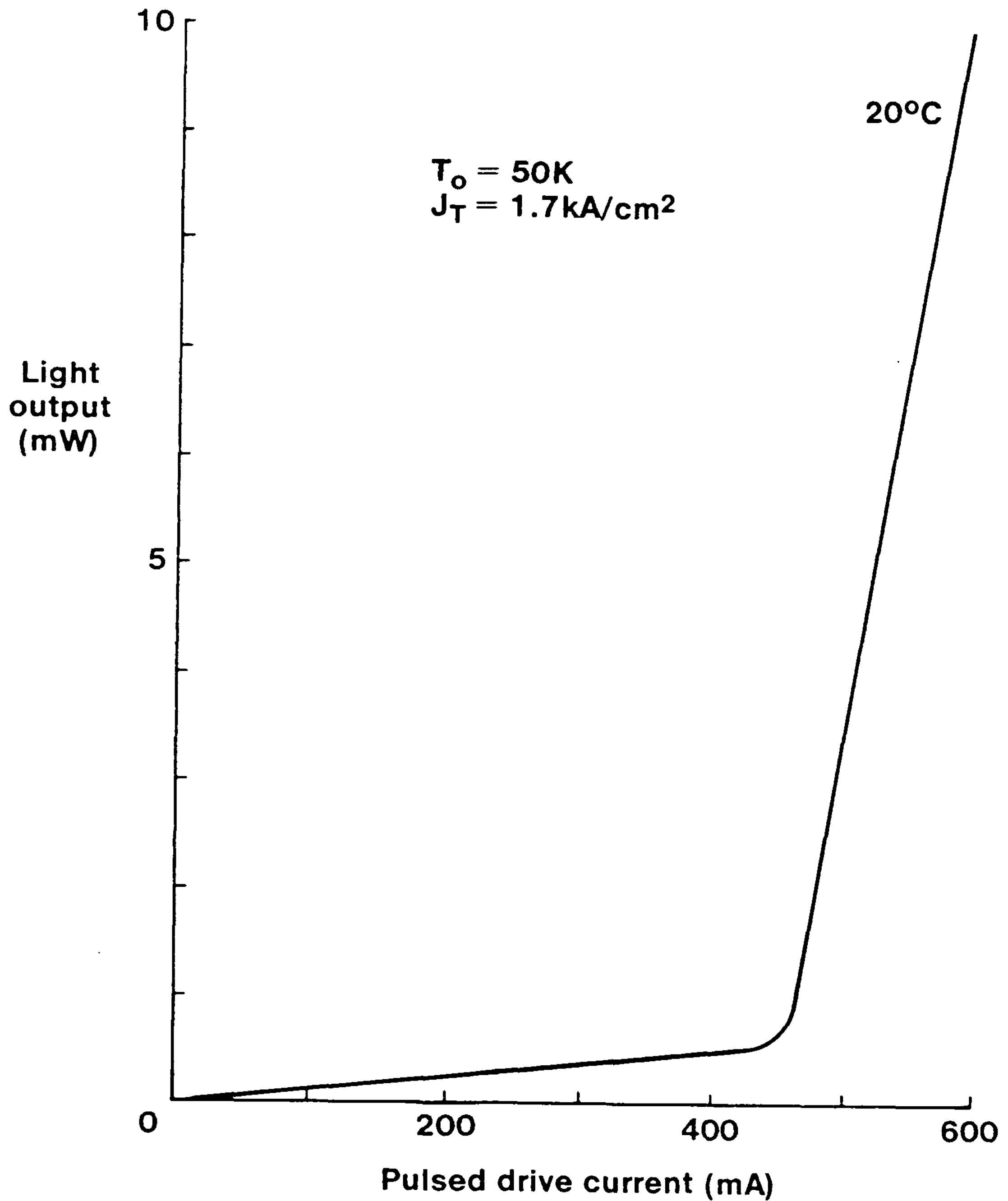

Figure (7.4): Light-current characteristic under pulsed drive current conditions for an all MOVPE 50μm stripe double heterostructure laser, fabricated from the epitaxial layers shown in figure (7.3).

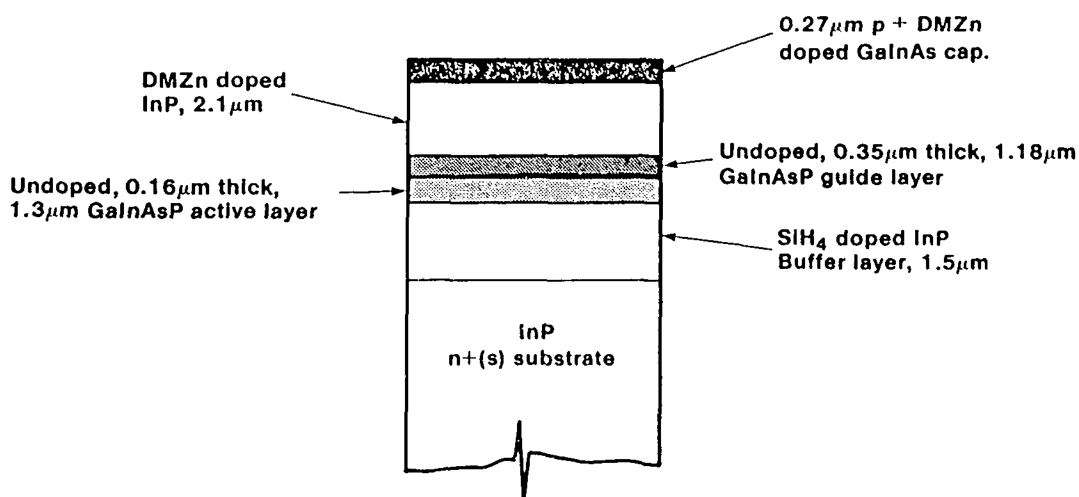

Figure (7.5): Schematic diagram of the sequence of epitaxial layers grown to produce ridge waveguide lasers.

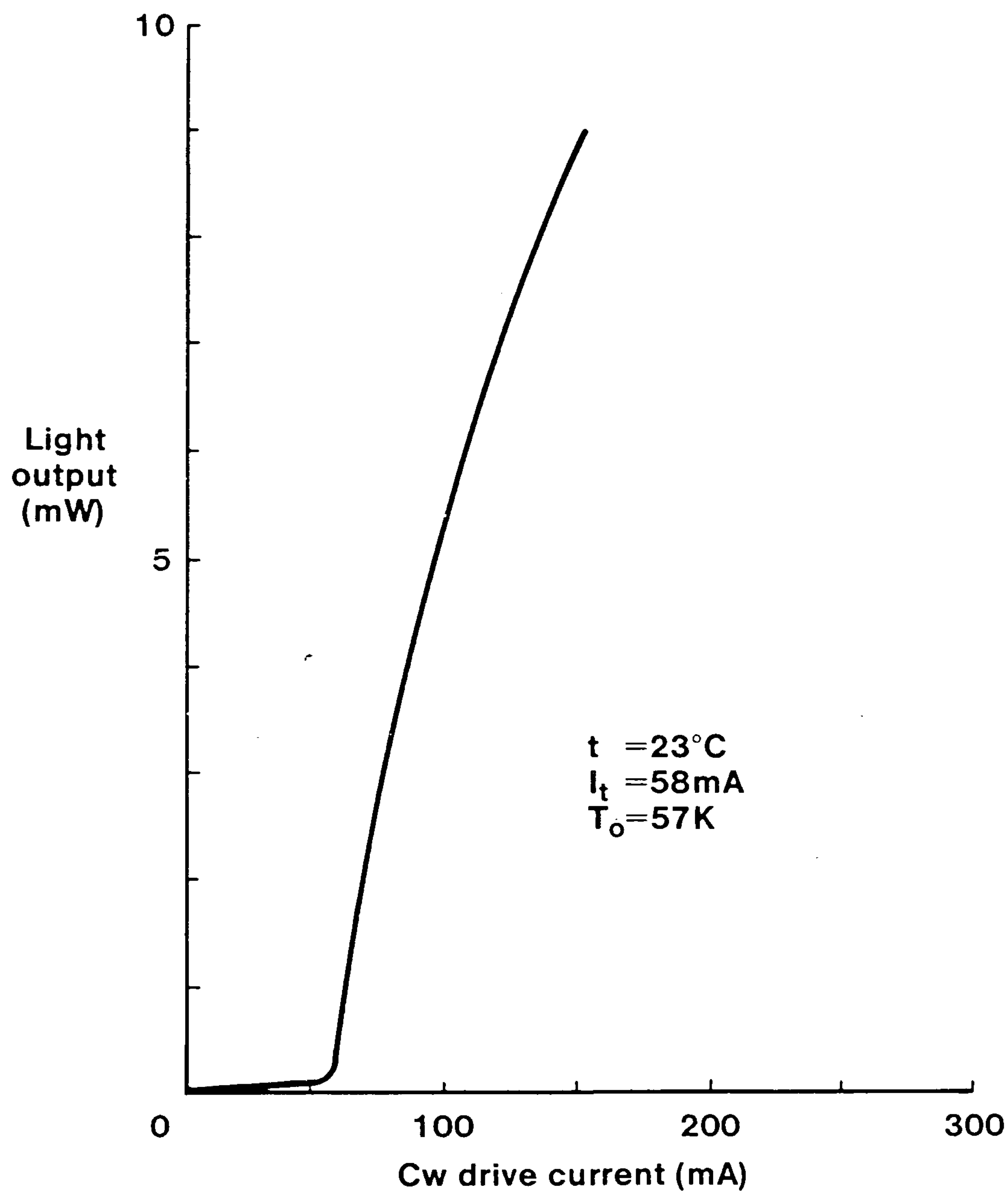

Figure (7.6): Light-current characteristic under CW drive conditions, for an all MOVPE ridge waveguide laser, fabricated from the epitaxial layers shown in figure (7.5).

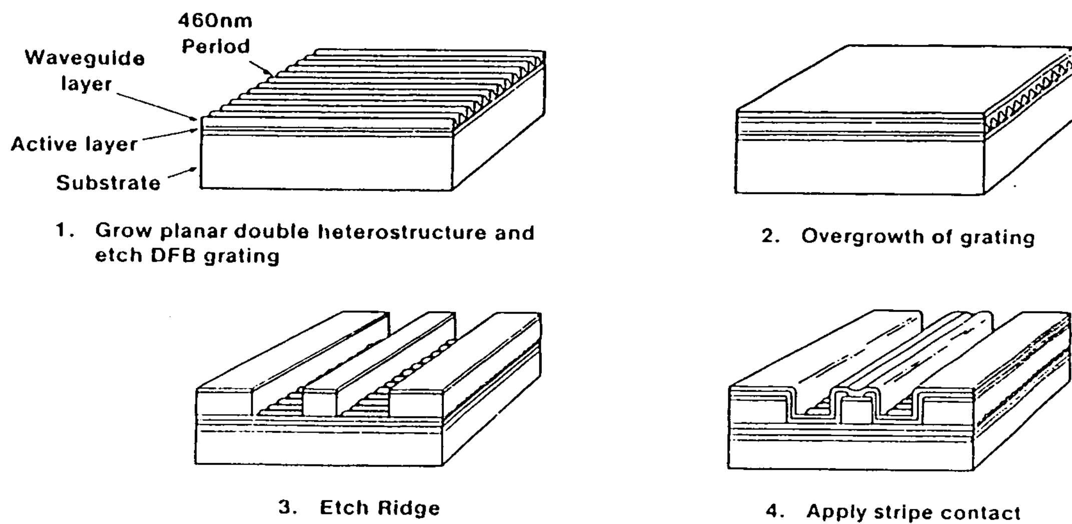

Figure (7.7): Sequence of fabrication steps required to produce a hybrid LPE/MOVPE distributed feed-back ridge waveguide laser. The grating is defined using electron beam lithography.

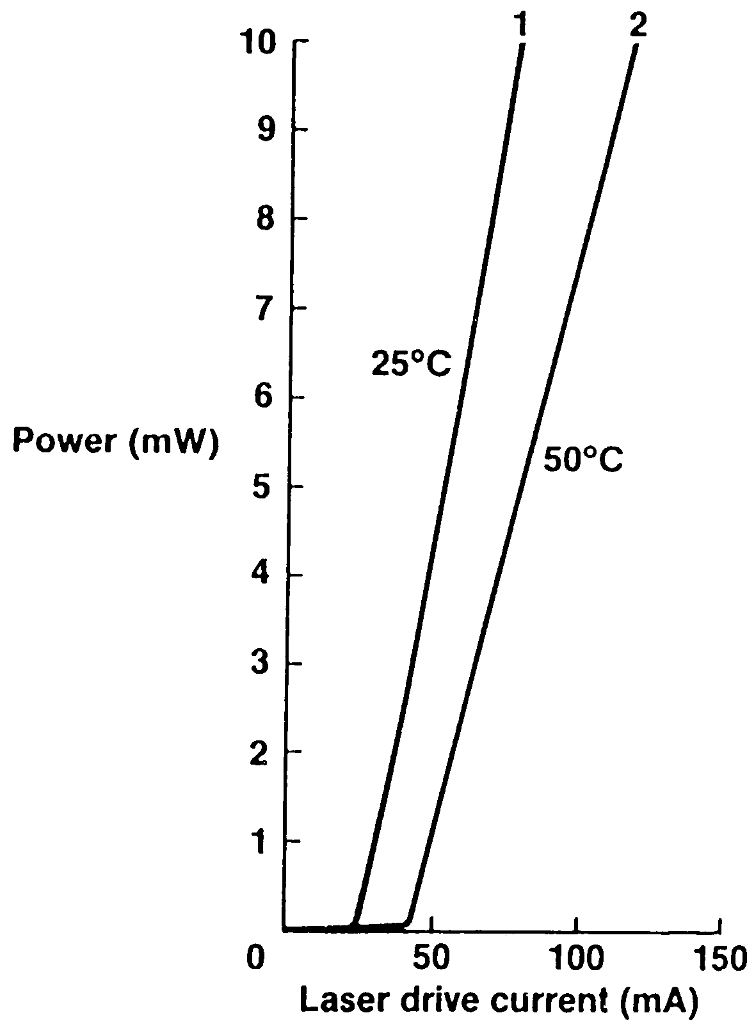

	Temp (°C)	Threshold (mA)
1)	25.1	24
2)	50.0	43

Figure (7.8): CW light-current characteristic for a hybrid LPE/MOVPE distributed feed-back ridge waveguide laser.

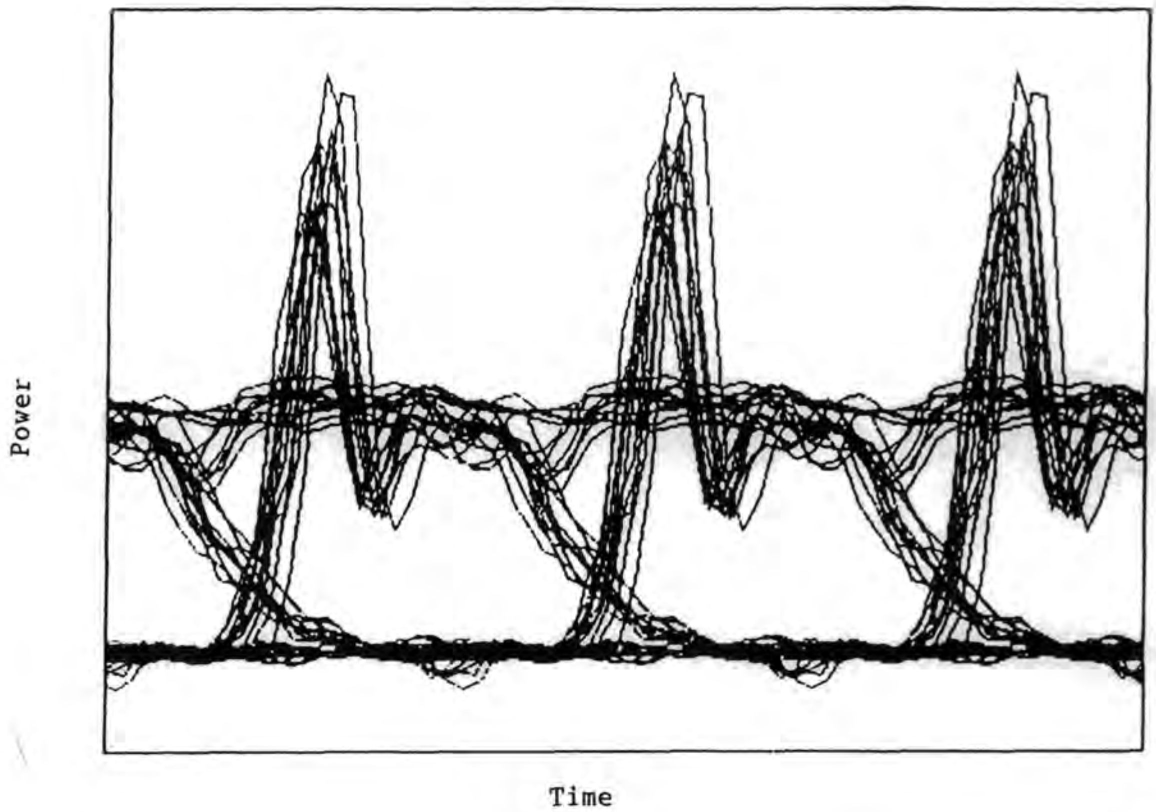

Figure (7.9): Eye diagram for a hybrid LPE/MOVPE distributed feed-back ridge waveguide laser operating at 2.4Gbs^{-1}.

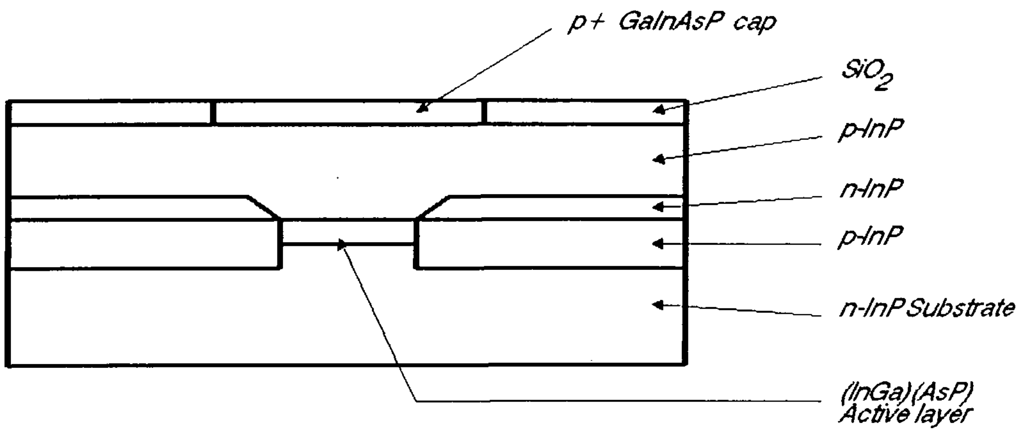

Figure (7.10): Schematic diagram of a buried heterostructure laser. (Not to scale.)

Chapter 8

MOVPE Safety

The nature of the reactants used in the MOVPE process requires considerable attention to be paid to issues of safety, more so than in many other semiconductor processes. The following section reviews the hazards and counter-measures taken to reduce risks to both personnel and the environment, to as low a level as possible.

Metal-Organic Chemicals

All of the group III and group II metal-organic precursors used in III/V MOVPE are spontaneously combustible in air, and react violently with water. They are normally packaged in all-welded stainless steel vessels, complete with inlet and outlet valves, suitable for direct connection to MOVPE reactors. Prior to opening the valves to allow passage of hydrogen through the container, the pipe joints are leak tested to avoid ingress of air and moisture, both for safety reasons, and to ensure that the highest quality of epitaxy is achieved. In the event of accidental pressure surges in the reactor, liquid metal-organic reagents can be moved into unexpected areas of pipework. Care has to be taken when disassembling pipework to avoid fires. Should a metal-organic fire take place, water fire extinguishers cannot be used. The reagents are sufficiently aggressive to react with carbon dioxide, limiting the use of this type of extinguisher. The best forms of quenching agent appear to be either dry sand or dry powder fire extinguishers.

When changing metal-organic sources, care is required to ensure that all traces of the compounds have been removed from pipes that are to be opened to air. Measures to achieve this are purging of pipework, or back-filling with dry nitrogen and evacuating the pipes connected to the bubbler.

The toxicity of metal-organic compounds has not been extensively investigated. Their pyrophoric nature, and the hermeticity of reactors, necessary for high quality growth, makes exposure to the chemicals unlikely. Obvious chemicals to which exposure should be

avoided, are compounds of elements which are toxic such as beryllium.

Phosphorus

The growth of InP based epitaxial layers, results in the deposition of large amounts of phosphorus upon glassware and pipework. With time, this tends to adopt a fairly passive form and may form red phosphorus. However immediately after growth, both white and yellow deposits may be seen, which can smoulder in air or burn with a hot flame. This form of phosphorus, probably the white allotrope, is therefore a burn hazard and is also poisonous.

Hydrogen

Hydrogen is used as the carrier gas to transport reactants to the MOVPE growth zone. The explosive nature of the gas requires care to be taken to avoid mixing it with air. This is ensured by the use of high integrity pipework and seals, checked using leak detectors. As a further safety measure, strategically placed hydrogen detectors can be used to signal alarms should a hydrogen leak occur, and allow automatic close down of the reactor. Smoke and flame detectors can be similarly interlocked with the process to prevent hydrogen fuelling a fire external to the reactor.

It was common practice when growing GaAs compounds, to unload the reactor with hydrogen flowing into the atmosphere. Epitaxy of InP based compounds results in the deposition of phosphorus, which can act as an ignition source for hydrogen gas. It is desirable therefore to switch the carrier gas to nitrogen during unloading. More sophisticated apparatus now incorporates either glove boxes or automatic load locks to prevent moisture and oxygen entering the reaction tube.

The above problems are fairly easily contained given high quality components and knowledgeable users.

The Toxicity of Arsine and Phosphine

The major hazard associated with MOVPE, is the need to use highly toxic gaseous sources for the group V elements. The toxicity of substances is classified by a variety of exposure levels. The level most commonly encountered in the U.K., is called the "Toxic Limit Value" (TLV), and defines the concentration of gas to which a worker can safely and continuously be exposed during a normal working week. Another level is the "Toxic Concentration Low" (TC_{Lo}), which is determined by observing the toxic gas concentration that first triggers physiological changes in workers. A third, often used in laboratory toxicology experiments is the LC_{50} value. The "Lowest Lethal Concentration" (LC_{Lo}), is used to define gas concentrations that terminally affect workers. The TLVs for arsine and phosphine are 0.05ppm and 0.3ppm respectively. The TC_{Lo} for arsine is 3ppm, and the LC_{Lo} values for arsine and phosphine are 25ppm and 1000ppm respectively. The gas concentrations normally encountered at the exhaust of an MOVPE reactor, assuming no consumption of the hydrides, are of the order of 20000ppm and 5000ppm, for low pressure and atmospheric pressure reactors respectively. Clearly it is essential during normal working situations to avoid release of these gases into the working environment, and to ensure that the final emissions into the atmosphere are safe. Normal working practice in most laboratories is to reduce exposure levels and emission levels to below the detection limits of monitoring systems, which can detect concentrations below TLV levels. Of equal importance is the limitation of the effects of a large toxic gas release caused by equipment malfunction.

Safe Reactor Design and Operation

MOVPE reactors are placed in well extracted cabinets, so that should a leak of gas occur, for example due to a fractured reaction chamber, the toxic gases will be swept away from the operator. The whole of the gas handling apparatus and cabinets containing the gas sources are also heavily extracted, and any linking between cabinets is achieved using all-welded pipework which is sometimes placed coaxially in a secondary extracted pipe. The apparatus has to be

extensively helium leak tested to ensure good epitaxial results, but the considerations of safety place further demands upon the need for leak tightness. Reactors should be designed to fail safe in the event of loss of power, air or hydrogen. Prior to unloading of the reactor, it is essential to purge remaining traces of toxic gases and also hydrogen from the growth zone. Alternative methods to unloading directly into the atmosphere are to use glove boxes and load locks. Both of these alternatives can be cumbersome to use. Within production facilities, the identification of risks, and the design, implementation, and monitoring of safe operating procedures is essential. This is especially important for workers who may be operating the reactor repetitively on a ten runs per week basis. The use of interlocks to prevent unloading whilst toxic gases are flowing, and to prevent access to extracted areas during growth is desirable.

Gas Containment upon Equipment Failure

There are several measures that can be taken to limit the effect of component failures upon personnel. The most commonly expected serious failure is bursting or detachment of the diaphragm of the pressure regulators, which reduce the pressure of the toxic gases down to ≃2 bar. Under these circumstances, reactor components are subjected to pressures beyond their specified limits, and leakage to the surrounding atmosphere may occur. The extent of this problem may be reduced considerably by the use of several safety features. The first measure is to use gas cylinders which are fitted with restricted output orifices, such that only a limited flow can occur, which can be handled by the remainder of the system. This measure has now been almost universally adopted. Another feature is to fit the bonnets of regulators with vent pipes which route gas to remote exhausts away from operators. The siting of gas cabinets in extracted rooms separate to the main MOVPE work areas further isolates the most hazardous modules from personnel. The use of flow limiting valves in toxic gas lines, which sense that the flow rate of gas has exceeded a threshold value and then automatically shut off all flow is desirable, though the tendency of some models to shut off for no apparent reason has limited their widespread use.

The use of toxic gas monitors to close down automatically the

MOVPE process can be extended to trigger further safety features. Clean-rooms need a positive pressure compared with external corridor and work areas, and MOVPE facilities are no exception to this requirement. To reduce the spreading effects of a toxic gas release, monitors can automatically trip further extraction fans into operation to provide an overall negative pressure in the affected laboratory, whilst maintaining a high input flow of air to sweep the toxic gases out. High pressure shut off valves, located on the high pressure side of regulators, have recently become available. These can be automatically triggered shut, and in the event of fire, the air supply to them can be terminated by the melting of the plastic pipes.

Cylinder Changing, Handling and Storage

The highest level of risk encountered during MOVPE operations is during the changing of gas cylinders. The cylinder is removed from the above safety features, and the engineer is reliant upon the gas cylinder being tightly closed prior to removal of the protective cap. It is now normal for personnel to wear self-contained positive pressure breathing apparatus for protection, and to exclude other people from the immediate area whilst the cylinders are changed.

Prior to removal of a toxic gas cylinder from a gas cabinet, any over-pressure of the gas is relieved, and the pipework, including the regulator assembly, is purged with either nitrogen or hydrogen. The pipework through to the cylinder valve is then evacuated to remove any remaining traces of toxic gases.

Cylinders have to be handled with care during transportation, even though they are designed and tested to withstand severe impacts. It is necessary to ensure that all staff responsible for the movement of toxic gases are aware of the nature of the hazards. Cylinders should be stored in open ventilated areas, which are secure from tampering.

There are legal limits on the amount of arsine and phosphine that can be present at any one location. For arsine, the level is 10kg, equivalent to only four normally sized cylinders of pure arsine. Companies wishing to exceed these limits must subject themselves to rigorous scrutiny and communicate the hazardous nature of their operations to the local authorities. The latter action is in any case

sensible, should a major problem such as fire occur that would involve emergency services, or in the case of fire in the vicinity of the gas cylinders, evacuation of the immediately surrounding population.

Medical Aspects of Exposure to Arsine and Phosphine

The available medical knowledge upon the effects of exposure to arsine and phosphine is limited. This is due to the low level of incidents which have occurred using these gases; to the author's knowledge, no severe exposure to the gases has ever taken place in an MOVPE facility. One accident that has been reported was the exposure of dock workers to arsine whilst investigating the contents of a ship's hold, in which a leaking cylinder of gas was present [194]. The workers were treated, and subsequently made a full recovery, indicating that the effects of exposure to arsine are acute rather than chronic. Arsine affects the oxygen carrying ability of blood, so several changes of blood are necessary when treating patients.

The associated compounds of arsenic are also poisonous, arseneous oxide being a carcinogen. The routine monitoring of arsenic levels in workers is desirable, however many of the methods tried such as blood, hair and urine sampling have proved unreliable.

Arsine and Phosphine Monitoring

To ensure that workers are not exposed to arsine and phosphine and to determine the content of exhaust gases released to the atmosphere, it is necessary to monitor continuously the working environment. There are several types of monitor commercially available. One type functions by detecting chemiluminescent emissions from the gases, and a more commonly used type determines the transparency of a chemically impregnated paper tape that darkens upon exposure to the gases. In each case, a high avoidance of false alarms is required, to ensure that operators' respect for the system is retained, and to avoid unnecessary production losses. This can only be achieved by the use of detection systems that are very specific to the gases being monitored, and exclude for example, traces of hydrogen. Monitoring systems are usually remote from the MOVPE reactors to facilitate decision making in the event of an emission of gas in the

laboratory. The need for multi-point systems, at a reasonable cost, can lead to significant response delays. It is both necessary to monitor for gas releases and act immediately, and also to identify the affected area so that corrective action can subsequently be taken. For this to be achieved, it is desirable to operate two systems, one detecting several channels simultaneously, and the other serially polling through different channels. Alarm and automatic close down signals are then generated accordingly. Upon detection of high levels of toxic gases, evacuation of the laboratory, and if necessary the surrounding buildings, can be ordered.

One problem with monitoring systems, is that a high gas level on one serially addressed channel, can lead to cross talk onto a neighbouring channel. This is particularly significant if a poorly scrubbed exhaust is being monitored along with a working atmosphere.

All of the above requirements result in the adoption of a fairly complex group of measurement equipment, which constitutes both an increase in capital cost, and routine expenditure upon consumables and servicing.

Alternative Group V Sources

The need for alternative group V sources for reasons relating to control of epitaxial composition has been discussed previously. The relative pyrolysis inefficiency of phosphine in particular, also causes unwanted loading of scrubbing facilities. A major reason for the hazardous nature of arsine and phosphine is that they are supplied as gaseous mixtures at cylinder pressures of over a hundred bar. This enhances the spreading rate of any accidental release. The use of pure gas sources of arsine and phosphine, which are liquefied and have cylinder pressures of $\approx$14 bar and $\approx$40 bar respectively, reduces the release rate from the cylinder.

It is desirable to find alternative sources to arsine and phosphine, which ideally are, non-toxic, liquids at room temperature, and pyrolyse efficiently. The first objective is unlikely to be realised for arsenic sources, however the reduced emission risks associated with liquid bubbled sources of group V elements has encouraged work in this field. Alkyl type sources such as tertiarybutyl arsine are now being marketed by both conventional

metal-organic suppliers, and also gas companies who anticipate further restrictions on the use of arsine and phosphine.

Environmental Protection

The toxicity of the hydrides and other compounds of arsenic, also give cause for concern regarding air pollution. During the early days of MOVPE, it was normal to exhaust waste gases directly to the atmosphere, albeit diluted with significant amounts of air or nitrogen. Whilst this practice was acceptable for workers in the immediate vicinity, the compounds of arsine had to come to rest somewhere. Over the last few years, environmental concern has increased, particularly in the U.S.A., such that it has become difficult for some companies to gain licences to operate MOVPE reactors. It has become common to scrub the output gases from MOVPE reactors, maintaining the amounts of toxic gases released to below TLV concentrations, or better still, to undetectable levels. Emission levels of arsine and phosphine are monitored in the same manner as within laboratories.

One method of eliminating the hydrides, is by combustion in a flame stack. However, this produces toxic oxides, which require wet scrubbing, or subsequent filtration to render the output harmless.

Charcoal Adsorption

Charcoal can act as a very good adsorber of gases, including arsine and phosphine [195]. The effect can be enhanced or activated by the addition of trace elements to the charcoal. A simple method of MOVPE exhaust scrubbing is to pass the gases through activated charcoal. The volume of charcoal can be small, in which case it has to be changed each growth run, whereas a large drum of activated charcoal can scrub the exhaust of several reactors for several hundred growth runs. Once removed from the reactors, the charcoal has to be disposed of, and since the contents are still toxic, there remains concern regarding this method of gas scrubbing.

The arsine and phosphine adsorbed onto the charcoal, is still exothermically reactive with oxygen. Should air enter the container, the temperature can rise significantly, presenting both a fire hazard

and also causing desorption of the hydrides. A simple way around this problem, is to add oxygen or air to the MOVPE exhaust gases prior to the charcoal scrubber. This treatment has been found to produce a stable chemical mixture within the charcoal, and to enhance the total adsorption capacity.

Wet Scrubbers

The alternative method for toxic gas scrubbing, is to chemically react the gases with aqueous solutions of suitable compounds. For scrubbing arsine and phosphine, an oxidising solution of sodium hypochlorite and alkaline sodium hydroxide is used. The gases are passed through a venturi spray and are then forced through fine meshes which are continuously sprayed with scrubbing solution. Scrubbing efficiencies of better than 99.9% can be achieved.

The reaction chemistry is not completely understood, but is thought to follow the equations:

$$PH_3 + 4NaOCl + 3NaOH \rightarrow Na_3PO_4 + 4NaCl + 3H_2O$$

$$AsH_3 + 4NaOCl + 3NaOH \rightarrow Na_3AsO_4 + 4NaCl + 3H_2O$$

It is important to maintain the redox potential of the scrubbing solution at a high value to obtain good efficiency.

The advantages of this technique are that relatively safe arsenic and phosphorus salts are produced in solution. The liquid waste has still to be disposed of, however there is some interest in it being reprocessed. The disadvantages are that considerable quantities of scrubbing reactants are required, and the liquid nature of the process can lead to spillages.

The author has used both charcoal adsorption scrubbers and sodium hypochlorite based liquid scrubbers, and has found the former to be the more reliable. However further work is needed to understand the long term stability and pollution hazards of the waste from each of these methods.

Future Developments

During the late 1980's, devices containing epitaxial layers of InP and (GaIn)(AsP) alloys grown by MOVPE, have been transferred successfully from development laboratories to production houses. These devices are discrete, and are analogous to early silicon transistors. The growth of the layers to date, has taken place upon single two inch diameter substrates, and a high degree of lattice matching of layers to substrates has been sought after.

Future developments will be associated with the economies of scale obtained by multi-wafer epitaxy, and with a drive towards integration of electronic and opto-electronic components. Small scale integration has been reported for photo-diodes with first stage FET amplifiers [4], and for the integration of DFB lasers with monitor photo-diodes [197,198]. The integration of lasers with driving transistors also has been demonstrated [199]. The integration of further components however, such as complete laser monitor and driving circuits, or complete repeater circuits, requires that major improvements in wafer uniformity and size be achieved.

There has been much speculation upon the feasibility of the growth of III/V epitaxial layers upon silicon substrates, the objectives ranging from lowering substrate costs, to the integration of silicon integrated circuits with opto-electronic components. The performance of computers is beginning to become limited by the long information transmission times between processors and across chips, the use of optical signals to transmit information would circumvent this problem. The growth of lasers upon silicon substrates has been demonstrated, but severe problems remain with the elimination of defects, and with device degradation [200].

It would appear that MOVPE is likely to remain a popular crystal growth technique for some time, even though the exact form may change to embrace MOMBE. The problems associated with the toxicity of the group V hydride sources, may be overcome with the advent of high quality organic group V precursors. The move away from the use of arsine and phosphine may be hastened by legislation and public concern.

Appendix 1

Atmospheric Pressure Reactor B at STL

The majority of the work reported in this thesis was undertaken upon MOVPE reactor B at STL. The gas circuit of this apparatus is shown in figure (A.1), and the front-piece of the thesis shows photographs of the reactor. The system was heavily modified during the work, and is described in its final form upon the author's departure from STL.

The reactor was originally constructed entirely at STL by E.J.Thrush and L.Beeson in 1983.

Vent-Run Design

The reactor is of a conventional vent-run design utilising fast switching valve manifolds purchased from Thomas Swan & Co. The vent-run design allows reactants to be passed through pipework prior to being directed into the reactor, enabling adsorption and desorption processes to equilibrate, and allowing stable conditions to be obtained within the metal-organic bubblers. The final selection of reactants for growth was determined by the valve manifolds switching the flows from vent to run, and the manifolds were positioned as close as possible to the reaction chamber, to prevent gas diffusion causing diffuse hetero-interfaces. Two manifolds were used, one for arsine and phosphine and the second for other reactants. This allowed mixing of hydrides and alkyls to take place in the reaction tube, so avoiding long lengths of pipes or dead volumes where pre-reactions could cause deposition of unwanted compounds.

A glass tube packed with quartz wool, was introduced into the vent line to allow room temperature reactions between the metal-alkyls and the hydrides to be observed.

Pressure and Flow Balancing

The flow of gas to the reaction chamber was dependent upon a stable pressure being maintained in the alkyl bubblers. This was achieved by dynamically pressure balancing the vent and run lines to

the same pressure, using a differential baratron transducer to determine any pressure discrepancy. The signal from this transducer was used by an electronic system to control a valve that allowed nitrogen to be added to the vent line, down stream of the switching manifold. An impedance in the vent line caused the pressure to change according to the amount of nitrogen added.

Further fine control of reactor pressure was possible by maintaining the same total flow rate of reactants through the growth tube by adding additional variable amounts of hydrogen to two further vent-run valves.

The reactor ran at slightly above atmospheric pressure, the exact pressure being determined by the exhaust impedance, extraction, and barometric conditions.

Mass Flow Controllers and Reactant Lines

Most of the mass flow controllers were purchased from Unit Instruments, with critical dopant and matrix elements utilising controllers with an auto-zero capability. One of the trimethylgallium lines had the facility to add further hydrogen, enabling the manifold gas injection velocity to be varied without changing the mole fraction of trimethylgallium reaching the reaction tube. The trimethylindium line incorporated an ultrasonic reagent concentration monitor which has been described in chapter (4). The trimethylindium lines and valves were heated throughout their length to avoid condensation since the source was held at 50°C.

The sources were isolated from the rest of the reactor by normally closed air operated valves. Normally open valves were used in tandem with the isolation valves to allow a flow of hydrogen to pass to the mass flow controllers when the reactants were isolated.

Metal-Organic Sources

Four metal-organic sources were used, trimethylindium, two trimethylgallium and one ferrocene. The source temperatures were 50°C, -10°C and -7°C respectively. Each was held in a water bath, controlled to better than 0.1°C, except the trimethylindium which was held in a bath containing high flash point oil.

Gaseous Sources

The main hydrogen supply to the reactor was purified using a palladium diffuser. Nitrogen, used during unloading of the reactor was dried by passing it through a molecular sieve.

The dopants used were dimethylzinc, silane and hydrogen selenide, mainly supplied from commercial gas cylinders. Arsine was used at a concentration of 10%, and phosphine was used at 100%. The hydride regulator assemblies could be purged and leak tested, and flow limit valves were fitted. Molecular sieves were used to dry the arsine and phosphine.

Reaction Chamber

The reaction chamber was based upon the Bass cell design [196], modified to allow separate injection of group V and group III reactants. The chamber was manufactured from circular cross section quartz glass. This design probably suffered from considerable swirling of the gases due to the large entrance angle where the diameter of the tube changed from 10mm to 35mm. The reaction tube incorporated a water jacket, allowing the temperature of the tube to be controlled from -13°C to 70°C. A small nozzle was introduced at the entrance to the reactor tube to induce gas mixing.

The substrates were positioned upon a silicon carbide coated graphite susceptor which was angled in the gas stream, with the rear of the susceptor raised to the centre of the tube. A half of a two inch diameter wafer could be grown upon in one growth run. The susceptor was inductively heated using an RF field from a helical coil surrounding the growth tube.

Exhaust and Toxic Gas Monitoring

The exhaust gases were first taken to a small charcoal filter close to the reaction chamber where particulate arsenic dust and phosphorus was removed from the gas stream. The gases were then taken to a large drum of activated charcoal, where the arsine and phosphine was adsorbed to prevent discharge of toxic gases into the atmosphere.

The exhaust was measured for breakthrough of toxic gases using an arsine-phosphine monitor.

The work areas and gas cabinet were also monitored for toxic gas levels using an arsine-phosphine detector, and the gas system and reaction chamber were housed in extracted enclosures.

Computer Control and In-situ Monitoring

The mass flow controllers, susceptor temperature, vent-run valves, and source isolation valves were all computer controlled using software supplied by Thomas Swan & Co. The computer also recorded flow rates, valve states, bath and line temperatures, susceptor temperature, differential and reactor pressure, and water vapour levels available from hygrometers placed in the gas lines. An oxygen monitor was also used to detect oxygen contamination of the system down to 0.02ppm levels.

Leak Testing and Vacuum System

A comprehensive vacuum manifold allowed a vacuum to be applied selectively to many areas of the reactor. This was used for regeneration of the molecular sieves, and to enable helium leak checking of the reactor. This was undertaken to ensure safe operation of the system, and to eliminate ingress of air and moisture which would affect the quality of the epitaxy. Helium leak checking was performed down to 3.10^{-9} $mbls^{-1}$ air equivalent, and vacuums of $\approx 5.10^{-5}$ torr were obtained for the complete reactor.

Acknowledgements

The work detailed in this thesis would not have been possible without the efforts of many other people. I would like to thank my colleagues at S.T.L., notably George Antell, Derek Bolger, Alan Briggs, Cliff Cureton, Nobby Denton, Brian Garratt, Rick Glew, David Greene, Julia Jowett, Sally Kitching, Keith Scarrott, John Stagg, Joe Trigg, and Ted Thrush; for help, stimulating discussions, and patience on the occasions when the MOVPE reactor defied my efforts to persuade it to function correctly.

Exchange of information between the JOERs partners, namely Plessey, BTRL, Oxford University, UMIST, Queen Mary College, St Andrews University, Epichem Ltd, and Loughborough Consultants, led to major progress in MOVPE in the U.K., and I wish to acknowledge the contribution that these establishments have indirectly made to this thesis.

Dr Nick Collings and Dr Rex Britter of Cambridge University Engineering Department gave valuable assistance with fluid dynamic modelling of gas flows. I am particularly indebted to Dr D.J.Nicholas of UMIST Solid State Electronics group for the low temperature photoluminescence results, Dr A.Norman of Oxford University Metallurgy Department for the TEM work, and Dr D.Sykes and Dr A.Chew of Loughborough Consultants for SIMS analysis.

Valuable discussions were held with colleagues in North America from A.T&T Bell Labs, Bellcore, and Bell Northern Research.

Professor J.Woods of the Applied Physics Department at the University of Durham has assisted in the submission of this work for the MSc degree.

The work at S.T.L. was funded by STC plc and by the Department of Trade and Industry under the Joint Opto-Electronics Research Scheme (JOERS). I would like to thank the Optical Devices Division of STC Defence Systems for permission to release this thesis.

Assistance in proof reading was given by Tina Dorling and Mr.& Mrs. Butler, and typing assistance was given by V.Trudgen and S.Elven.

References

1. K.C.Kao, G.A.Hockman; IEE Proceedings Vol.133, Pt.J, No.3, June 1986, pp 191-198. First published in IEE Proceedings, July 1966.

2. J.Gowar; Optical Communication Systems, Prentice Hall International, London.

3. J.R.Stern, C.E.Hoppit, D.B.Payne, M.H.Reeve, K.Oakley; 14th European Conference on Optical Communications, Brighton, 11-15 Sept, 1988, part 1, pp 203-206.

4. P.Dawe, D.Spear, W.Lee, G.Antell, S.Bland; 14th European Conference on Optical Communications, Brighton, 11-15 Sept, 1988, part 2, pp 21-24.

5. Internal STC Document.

6. G.H.Olsen; VPE of GaInAsP, GaInAsP Semiconductors, Wiley, 1982, pp 11-41.

7. H.Manasevit, Recollections and Reflections of MOCVD, Journal of Crystal Growth, 55(1981).

8. A.Y.Cho; Thin Solid Films, Vol 100, pp 291-315.

9. C.T.Foxen, B.A.Joyce, from a course on optical communications at Essex University, U.K., March 1988.

10. Third Biennial OMVPE Workshop, Brewster, Massachussettes, U.S.A., 21-23 Sept 1987.

11. G.Stringfellow; Third Biennial OMVPE Workshop, Brewster, Massachussettes, U.S.A., 21-23 Sept 1987.

12. R.Bhat; J.Elec.Materials, 14(4),1985, pp 443-448.

13. M.Naitoh, M.Umeno; Jap.J.App Phys, 26(9), Sept 1987, pp L1538-L1539.

14. R.M.Lum, J.K.Klingert, M.G.Lamont; J.Crystal Growth; 89(1988), pp 137-142.

15. M.Koppitz, O.Vestavick, W.Pletschen, A.Mircea, M.Heyan, W.Richter; J.Crystal Growth, 68(1984), pp 136-141.

16. T.F.Kuech, E.Veuhoff; J.Crystal Growth, Proceedings of the 1984 MOVPE conference, pp 148-156.

17. N.Buchan, C.Larsen, G.Stringfellow; App.Phys.Lett, 51(13), 28 Sept 1987, pp 1024-1026.

18. R.Moss, J.Evans; J.Crystal Growth, 55(1981) pp 129-134.

19. J.P.Duchemin, J.P.Hirtz, M.Razeghi, M.Bonnet, S.Hersee; J.Crystal Growth, 55(1981) pp 64-73.

20. M.Razeghi, M.Poison, J.P.Larivain, J.P.Duchemin; J.Elec. Materials, 12(2), 1983.

21. C.Cheng, K.Jones, K.Motyl; Prog.Crystal Growth and Charact., 1986, Vol 12, pp 319-333.

22. G.E.Coates; Organo-Metallic Compounds; Methuin & Co, 1960.

23. S.Bass, M.Skolnick, H.Chudzynska, L.Smith; J.Crystal Growth, 75(1986), pp 221-226.

24. Q.M.C. report to JOERS, 1988.

25. K.Fry, C.Kuo, C.Larsen, R.Cohen, G.Stringfellow, A.Mellas; J.Elec. Materials, 15(2), March 1986, pp 91-96.

26. S.Sugou, A.Kameyama, H.Katsuda, Y.Miyamoto, K.Furuya, Y.Suematsu; Elec.Lett., 24.11.83, 19(24), pp 1036-1037.

27. R.Bhat, M.Koza, B.Skromme; App.Phys.Lett, 50(17), 27.4.87, pp 1194-1196.

28. C.Chen, C.Larsen, G.Stringfellow; Inst.of Physics conference series 83, chap 3, (GaAs and related compounds 1986).

29. C.H.Chen, D.S.Cao, G.B.Stringfellow; J.Elec.Mat., 17(1), 1988, pp 67-73.

30. D.Bradley, M.Faktor, M.Scott, E.White; J.Crystal Growth, 75(1986), pp 101-106.

31. S.Adachi; J.Appl.Phys, 53(12), Dec.1982, pp 8775-8791.

32. E.J.Thrush, C.G.Cureton, J.M.Trigg, J.P.Stagg, B.R.Butler; Chemtronics, June 1987, Vol.2, pp 62-68.

33. A.R.Clawson; J.Vac.Sci.Technology A; 3(3), May 1985, pp 1040-1041.

34. A.R.Clawson, D.I.Elder; J.Elec.Mat., Vol 15(2), March 1986, pp 111-116.

35. A.T.R.Briggs, B.R.Butler; J.Crystal Growth, 85(1987), pp 535-542.

36. E. Kuphal, Flüssigphasenepitaxie von $InP/In_{1-x}Ga_xP_{1-y}As_y$ - Heterostrukturen. Teil II:Elektrische Eigenschaften von InP und $In_{0.53}Ga_{0.47}As$, Techn. Bericht, 65, TBr 20 des FI der DBP beim FTZ (1982).

37. W. Walukiewicz, J. Lagowski, L. Jastrzebski, P. Rava, M. Lichtensteiger, C.H. Gatos and H.C. Gatos, Journal of Applied Physics, 51(5), May 1980, pp 2659-2668.

38. T. Ambridge, J.L. Stevenson and R.M. Redstall, Journal of the Electrochemical Society, 127, (1), Jan. 1980, pp 222-228.

39. S.J. Bass, C. Pickering and M.L. Young, Journal of Crystal Growth, 64, (1983) pp 68-75.

40. C.C. Hsu, J.S. Yuan, R.M. Cohen and G.B. Stringfellow, Journal of Crystal Growth, 74, (1986) pp 535-542.

41. K. Uwai, O. Mikami, N. Susa; Electronic Lett; 14 Feb. 1985, Vol 21 (4), pp 131-132.

42. S.J. Bass and M.L. Young, Journal of Crystal Growth, 68, (1984), pp 311-318.

43. A.M. Huber, M. Razeghi and G. Morillot, Gallium Arsenide and Related Compounds 1984, Institute of Physics Conference Series No 74, Chapter 3, pp 223-228.

44. S.J. Bass, Journal of Crystal Growth, 47, (1979), pp 613-618.

45. E. Veuhoff, T.F. Kuech and B.S. Meyerson, Journal of the Electrochemical Society, 132, 8 August 1985, pp 1958-1961.

46. T.F. Keuch and R. Potemski, Applied Physics Letters, 47, (8), 15th October 1985, pp 821-823.

47. H. G. B. Hicks and P.D. Greene, Gallium Arsenide and Related Compounds, Institute of Physics Conference Series, No.9, 1970, pp 92-99.

48. M.E.Weiner, Journal of the Electrochemical Society, 119(4) April 1972, pp 496-503.

49. M.A. Di Forte-Poisson, C. Brylinski and J.P. Duchemin, Applied Physics Letters 46(5), 1st March 1985, pp 476-478.

50. L.D. Zhu, K.T. Chan and J.M. Ballantyne, Applied Physics Letters, 47(1), 1st July 1985, pp 47-48.

51. J.P. André, E.P. Menu, M. Erman, M.H. Meynadier and T. Ngo, Journal of Electronic Materials, 15, 2 March 1986, pp 71-74.

52. A.H. Moore, M.D. Scott, J.I. Davies, D.C. Bradley, M.M. Faktor and H. Chudzynaska, Journal of Crystal Growth, 77, (1986), pp 19-22.

53. J.M.Boud et al; GaAs and related compounds, Crete, 1987.

54. K.Nakajima, S.Komiya, K.Akita, T.Yamaoka, O.Ryuzan; J.Electrochemical Society; Solid State Science & Technology, July 1980, pp 1568-1572.

55. A.Rosiewicz, C.Park, B.Butler, C.Jones, M.Palin; IEE Proceedings (J), 132(6), Dec.'85, pp 319-324.

56. T.Glisson, J.Hauser, M.Littlejohn, C.Williams, J.Electronic Materials, 7(1), 1978, pp 1-17.

57. K.Nakajima, A.Yamaguchi, K.Akita, T.Kotani; J. Appl. Phys., 49(12), 1978, pp 5944-5950.

58. R.Nahory, M.Pollack, W.Johnston, R.Barns; Appl. Phys. Lett., 33(7), 1978, pp 659-661.

59. G.Olsen, C.Nuese, R.Smith; J.App.Phys.,49(11), Nov.'78, pp 5523-5529.

60. E.Thrush, J.Whiteaway, G.Whale-Evans, D.Wight, A.Cullis; J.Crystal Growth, 68(1984) pp 412-421.

61. P.Charsley, R.S.Deol; J.Crystal Growth, 74(1986), pp 663-666.

62. S.J.Bass, not published.

63. J.P.André, E.Menu, M.Erman, M.Meynadier, T.Ngo; J.Electronic Materials, 15(2), March 1986, pp 71-79.

64. L.Zhu, P.Sulewski, K.Chan, K.Muro, J.Balantyne, A.Sievers; J.App.Phys, 58(8), 15.10.85, pp 3145-149.

65. M.Kane, D.Anderson, L.Taylor, S.Bass; J.Surface Science, 170(1986), pp 470-479.

66. K.Chan, L.Zhu, J.Balantyne; App.Phys.Lett., 47(1), 1.7.85.

67. L.Aina, M.Mattingley, R.Potter; App.Phys.Lett., 51(21), 23.11.87, pp 1735-1737.

68. M.Kane, D.Anderson, L.Taylor, S.Bass; J.App.Phys., 60(2), 15.7.86.

69. A.Mircea,R.Mellet, B.Rose, D.Robein, H.Thibierge, G.Leroux, P.Daste, S.Godefroy, P.Ossart; J.Elec.Mat., 15(4), July'86, pp 205-213.

70. M.Razeghi, B.de Cremoux, J.Duchemin; J.Crystal Growth, 68(1984), pp 389-397.

71. M.Sato, M.Suzuki; Jap.J.App.Phys., 26(3), March'87, pp 428-433.

72. A.Koukitu, H.Seki; J.Crystal Growth, 76(1986), pp 233-242.

73. R.Nahory, M.Pollack, W.Johnston; App.Phys.Lett., 33(7), 1.10.78, pp 658-661.

74. E.Kuphal; J.Crystal Growth, 67(1984), No.3, pp 441-457.

75. J.Hayes, A.Adams, P.Greene; GaInAsP alloy semiconductors; editor T.Pearsall; Wiley & Sons, 1982, p 189.

76. M.Faktor, Queen Mary College, London; Private Communication, 1986.

77. J.Stagg; Chemtronics, 3(1), March'88, pp 44-49.

78. O.Kayser, H.Heinecke, A.Brauers, H.Luth, P.Balk; Chemtronics, 3, June '88, pp 90-93.

79. S.Bass, R.S.R.E; private communication, 1987.

80. A.Mircea, R.Azoulay, L.Dugrand, R.Mellet, K.Rao, M.Sacilotti; J.Elec.Mat., 13(3), 1984, pp 603-620.

81. B.S.Massey; Mechanics of fluids, Van Nostrand Reinhold (UK), 5th ed., ISBN 044230552-4.

82. Experiments undertaken during 1987 at the University of Cambridge Department of Engineering.

83. C.Baauw, C.Miner; J.Crystal Growth, 84(1987), pp 191-195.

84. J.Crank; The Mathematics of Diffusion; 1975, 2nd ed., Oxford, Clarendon, ISBN 0198534116.

85. W.Boynton, W.Brattain, International Critical Tables, Vol 5, McGraw Hill, 1929, pp 62-63.

86. M.M.Faktor, I.Garrett; Growth of Crystals from the Vapour; Chapman and Hall, 1974, ISBN 0412113201, p 169.

87. E.Johnson, G.Legg; SPIE Vol 796, Growth of Compound Semiconductors.

88. N.Mason, P.Walker; 2nd European Workshop on MOVPE, St. Andrews, Scotland, June 1988, PS7-70.

89. C.Goodings, N.Mason, P.Walker, D.Jebb; 2nd European Workshop on MOVPE, St. Andrews, Scotland, June 1988, PS7-71.

90. J.Duchemin, M.Razeghi, J.Hirtz, M.Bonnet; Inst. Phys. Conf. Ser. No 63, Chapter 3, (GaAs and related compounds, 1981), pp 89-94.

91. P.Spurdens, A.Nelson, S.Cole, R.Walling, D.Button; 3rd biennial MOVPE workshop, Brewster, Mass., U.S.A, Sept. 1987.

92. H.Haspekto, U.Büttner, E.Sasse, U.König; Journal of Crystal Growth, 84(1987), pp 196-198.

93. M.Di Forte-Poisson, C.Brylinski, J.Duchemin; App.Phys.Lett., 46(5), 1.3.85, pp 476-478.

94. C.Hsu, J.Yuan, R.Cohen, G.Stringfellow; J.Crystal Growth, 74(1986), pp 535-542.

95. C.Hsu, J.Yuan, R.Cohen, G.Stringfellow; J.App.Phys., 59(2), 15.1.86, pp 395-398.

96. A.Clawson, T.Vu, D.Elder; J.Crystal Growth, 83(1987), pp 211-218.

97. T.Kuech, E.Veuhoff, B.Mayerson; J.Crystal Growth; 68(1984), pp 48-53.

98. E.Woelk, H.Beneking; J.App.Phys., 63(8), 15.4.88, pp 2874-2876.

99. T.Kawabata, H.Ishiguro, S.Koike; J.App.Phys., 64(7), 1.10.88, pp 3684-3688.

100. P.Spier, U.Koerner, A.Nowitzki, F.Grotjahn, F.Tegude, K.Wünstal; (SEL, Germany), unpublished.

101. A.Nelson, R.Moss, P.Spurdens, S.Cole, S.Wong; Br.Telecom Technol.J., Vol.4 #2, April 1986, pp 85-103.

102. M.Vilela, J.Sallese, P.Basmaji, P.Gibart, J.Portal; 2nd European workshop on MOVPE, St. Andrews, Scotland, June 1988, PS3-35.

103. A.Nelson, L.Westbrook; J.App.Phys., 55(8), 15.4.84, pp 3103-3108.

104. B.Rose, C.Kazmierski, D.Robein; 2nd European workshop on MOVPE, St. Andrews, Scotland, June 1988, PS3-37.

105. J.Wiley; Semiconductors and Semimetals, Vol.10, eds: R.Willardson and A.Beer, Acedemic Press, New York, 1975, p 162.

106. C.Blaauw, B.Emmerstorfer, A.Springthorpe; J.Crystal Growth, 84(1987), pp 431-435.

107. C.Blaauw, R.Bruce, C.Miner, A.Howard, B.Emmerstorfer, A.Springthorpe; 2nd European workshop on MOVPE, St. Andrews, Scotland, June 1988, PS3-36.

108. K.Huang, B.Wessels, J.Mat.Sci.Lett., 6(1987), pp 1310-1312.

109. Diffusion in the III/V Compound Semiconductors, H.C. Casey Jnr., Bell Labs, Murray Hill, NJ, USA.

110. G.van Gurp, P.Bondeivijn, G.Fontiyn, D.Tjaden, Phillips Eindhoven, The Netherlands; to be published.

111. S.Cole, J.S.Evans, A.W.Nelson, S.Wong; ICMOVPE '88, Hakone, Japan.

112. S.Cole, J.S.Evans, M.J.Harlow, A.W.Nelson, S.Wong, Elec. Lett, 24(15), 21.7.88, pp 929-931.

113. B.Rose, C.Kazmierski, 2nd European Conference in MOVPE, St. Andrews, Scotland, June 1988, PS37.

114. S.J.Pearton, J.W.Corbett, T.S.Shi, App.Phys. A, 43, (1987), pp 153-195.

115. J.Chevallier, A.Jalil, B.Theys, J.C.Pesant, M.Aucouturier, B.Rose, C.Kazmierski, A.Mircea; Proceedings of ICDS 15, Budapest, 22-26 August '88. Also see: Semicond.Sci. and Tech., 4(1989), pp 87-90.

116. B.Pajot, J.Chevallier, B.Theys, B.Rose, Proceedings of ICDS 15, Budapest, 22-26 August '88. Also see: Semiconductor Sci. and Tech., 4(1989),pp 91-94.

117. K.Uwai, H.Nakagome, K.Takahei; App.Phys.Lett., 50(15), 13.4.87, pp 977-979.

118. J.Long, V.Riggs, W.Johnston; J.Crystal Growth, 69(1984), pp 10-14.

119. A.Macrander, J.Long, V.Riggs, A.Bloemake, W.Johnston; App.Phys.Lett., 45(12), 15.12.84, pp 1297-1298.

120. S.Chu, S.Nakahara, J.Long, V.Riggs, W.Johnston; J.Electrochemical Soc., Solid State Science and Technology, Nov. 1985, pp 2795-2798.

121. K.Huang, B.Wessels; J.App.Phys., 60(12), 15.12.86, pp 4342-4344.

122. M.Sugawara, M.Kondo, K.Nakai, A.Yamaguchi, K.Nakajima; App.Phys.Lett., 50(20), 18.5.87.

123. T.Takanohashi, K.Nakai, K.Nakajima; Jap.J.App.Phys., 27(1), Jan.1988, pp L113-L115.

124. F.Shishiyanu, Y.Gh.Gheorghiu, S.Palzov; Phys.Stat.Sol.(a) 40, 1977, p 29.

125. K.Hess, S.Zehr, W.Cheng, D.Perrachione; J.Elec.Mat., 16(2), 1987, pp 127-131.

126. B.Tell, U.Koren, B.Miller; J.App.Phys, 61(3), 1.2.87.

127. C.Zah, C.Caneau, S.Menocal, F.Favire, T.Lee, A.Dentai, C.Joyner; Elec.Lett., 24(11), 26.5.88, pp 695-697.

128. Hess; ICMOVPE IV, Hakone, Japan, May 1988.

129. H.Temkin, G.J.Dolan, M.B.Pannish, S.Chu; App Phys Lett, 50(7), 16.2.87, pp 413-415.

130. H.Arnot, M.Watt, C.Sotomayor-Torres, R.Glew, R.Cusco, J.Bates, S.P. Beaumont; Superlattices and Microstructures, Vol 5, no.3, 1989, pp 459-463.

131. K.Karey, R.Hull, J.Fouquet, F.Kellert, G.Trott.

132. M.Razeghi; unpublished.

133. M.B.Pannish; J.Crystal Growth, 81(87), pp 249-260.

134. Y.Guldner, J.Vieren, P.Voisin, M.Voos, M.Razeghi, M.Poisson; App.Phys.Lett, 40(10), 15.5.82, pp 877-879.

135. L.Taylor, M.Kane, S.Bass; Appl.Phys.Lett, 51(3), 20.7.88, pp 180-182.

136. M.Razeghi, J.Duchemin, J.Portal; Appl.Phys.Lett, 46(1), 1.1.85, pp 46-48.

137. J.Portal, R.Nicholas, M.Brummell, L.Brunel, S.Huant, M.Razeghi, M.Laviron; J.Semicond.Sci.Tech., 1(1986), pp 3-6.

138. M.Razeghi, P.Maurel, A.Tardella, L.Dmowski, D.Gauthier, J.Portal; J.Appl.Phys., 60(7), 1.10.88, pp 2453-2456.

139. T.Fukui, H.Saito; Jap.J.Appl.Phys., 23(8), Aug '84, pp L521-L523.

140. P.Gourley, R.Biefeld, L.Dawson; App.Phys.Lett., 47(5), 1.9.85, pp 482-484.

141. B.Miller, E.Schubert, U.Koren, O.Ourmazd, A.Dayem, R.Capik; App.Phys.Lett, 49(20), 17.11.86, pp 1384-1386.

142. C.Kuo, K.Fry, G.Stringfellow; Appl.Phys.Lett, 47(8), 15.10.85, pp 855-857.

143. D.Grützmacher, K.Wolter, H.Jürgesen, P.Balk; Appl.Phys.Lett, 52(11), 14.3.88, pp 872-873.

144. S.Barnett, G.Brown, S.Courtney, S.Bass, L.Taylor; J.Appl.Phys, 64(3), 1.8.88, pp 1185-1190.

145. R.Moss, P.Spurdens; Elec.Lett, 8.11.84, Vol 20(23), pp 978-980.

146. D.Moroni, J.André, E.Menu, Ph.Gentric, J.Patillon; J.App.Phys, 62(5), 1.9.87, pp 2003-2008.

147. M.Skolnick, P.Tapster, S.Bass, A.Pitt, M.Apsley, S.Aldred; J.Semicond.Sci.Tech., 1(1986), pp 29-40.

148. M.Skolnick, P.Tapster, S.Bass, M.Apsley, A.Pitt, S.Aldred, N.Chew, A.Cullis, C.Warick; Appl.Phys.Lett, 48(21), 26.5.88, pp 1455-1457.

149. M.Razeghi, J.Duchemin, J.Crys.Growth, 70(1984), pp 145-149.

150. M.Panish, H.Temkin, R.Hamm, S.Chu; App.Phys.Lett, 49(3), 21.7.86, pp 164-166.

151. G.Thompson; Physics of Semiconductor Laser Devices; Wiley 1980.

152. M.Razeghi, P.Hirtz, R.Blondeau, J.P.Laravain, L.Noel, B.de Cremoux, J.Duchemin; Elec.Lett, 4.2.82, 18 (3), pp 132-133.

153. M.Razeghi, P.Hirtz, R.Blondeau, J.P.Laravain, B.de Cremoux, J.Duchemin; Elec.Lett, 3.9.81, Vol 17 (18), pp 643-644.

154. J.Hirtz, J.Duchemin, P.Hirtz, B.de Cremoux, T.Pearsall, M.Bonnet, Elec.Lett, 10.4.80; Vol 16 (8), pp 276-277.

155. M.Razeghi, J.P.Hirtz, P.Hirtz, R.Blondeau, J.P.Laravain, B.de Cremoux, J.Duchemin; Elec.Lett, 20.8.81, Vol 17 (17), pp 597-598.

156. M.Razeghi, P.Hirtz, R.Blondeau, B.de Cremoux, J.Duchemin; Elec.Lett, 23.6.83, 19(3), pp 481-483.

157. J.P.Hirtz, M.Razeghi, J.Laravain, S.Hersee, J.Duchemin; Elec.Lett, 5.2.81, 17(3), pp 113-115.

158. A.Nelson, R.Moss, P.Spurdens, S.Cole, S.Wong; Br.Telecom J., Vol 4(2), April '86, pp 85-103.

159. B.Rose, P.Devoldere, A.Mircea, D.Robein, M.Trotte; Elec.Lett, 6.6.85, Vol 21 (12), pp 521-522.

160. W.Devlin, J.Sidhu, S.Cole, M.Harlow, L.Westbrook, A.Nelson, J.Regnault; Elec.Lett, 22.5.86, Vol 22(11), pp 584-585.

161. R.Dupuis, H.Temkin, L.Hopkins; Elec.Lett, 17.1.85, 21(2), pp 60-62.

162. A.Rashid, R.Murison, J.Haynes, G.Henshall, T.Stockton, A.Janssen; J. Lightwave Tech. 6(1), Jan 1988, pp 25-29.

163. D.Lesterlin, J.Charil, B.Rose, M.Gilleron, P.Correc, J.Bouley; CNET, France.

164. A.Talneau, D.Rondi, M.Krakowski, R.Blondeau; Elec.Lett, 12.5.88, 24(10), pp 609-611.

165. B.Butler, A.Briggs, E.Thrush, B.Garrett, J.Stagg; Chemtronics, March 1988, pp 31-34.

166. M.Oishi, M.Nakao, Y.Itaya, K.Sato, Y.Imamura; IEEE J.Quantum Elec., QE-23(6), June '87, pp 822-827.

167. H.Yamada, T.Sasaki, S.Takano, T.Numai, M.Kitimura, I.Mito; Elec.Lett, 4.2.88, 24(3), pp 147-149.

168. T.Saaki, H.Yamada, S.Takano, M.Kitamura, I.Mito, T.Suzuki; J.Crystal Growth, 93(1988) pp 838-842.

169. Y.Miyamoto, C.Wantanabe, M.Nagashima, F.Furuya, Y.Suematsu, Y.Tohmori, S.Arai; Transactions of the IECE of Japan, Vol E, 68(12), Dec.'85, pp 796-797.

170. A.Rosiewicz, B.Butler, R.Hinton; IEE Proc.J, Vol 132(1), Feb.'85, pp 97-100.

171. M.Razeghi, R.Blondeau, K.Kazmierski, M.Krakowski, J.Duchemin; Appl.Phys.Lett, 46(2), 15.1.85, pp 131-133.

172. M.Krakowski, R.Blondeau, K.Kazmierski, M.Razeghi, J.Ricciardi, P.Hirtz, B.de Cremoux; J.Lightwave Tech, LT-4(10), Oct '86.

173. D.Cooper, S.Cole, W.Devlin, R.Hobbs, A.Nelson, J.Regnault, A.Skeats, S.Sim, P.Spurdens; Elec.Lett, 28.4.88, 24(9), pp 519-521.

174. R.Spillet; European Conference on Optical Communications, Brighton, Sept'88, pp 328-336.

175. T.Kawabata, H.Ishiguro, S.Koike; J.Appl.Phys, 64(7), 1.10.88, pp 3684-3688.

176. T.Yanase, Y.Kato, I.Mito, K.Kobayashi, H.Nishimoto, A.Usui; unpublished?

177. M.Nagashima, Y.Miyamoto, K.Furuya, Y.Suematsu, C.Wantanabe, S.Yang; Transactions of the IECE of Japan, Vol E,68, no 9, Sep'85, pp 563-565.

178. D.P.Wilt, J.Long, W.Dautremont-Smith, M.Focht, T.Shen, R.Hartman; Elec.Lett, 31.7.86, Vol 22(16), pp 869-870.

179. C.Zah, J.Osinski, S.Menocal, N.Tabatabaie, T.Lee, A.Dentai, C.Burrus; Elec.Lett, 2.1.87, 23(1), pp 52-53.

180. S.Yamakoshi, K.Tanaka, K.Wakao, O.Aoki, K.Nakai; Proc. ECOC, 1986, pp 41-44.

181. B.Miller, U.Koren, R.Capik, Y.Su; Appl.Phys.Lett, 51(26), 28.12.87, pp 2260-2262.

182. T.Tanbun-ek, R.Logan, J.Van der Ziel; Elec.Lett, 24.11.88, Vol 24(24), pp 1483-1484.

183. K.Wakao, K.Nakai, T.Sanada, M.Kuno, T.Odagawa, S.Yamakoshi; IEEE J.Quantum Elec, Vol QE23(6), June '87, pp 943-947.

184. T.Sanada, K.Nakai, K.Wakao, M.Kuno, S.Yamakoshi; Appl.Phys.Lett, 51(14), 5.10.87, pp 1054-1056.

185. W.Cheng, D.Renner, K.Hess, S.Zehr; Appl.Phys.Lett, 63(3), 1.8.88, pp 1570-1573.

186. Y.Miyamoto, M.Cao, K.Furuya, Y.Suematsu; Jap.J.App.Phys, 26(3), March '87, pp L176-L178.

187. A.Nelson, R.Moss, J. Regnault, P.Spurdens, S.Wong; Elec. Lett, 11.4.85, Vol 21(8), pp 329-331.

188. U.Koren, B.Miller, Y.Su, T.Koch, J.Bowers; App. Phys. Lett., 51(21) 23.11.87, pp 1744-1746.

189. M. Kitamura, S.Takano, N.Henmi, T.Sasaki, H.Yamada, Y.Shinohara, H.Hasumi, I.Mito; Elec. Lett., 4.8.88, Vol 24(16), pp 1045-1046.

190. T.Sasaki, N.Henmi, S.Takano, H.Yamada, M.Kitimura, H.Hasumi, I.Mito; 14th European Conference on Optical Communications, Brighton, 11-15 Sept. 1988, Part 1, pp 364-367.

191. H.Ishiguro, T.Kawabata, S.Koike; App. Phys. Lett, 52(25), 20.6.88, pp 2099-2101.

192. A.Kasukawa, Y.Imajo, T.Makino; Elec. Lett. 19.1.89, Vol 25 #2, pp 104-105.

193. R.Glew, B. Garrett, P. Greene; to be published.

194. S.P.Wilkinson, P McHuch, S.Horsley, H.Tubbs, M.Lewis, A.Thould, M.Winterton, V.Parsons, R.Williams; British Medical J., 1975(3), pp 559-563.

195. G.Haacke, J.S.Brinen, H.Burkhard; J.Electrochemical Soc. (Solid State Sci. Tech.), March '88, pp 715-718.

196. S.Bass, P.Oliver; Inst.Physics Conference Series, No 33b, 1977, Chap.1, pp 1-10.

197. N.Dutta, T.Cella, J.Zilko, A.Piccirilli, R.Brown; Elec. Lett, 17.3.88, Vol 24(6), pp 335-336.

198. M.Usami, S. Akiba, K.Utaka, Y.Matsushima; IEE Proc.J., Vol 135, #4, Aug '88, pp 289-297.

199. H.Back, F.Fiedler, N.Grote, N.Bouadma, B.Rose, P.Devoldere, F. Tegude, P.Speier, K.Wünstel; EFOC/LAN '88, 5.1, pp 161-166.

200. M.Razeghi, M.Defour, F.Omnes, P.R.Maurel, J.Chazelas, F.Brillovet; App.Phys.Lett, 53(9), 29.8.88, pp 725-727.